ON THE CAPACITY OF RATE ADAPTIVE MODULATION SYSTEMS OVER FADING CHANNEL

MO RONGHONG

NATIONAL UNIVERSITY OF SINGAPORE

2004

ON THE CAPACITY OF RATE ADAPTIVE MODULATION SYSTEMS OVER FADING CHANNEL

MO RONGHONG
(B.Sc., M.Sc.)

A THESIS SUBMITTED FOR THE DEGREE OF DOCTOR OF PHILOSOPHY IN ELECTRICAL ENGINEERING
DEPARTMENT OF ELECTRICAL & COMPUTER ENGINEERING
NATIONAL UNIVERSITY OF SINGAPORE

2004

ACKNOWLEDGEMENTS

This thesis would not have been completed without the help of many people.

First and foremost, I would like to express my heartfelt gratitude to my supervisor, Dr. Chew Yong Huat, for his consistent support, patient guidance and valuable advice throughout my study in NUS. I am indebted to him for encouraging me to take all the challenges and get through all the difficulties during the study. His deep insight, rigorous style of problem solving and always availability to listen to my questions kept me motivated during the work of my research. Not only his conscious attitude towards research work but also his never giving up facing difficulties leaves indelible impact on me forever.

Special thanks go to professor Tang Sing Hai and associate professor C.C. Ko for offering me the opportunity to study in NUS. I would like to thank Mr. Hu Xiaoyu and Miss Wun Hau Sze for their collaboration on my work. I would also like to thank NUS and ECE-I^{2}R Joint Laboratory for giving me the scholarship and providing a wonderful technical environment. I would also like to thank all my friends in this laboratory for the great help when I was in trouble.

I am also deeply grateful to all my friends. Their friendship accompanies me fighting all the difficulties during this phase of my life. I also express my thanks to all my tennis partners, who made this exercise the most efficient relaxation after hard working.

Last but not least, I am and always grateful to my family, for their substantial support with their endless love and care, advice and encouragement in my life.

TABLE OF CONTENTS

SUMMARY

This thesis studies the capacity achieved by adaptive modulation systems employing various techniques over flat and frequency selective fading channel.

The realization of adaptive modulation relies on the precise tracking of channel conditions. The effect of imperfect channel estimation on the bit error rate (BER) performance is studied. Numerical results show that the BER performance strongly depends on the correlation coefficient ρ of the true fading gain and the estimated fading gain. An approximate method to reduce the complexity in BER computation with small amplitude error is proposed. It is proved to be a good match at practical SNR and at higher ρ. For the first time, a framework is proposed to quantify the effect of imperfect channel estimation on capacities achieved by adaptive modulation systems. With channel estimation error, some higher order multi-level quadrature amplitude modulation (MQAM) constellations cannot be used due to the presence of error floor.

A thorough study on the channel capacity and some performance metrics such as the average time duration to stay in one MQAM constellation and the channel inter-access time of an optimal multiple access channel allocation scheme is conducted. A suboptimal SNR(signal-to-noise-ratio)-priority-based channel allocation scheme combined with adaptive modulation is proposed to overcome the long channel inter-access time of the optimal channel allocation scheme. To meet the requirement of future generation wireless systems, a dual-class system accommodating QoS (quality of service) and best effort (BE) services is proposed and studied. The system throughput achieved by this dual-class

allocation scheme is shown to be higher than that of conventional fixed rate fixed slot duration systems.

Adaptive modulation can be extended to code division multiple access (CDMA) systems by employing adaptive processing gain (PG) technique. A flaw present in the study of capacity of adaptive CDMA systems in most of the literatures is corrected by considering a minimum PG constraint, $G_{\min}$. A combined adaptive PG adaptive MQAM technique is proposed to overcome the difficulty introduced by $G_{\min}$. The system capacities achieved by rate adaptive CDMA systems combined with various power control schemes over frequency selective fading channel have been studied. The proposed power control schemes make use of the information of channel fading and user location to achieve higher system capacity without the need of complicated algorithm as reported in some literatures.

Rate adaptation in CDMA systems can be realized by adjusting the spreading chip rate. The variance of multiple access interference (MAI) is derived under a practical interference model taking into account the non-orthogonality of spreading codes, the difference of carrier frequency and the power spectral density for different spreading signals. Various configurations of multiple chip rate CDMA (MCR/CDMA) systems are evaluated in terms of system capacity. For the first time, comparison on capacity achieved by MCR and multiple processing gain (MPG) systems is conducted. The study shows that MCR systems perform not worse than MPG systems in terms of system capacity. With the proper control of spectrally overlaid configuration of MCR systems, the capacity gain achieved by MCR systems can be much higher.

NOMENCLATURE

AGC	Automatic gain control
AWGN	Additive white Gaussian noise
BE	Best effort
BER	Bit error performance
BS	Base station
CBR	Constant bit rate
CDF	Cumulative distribution function
CDMA	Code division multiple access
CSI	Channel state information
EGC	Equal gain combining
FDMA	Frequency division multiple access
GPRS	General packet radio system
IQ	In-phase and quadrature
LCR	Level crossing rate
MAC	Media access control
MAI	Multiple access interference
MCR	Multiple chip rate
MMSE	Minimum mean square error
MPG	Multiple processing gain
MQAM	Multi-level quadrature amplitude modulation
MS	Mobile station
MRC	Maximal ratio combining

MUD	Multi-user detection
OVSF	Orthogonal variable spreading gain
PDF	Probability density function
PG	Processing gain
PSAE	Pilot symbol assisted estimation
PSD	Pulse spectral density
PTAE	Pilot tone assisted estimation
QoS	Quality of service
QAM	Quadrature amplitude modulation
SC	Selection combining
SINR	Signal-to-noise-interference ratio
SIR	Signal-to-interference ratio
SNR	Signal-to-noise ratio
TDMA	Time division multiple access
TDD	Time division duplex

LIST OF FIGURES

LIST OF TABLES

LIST OF SYMBOLS AND NOTATIONS

α	Channel fading amplitude
θ	Phase
$\hat{\alpha}$	Estimated fading amplitude
$\hat{\theta}$	Estimated phase
$\dot{\alpha}$	Derivative of fading amplitude
β	Average packet loss
Ω	Variance of channel fading gain
$\hat{\Omega}$	Variance of estimated channel fading gain
Ω_e	Variance of estimation error
$\dot{\Omega}$	Variance of derivative of fading amplitude
σ_n	Standard deviation of AWGN
ρ	Correlation coefficient of α and $\hat{\alpha}$
ψ	Phase estimation error
λ	Ratio of $\alpha / \hat{\alpha}$
γ	Instantaneously received SNR
$\bar{\gamma}_s$	Average transmitted SNR per symbol
$\bar{\gamma}_b$	Average transmitted SNR per bit
γ_0	Cutoff received SNR
$\gamma_{\min}$	Minimum SIR requirement
μ	Average received SNR

τ	Transmission delay
ς	Cell radius
χ	Interference coefficient
ω	Carrier frequency
$\Phi(t)$	Pulse function
ϑ	Ratio of chip durations
$a_{th,i}, b_{th,i}$	SNR thresholds for 2^i QAM being employed
B	Channel bandwidth
C	Channel capacity or bandwidth efficiency
d	Unit distance of MQAM constellation
$\overline{E}_s$	Average symbol energy
f_D	Doppler frequency
f_c	Carrier frequency
G	Processing gain
$G_{\min}$	Minimum processing gain
h	Complex channel fading gain
$\hat{h}$	Estimated fading gain
$H(f)$	Transfer function
i	The number of bits per MQAM symbol
I	Multiple access interference
K	Number of users allowed for transmission
L	Number of receivers in diversity reception system

L_{CR}	Level crossing rate
M	MQAM constellation
N_0	Two-sided power density of AWGN
$n(t)$	AWGN
N	Number of users admitted in the system
P_i	Probability that 2^i QAM being used
$\overline{p}$	Average transmission power
p_t	Transmission power
p_r	Received power
Q	Number of services
$r(t)$	Received signal
r	Ratio of variance of channel fading gain to variance of estimated channel fading gain
R	Transmission rate
s	Transmitted symbol
$\hat{s}$	Estimated symbol
S	Signal energy
$S(f)$	Power spectral density
T_c	Chip duration
T_s	Symbol duration
T_f	Frame duration
z	Distance between mobile users and the base station

CHAPTER I

INTRODUCTION

1.1 Motivation

Future generation wireless systems are required to support the simultaneous transmission of diverse information source including voice, data, image and video conferencing with variable quality of service (QoS). Two challenges imperative to the development of multimedia capability of future wireless systems are hostile transmission environment and limited radio resources. The impairments imposed by channel fading (large-scale and small-scale), path loss and co-channel interference on radio signals transmitted over air interface result in the degradation of transmission quality. Thus extra bandwidth and power are needed if a pre-defined transmission quality has to be maintained. However the extreme scarcity of available radio spectrum limits the extent to expand the signal bandwidth to meet the data rate requirement of future generation systems. To this end, the primary concern and the dominant goal of future wireless systems focus on exploring transmission technologies to achieve efficient utilization of radio resources without sacrificing service quality. Emerging technologies to improve bandwidth efficiency are becoming a necessity and are of researchers' interest, especially in broadband applications.

Bandwidth efficiency can be enhanced through the design of cell size, co-channel reuse factor, space diversity technology and multiple access techniques such as time division multiple access (TDMA), frequency division multiple access (FDMA) and CDMA.

Strategies through adaptive modulation, intelligent coding format and smart media access control are alternative solutions. Among them, adaptive modulation, which is able to dynamically adjust the allocation of radio resources to take advantage of the time varying nature of transmission environment and traffic characteristics, is a promising technique due to its potential to achieve high bandwidth efficiency.

There are two categories of adaptive modulation, one is based on instantaneous traffic conditions and the other is based on instantaneous channel conditions. The adaptive modulation based on channel conditions, which requires accurate estimation of channel quality at receiver and the reliable feedback of channel state information from receiver to transmitter, was well recognized and attracted much of research attention [1-3]. Adaptive modulation was first proposed around 60's. Due to the lack of sound channel estimation technique and the constraints on hardware complexity, its application to wireless communications did not take off immediately after emerge of the concept. Recently, driven by the need of technologies to achieve high bandwidth efficiency, the research in this area has been brought out again. Adaptive modulation is part of V.34 modem standard [4]. It was first proposed and successfully implemented for two-way data transmission over cable [5]. Other important indications of the popularity of adaptive modulation technique are the current proposals for the third-generation (3G) wireless systems and the Enhanced Global Packet Radio Systems (EGPRS) [6,7]. The adoption of adaptive modulation in the next or the fourth-generation (4G) wireless systems is also inevitable [8].

Bandwidth efficiency achieved by adaptive modulation technique depends on the statistical characteristics of radio channel, the accuracy in the measurement of channel quality and the selection criterion of suitable modulation mode at the transmitter. This thesis will study the capacity or bandwidth efficiency and the BER performance achieved by various adaptive modulation techniques over fading channel theoretically. The effects of imperfect channel estimation on capacity and BER performance are also investigated.

1.2 Principles of adaptive modulation technique

Radio signal transmitted over wireless channel is affected by various detrimental effects, such as path loss, multipath fading and shadowing. Both the amplitude and the phase of the received signal fluctuate, as a function of time. Furthermore, if transmission rate is higher than channel's coherent bandwidth, transmitted signals experience frequency selective fading inflicted by the dispersion over time. Under these circumstances, radio signals are severely corrupted and suffer from bursts of bit errors. In currently deployed wireless systems, radio signals are transmitted at a fixed rate and fixed modulation constellation. These non-adaptive systems require a fixed link margin to guarantee acceptable performance when radio channel undergoes the worst channel conditions and do not take the time varying nature of channel fading into consideration thus result in insufficient utilization of radio resources.

If the variation of channel conditions over time can be tracked accurately and channel state information is known to both transmitter and receiver, an effective approach to combat the time variation of channel fading is to employ adaptive modulation, through adapting certain parameters of the transmitted signal to instantaneous channel conditions without sacrificing system performance. The main idea behind adaptive modulation technique is the real-time balancing of the link budget to take advantage of channel conditions. For example, when channel conditions are good, higher transmission rate or higher order modulation constellation is employed to increase bandwidth efficiency, whereas when channels are in poor conditions, lower transmission rate or more robust lower-order modulation constellation is invoked to maintain transmission quality. An illustration of adaptive modulation systems is shown in Fig.1.1.

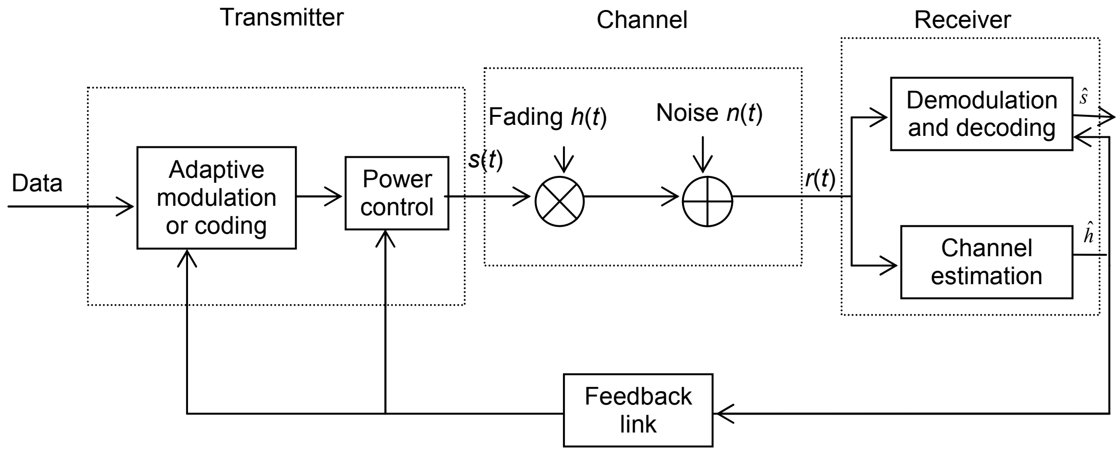

Fig.1.1 A block diagram of adaptive modulation systems

The transmission parameters to be adapted include transmission power, modulation constellation, signal bandwidth, processing gain (PG, applying to CDMA systems), the number of sub-channels (applying to multi-carrier modulation systems), or any combination of these parameters [1-3,9-14]. Among them, transmission power and modulation constellation are fundamental considerations to realize transmission adaptation. Adaptive transmission power is to adjust the power of transmitted signals according to channel fluctuations through power control. This strategy will cause the peak-power problem. Under multiple access environment, adaptive transmission power may result in extra interference to co-channel users thus reducing system capacity if proper coordination is not performed among the users. Adaptive constellation is achieved by changing the modulation constellation size used based on channel conditions and can be implemented either by changing the transmission power simultaneously or by maintaining the signal transmission power as a constant. In a CDMA system, adaptive PG and adaptive spreading bandwidth (or spreading chip rate) are powerful techniques achieved by adjusting PG or spreading bandwidth to capture the time variation of channel conditions. The focus of this thesis is to study the capacity of flat fading channel employing adaptive rate adaptive power and adaptive rate constant power, and the capacity of adaptive CDMA systems employing adaptive PG technique over frequency selective fading channel.

The adaptive modulation technique only works under duplex mode. The simplest duplex operation for adaptive modulation is the time division duplex (TDD), where both the base station (BS) and the mobile station (MS) transmit over the same radio channel, but in different time slots. With this arrangement, both the MS and the BS experience identical channel fading gain due to the reciprocity of channel conditions in both directions. Hence, it will be sufficient for channel estimation to be made either at the BS or at the MS. As an example, a possible signaling format for TDD mode adaptive transmission systems is shown in Fig.1.2. In the uplink transmission (from MS to BS), the channel quality measured at the BS is used to decide the adaptation of transmission parameters used by both the MS and the BS. The MS will obtain the transmission parameters from the signaling header sent from the BS. Because the BS has the channel information for all mobiles, it is able to schedule which mobile to transmit, in order to achieve maximum system throughput.

To facilitate the operation of adaptive modulation technique, a channel quality indicator which reflects the instantaneous channel conditions needs to be identified. There are many metrics suitable as an indicator. At the link layer, packet error rate (PER) can be used as an indicator, while at the physical layer, signal-to-interference-noise ratio (SINR) is a typical choice since it is directly related to BER performance. Once the channel quality indicator is specified, the measurement of channel quality is performed at the receiver and the measured results are fed back to the transmitter with the aid of a feedback link. At the transmitter, the parameters of transmitted signals to be adapted are grouped into a set of modulation modes. The goal of adaptive modulation is to ensure that the most efficient mode is in use. The criterion for the selection of each modulation mode is determined based on some pre-defined requirements of transmission quality, for example, a given average BER performance. The selection of modulation mode is performed by comparing the measured channel quality against the selection criteria.

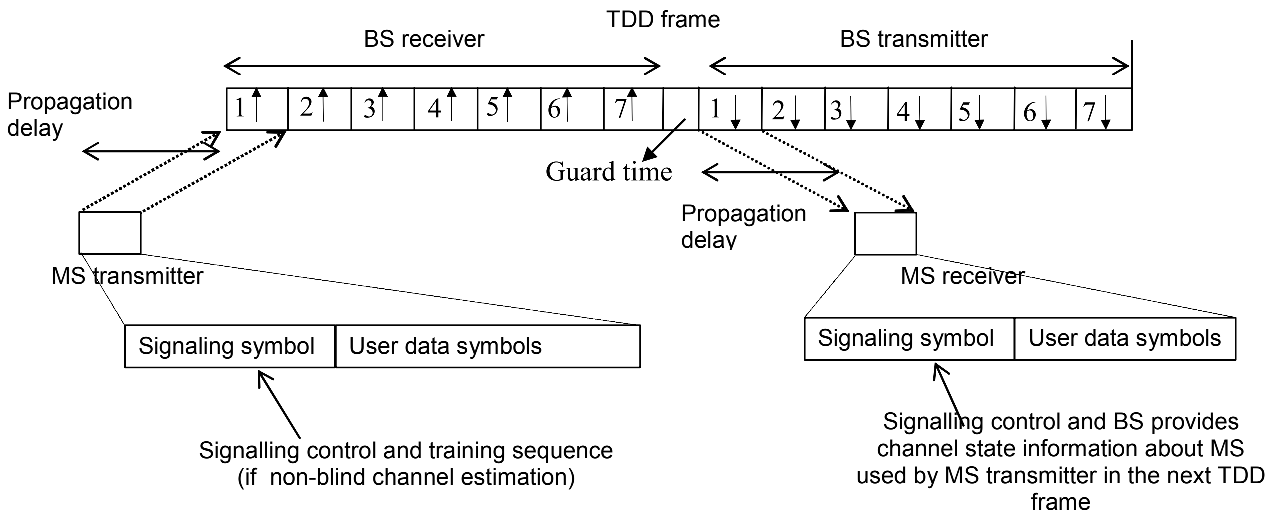

Fig.1.2 A TDD frame structure for signaling of adaptive modulation systems

The basic assumption for the implementation of adaptive modulation systems is that the channel cannot vary too fast with respect to the duration of one transmission interval so that the channel conditions can be tracked precisely, otherwise the transmission parameters selected might be badly matched to the instantaneous channel conditions. For fast varying channel, estimation error and feedback delay badly affect the sound selection of the modulation mode. Hence the choice of adaptation rate or how frequently the channel estimation should be performed is very important. However there exists trade off between adaptation rate and signaling overhead.

1.3 Previous work on adaptive modulation techniques

Intensive studies on the performance of adaptive modulation have been carried out for decades. The advance of adaptive transmission was as early as 1968, when Hayes proposed this efficient approach to mitigate the detrimental effect of channel fading [1]. Transmission power adaptation scheme was proposed in [1] while a variable symbol duration scheme adaptive to channel conditions was suggested in [2]. The effects of block size, fading rate and co-channel interference were also investigated in [2]. The disadvantages of the adaptation of transmission power were the peak-power problem, lower power efficiency and the possible increase of co-channel interference level, while variable symbol duration was realized at the cost of varying signal bandwidth. The adoption of multi-level star-QAM (quadrature amplitude modulation) in adaptive modulation systems over flat Rayleigh fading channel was proposed in [10] and it was found that adaptive modulation had better performance over fixed modulation. The adoption of square-QAM to implement adaptive modulation was suggested and studied in

[9]. Both studies showed that MQAM was promising to achieve high bandwidth efficiency and had the capability to combat peak-power problem by keeping transmission power as a constant. A methodology for combining coding scheme with a general class of adaptive modulation techniques was derived in [15]. The BER performance and bandwidth efficiency achieved by applying this methodology to MQAM were evaluated. The bandwidth efficiency of adaptive modulation systems employing variable-rate fixed power non-coherent M-FSK (M-ary frequency shift keying) was proposed in [16]. The method of reliably transmitting control information in adaptive modulation was suggested in [9]. The optimization of criterion for the selection of suitable modulation modes or switching levels based on a defined cost function over slow Rayleigh fading channel was studied in [13,17].

The adaptive modulation realized by the combination of adaptive rate and adaptive power over flat fading channel was studied in [18-21] in terms of Shannon capacity and achievable capacity employing adaptive MQAM. It was also demonstrated in [18] that adaptive-rate adaptive-power modulation achieved a 5-10dB power gain over a fixed rate system having power adaptation only and up to 20dB relative to non-adaptive modulation. The extra Shannon capacity achieved by variable power variable rate over constant power variable rate was marginal for most types of fading channels [18-20]. Under single user environment, the optimal power control strategy over flat fading channel was identified to be “watering filling” over time, where more power was allocated as channel is in favorable conditions [20]. A large class of adaptive modulation techniques, including continuous rate adaptation under average BER constraint and instantaneous BER constraint, discrete rate adaptation under average BER constraint and instantaneous BER constraint, were examined in [22]. The general form of rate, power and BER adaptation for the maximization of bandwidth efficiency achieved by these schemes was also obtained in [22]. The jointly optimal rate and power adaptation of adaptive modulation system employing average BER constraint was derived in [23].

Adaptive modulation technique can be applied to multiple access channels. An adaptive modulation technique where the modulation constellation size and symbol duration (signal bandwidth) were dynamically assigned based on the average perceived channel conditions was proposed for TDMA system [24,25]. The achieved average bit rate of the proposed technique over Rayleigh flat fading channel was studied theoretically [25]. Through simulation, the bandwidth efficiency achieved over frequency selective fading channel was investigated. It was shown that the adaptive MQAM and symbol rate technique achieved higher bandwidth efficiency than the fixed modulation system and system with adaptive MQAM only over both flat and frequency selective fading channel. The delay-spread immunity over frequency selective fading channel was significantly improved as well. An extended work of [24], which combined the adaptive MQAM and symbol duration with dynamic assignment of TDMA time slot to each user based on its channel conditions, was conducted in [26]. The average bit rate obtained for an adaptive MQAM and symbol duration system with coding was investigated for TDMA systems in [27]. The throughput performance, which is defined as the number of bits successfully sent during each transmitted symbol, was evaluated for a number of adaptive modulation techniques under the consideration of co-channel interference [28]. It showed that the adaptive modulation adjusted to SINR of individual user provided a higher throughput than the SINR balancing power control scheme where all co-channel users have the same

SINR. Under multiple access environment, channel capacity is characterized by a rate region, where each point in the region is an achievable rate vector transmitted by all users simultaneously. The comparison study on capacity regions for different multiple access schemes was conducted in [29] by assuming that channel state information is known to receiver only. The Shannon capacity regions of downlink broadcast fading channel with adaptive rate and power were identified under different multiple access schemes in [30]. An asymptotical power control strategy, which is based on the channel conditions of individual user, was investigated in [31] under the consideration of co-channel interference and was shown to be optimal as observation time was long enough. The optimal power control strategy of multiple access fading channel was to assign the channel to the user with the best channel conditions, and power allocation was performed based on the instantaneous channel conditions of the user assigned the entire channel [32]. Obviously this optimal strategy excludes the transmission of data from users with poor channel conditions and does not consider the fairness of channel allocation. Another significant issue in such a system was the long channel inter-access time, which is defined as the time interval one user with poor channel conditions has to wait for its channel conditions to be the best. The channel capacity achieved by this optimal strategy and some proposed channel allocation schemes will be investigated in this thesis.

The application of adaptive transmission techniques to a CDMA system is still ongoing since CDMA was proposed as a candidate of future generation wireless systems. Other than the adaptive modulation techniques realized by adaptive modulation constellation and transmission power, adaptive modulation in a CDMA system can also be achieved through adapting PG or chip rate (spreading bandwidth) to the channel conditions.

Adaptive PG was shown to be an efficient solution to realize adaptive modulation in a CDMA system [33]. The rate adaptation of a CDMA system realized by means of adaptive chip rate was studied in [34]. The capacity and BER performance of CDMA systems employing MQAM was studied in [35,36]. The comparison study of single-code and multi-code CDMA systems was carried out in [37] and it showed that multi-code system was much more robust against multipath fading channel. The BER performance comparison of CDMA system employing multiple PG, multi-code and MQAM over both additive white Gaussian noise (AWGN) channel and multipath Rayleigh fading channel was performed in [38]. It was concluded that both multi-code and multiple PG schemes achieved similar performance, while MQAM caused severe performance degradation for users requesting high bit rate service. The study on the capacity of multi-rate system adopting multiple PG and multiple chip rate (MCR) with constant PG will be conducted in Chapter VI of this thesis. The throughput of CDMA systems achieved by adaptive modulation technique was investigated in [39]. The results showed that adaptive symbol rate (through adaptive PG or adaptive chip rate) achieved higher throughput than the adaptive constellation size and adaptive code allocation scheme, while adaptive constellation size performed better than adaptive code allocation scheme. Adaptive coding and modulation using M-ary orthogonal modulation and RAKE receiver was investigated in [40] and was found to have significant improvement in the average throughput and BER performance over fixed coding systems. The capacity of CDMA systems achieved with rate adaptive modulation over multipath fading channel was investigated in [41,42], where the rate adaptation was used to explore the channel fading only. The capacity obtained was in terms of lower bound. Some new adaptive rate/power schemes based on the channel fading or the user location will be proposed and investigated in this thesis.

1.4 Thesis outline

Adaptive modulation techniques are promising to achieve high bandwidth efficiency over fading channel. The implementation of adaptive modulation technique depends on channel characteristics and estimation techniques. Available statistical models to characterize fading channels and widely used channel estimation techniques are summarized in Chapter II. The BER performance obtained with and without channel estimation error is investigated in Chapter II as well. The channel capacity achieved by adaptive modulation techniques over flat fading channel under single user environment is studied in Chapter III. Since channel estimation is crucial to the performance of adaptive modulation systems, a framework to study the effect of imperfect channel estimation on channel capacity is presented. This framework is obtained regardless of specific estimation techniques thus can be used to evaluate the capacity of adaptive modulation systems employing any estimation technique.

Under multiple access environment, the optimal channel allocation strategy to achieve channel capacity is to assign radio channel to the user observing the best channel conditions. Chapter IV first investigates the capacity achieved by this optimal channel allocation scheme. The significant disadvantage of this optimal channel allocation strategy is the possible long channel inter-access time. An SNR-priority-based channel allocation scheme is proposed to overcome this difficulty. This is a suboptimal channel allocation strategy conceived to combat the channel inter-access time problem by allowing a number of users observing the first few best channel conditions to share the radio channel. The capacity achieved by this suboptimal strategy is presented in Chapter IV also. Both the optimal and the proposed SNR-priority-based strategy are only suitable for delay non-sensitive services. In order to accommodate real-time services with stringent delay constraint, another channel allocation strategy able to serve both QoS and best effort (BE) services is proposed. Analysis on system throughput and packet loss is carried out in this chapter.

Studies in Chapter IV are extended to interference limited CDMA systems. In a CDMA system, rate adaptive capability can be implemented using adaptive PG, adaptive chip rate, adaptive modulation constellation and adaptive multi-code modulation. A combined adaptive PG and adaptive constellation scheme is proposed to combat the problem caused by minimum PG constraint. Three adaptive rate adaptive power schemes are proposed to take advantage of the information of multipath channel fading and large-scale path loss. Capacities achieved by these proposed adaptive rate adaptive power schemes are investigated in Chapter V. A dual-class CDMA system employing different power control schemes to support voice and data services is proposed and studied.

The multiple access interference (MAI) of multiple PG and MCR systems exhibits different characteristics from that of single chip rate constant PG systems. Firstly the statistical nature of MAI of MCR systems is derived. With the knowledge of the variance of MAI, the system capacity obtained from different configurations of MCR systems is then studied. The comparison study on system capacity for MCR and multiple PG (MPG) systems is performed in Chapter VI. Finally, conclusions based on the studies of this thesis are given in Chapter VII.

1.5 Thesis contributions

This section summarizes all the main contributions by the author.

In Chapter II, the BER performance of coherent MQAM systems over flat fading channel with and without channel estimation error is investigated. An approximate method to evaluate the BER performance of coherent detection systems under imperfect channel estimation with amplitude error only is proposed. With this approximate method, a simple closed form solution is obtained. The complexity in the BER computation caused by the exact method is significantly reduced. Numerical results show that this approximate method gives a good match within a practical SNR range and at high correlation coefficient between the estimated and the true fading gain.

In Chapter III, the capacity of adaptive MQAM systems over flat fading channel is studied under perfect and imperfect channel estimation. A framework to evaluate the effect of imperfect channel estimation on channel capacity is introduced. This framework can be applied to evaluate the channel capacity of adaptive modulation systems employing any estimation technique once the joint probability density function (PDF) between the estimated fading amplitude and the true fading amplitude, and the joint PDF between the estimated fading phase and the true fading phase are known. An equivalent receiver circuit is conceived to convert the effect of channel estimation error into an equivalent imperfect I and Q demodulator. By using this equivalent receiver structure, extra margins required in the SNR threshold intervals for the selection of suitable MQAM constellation in order to maintain the targeted BER performance can be obtained. Prior to this work, such margins are given through experiences, rather than obtained from any quantitative analysis based on channel characteristics and estimation techniques. Once the channel estimation technique is specified, with the joint PDFs mentioned above known, this framework is valuable for the choice of parameters associated with the selected channel estimation technique, such as the frequency to perform the estimation, the length of training sequence, etc., to maintain the given SNR margins. The effect of channel estimation error on the capacity achieved by diversity reception systems with selection combining (SC) is investigated as well. The study shows that diversity reception techniques improve capacity caused by estimation error at the cost of implementation complexity.

In Chapter IV, the capacity of multiple access Rayleigh and General Gamma fading channel employing an optimal channel allocation and rate adaptive modulation techniques is first derived. The PDF of the highest SNR is obtained. The average time duration for the process to stay in one MQAM constellation is derived by employing the first order Markov model and level crossing rate (LCR). This time duration is helpful and can be used as a guideline for the design of frame size in practical systems. Channel inter-access time is an important parameter directly related to the service QoS requirements in a multiple access environment. A methodology to quantify the channel inter-access time of the optimal channel allocation scheme based on the statistical characteristics of channel and the number of users contending for channel access is introduced. A suboptimal SNR-priority-based channel allocation scheme combined with adaptive modulation is proposed to overcome the problem of long channel inter-access time of the optimal channel allocation system. The capacity achieved by the proposed SNR-priority-based channel allocation scheme is studied by employing order statistics. Another channel allocation scheme to accommodate both QoS and BE services is proposed and investigated. The system throughput and the packet loss performance of this channel allocation scheme combined with adaptive modulation are investigated in detail. Although the schemes studied here are simple, the analysis is concrete and new, and is useful for designers to perform system design.

In Chapter V, capacities of CDMA systems employing rate adaptive modulation technique over frequency selective fading channel are studied. A flaw present in the study of adaptive CDMA systems in the literatures is corrected by giving a minimum PG constraint ($G_{\min}$). A combined adaptive PG and adaptive MQAM scheme is proposed to overcome the $G_{\min}$ constraint. Three power control schemes combined with rate adaptive modulation are proposed to improve the capacity of adaptive CDMA systems. In scheme I, the transmission power after path loss is compensated for is kept as a constant and the transmission rate is adapted to the received SIR. In scheme II, the transmission power after path loss is compensated for is adapted based on the channel fading of individual user rather than being kept as a constant and the transmission rate is adapted to the received SIR. In scheme III, the transmission power is allocated according to the mobile location and the transmission rate is adapted to the received SIR. Scheme III has the potential to improve the system capacity through reducing the other cell interference. Expressions to obtain the system capacity achieved by these power control schemes with combined adaptive PG adaptive MQAM are derived and results show that all these schemes are promising to improve system capacity. A dual-class CDMA system supporting both voice and data services is proposed to meet the QoS requirements of multimedia capability of future wireless systems. In this dual-class system, perfect power control is assumed for voice users, while scheme I is adopted for data users. The capacity achieved by this dual-class CDMA system and the power consumption for different numbers of voice and data users are derived.

In Chapter VI, capacities achieved by MCR systems are investigated based on a practical interference model which takes into account the non-orthogonality of spreading codes with different chip rates, the difference of carrier frequencies, and the effect due to the receiver filter of the desired user and the power spectral density (PSD) of transmitted signals from interference users with different spreading bandwidth for the first time. Different configurations of MCR systems are evaluated in terms of system capacity. The analytical results obtained give useful guidelines on designing the MCR system architecture. The comparison study on the capacities achieved by MCR and MPG systems is conducted and new conclusions are drawn. The study shows that the MCR system performs not worse than the MPG system. With good control of spectrum allocation in the spectral overlay structure, MCR systems can achieve significant capacity gain over MPG systems.

CHAPTER II

FADING CHANNEL MODELS, CHANNEL ESTIMATION TECHNIQUES AND MULTILEVEL MODULATION

The performance of adaptive modulation systems depends on the statistical characteristics of fading channel and the channel estimation techniques. This chapter first reviews the widely used statistical models of fading channel, channel estimation techniques and MQAM modulation technique. The BER performance of MQAM over different fading channels in the presence of AWGN noise is presented. The effect of imperfect channel estimation on BER performance is investigated first by an exact method. An approximate method which reduces the complexity in BER computation with amplitude estimation error while provides sufficiently good evaluation of BER performance is then proposed and studied. The conditions for the effectiveness of this approximate method are given.

2.1 Channel model descriptions

Radio signals transmitted over wireless channel experience amplitude and phase fluctuations at the receiver caused by the combination of randomly delayed paths due to scattering, reflection and diffraction of propagation environment present along the traveling path from transmitter to receiver. As a result of the constantly changing transmission environment, the time-varying land mobile radio channel can be characterized by three mutually independent, multiplicative propagation phenomena:

small-scale multipath fading, large-scale shadowing effect and path loss [43-45]. Multipath fading is used to describe the rapid fluctuations of the phase and amplitude of transmitted signal over a short period of time (on the order of seconds) or travel distance (on the order of a few wavelength) caused by the interference between multiple versions of transmitted signals arriving at the receiver at slightly different time. Path loss predicts the mean signal strength determined by the geometry of the path profile as the transmitter-receiver (T-R) separation distance is larger than a few tens or hundreds of meters. The path loss model fails to consider the fact that the measured mean signal strength varies with locations even with the same T-R distance. The shadowing effect is thus introduced to describe the additional fluctuations of signal strength about the distance-dependent mean at a specific transmitter-receiver distance.

In generic studies, there are two categories of model which describe a wireless radio channel: the propagation model and statistical model. The propagation model is concerned with those physical phenomena which could affect the propagating signals. Among them are free space signal loss, reflection, surface wave, antenna structure, etc. As an alternative and the most widely used models, in the context of wireless communications, the wireless channel is usually evaluated on a statistical basis: no specific terrain data is considered, and channel parameters are modeled as random variables. The statistical models employed to describe the nature of signal transmitted over radio channels are summarized and reviewed in the following.

1) Path loss

In statistical model where the effects of large scale propagation mechanism are simplified as an average attenuation, path loss can be expressed as a function of the distance between transmitter and receiver

$$p_z \propto p_{z_0} (\frac{z}{z_0})^{-n}, \tag{2-1}$$

where p_z, p_{z_0} are the signal power as the distance between transmitter and receiver is z and z_0 respectively. The value of n depends on the specific propagation environment. For example, in free space, n is set to 2, for other environments, n will have a larger value.

2) Shadowing effect

Shadowing effect is usually modeled by a log-normal distribution. The PDF of local-mean power measured in dB received at an arbitrary distance between transmitter and receiver can be expressed as

$$f_Y(y) = \frac{1}{\sqrt{2\pi}\sigma_p} \exp(-\frac{(y-\overline{Y})^2}{2\sigma_p^2}), \tag{2-2}$$

where $\overline{Y} = E[Y]$ is the mean value of local mean power in dB, σ_p is the standard deviation or shadowing spread in dB ranging from 6dB to 12dB [46].

3) Multi-path fading

For a typical narrowband flat fading where all the spectral components of signal are affected in a similar manner, the time varying nature of the received envelope of an individual multipath component can be modeled by Rayleigh, Rician and Nakagami-*m* distribution. Rayleigh distribution characterizes the statistical nature of fading that occurs when there are a large number of scatterers contributing to the signal received at the receiver, as in the case where there is no light-of-sight propagation from transmitter to receiver. The PDF of amplitude of Rayleigh distributed fading gain can be expressed as

$$f_\alpha(\alpha) = \begin{cases} \frac{2\alpha}{\Omega}\exp(-\frac{\alpha^2}{\Omega}) & 0 \le \alpha \le \infty \\ 0 & \alpha < 0 \end{cases}, \tag{2-3}$$

Rician distribution is used to describe the statistical characteristics of channel fading when there are fixed scatterers or signal reflectors in the medium thus leading to dominant signal propagation path present, as the case of a light-of-sight propagation. The PDF of Rician distribution is given by

$$f_\alpha(\alpha) = \begin{cases} \frac{2\alpha}{\Omega}\exp(-\frac{(\alpha^2 + A_p^2)}{\Omega}) I_0(\frac{2A_p\alpha}{\Omega}) & \alpha \ge 0, A_p \ge 0 \\ 0 & \alpha < 0 \end{cases}. \tag{2-4}$$

In (2-3) and (2-4), $\Omega = E[\alpha^2]$, and in (2-4), A_p is the amplitude of the dominant signal and $I_0(\cdot)$ is the modified Bessel function of the first kind and zero-order. Rician factor defined as A_p^2/Ω completely specifies the Rician distribution. As $A_p \to 0, A_p^2/\Omega \to 0$, the Rician distribution degenerates to a Rayleigh distribution.

Another model useful to characterize multipath fading channel is Nakagami-*m* distribution. Nakagami-*m* distribution can approximate different fading environments including those characterized by Rayleigh and Rician distributions with *m* being chosen appropriately. The amplitude attenuation modeled by Nakagami-*m* distribution is given by

$$f_\alpha(\alpha) = \begin{cases} \dfrac{2m^m}{\Gamma(m)\Omega^m}\alpha^{2m-1}\exp(-\dfrac{m}{\Omega}\alpha^2) & \alpha \geq 0 \\ 0 & \alpha < 0 \end{cases}, \tag{2-5}$$

where *m* is a shape parameter and $\Omega = E[\alpha^2]$ controls the spread of the distribution. The value of *m* determines the severity of fading, less severe fading associated with larger value of *m*. And *m*=1 corresponds to Rayleigh fading.

For wideband signals propagating through a frequency selective fading channel where the spectral components are affected by different amplitude gains and phase shifts, the multipath fading is modeled as a linear filter with its equivalent lowpass impulse response given by

$$h(t) = \sum_{l=1}^{L} \alpha_l e^{-j\theta_l} \delta(t - \tau_l), \tag{2-6}$$

where all α_l are statistically independent random variables whose distributions follow the above mentioned models. θ_l, τ_l and L are the phase of fading gain for the *l*th path, propagation delay for the *l*th path and the number of paths. The distribution of variance of α_l with respect to different paths is referred to as power delay profile. It is another significant distribution to characterize frequency selective fading channel. Typically it is modeled as a decaying function

$$\Omega_l = \Omega_0 e^{-\delta(l-1)}, \quad l = 1,2,\cdots L, \tag{2-7}$$

where δ is a decaying factor reflecting the rate at which decaying occurs. As $\delta = 0$, power delay profile is uniformly distributed. Ω_0 is the normalized factor and normally defined by $\sum_{l=1}^{L} \Omega_l = 1$.

4) Suzuki distribution [47]

The statistical nature of amplitude of the channel fading gain can be characterized by Suzuki distribution. The PDF of amplitude α is

$$f_\alpha(\alpha) = \int_0^\infty \frac{\alpha}{\sigma_s^2} \exp(-\frac{\alpha^2}{2\sigma_s^2}) \frac{1}{\sqrt{2\pi}\sigma_s v_s} \exp(-\frac{(\log\sigma_s - \mu_s)^2}{2v_s^2}) d\sigma_s, \tag{2-8}$$

where σ_s, μ_s, v_s are the distribution parameters. For $v_s = 0$, Suzuki distribution is identical to Rayleigh distribution. In the practical, the values of v_s, μ_s can be estimated through measurements using the following log-moment estimates,

$$\begin{aligned} \hat{v}_s &= \sqrt{<(\log\hat{\alpha})^2> - <\log\hat{\alpha}>^2 - \frac{\pi^2}{24}}, \\ \hat{\mu}_s &= <\log\hat{\alpha}> - \frac{1}{2}[\log 2 - U], \end{aligned} \tag{2-9}$$

where $\hat{\alpha}$ is the estimated value of α through measurement, U is the Euler's number and $\langle \bullet \rangle$ denotes the arithematic mean.

It has been demonstrated that Suzuki distribution can achieve good fits to the measured data for a variety of physical channels [47]. However due to its complicated mathematical form and the inconvenience caused by this no closed form solution when performing BER evaluation, it is not widely used.

5) General Gamma distribution [48,49]

Generally, the signal transmitted over the air experiences small-scale multi-path fast fading and large-scale slow shadowing simultaneously. The statistical nature of multi-path fading and shadowing can be well represented by Rayleigh (or Rician) and log-normal distribution respectively. There is also an attempt to use General Gamma distribution as a distribution model which encompasses both multipath fading and shadowing together [48]. This distribution has been verified in [48] through physical measurement and parameter estimation to curve fit with General Gamma distribution. General Gamma distribution takes the form of

$$f_\alpha(\alpha)=\frac{c_g \alpha^{c_g d_g -1}}{\beta_g^{c_g d_g}\Gamma(d_g)}\exp\left(-\left[\frac{\alpha}{\beta_g}\right]^{c_g}\right), \tag{2-10}$$

where d_g, β_g, c_g are distribution parameters and $\Gamma(d_g)=\int_0^\infty x^{d_g-1}e^{-x}dx$ is the Gamma function. It has been shown in [49] that the product of $c_g d_g$ predicts the severity of the fast fading, while parameter c_g represents the shadowing fading. The General Gamma distribution contains many well-known distributions as special cases [49]. The parameters of General Gamma distribution can be obtained by performing log-moment estimates,

$$\hat{c}_g = \left| \frac{\left[\left\langle (\log \hat{\alpha})^2 \right\rangle - \langle \log \hat{\alpha} \rangle^2 \right] \phi''(\hat{d}_g)}{\left\langle (\log \hat{\alpha})^3 \right\rangle - \langle \log \hat{\alpha} \rangle^3 \phi'(\hat{d}_g)} \right|,$$

$$\hat{\beta}_g = \exp(\langle \log \hat{\alpha} \rangle - \frac{\phi'(\hat{d}_g)}{\hat{c}_g}), \tag{2-11}$$

$$\frac{\phi''(\hat{d}_g)}{[\phi'(\hat{d}_g)]^{3/2}} = \left| \frac{\left\langle (\log \hat{\alpha})^3 \right\rangle - \langle \log \hat{\alpha} \rangle^3}{\left[\left\langle (\log \hat{\alpha})^2 \right\rangle - \langle \log \hat{\alpha} \rangle^2 \right]} \right|,$$

$$\phi^{(n)}(\hat{\alpha}) = \frac{d^n}{d\hat{\alpha}^n} \log\Gamma(\hat{\alpha}),$$

where $\hat{\alpha}$ denotes the estimated values through measurement in the experiment and $|\bullet|$ denotes taking absolute values.

To verify how good the General Gamma model matches the statistical nature of channel represented by Rayleigh fading and log-normal shadowing, a simulation is performed and the result is shown in Fig.2.1. This figure shows the resemblance between General Gamma distribution having $c_g = 0.76$, $c_g d_g = 2.3$, $\beta_g = 0.28$ and the simulated results generated by the combination of Rayleigh ($\Omega = 1$) and lognormal shadowing (shadowing spread $\sigma_p = 8\text{dB}$). From this figure, it can be seen that General Gamma distribution is valid to describe the fading process caused by the combination of Rayleigh fading and log-normal shadowing. This statistical model will be employed in the analysis of capacity and BER performance in this chapter and Chapter III.

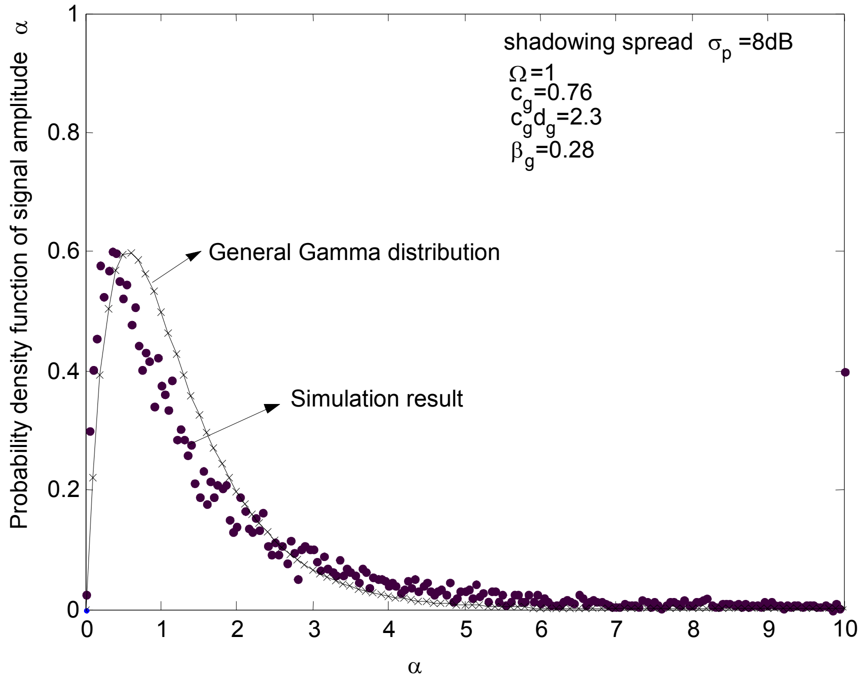

Fig.2.1 Simulated results for combined Rayleigh - Lognormal distribution and General Gamma distribution

2.2 Channel estimation techniques

Two categories of channel estimation techniques are employed in the identification of channel fading. One class is to provide embedded references for the demodulator to perform estimation of channel conditions [50,51]. The other is blind channel estimation where the input to the channel is not available for processing at the receiver [52]. So far, the pilot tone assisted estimation (PTAE) and the pilot symbol assisted estimation (PSAE) are commonly used estimation techniques and have been proven to be effective in channel fading estimation [50]. In PTAE, a tone is transmitted together with the data symbols by assuming that both are equally affected by the channel fading as depicted in Fig.2.2. The tone provides the receiver with explicit amplitude and phase reference for detection. The channel conditions can be estimated by observing the effect of fading on the amplitude and phase of the tones. The key in PTAE is the placement of tone location. In PSAE pilot symbols are periodically inserted into the data symbols to estimate the fading, as shown in Fig.2.3. The data is formatted into frames of *L* symbols, with the first symbol in each frame used for the pilot symbol [51]. The pilot sequences are multiplexed with data symbols. The receiver has prior knowledge of the pilot sequences and thus can extract them from the received signal and estimate the effect of channel fading. The estimates of fading experienced by the data symbols are obtained by interpolating the fading experienced by the pilot symbols. In PTAE, pilot tones are inserted in frequency domain while in PSAE, pilot symbol is added in time domain. In blind estimation, only the received signal is available for the processing in the identification and estimation of channel. The essence of blind estimation rests on the exploitation of characteristics of the channel fading and statistical properties of input sequences.

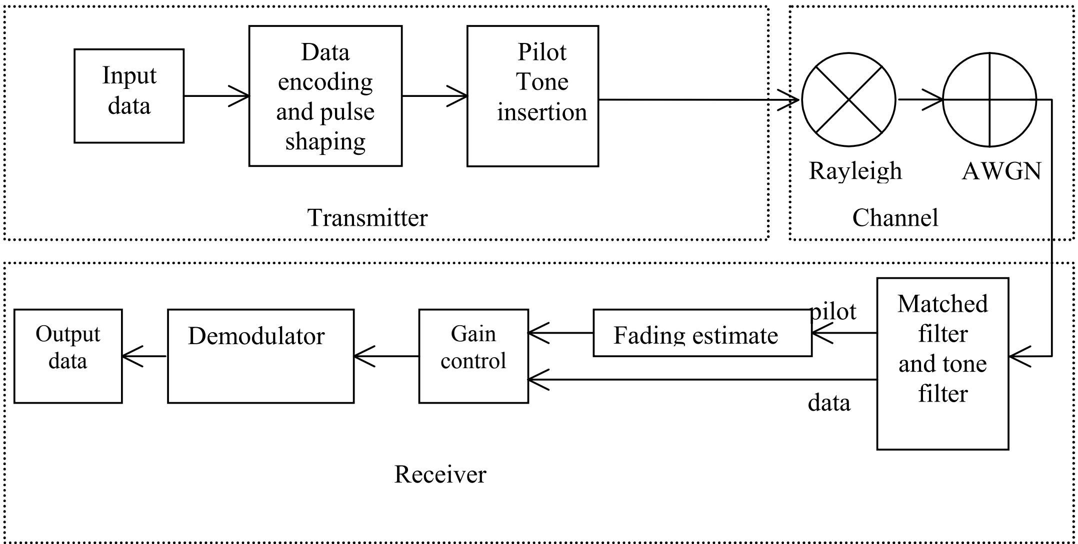

Fig.2.2 A functional block diagram for PTAE

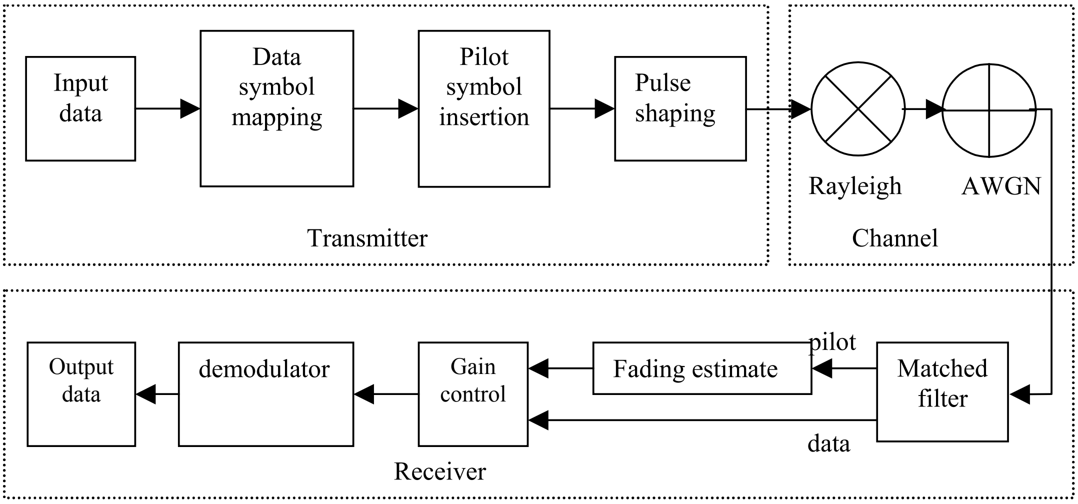

Fig.2.3 A functional block diagram for PSAE

In coherent systems, at the receiver side, the estimated channel state information can be used to assist data symbol recovering. Moreover, if the estimated channel state information is available at the transmitter side and adaptive modulation is employed, this information can be used for the control of transmission power, constellation size, and even for the channel allocation. Hence the effect of imperfect channel estimation on the performance of adaptive modulation systems is multifold. To guarantee transmission quality, the choice of estimation techniques should be considered carefully.

With channel estimation error, the estimated complex channel fading gain can be expressed as $\hat{h}=h+e$, where $\hat{h}=\hat{\alpha}e^{j\hat{\theta}}$ is the estimated fading gain and $h=\alpha e^{j\theta}$ is the true fading gain, respectively, while $\hat{\alpha},\alpha$ and $\hat{\theta},\theta$ are fading amplitudes and phases, respectively. For different estimation techniques, the joint PDF of $\hat{\alpha}$ and α, $\hat{\theta}$ and θ are different. To illustrate how to evaluate the effect of imperfect channel estimation on BER performance, h and $\hat{h}$ are assumed to be complex Gaussian random variables, thus estimation error e can be modeled as a complex Gaussian random variable. This is true for the PSAE estimation technique where the estimated fading gain is just the weighted sum of complex Gaussian random variables. However, the method introduced in the following can be applied to evaluate any kind of estimation techniques in case that the joint PDF of α and $\hat{\alpha}$, $\hat{\theta}$ and θ are known.

The joint PDF of fading amplitude of α and $\hat{\alpha}$ are expressed as [53]

$$f_{\alpha,\hat{\alpha}}(\alpha,\hat{\alpha}) = \frac{4\alpha\hat{\alpha}}{(1-\rho)\Omega\hat{\Omega}}\exp\left[-\frac{1}{(1-\rho)}\left(\frac{\alpha^2}{\Omega}+\frac{\hat{\alpha}^2}{\hat{\Omega}}\right)\right]I_0\left(\alpha\hat{\alpha}\frac{\sqrt{\rho}}{(1-\rho)\sqrt{\Omega\hat{\Omega}}}\right), \qquad (2\text{-}12)$$

where $\hat{\Omega}=E\left[\hat{\alpha}^2\right]$, $\Omega=E\left[\alpha^2\right]$, and $\rho=\mathrm{cov}(\alpha^2,\hat{\alpha}^2)/\sqrt{\mathrm{var}(\alpha^2)\mathrm{var}(\hat{\alpha}^2)}$ is the correlation coefficient between $\hat{\alpha}^2$ and α^2.

The joint PDF of phase and phase estimate $\theta,\hat{\theta}$ can be expressed as [54]

$$f_{\theta,\hat{\theta}}(\theta,\hat{\theta})=\frac{1-\rho}{4\pi^2}\frac{(1-q^2)^{1/2}+q(\pi-\cos^{-1}q)}{(1-q^2)^{3/2}},0\le\theta,\hat{\theta}\le 2\pi, \qquad (2\text{-}13)$$

where $q=\sqrt{\rho}\cos(\theta-\hat{\theta})$. The PDF of phase estimation error $\psi=\theta-\hat{\theta}$ can be derived as [55]

$$f_{\Psi}(\psi)=\frac{1-\rho}{4\pi^2}\frac{(1-q^2)^{1/2}+q(\pi-\cos^{-1}q)}{(1-q^2)^{3/2}}(2\pi-|\psi|), \qquad (2\text{-}14)$$

and $q=\sqrt{\rho}\cos\psi$.

2.3 Multi-level quadrature modulation technique (MQAM)

MQAM is a bandwidth efficient modulation technique which is widely employed in adaptive modulation systems. The high bandwidth efficiency of MQAM is obtained by simultaneously modulating two separate bit streams from the information sequences onto two quadrature carriers $\cos 2\pi f_c t$ and $\sin 2\pi f_c t$, where f_c is the carrier frequency. Gray-coding is applied to assign bit sequences to their respective constellation points, ensuring that the nearest neighbouring constellation points have a Hamming distance of *1* to minimize BER.

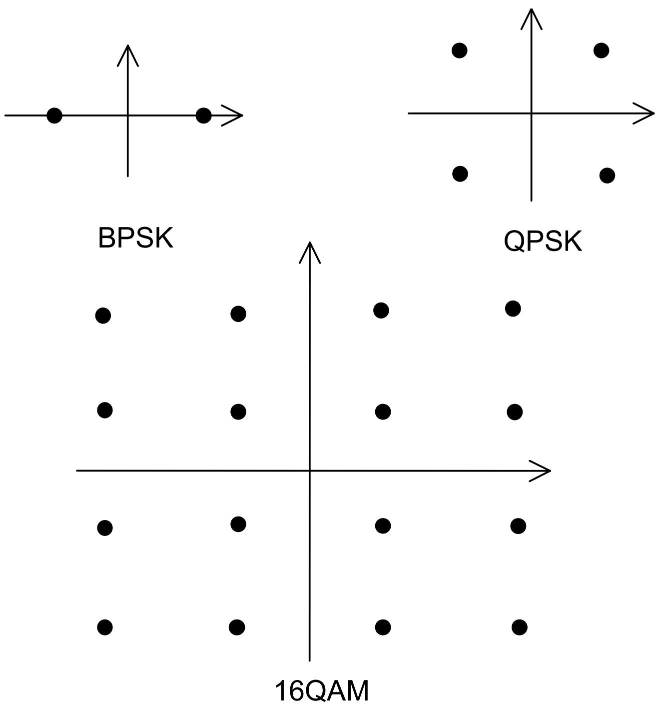

Fig.2.4 Illustration of MQAM constellations

For M-QAM, *M*-ary denotes the number of signal points or the constellation size in the signal space. The constellations of square MQAM for some values of *M* are shown in Fig.2.4. This leads to the application of MQAM technique to fading channel to combat channel distortions by varying the constellation size according to the channel conditions: as channel is not in a deep fade, higher order constellation is used, while as channel enters a deep fade, lower order constellation size is employed to provide an acceptable BER performance but maintain a constant transmission power. If the required BER is specified and constellation size is changed accordingly, a variable data rate and throughput is obtained. This system is defined as variable rate MQAM system.

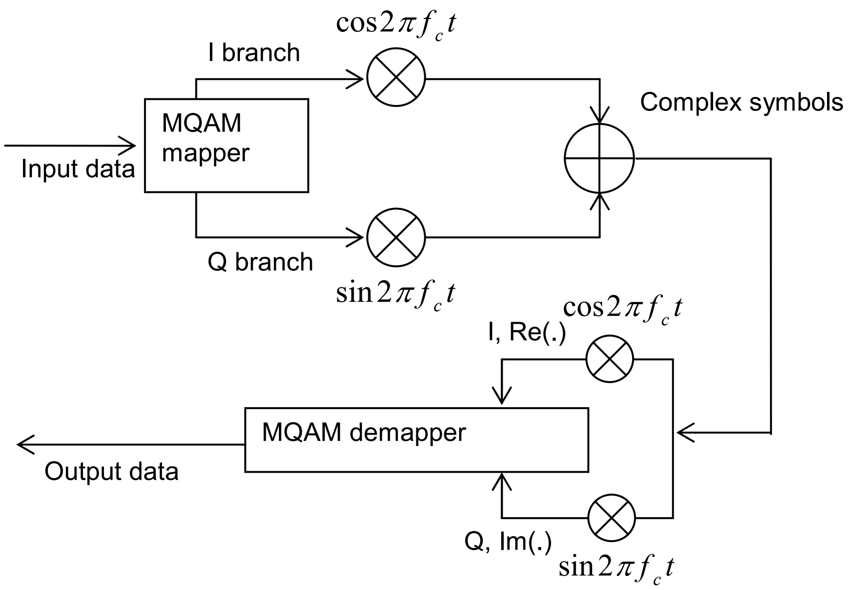

Fig.2.5 MQAM modulation and demodulation

The modulation and demodulation of a square MQAM signal is shown in Fig.2.5. The data bit stream is split into in-phase (I) and quadrature (Q) bit streams at the modulator. For example, for 16-QAM, the first and the third bits are passed to the in-phase bit stream, while the second and the fourth bits are passed to the quadrature bit stream. Gray coding is employed as I and Q components are mapped to form complex symbols. The demodulator first de-maps the received complex symbol into I and Q components where decision is made independently. Fig.2.6 shows the bit mapping of 16-QAM.

Due to the symmetry of I and Q components in M-QAM modulation, the average BER performance of MQAM is then equal to the BER of either I or Q component or $P_e = \frac{1}{2}(P_{e,I} + P_{e,Q}) = P_{e,I}$, where $P_{e,I}$, $P_{e,Q}$ is the BER for the respective data stream in I and Q component. Square MQAM is assumed in this study. However, the analysis can be easily extended to other MQAM techniques, for example Star MQAM. The only difference is the dependence of BER performance on MQAM constellations.

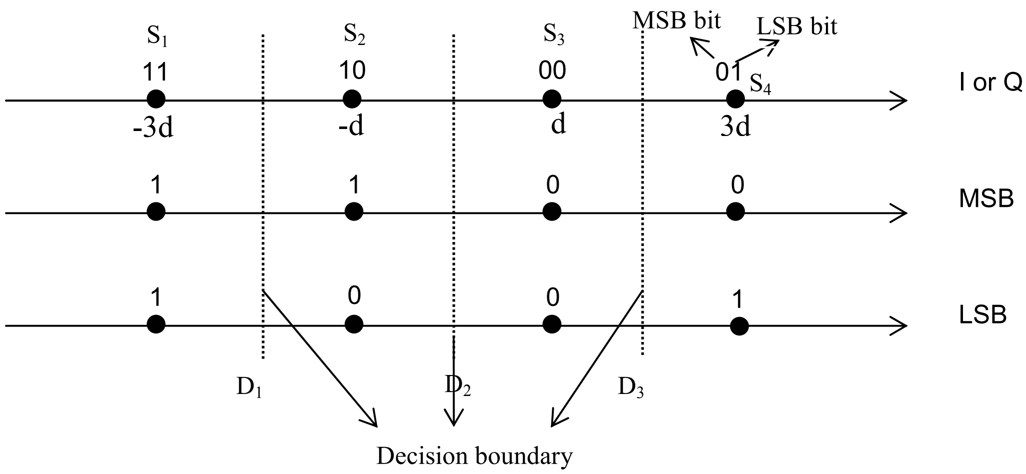

Fig.2.6 bit-by-bit mapping for 16QAM

2.3.1 BER performance of gray-coded MQAM over AWGN channels

A. Exact approach to compute BER

In this approach, BER is computed for each bit separately. Considering the I component only, average BER is obtained by averaging over all bits of the I component. Taking

16-QAM as an example, the bits of the I component can be further split into the most significant bits (MSB) and the least significantly bits (LSB), where MSB and LSB refer to the left and the right bits respectively as shown in Fig.2.6. The decision boundaries D_1 and D_3 are used to compute the BER for LSB bits whilst D_2 is used to compute the BER for MSB bits. Therefore, for 16-QAM, $P_{e,I} = \frac{1}{2}(P_{e,I,MSB} + P_{e,I,LSB})$.

For an AWGN channel, the BER for each MSB and LSB bit is computed according to decision statistics $\hat{s}_I = s_I + n$, where $\hat{s}_I, s_I$ are the detected signal and the transmitted signal respectively. n is AWGN with variance $\sigma_n^2 = N_0/2$. For example, for MSB bits, a bit error occurs when $n < -d$ for signal point S3, $n < -3d$ for signal point S4, $n > d$ for signal point S2 (same probability as S1) and $n > 3d$ for signal point S1 (same probability as S4). Likewise for LSB bits, a bit error occurs when $d < n < 5d$ for signal point S1, $-5d < n < -d$ for signal point S4 (same probability as S1), $n > d$ or $n < -3d$ for signal point S3, and, $n > 3d$ or $n < -d$ for signal point S2 (having same probability as S3).

The average BER performance for one MQAM constellation size can then be obtained as

$$P_e = \sum_j w_j Q\left((a_j + b_j)\sqrt{\bar{\gamma}_s}\right), \tag{2-15}$$

where $\bar{\gamma}_s = \bar{E}_s / N_0$ is signal-to-noise ratio (SNR) per symbol. The symbol energy $\bar{E}_s$ can be expressed as a function of d, for BPSK, $\bar{E}_s = d^2$, QPSK, $\bar{E}_s = 2d^2$, 16-QAM, $\bar{E}_s = 10d^2$, 64-QAM, $\bar{E}_s = 42d^2$. The SNR per bit is defined as $\bar{\gamma}_b = \bar{\gamma}_s / \log_2 M$. Now we illustrate how to obtain the coefficients w_j, a_j, b_j. Taking the LSB bit of signal S_1 shown in Fig.2.6 as an example, the BER of these LSB bit is calculated to be

$$
\begin{aligned}
P_e &= \frac{1}{4}Q\left(\frac{3d-2d}{\sigma_n}\right)-\frac{1}{4}Q\left(\frac{3d+2d}{\sigma_n}\right)\\
&= \frac{1}{4}Q\left((3-2)\sqrt{\frac{d^2}{\sigma_n^2}}\right)-\frac{1}{4}Q\left((3+2)\sqrt{\frac{d^2}{\sigma_n^2}}\right)\\
&= \frac{1}{4}Q\left((3-2)\sqrt{\frac{2\overline{E}_s}{10N_0}}\right)-\frac{1}{4}Q\left((3+2)\sqrt{\frac{2\overline{E}_s}{10N_0}}\right)\\
&= \frac{1}{4}Q\left(\frac{(3-2)}{\sqrt{5}}\sqrt{\overline{\gamma}_s}\right)-\frac{1}{4}Q\left(\frac{(3+2)}{\sqrt{5}}\sqrt{\overline{\gamma}_s}\right) \qquad (2\text{-}16)
\end{aligned}
$$

Hence the coefficients (w_j, a_j, b_j) are obtained as $\left(\frac{1}{4},\frac{3}{\sqrt{5}},-\frac{2}{\sqrt{5}}\right)$ and $\left(-\frac{1}{4},\frac{3}{\sqrt{5}},\frac{2}{\sqrt{5}}\right)$ respectively. The coefficients for other bits of the I component can be obtained similarly. The coefficients w_j, a_j, b_j are listed in Table A.1 to Table A.4 of Appendix A, for several constellations respectively.

B. Approximate approach to compute BER

As MQAM is employed to transmit signals over AWGN channel, a loose bound for the BER performance as ideal coherent detection being used can be obtained as $P_e \le 0.2\exp[-\frac{\overline{E}_s}{N_0}\frac{1.5}{(M-1)}]$ [56]. For square MQAM, as $M \ge 4$, a more precise approximation on the average BER performance over AWGN channel is calculated as [57]

$$
P_e = \frac{4}{\log_2 M}\left(1-\frac{1}{\sqrt{M}}\right)\sum_{j=1}^{\sqrt{M}/2} Q\left[(2j-1)\sqrt{\frac{3\overline{\gamma}_s}{(M-1)}}\right], \qquad (2\text{-}17)
$$

where $Q(x)$ is defined as

$$Q(x) = \frac{1}{\sqrt{2\pi}} \int_x^{\infty} e^{-y^2/2} dy . \tag{2-18}$$

In this approximation, each symbol is assumed to cause only one bit error. The BER performance obtained for (2-15) and (2-17) under different SNR is shown in Fig.2.7. It can be seen that the average BER obtained from approximate method matches well with that obtained from the exact method.

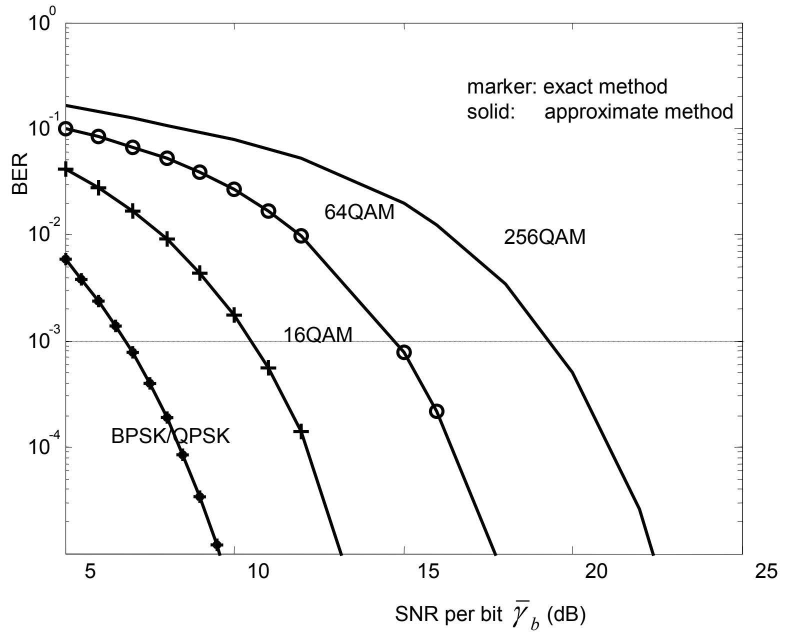

Fig.2.7 BER performance of MQAM over AWGN channels

As adaptive modulation is employed, SNR can be selected as channel quality indicator to decide which constellation is used. At receivers, the instantaneous SNR is first measured and fed back to transmitters. The selection of suitable constellation for transmitter is performed by comparing the instantaneous SNR against the pre-defined SNR threshold intervals. The SNR threshold intervals are determined based on the required BER performance.

As an example, for some constellations, the threshold intervals in terms of SNR per symbol ($\bar{\gamma}_s$) obtained for a targeted BER=10^{-3} is listed in Table 2.1.

TABLE 2.1 SNR Threshold intervals for selection of MQAM constellation

Constellation	BPSK	QPSK	16QAM	64QAM	256QAM
I	1	2	4	6	8
$a_{th,i}$	6.8dB	9.8dB	16.6dB	22.6dB	31dB
$b_{th,i}$	9.8dB	16.6dB	22.6dB	31dB	∞

2.3.2 BER performance of MQAM over fading channel with perfect channel estimation

As signal is transmitted over fading channel, the received signal is expressed as $r(t)=h(t)s(t)+n(t)$. If channel fading gain can be estimated precisely, receivers can make use of this channel state information to recover the signal corrupted by channel fading. For a coherent detection system, the estimated channel fading gain is used to control the local oscillator. Fig.2.8 shows an ideal case when channel estimation is perfect. Assuming signal is transmitted at a given constant average power, automatic gain control (AGC) can be used to scale the received faded signal so that the recovered signal constellation before making decision remains unchanged regardless of channel fading gain. Note that the noise will be scaled by the same factor and hence there is no effect on the received SNR, before and after applying AGC.

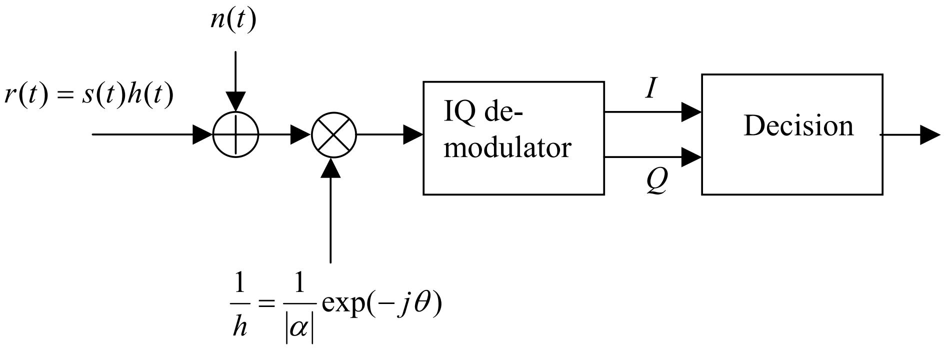

Fig.2.8 Receiver structure with perfect channel estimation

Conventionally, in a coherent detection system, the decision variable is constructed as $\hat{s} = r/\hat{h}$. Under perfect channel estimation where $h = \hat{h}$, the decision variable for the I component is constructed as $\hat{s}_I = \frac{r_I}{h} = s_I + \frac{n}{\alpha}$, where r_I is the received signal in the I component. The effect of phase shift on noise is not taken into account since statistically it can be ignored.

A. Exact method

As MQAM signal transmits over fading channels and assuming ideal coherent detection, the BER over fading channel conditioned on fading state α is given by $P_{e|\alpha} = \sum_j w_j Q\left[(a_j + b_j)\sqrt{\bar{\gamma}_s \alpha^2}\right]$. The average BER can be obtained by averaging this conditional BER over all fading gains,

$$P_e = \sum_j \int_0^\infty w_j Q\left[(a_j + b_j)\sqrt{\bar{\gamma}_s \alpha^2}\right] f_\alpha(\alpha) d\alpha, \tag{2-19}$$

where α is a random variable having PDF $f_\alpha(\alpha)$ introduced in Section 2.1 of Chapter II. Using the alternative form for the Q-function [58]

$$Q(x)=\frac{1}{\pi}\int_{0}^{\pi/2}\exp\left(-\frac{x^2}{2\sin^2\theta}\right)d\theta, \tag{2-20}$$

For Rayleigh fading channels, (2-19) can be simplified as

$$P_e=\sum_{j}\frac{1}{2}w_j\left(1-\sqrt{\frac{\bar{\gamma}_{s,j}}{1+\bar{\gamma}_{s,j}}}\right), \tag{2-21}$$

where $\bar{\gamma}_{s,j}=\Omega(a_j+b_j)^2\,\bar{\gamma}_s/2=(a_j+b_j)^2\,\mu/2$. $\mu=\Omega\bar{\gamma}_s$ is the average received SNR per symbol. The average received SNR per bit is defined as $\mu_b=\mu/\log_2 M$. The coefficients w_j, a_j, b_j are listed in Table A.1 to Table A.4 of Appendix A, for various constellations.

B. Approximate method

As signal is transmitted over fading channels, the average BER can be approximated using (2-17) and is written as

$$P_e=\int_{0}^{\infty}\frac{4}{\log_2 M}\left(1-\frac{1}{\sqrt{M}}\right)\sum_{j=1}^{\sqrt{M}/2}Q\left[(2j-1)\sqrt{\frac{3\bar{\gamma}_s}{(M-1)}\alpha^2}\right]f_\alpha(\alpha)d\alpha\,. \tag{2-22}$$

If Rayleigh fading channel is considered, a closed form solution for the average BER performance can be obtained as

$$P_e=\frac{4}{\log_2 M}\left(1-\frac{1}{\sqrt{M}}\right)\sum_{j=1}^{\sqrt{M}/2}\frac{1}{2}\left[1-\sqrt{\frac{(\bar{\gamma}_s)_j}{1+(\bar{\gamma}_s)_j}}\right], \tag{2-23}$$

where $(\bar{\gamma}_s)_j=\frac{3(2j-1)^2}{2(M-1)}\mu$. The BER performance as a function of the average received SNR per bit μ_b over Rayleigh and General Gamma fading channel is shown in Fig.2.9. It indicates that the approximate method can accurately evaluate the BER performance over flat fading channel.

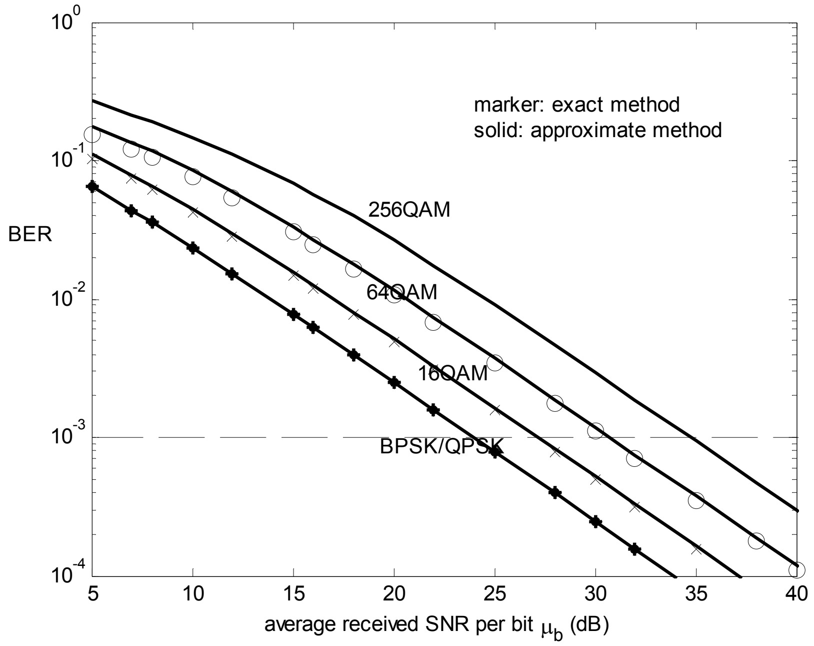

(a) BER performance over Rayleigh fading channel

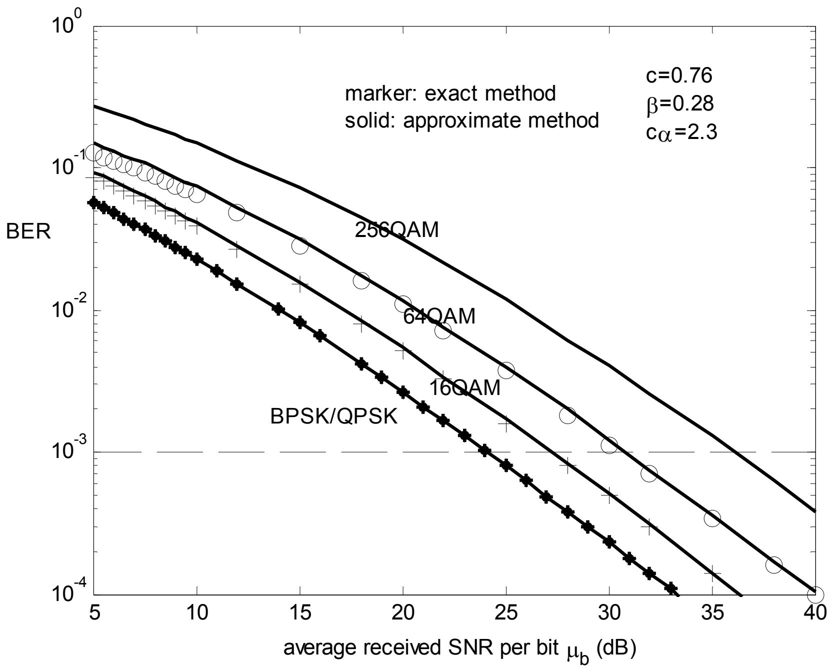

(b) BER performance over General Gamma fading channel

Fig.2.9 BER performance over fading channel with perfect channel estimation

2.3.3 Effect of channel estimation error on BER performance

In coherent detection systems, the estimated channel gain and phase are used to control the gain and phase of the local oscillator in the IQ demodulator – this processing results in a significant increase in symbol errors if channel estimation errors exist. Therefore the receiver performance is affected by the accuracy of channel estimation. In practical situation, however, channel estimation errors are unavoidable, due to the presence of AWGN. The receiver structure under imperfect channel estimation is shown in Fig.2.10(a). Note that in Fig.2.10(a), the received signal is scaled by the estimated channel fading gain, rather than the true fading gain as shown in Fig.2.8 where the channel estimation is perfect. Under channel estimation error, this scaling results in amplitude and phase errors as shown in Fig.2.10(b). Without the change of decision boundaries, these errors would therefore cause larger bit errors. In this section, the effect of imperfect channel estimation on BER performance of MQAM systems is investigated under the situations with amplitude estimation error only and with both amplitude and phase estimation errors. Two different approaches are adopted to compute the BER performance. One is the study by Tang in [58]. Its drawbacks are the computation complexity and the difficulty to be used to generate simulation samples. To overcome these difficulties, an approximate approach which treats the estimation error as signal level dependent Guassian noise is proposed and its accuracy is studied for the situation with amplitude error only.

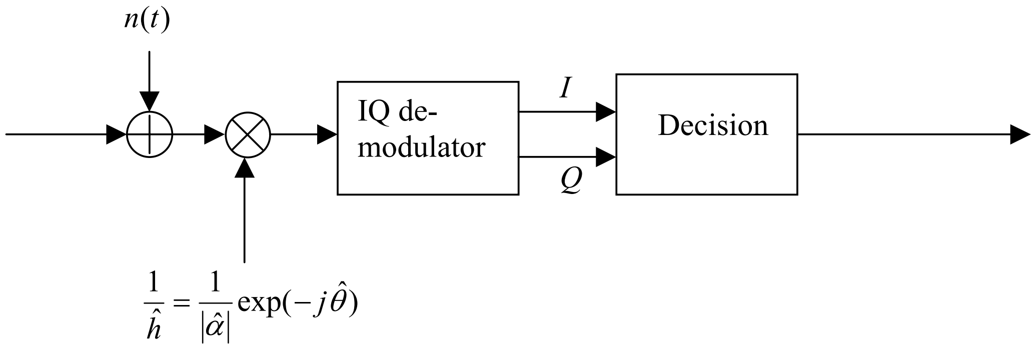

(a) Receiver structure with imperfect channel estimation

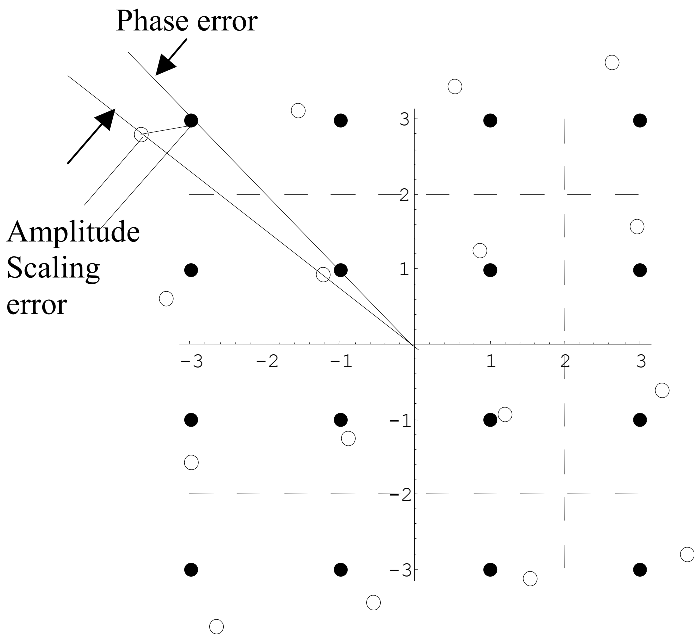

(b) The recovered signal constellation and the decision regions in an imperfect IQ demodulation

Fig.2.10 Effect of channel estimation error on receiver structure and recovered constellation

A. Exact approach of BER computation

(a) BER performance with amplitude error only

In this case, $\hat{\theta}=\theta$ and $h/\hat{h}=\alpha/\hat{\alpha}$, the decision variable for symbol detection is

$$\hat{s}_I = s_I \frac{\alpha}{\hat{\alpha}} + \frac{n}{\hat{\alpha}}. \tag{2-24}$$

To obtain the average BER with amplitude estimation error, we first derive the BER conditioned on α and $\hat{\alpha}$. The average BER is then obtained by averaging the conditional BER over the joint PDF of α and $\hat{\alpha}$ given in (2-12). We take 16-QAM as an example and consider the I component. By referring to decision boundaries shown in Fig.2.6, the conditional BER is obtained as

$$\begin{aligned} P_e(e|\alpha,\hat{\alpha}) = & \frac{1}{4}Q\left(\frac{3d\alpha}{\sigma_n}\right) + \frac{1}{4}Q\left(\frac{d\alpha}{\sigma_n}\right) + \frac{1}{4}Q\left(\frac{3d\alpha - 2d\hat{\alpha}}{\sigma_n}\right) - \frac{1}{4}Q\left(\frac{3d\alpha + 2d\hat{\alpha}}{\sigma_n}\right) + \\ & \frac{1}{4}Q\left(\frac{-d\alpha + 2d\hat{\alpha}}{\sigma_n}\right) + \frac{1}{4}Q\left(\frac{d\alpha + 2d\hat{\alpha}}{\sigma_n}\right) \end{aligned}. \tag{2-25a}$$

The first two terms are obtained for the two MSB bits, while the last four terms are for LSB bits.

The average BER is derived to be

$$P_e = \int_0^\infty \int_0^\infty P_e(e|\alpha,\hat{\alpha}) f_{\alpha,\hat{\alpha}}(\alpha,\hat{\alpha}) d\alpha d\hat{\alpha}. \tag{2-25b}$$

Substitute (2-12) into (2-25b) and with some re-arrangements, the average BER can be expressed as [55]

$$P_e = \sum_j w_j I(a_j, b_j, \mu, r, \rho) \tag{2-26a}$$

and

$$I(a_j, b_j, \mu, r, \rho) = \frac{1-\rho}{\pi} \int_0^{\pi/2} \int_{-\pi/2}^{\pi/2} \frac{\sin(2\theta) J_2\left(\sqrt{\rho}\sin(2\theta)\sin\phi + 1, \sqrt{1-\rho\mu}\left(a\cos\theta + (b\sin\theta)/\sqrt{r}\right)\right)}{\left(\sqrt{\rho}\sin(2\theta)\sin\phi + 1\right)^2} d\phi d\theta$$

(2-26b)

where

$$J_2(x,y)=\frac{1}{2}-\frac{3y}{4\sqrt{2x+y^2}}+\frac{y^3}{4(2x+y^2)^{3/2}} \tag{2-27}$$

and $r=\Omega/\hat{\Omega}$. μ and ρ are the average received SNR and the correlation coefficient between $\hat{\alpha}^2$ and α^2, repsectively. The values of coefficients w_j, a_j, b_j for various constellations are listed in Table A.1 to Table A.4 of Appendix A respectively.

(b) BER with both amplitude and phase estimation error

In this case, the decision variable is constructed as

$$\hat{s}=\frac{r}{\hat{h}}=\frac{\alpha}{\hat{\alpha}}e^{j(\theta-\hat{\theta})}s+\frac{n}{\hat{\alpha}}. \tag{2-28a}$$

Considering I component and $s=s_I+js_Q$, (2-28a) becomes

$$\hat{s}_I=(s_I\cos\psi+s_Q\cos\psi)\frac{\alpha}{\hat{\alpha}}+\frac{n}{\hat{\alpha}}, \tag{2-28b}$$

where s_I, s_Q are the signal components projected on the I and Q components, respectivelly. For 16-QAM, $s_I, s_Q \in \{-3d, -d, d, 3d\}$, however, only positive values of s_Q need to be considered due to the symmetry. Under combined amplitude and phase error, the conditional BER can be obtained from (2-28b) referring to the decision boundaries shown in Fig.2.6. Unlike the case with amplitude error only, the conditional BER is further conditioned on ψ. The average BER is obtained as [55]

$$P_e = \sum_j w_j I(a_{1j}, a_{1j}, b_j, \mu, r, \rho), \tag{2-29}$$

where

$$I(a_{1j}, a_{1j}, b_j, \mu, r, \rho) = \frac{1-\rho}{\pi} \int_{-2\pi}^{2\pi} \int_{0}^{\pi/2} \int_{-\pi/2}^{\pi/2} \frac{\sin(2\theta) f_\psi(\psi)}{\left(\sqrt{\rho}\sin(2\theta)\sin\phi + 1\right)^2} \bullet$$

$$J_2\left(\sqrt{\rho}\sin(2\theta)\sin\phi + 1, \sqrt{1-\rho\mu}\left((a_1\cos\psi + a_2\sin\psi)\cos\theta + (b\sin\theta)/\sqrt{r}\right)\right) d\phi\, d\theta\, d\psi \; .$$

(2-30)

The function $f_\psi(\psi)$ is defined in (2-14). The coefficients for various constellations are listed in Table A.5 to Table A.8 in Appendix A. μ and ρ are the average received SNR and the correlation coefficient between $\hat{\alpha}^2$ and α^2, repsectively

The BER performances under imperfect channel estimation are shown in Fig.2.11-Fig.2.14 for different estimation conditions. Comparing Fig.2.11 and 2.12 with Fig.2.9 (a), it can be seen that imperfect channel estimation causes error floor in BER performance which is not present when perfect channel estimation is assumed. It is also observed that amplitude and phase error together degrade the BER performance much severe than amplitude error alone. This is because the phase error causes extra impairments in coherent symbol detection. The BER performance is affected by the correlation coefficient ρ badly as shown in Fig.2.13 and 2.14 using 16QAM as an example. The error floor increases significantly as the decrease of ρ. For example, with both amplitude and phase error, the error floor goes beyond 10^{-2} for $\rho = 0.99$ while it is below 10^{-3} for $\rho = 0.9999$.

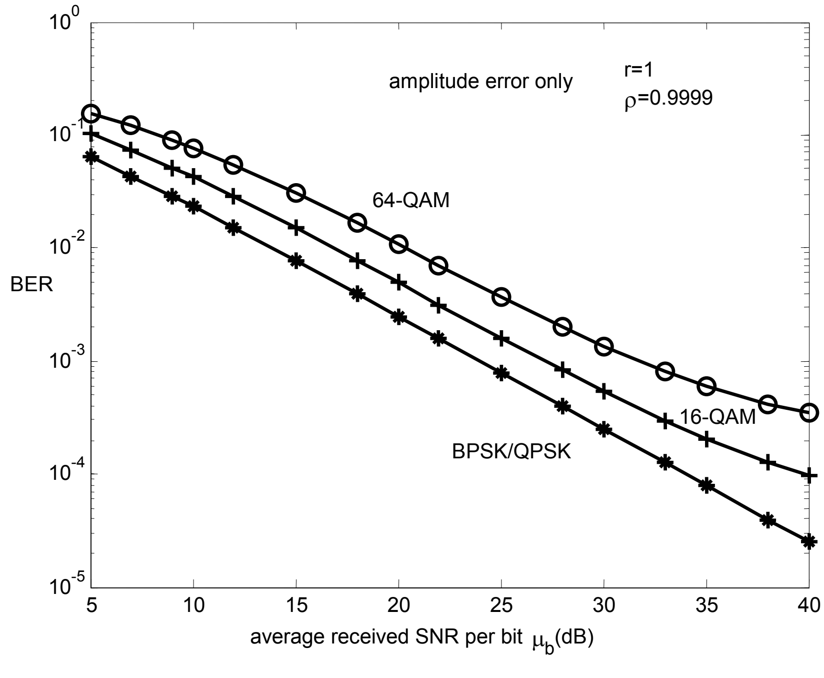

(a) $\rho = 0.9999$

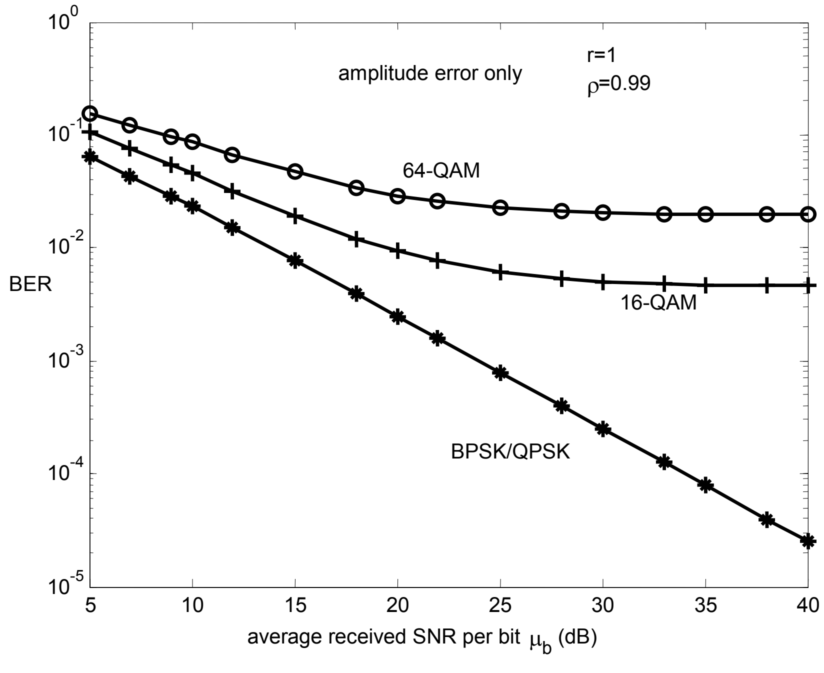

(b) $\rho = 0.99$

Fig.2.11 BER performance over fading channel with amplitude error alone

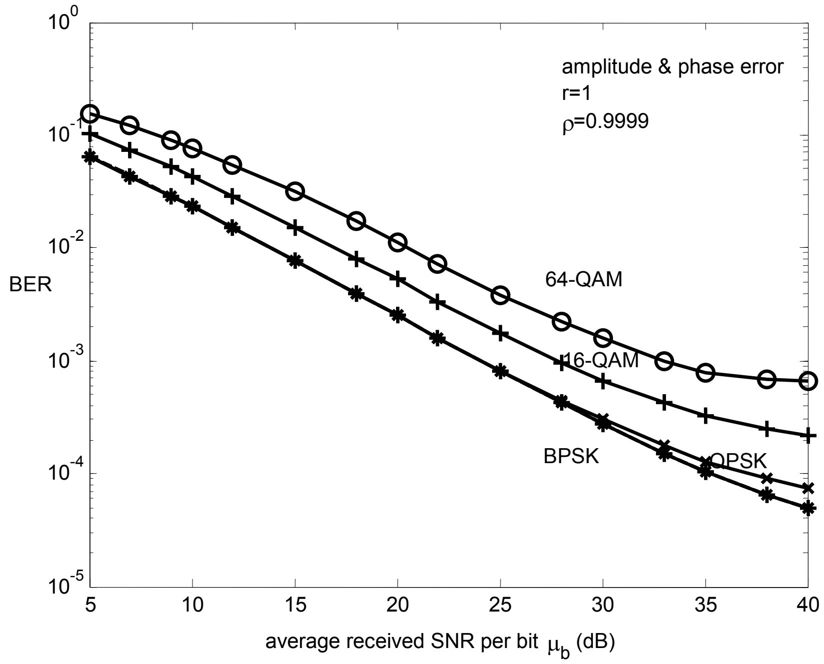

Fig.2.12 BER performance with amplitude and phase error over fading channel

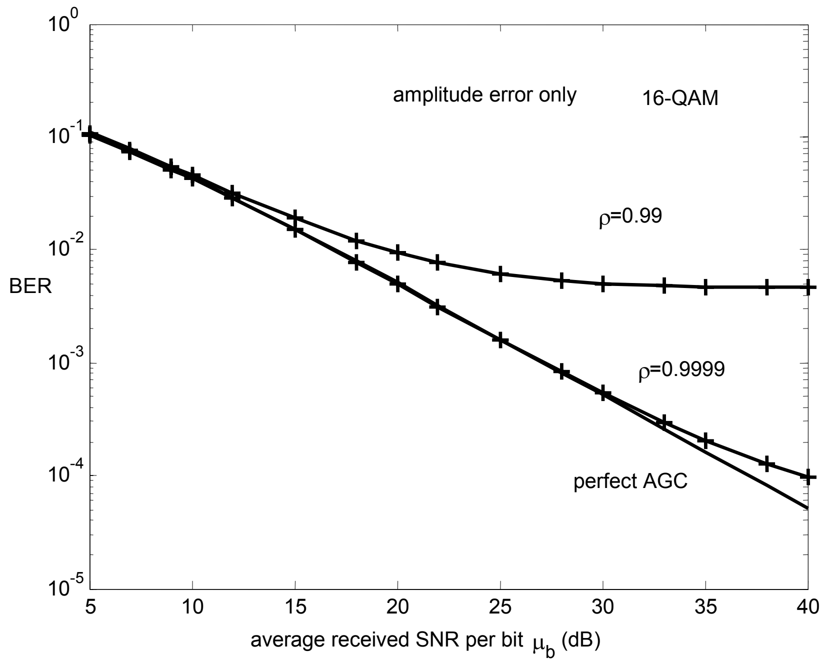

Fig.2.13 BER performance with amplitude error alone vs SNR

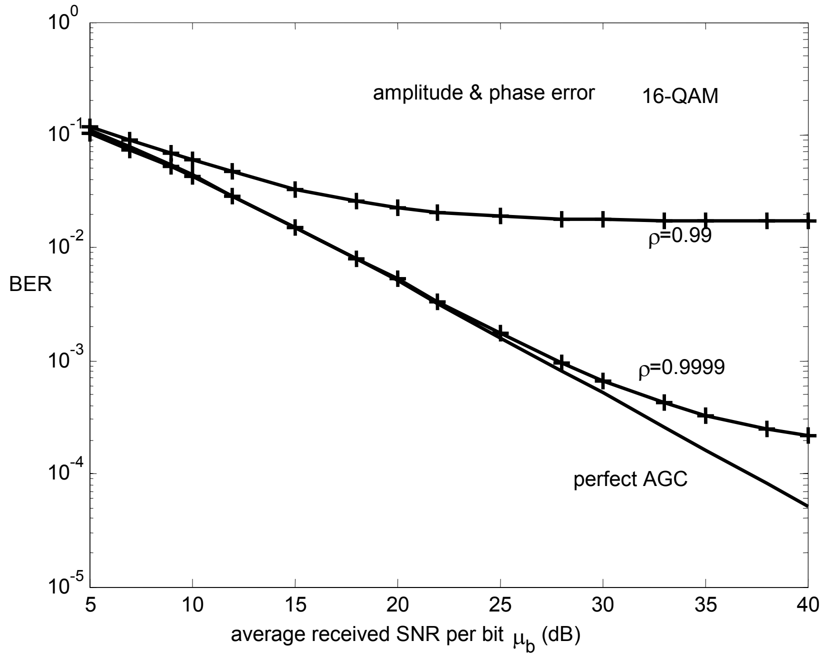

Fig.2.14 BER performance with amplitude and phase error vs SNR

The results and observations obtained here show that understanding how the channel estimation errors affect the rate adaptive modulation systems is very important because the channel estimation error might result in the fact that higher order constellations become unusable. In practical, the amount of channel estimation error can be controlled by the selection of training sequence, the interpolation order and frame length as shown in [59].

B. Approximate method to evaluate BER

The BER computation with channel estimation error requires numerical integration which grows with the constellation size in the earlier study. Here we introduce an approximate method to obtain closed form solution for the BER performance with amplitude estimation only. The main idea behind this approximate method is to treat the effect of estimation error *e* as an equivalent signal level dependent Gaussian noise. The underlined assumption is that the estimated error e is small and the estimated fading gain α is uncorrelated with the estimated error. This assumption is true if α and $\hat{\alpha}$ are highly correlated. The investigation on the correlation coefficient ρ_e between $\hat{\alpha}^2$ and $|e|^2$ conducted in part (b) of this section will verify that the assumption approximately holds. Hence the accuracy of this approximation strongly relies on the correlation of α and $\hat{\alpha}$.

(a) BER performance with amplitude error

In this case, considering I component only, the decision variable of (2-24) obtained from Fig.2.10 (a) can be rewritten as

$$\hat{s}_I = \frac{\alpha s_I + n}{\hat{\alpha}} = \frac{(\hat{\alpha} - |e|) s_I + n}{\hat{\alpha}} = s_I - \frac{|e| s_I - n}{\hat{\alpha}} = s_I + n', \tag{2-31}$$

where the estimation error e is a complex Gaussian random variable and $|e| = \hat{\alpha} - \alpha$. $n' = \frac{|e| s_I - n}{\hat{\alpha}}$ is the effective noise including both AWGN and the effect due to estimation error. It can be seen that the effective noise depends on the signal power level in MQAM constellation.

However for MSB bits, where the decision boundary is zero (for example, D_2 in Fig.2.6), this approximation is not valid since the amplitude estimation error will not affect the BER performance. The decision variable for MSB bits is constructed as $\hat{s}_I = \alpha s_I + n$. Therefore in the following computation, the BER performance under amplitude estimation error will be partitioned into two parts. One part is the BER obtained for MSB bits, while the other part is the BER obtained for the remaining bits with decision variable defined by (2-31). The BER performance with amplitude error only is then expressed as

$$P_e = P_{e,MSB} + P_{e,other}, \tag{2-32}$$

where

$$P_{e,MSB} = \frac{1}{2}\sum_j w_j Q\left(1 - \sqrt{\frac{\Omega a_j^2 \bar{\gamma}_s / 2}{1 + \Omega a_j^2 \bar{\gamma}_s / 2}}\right) \tag{2-33}$$

and coefficients w_j, a_j are listed in Table A.1 to Table A.4 of Appendix A for various constellations respectively. The computation of $P_{e,other}$ will be presented in the following.

n' can then be approximated as a Gaussian random variable conditioned on $\hat{\alpha}$, $|e|$ and s_I (the I component of the signal), the variance of n' is

$$\sigma_{n'}^2 = \frac{1}{\hat{\alpha}^2}\left(|e|^2 s_I^2 + \frac{N_0}{2}\right). \tag{2-34}$$

Since the estimation error e is a Guassian random variable, its amplitude follows Rayleigh distribution. The variance Ω_e of the estimation error e can be calculated as

$$\Omega_e = E[|e|^2] = E\left[(\hat{\alpha} - \alpha)^2\right] = E[\hat{\alpha}^2] + E[\alpha^2] - 2E[\alpha\hat{\alpha}], \tag{2-35}$$

where $E[\bullet]$ denotes the expectation. With amplitude estimation error, $E\left[\alpha^2\right] = \Omega$, $E\left[\hat{\alpha}^2\right] = \hat{\Omega}$, the PDF of $|e|$ is obtained as

$$f_{|e|}(|e|) = \frac{2|e|}{\Omega_e}\exp\left(-\frac{|e|^2}{\Omega_e}\right). \tag{2-36}$$

Now taking 16-QAM as an example, using (2-31) and decision boundaries shown in Fig.2.6, the BER of bits except MSB bits of 16-QAM conditioned on $\hat{\alpha}$ and $|e|$ is calculated to be

$$P_{e,other}(e|\hat{\alpha},|e|) = \frac{1}{4}Q(\frac{3d-2d}{\sigma_{n'}}) - \frac{1}{4}Q(\frac{3d+2d}{\sigma_{n'}}) + \frac{1}{4}Q(\frac{-d+2d}{\sigma_{n'}}) + \frac{1}{4}Q(\frac{d+2d}{\sigma_{n'}}). \tag{2-37}$$

Substitute (2-34) into (2-37) and with some re-arrangements, the BER performance conditioned on estimated channel fading amplitude $\hat{\alpha}$ and $|e|$ is

$$P_{e,other}(e|\hat{\alpha},|e|) = \sum_j w_j Q\left(\sqrt{\left(1+\frac{b_j}{a_j}\right)^2 \gamma_j}\right), \tag{2-38}$$

where $\gamma_j = \dfrac{\hat{\alpha}^2 a_j^2 d^2}{|e|^2 a_j^2 d^2 + N_0/2}$. The values of coefficients w_j, a_j, b_j for various constellations are listed in Table A.1 to Table A.4 of Appendix A respectively.

Assuming that e and $\hat{\alpha}$ are uncorrelated, the PDF of γ_j can be expressed as

$$f_{\gamma_j}(\gamma_j) = \int_{\frac{N_0}{2a_j^2 d^2}}^{\infty} \frac{z}{\Omega_e}\exp\left(\left(-z-\frac{N_0}{2a_j^2 d^2}\right)\Big/\Omega_e\right)\frac{1}{\hat{\Omega}}\exp\left(-\frac{\gamma_j z}{\hat{\Omega}}\right)dz. \tag{2-39}$$

$$
\begin{aligned}
P_{e,other} &= \sum_j w_j \int Q\left(\sqrt{\left(1+\frac{b_j}{a_j}\right)^2 \gamma_j}\right) f_{\gamma_j}(\gamma_j)\,d\gamma_j \\
&= \sum_j w_j \int_0^\infty \frac{1}{\pi}\int_0^{\pi/2} \exp\left(-\left(1+\frac{b_j}{a_j}\right)^2 \frac{\gamma_j}{2\sin^2\theta}\right) \int_{\frac{N_0}{2a_j^2 d^2}}^\infty \frac{z}{\Omega_e}\exp\left(-\left(z-\frac{N_0}{2a_j^2 d^2}\right)\Big/\Omega_e\right)\frac{1}{\hat{\Omega}}\exp\left(-\frac{\gamma_j z}{\hat{\Omega}}\right) dz\,d\theta\,d\gamma_j \\
&= \frac{1}{2}\sum_j w_j \left\{1-\sqrt{\left(1+\frac{b_j}{a_j}\right)^2 \frac{\hat{\Omega}}{\Omega_e}} \exp\left(\left(\hat{\Omega}\left(1+\frac{b_j}{a_j}\right)^2+\frac{1}{a_j^2\bar{\gamma}_s}\right)\Big/2\Omega_e\right) Q\left(\sqrt{\left(\hat{\Omega}\left(1+\frac{b_j}{a_j}\right)^2+\frac{1}{a_j^2\bar{\gamma}_s}\right)\Big/\Omega_e}\right)\right\}
\end{aligned}
$$

(2-40)

The BER performance obtained from the approximate method for amplitude error only is shown in Fig.2.15 and Fig.2.16. As correlation coefficient ρ is high, the approximate method can effectively evaluate the BER performance. It can be seen that, for small channel estimation error (or highly correlated estimated and true fading gain), the approximate method can predict the error floor rather well.

In this section, a closed form solution is obtained for BER performance for amplitude error only. As both amplitude and phase errors are present, it is not so straightforward to obtain the parameters for the Gaussian approximation. We leave this to future investigation.

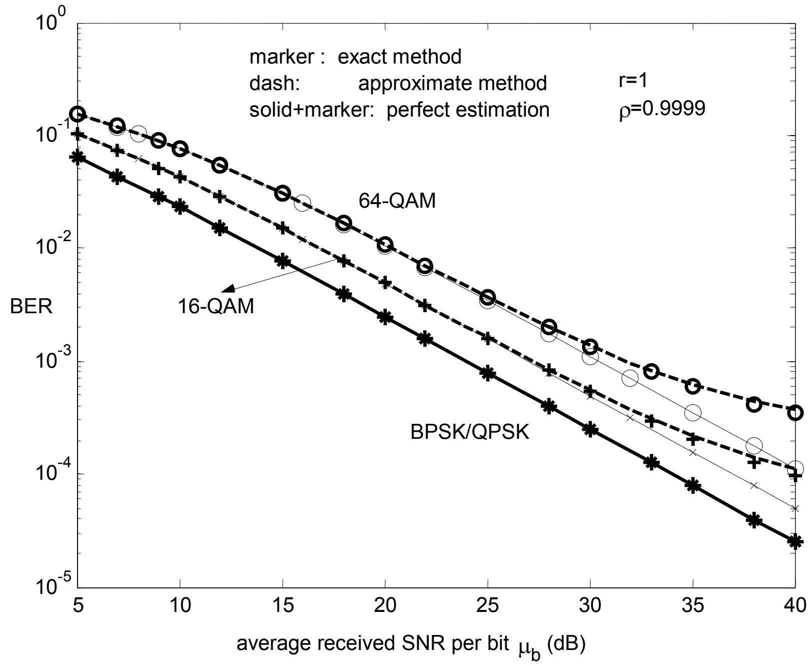

Fig.2.15 Average BER obtained from approximate method with amplitude error alone ($\rho=0.9999$)

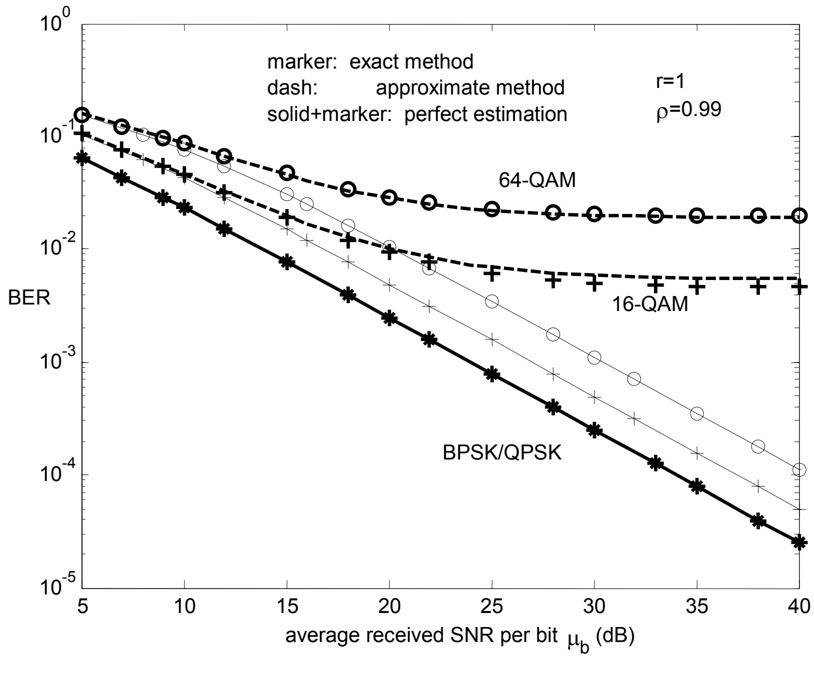

Fig.2.16 Average BER obtained from approximate method with amplitude error alone ($\rho=0.99$)

(b) Investigation on correlation between $\hat{\alpha}$ and $|e|$

The correlation coefficient between $\hat{\alpha}$ and e can be defined as

$$\rho_e = \left[\mathrm{cov}\left(\hat{\alpha}^2, |e|^2\right)\right] / \left[\sqrt{\mathrm{var}\left(\hat{\alpha}^2\right)\mathrm{var}\left(|e|^2\right)}\right], \tag{2-36}$$

where

$$\mathrm{cov}\left(\hat{\alpha}^2, |e|^2\right) = E\left[\hat{\alpha}^2 |e|^2\right] - E\left[\hat{\alpha}^2\right] E\left[|e|^2\right]. \tag{2-37}$$

Using $|e| = \hat{\alpha} - \alpha$,

$$E\left[\hat{\alpha}^2 |e|^2\right] = E\left[\hat{\alpha}^2 (\hat{\alpha}-\alpha)^2\right] = \int_0^\infty \int_0^\infty \hat{\alpha}^2 (\hat{\alpha}-\alpha)^2 f_{\hat{\alpha},\alpha}(\hat{\alpha},\alpha)\, d\hat{\alpha}\, d\alpha \tag{2-38}$$

and

$$E\left[|e|^2\right] = E\left[(\hat{\alpha}-\alpha)^2\right] = \int_0^\infty \int_0^\infty (\hat{\alpha}-\alpha)^2 f_{\hat{\alpha},\alpha}(\hat{\alpha},\alpha)\, d\hat{\alpha}\, d\alpha . \tag{2-39}$$

The joint PDF of $\hat{\alpha}, \alpha$ is defined in (2-12). Since the estimation error e is a complex Gaussian random variable, its amplitude $|e|$ should be a random variable having Rayleigh distribution. The standard deviations of $\hat{\alpha}^2$ and $|e|^2$ are $\sqrt{\mathrm{var}\left(\hat{\alpha}^2\right)} = \hat{\Omega}$ and $\sqrt{\mathrm{var}\left(|e|^2\right)} = \Omega_e$.

The correlation coefficients ρ_e are shown in Table 2.2. With r=1, the increase of correlation coefficient ρ between α and $\hat{\alpha}$ results in low correlation between $\hat{\alpha}$ and $|e|$. Hence it can be predicted that as α and $\hat{\alpha}$ become highly correlated, the approximate method can evaluate BER performance under imperfect channel estimation more precisely. As $r \neq 1$, even α and $\hat{\alpha}$ are highly correlated, the correlation between

$\hat{\alpha}$ and $|e|$ are very high. In this case, the underlined assumption of proposed approximate method is not guaranteed so that it is not valid to approximate BER performance.

TABLE 2.2 Correlation coefficients ρ_e between $\hat{\alpha}$ and $|e|$ for various ρ and r

ρ_e (ρ / r)	0.9999	0.9995	0.999	0.995	0.99	0.95	0.9	0.85	0.8
1	0.00016	0.00068	0.0013	0.0054	0.0099	0.04	0.072	0.1	0.13
0.9	0.98	0.93	0.86	0.58	0.43	0.23	0.22	0.24	0.26
1.05	0.92	0.69	0.52	0.015	0.071	0.013	0.033	0.058	0.083

2. 4 Summary

In this chapter, the widely used channel models, channel estimation techniques and MQAM modulation technique are reviewed. The BER performances of MQAM over Rayleigh and General Gamma fading channel are investigated. The effect of imperfect channel estimation on BER performance over Rayleigh fading channel is studied. The numerical results show that with channel estimation error, error floors are present even employing coherent detection. Higher correlation between α and $\hat{\alpha}$ results in small error floor and gives better BER performance. An approximate method which gives closed form solution for BER performance and has lower complexity in BER computation for amplitude estimation error is introduced. The analysis shows that this method is valid and gives good approximation at higher correlation coefficient ρ between α and $\hat{\alpha}$. Within a practical SNR range, the approximate method can predict the BER performance with good accuracy.

CHAPTER III

CAPACITY OF FADING CHANNEL EMPLOYING RATE ADAPTIVE MODULATION TECHNIQUE

As signal is transmitted over fading channel, insufficient usage of bandwidth is unavoidable if system is designed to work under worst case conditions. Adaptive modulation is employed to improve bandwidth efficiency of fading channel without sacrificing transmission quality. In this chapter, channel capacity or bandwidth efficiency achieved by adaptive modulation over different fading channels is investigated first under perfect channel estimation. A framework to study the effect of channel estimation error on capacity of rate adaptive modulation systems is then proposed. With the introduction of this framework, the effect of channel estimation error on the SNR threshold intervals is quantified based on the channel characteristics and the estimation techniques. The SNR threshold intervals for the selection of suitable MQAM constellation under the consideration of channel estimation error are obtained by employing the proposed framework. Channel capacities of adaptive MQAM systems with and without diversity reception are derived under different estimation conditions.

3.1 System model description of adaptive modulation technique

In adaptive modulation systems, channel state information is available at both receiver and transmitter. The estimated channel fading is used not only for the coherent detection of transmitted signal, but also for the adaptation of parameters of transmitted signal at the transmitter, as shown in Fig.3.1. For the operation of adaptive modulation systems, the measurement of channel quality should be performed at the receiver and selection criterion of suitable modulation mode should be given at the transmitter.

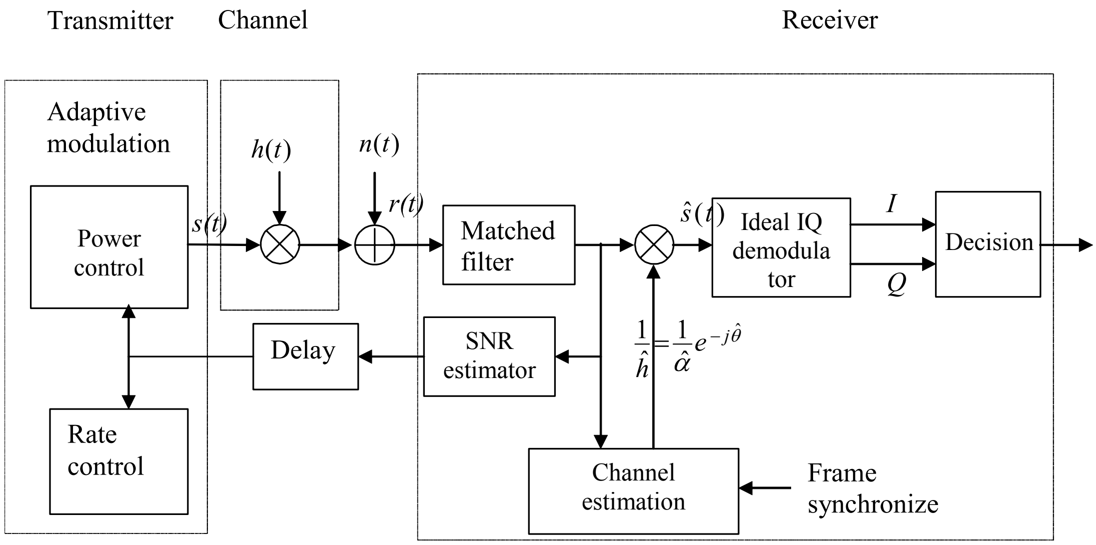

Fig.3.1 Receiver and transmitter structure of adaptive modulation systems

If SNR is specified as a channel quality indicator, the selection criterion turns out to be the SNR threshold intervals. The transmission parameters for the next transmission are determined by comparing the measured SNR at the receiver against the SNR threshold intervals which are defined based on certain transmission requirements, for example, the targeted BER. Fig.3.2 shows how the constellation size of MQAM is adapted to the instantaneous SNR. The suitable MQAM constellation size is obtained by checking which SNR threshold interval the received SNR falls in.

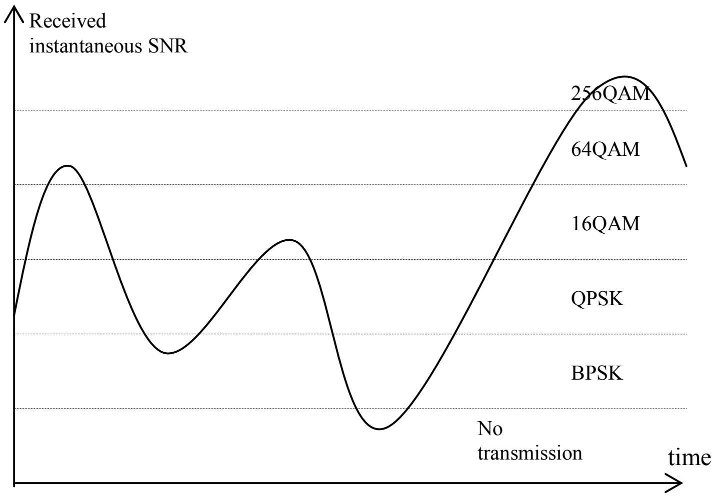

Fig.3.2 An illustration of modulation mode adaptation

If channel conditions can be tracked perfectly, the SNR threshold intervals are obtained from the BER performance over AWGN channels, with the equivalent receiver circuit shown in Fig.3.3(b). The obtained SNR threshold intervals for the selection of MQAM constellation size based on Fig.3.3 are shown in Table 2.1.

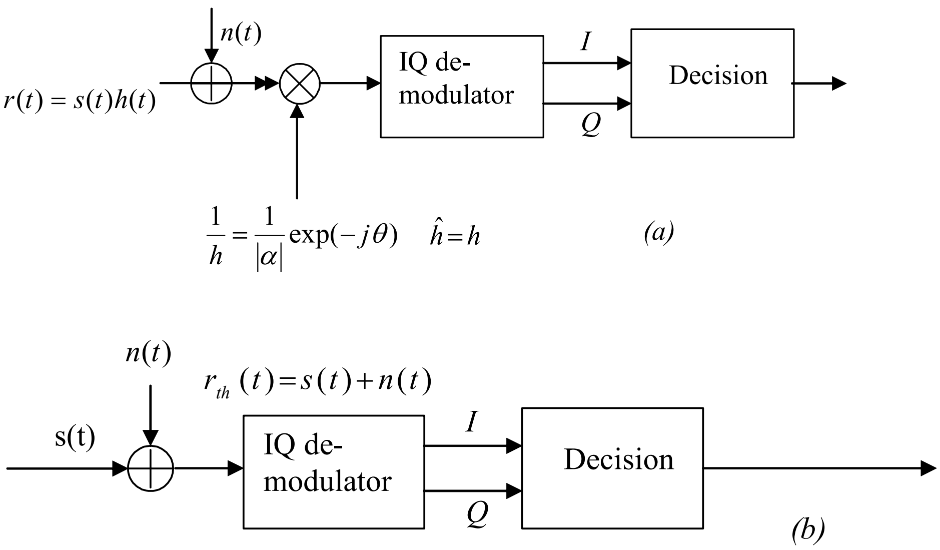

Fig.3.3 Equivalent circuit to determine SNR threshold intervals under perfect channel estimation

In the presence of channel estimation error, due to the mismatch of h and $\hat{h}$, extra impairment is introduced by the estimation error during coherent symbol detection. To ensure the transmission quality, the adaptation of parameters has to take both AWGN and the effect of channel estimation error into account. How to adapt transmitter parameters to channel conditions and how to obtain the SNR threshold intervals with channel estimation error will be studied in this chapter.

To investigate capacity achieved by adaptive modulation systems, the PDF of received SNR should be known. The instantaneously received SNR conditioned on channel fading gain $h=\alpha e^{j\theta}$ is derived to be

$$\gamma=\frac{E[|s|^2]}{E[|n/h|^2]}=\alpha^2\frac{\overline{E}_s}{N_0}=\alpha^2\overline{\gamma}_s, \tag{3-1}$$

where $\bar{\gamma}_s$ is the transmitted SNR regardless of channel conditions. With the knowledge of PDF of α, the PDF of SNR denoted as $f_\gamma(\gamma)$ can be obtained using (3-1). If MQAM is used to realize rate adaptive modulation, the probability that one specific constellation size is selected can be derived by integrating $f_\gamma(\gamma)$ over the corresponding SNR threshold intervals. Achievable capacity by rate adaptive MQAM modulation can be obtained. Capacity analysis obtained with and without channel estimation error is carried out in Section 3.4 of this chapter.

3.2 Shannon capacity achieved over flat fading channel with perfect channel estimation

For a given received SNR γ, the maximum transmission rate over radio channel is generally represented by Shannon capacity, which is given as

$$C = B\log_2(1+\gamma)\,. \tag{3-2}$$

As the received SNR varies over time, Shannon capacity of flat fading channel conditioned on γ is

$$C(\gamma) = B\log_2(1+\gamma)\,. \tag{3-3}$$

The average achievable channel capacity is obtained by averaging (3-3) over all possible fading states, i.e.,

$$C = \int_0^\infty B\log_2\left[1+\gamma\right] f_\gamma(\gamma)\,d\gamma\,. \tag{3-4}$$

Eq.(3-4) represents the capacity achieved over fading channel as channel state information is available at the receiver only. As channel state information is known to both receiver and transmitter, power control can be performed at the transmitter to improve channel capacity. It has been proven in [20] that the optimal power control strategy for flat fading channel is "water filling" over time. In mathematics, the transmission power can be obtained as

$$p(\gamma) = \frac{\overline{p}}{\gamma_0} - \frac{\overline{p}}{\gamma}, \quad \gamma \geq \gamma_0\,, \tag{3-5}$$

where $\overline{p}$ is the average transmission power and γ_0 is the cut-off SNR. If the received SNR is smaller than γ_0, transmitter is not allowed to transmit any data. γ_0 can be defined from

$$\int_{\gamma_0}^{\infty}\left(\frac{\overline{p}}{\gamma_0}-\frac{\overline{p}}{\gamma}\right)f_\gamma(\gamma)d\gamma=\overline{p}. \tag{3-6}$$

With this optimal power allocation strategy, the instantaneous SNR is rewritten as

$$\gamma_{opt}=\frac{E[|s|^2]}{E[|n/h|^2]}=\gamma\left[\frac{1}{\gamma_0}-\frac{1}{\gamma}\right]. \tag{3-7}$$

Substitute γ_{opt} into (3-4), Shannon capacity is obtained as

$$C=\int_{\gamma_0}^{\infty}B\log_2\left(\frac{\gamma}{\gamma_0}\right)f_\gamma(\gamma)d\gamma. \tag{3-8}$$

For Rayleigh fading channel, the PDF of SNR is

$$f_\gamma(\gamma)=\frac{1}{\mu}e^{-\frac{\gamma}{\mu}}, \tag{3-9}$$

where $\mu=E[\gamma]=\Omega\frac{\overline{E}_s}{N_0}=\Omega\overline{\gamma}_s$ is the average received SNR and $\Omega=E[\alpha^2]$.

For fading channel characterized by General Gamma distribution, the PDF of instantaneous SNR is obtained from (2-10) and is given as

$$f_\gamma(\gamma)=\frac{1}{2\sqrt{\gamma}}\sqrt{\frac{1}{\overline{\gamma}_s}}\frac{c_g\left(\gamma/\overline{\gamma}_s\right)^{(c_gd_g-1)/2}}{\beta_g^{c_gd_g}\Gamma(d_g)}\exp\left[-\left(\frac{\gamma}{\beta_g^2\overline{\gamma}_s}\right)^{c_g/2}\right]. \tag{3-10}$$

The Shannon capacity obtained over Rayleigh and General Gamma fading channel with and without channel state information available at transmitter is shown in Fig.3.4. It can be seen that as transmission rate is adaptive to instantaneous conditions, adaptive transmission power as well only yields a negligible capacity gain, as reported in [19,20]. Therefore, from now onwards, the study will focus on a rate adaptive constant transmission power system. The other reasons for the adoption of constant transmission power rate adaptive technique are: 1) Power adaptation may sometimes result in uncontrollably large interference to co-channel cells when the communication link between mobile and the home base station is in deep fades whilst the link between mobile and the base station in co-channel cell is in good conditions. 2) Heavy signaling overheads may be reduced since no instruction information of power adaptation is needed. 3) The complexity of transmitter structure is reduced.

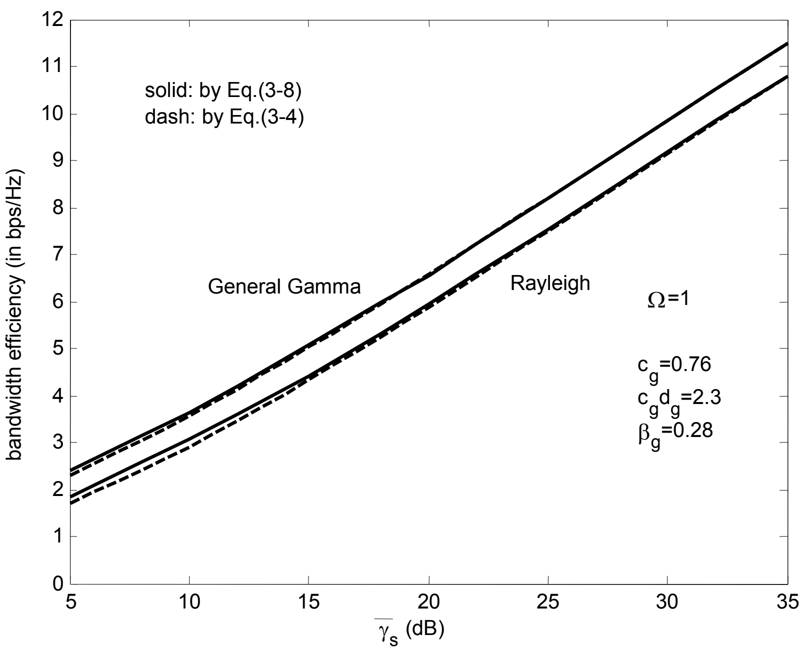

Fig.3.4 Channel capacities with and without power adaptation

3.3 Capacity achieved by rate adaptive MQAM modulation with perfect channel estimation

MQAM modulation scheme is widely used to implement adaptive modulation. Square MQAM is assumed in the following study.

The probability that one constellation is used is calculated to be

$$P_i = \int_{a_{th,i}}^{b_{th,i}} f_\gamma(\gamma) d\gamma , \tag{3-11}$$

where i is the bit/symbol of a specific constellation, for example, for 16QAM, i=4. $a_{th,i}, b_{th,i}$ are the ranges of the SNR threshold intervals for 2^i QAM constellation being used and defined in Table 2.1. Channel capacity achieved by adaptive MQAM is then obtained as

$$C = \sum_i iP_i . \tag{3-12}$$

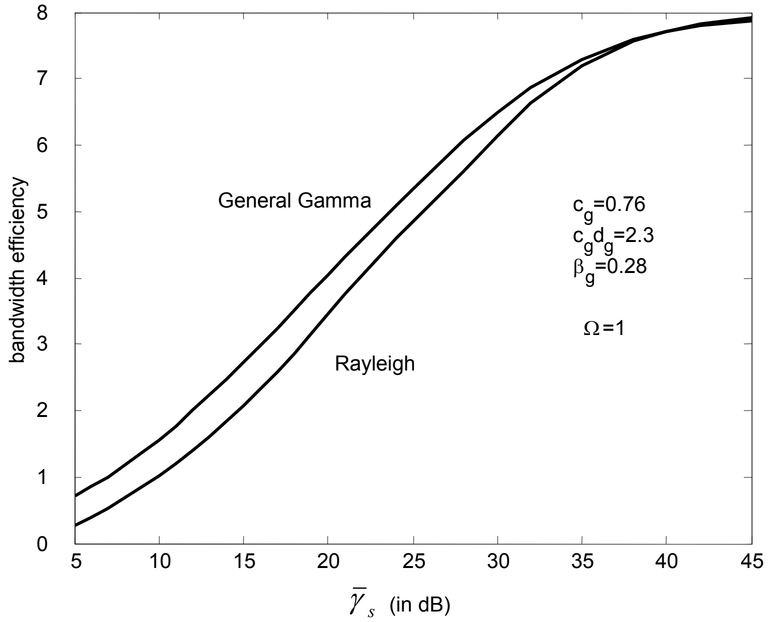

Fig.3.5 Channel capacity employing MQAM adaptive modulation

The capacities achieved by adaptive MQAM are shown in Fig.3.5 for Rayleigh and General Gamma fading channel respectively.

3.4 Effect of channel estimation error on channel capacity

Adaptive modulation technique requires that the instantaneous channel fading can be accurately estimated. The effect of channel estimation error on the BER performance of coherent detection system is studied in Chapter II, Section 2.3.3. It shows that channel estimation error causes the degradation of BER performance and results in error floor. When designing a practical coherent rate adaptive modulation system, such channel estimation errors have to be taken into consideration to maintain the transmission quality. Under the consideration of imperfect channel estimation, one way to implement rate adaptive modulation is to adjust the transmitter parameters based on the received SNR, while the estimation error is encompassed in the determination of SNR threshold intervals. The consequence of this approach is, given a received SNR, the selection of one specific MQAM constellation will be based on the new SNR threshold intervals compared to the case with perfect channel estimation. In other words, the new SNR threshold intervals have to be employed when the receiver decides which constellation size is used. Hence the first step to evaluate the effect of imperfect channel estimation on capacity is to investigate how the estimation error affects the SNR threshold intervals.

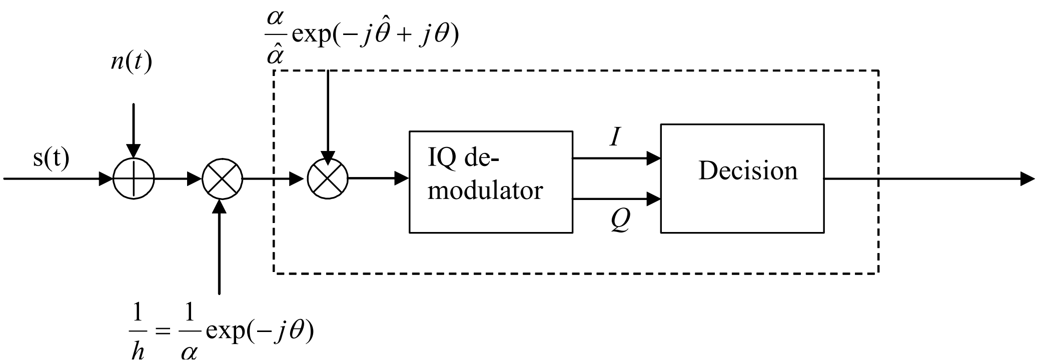

(a)

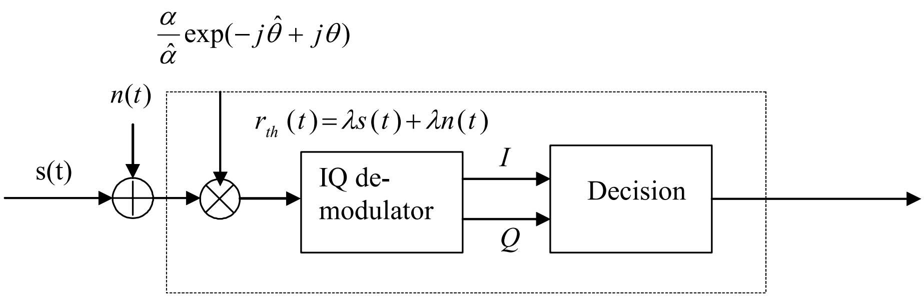

(b)

Fig.3.6 (a) Receiver structure (b) Equivalent circuit to determine SNR threshold intervals under imperfect channel estimation

Under imperfect channel estimation, the receiver structure for coherent detection is shown in Fig.2.10(a) which can be reconstructed as Fig.3.6(a). From Fig.3.6(a), it can be seen that the effect of channel estimation errors results in the fact that the signal constellation which has been recovered is further scaled by a factor $\lambda = |\alpha/\hat{\alpha}|$ and rotated by an angle ψ before decision making. Note that the noise is also scaled by λ. Comparing Fig.3.3(a) and Fig.3.6(a), under imperfect channel estimation, an equivalent circuit to include the effect of channel estimation errors in the determination of the SNR threshold intervals is to replace Fig.3.3(b) by Fig.3.6(b), where the imperfect channel estimation is replaced by an equivalent circuit with imperfect IQ modulator. In this equivalent circuit, investigating the effect of imperfect channel information is converted into investigating the system performance using imperfect IQ demodulator. For a given decision circuit, the degradation in BER performance can therefore be found.

To define the SNR threshold intervals for the selection of suitable MQAM constellation, a performance curve needs to be obtained. For ideal channel estimation, the performance curves as a function of received SNR obtained from the equivalent circuit shown in Fig.3.3(b) are represented by solid lines in Fig.3.7. The effect of imperfect channel estimation is equivalent to shifting this SNR threshold intervals toward high SNR end as shown by the dash lines obtained from equivalent circuits shown in Fig.3.6(b) in Fig.3.7. It can be seen that, to guarantee a maximum tolerable BER, an additional SNR margin for the choice of a particular constellation size has to be considered. Under imperfect channel estimation, the new threshold intervals can now be found using Fig.3.7, by drawing a horizontal line across and obtaining the SNR at these intersection points.

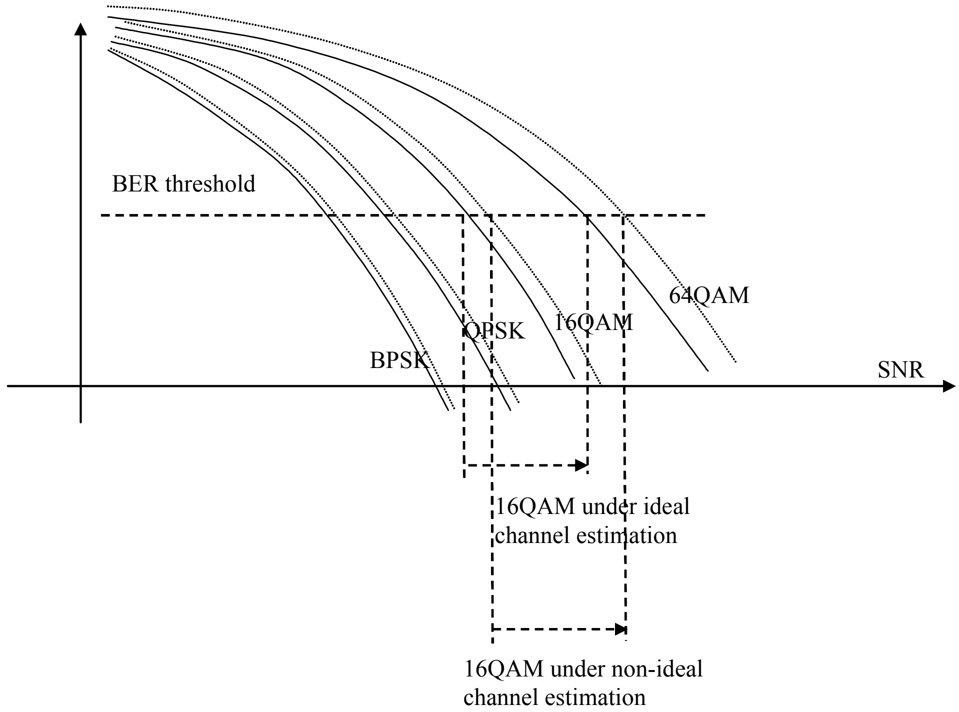

Fig.3.7 The shift of SNR threshold intervals

3.4.1 Derivation of SNR threshold intervals under imperfect channel estimation

With channel estimation error, referring to the equivalent circuit shown in Fig.3.6(b), the new SNR threshold intervals are obtained from

$$r_{th} = \lambda e^{j\psi} s + \lambda n \,, \tag{3-13}$$

where $\lambda = |\alpha/\hat{\alpha}|$ and $\psi = \theta - \hat{\theta}$ with its PDF defined in (2-14).

For the computation of the SNR threshold intervals, the joint PDF of α and $\hat{\alpha}$ and PDF of ψ should be known. For different channel estimation techniques, both distributions have different representations. For pilot symbol estimation technique, both α and $\hat{\alpha}$ are complex Gaussian random variables, their joint PDF is shown to be bivariate Rayleigh distribution and is given by (2-12) [48] [55].

The PDF of λ can be derived from (2-12) and is given to be

$$
\begin{aligned}
f(\lambda) &= \int_0^{\infty} \hat{\alpha} f_{\hat{\alpha},\alpha}(\lambda\hat{\alpha},\hat{\alpha})\,d\hat{\alpha} \\
&= \int_0^{\infty} \frac{4\lambda\hat{\alpha}^2}{(1-\rho)\Omega\hat{\Omega}} \exp\left[-\frac{1}{(1-\rho)}\left(\frac{\lambda^2\hat{\alpha}^2}{\Omega}+\frac{\hat{\alpha}^2}{\hat{\Omega}}\right)\right] I_0\left(\lambda\hat{\alpha}^2 \frac{\sqrt{\rho}}{(1-\rho)\sqrt{\Omega\hat{\Omega}}}\right) d\hat{\alpha}
\end{aligned}
\quad . \tag{3-14}
$$

Using integral representation [60]

$$
I_0(z) = \frac{1}{\pi} \int_{-\pi/2}^{\pi/2} e^{(-z\sin\delta)}\,d\delta\,, \tag{3-15}
$$

the PDF of λ can be obtained as

$$
f(\lambda) = \frac{4\lambda(1-\rho)W\left\{\left[W^2\tan^{-1}\sqrt{\frac{W+W_1}{W-W_1}} - \tan^{-1}\sqrt{\frac{W-W_1}{W+W_1}}\right] - W_1^2\left[\tan^{-1}\sqrt{\frac{W+W_1}{W-W_1}} + \tan^{-1}\sqrt{\frac{W-W_1}{W+W_1}}\right]\right\}}{\pi(W^2-W_1^2)^{3/2}\,\Omega\hat{\Omega}} \tag{3-16}
$$

where

$$
W = \frac{1}{\hat{\Omega}} + \frac{\lambda^2}{\Omega},\; W_1 = \frac{2\sqrt{\rho}}{\sqrt{\Omega\hat{\Omega}}}\lambda\,. \tag{3-17}
$$

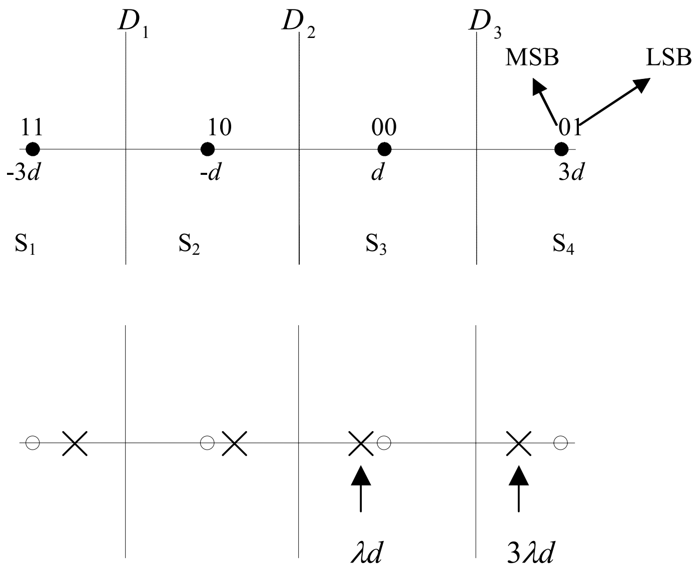

Fig.3.8 Signal points projected on in-phase direction

Under imperfect channel estimation with amplitude estimation error only, the recovered signal points projected onto the in-phase direction will deviate from the ideal position, as shown in Fig.3.8. A method similar to the computation of BER over AWGN channel is used to figure out the BER performance for a given value of λ. Taking 16-QAM as an example, for MSB bits, a bit error occurs when $n<-d$ for signal point S_3, $n<-3d$ for signal point S_4, $n>d$ for signal point S_2 and $n>3d$ for signal point S_1. For LSB, a bit error occurs when $3d-2d/\lambda<n<3d+2d/\lambda$ for S_1, $-2d/\lambda-3d<n<-2d/\lambda-3d$ for S_4, $n>2d/\lambda-d$ or $n<-2d\lambda-d$ for S_3, and, $n>2d/\lambda+d$ or $n<-2d/\lambda+d$ for S_2.

The conditional BER under a given λ is given by

$$p_{e|\lambda}=\sum_j w_j Q\left(\sqrt{\bar{\gamma}_s}\,(a_j+b_j/\lambda)\right). \tag{3-18}$$

The average BER under amplitude estimation error can be obtained by averaging (3-18) over λ and is given as

$$P_e = \int_{\lambda} \sum_{j} w_j \, Q\left(\sqrt{\bar{\gamma}_s}\,(a_j + b_j/\lambda)\right) f(\lambda)\, d\lambda \,. \tag{3-19}$$

The coefficients w_j, a_j, b_j are defined in Table A.1 to Table A.4 in Appendix A for various constellations respectively.

When both amplitude and phase estimation errors are present, the situation gets more tedious. Each signal point $I_j + jQ_j$ will undergo different degrees of impairment and has to be considered separately, as shown in Fig.3.9. However, the procedure of deriving the BER expression is the same for a given λ and ψ, followed by taking the average over the λ and ψ with their PDF defined in (3-16) and (2-14) respectively.

$$p_e = \int_{-2\pi}^{2\pi} \int_{\lambda=0}^{\infty} \sum_{j} Q\left\{\sqrt{\bar{\gamma}_s}\left[a_{1j}\cos\psi + a_{2j}\sin\psi) + b_j/\lambda\right]\right\} f(\lambda) f_{\psi}(\psi)\, d\lambda\, d\psi \,. \tag{3-20}$$

The coefficients of a_{1j}, a_{2j}, b_j, w_j are defined in Table A.5 to Table A.8 in Appendix A for various constellations respectively.

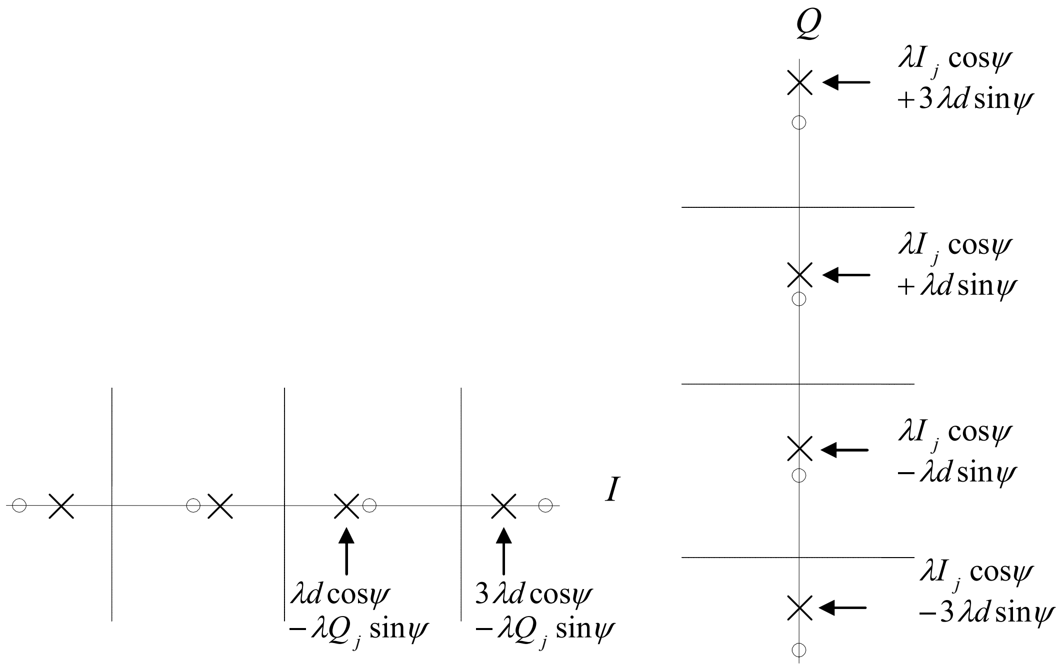

Fig.3.9 Signal points projected on I and Q direction with both amplitude and phase error

The BER performance curves obtained with channel estimation error are presented in Fig.3.10 to Fig.3.16 for different channel characteristics. Table 3.1 lists the minimum SNR for various MQAM constellations to achieve a BER performance of 10^{-3} under different channel estimation errors. The SNR threshold intervals for the selection of modulation constellation under imperfect channel estimation are shown in Table 3.2. It can be seen that the shift of SNR threshold intervals for higher order constellations is larger than that for lower order constellations, for given ρ and r. It is because that the higher order constellations are more sensitive to the same amount of error due to the smaller Euclidean distance between the signal points.

At low SNR, for given ρ and r, imperfect channel estimation causes negligible shift of SNR threshold intervals from that of perfect channel estimation since AWGN is the main impairment of source. From these BER performance curves, we can also see that error floor which is not observed in the BER performance curves under perfect channel estimation exist. This observation indicates that with channel estimation error, some higher order constellations ceases to be used since it cannot meet BER requirement, resulting in larger capacity loss. For example, as $\rho = 0.9999$, all four constellations can be employed. However, as $\rho = 0.999$, with amplitude error only, 64QAM cannot be used, while with amplitude and phase error, only BPSK and QPSK are the only constellations to meet the BER requirement of 10^{-3}. Fig.3.14 to Fig.3.16 show how the BER performance curves depend on r and ρ for various given average SNR $\bar{\gamma}_s$. The observation is that the dependence of BER on r is not noticeable as compared with correlation coefficient ρ.

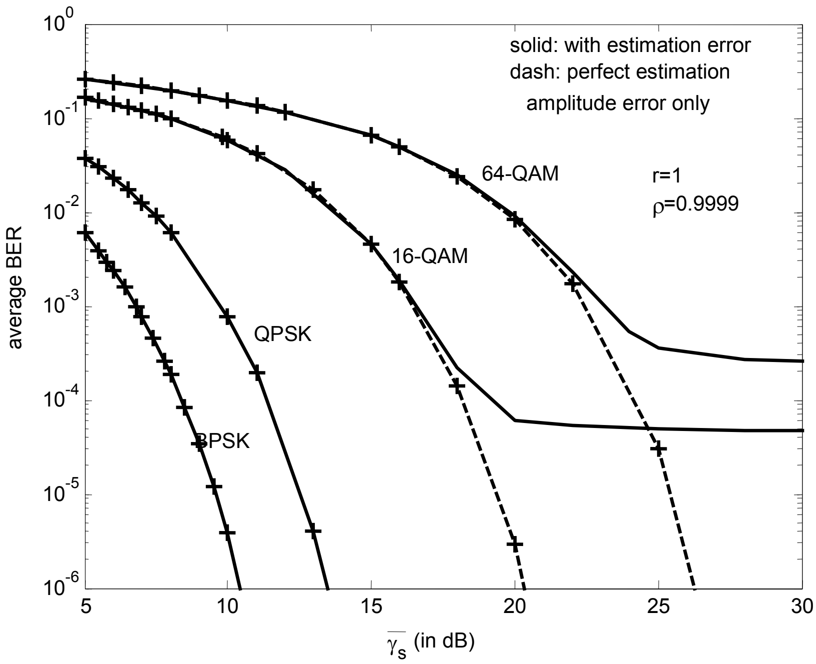

Fig.3.10 BER performance with amplitude estimation error $(\rho = 0.9999)$

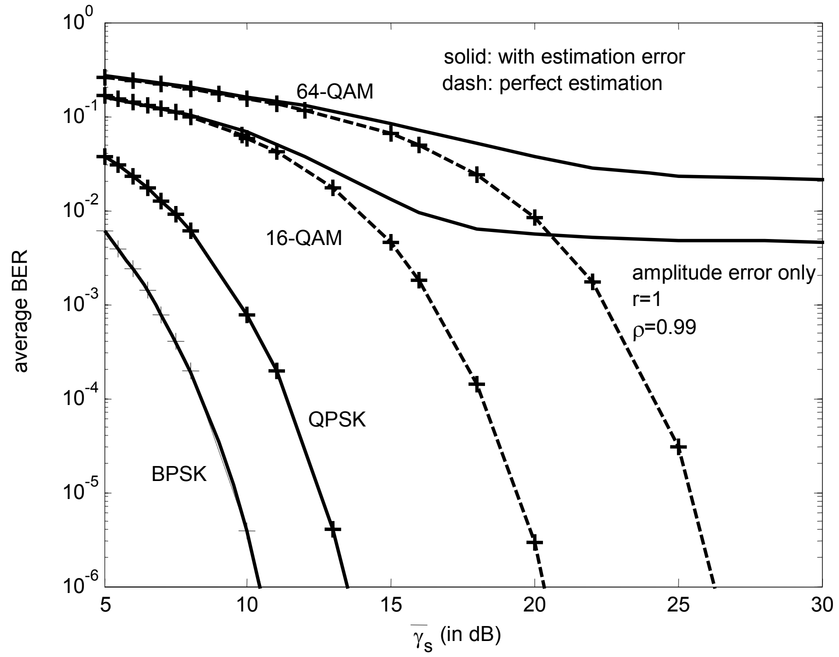

Fig.3.11 BER performance with amplitude estimation error $(\rho = 0.99)$

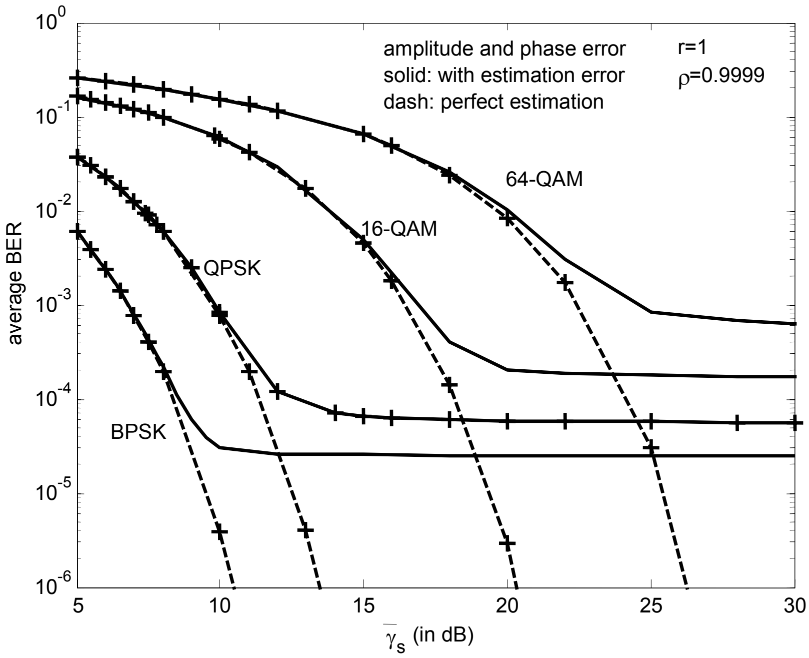

Fig.3.12 BER performance with amplitude and phase error $(\rho = 0.9999)$

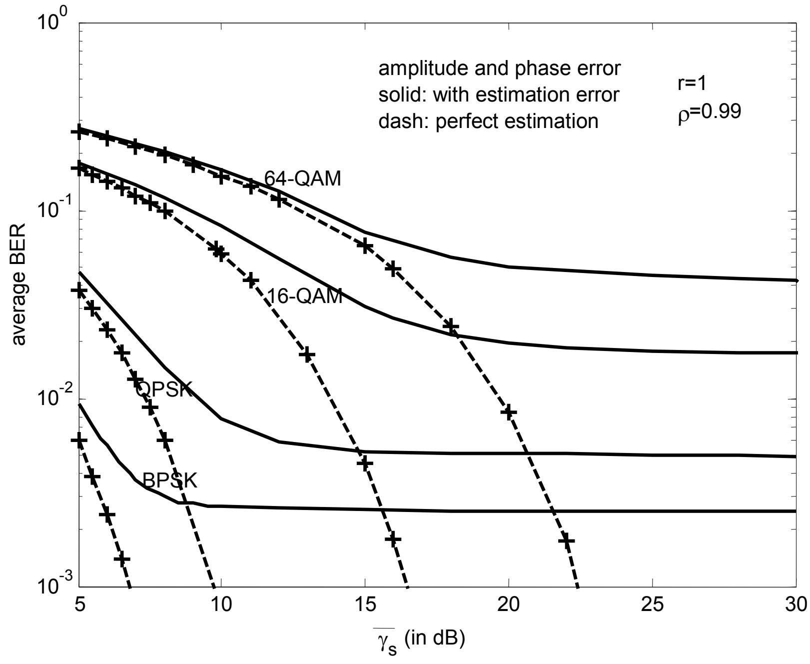

Fig.3.13 BER performance with amplitude and phase error ($\rho = 0.99$)

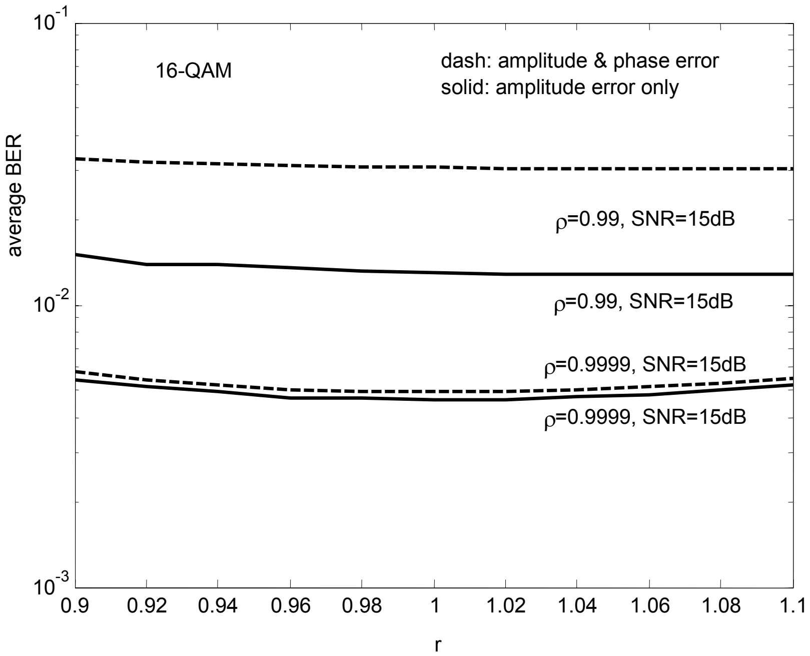

Fig.3.14 BER performance vs r

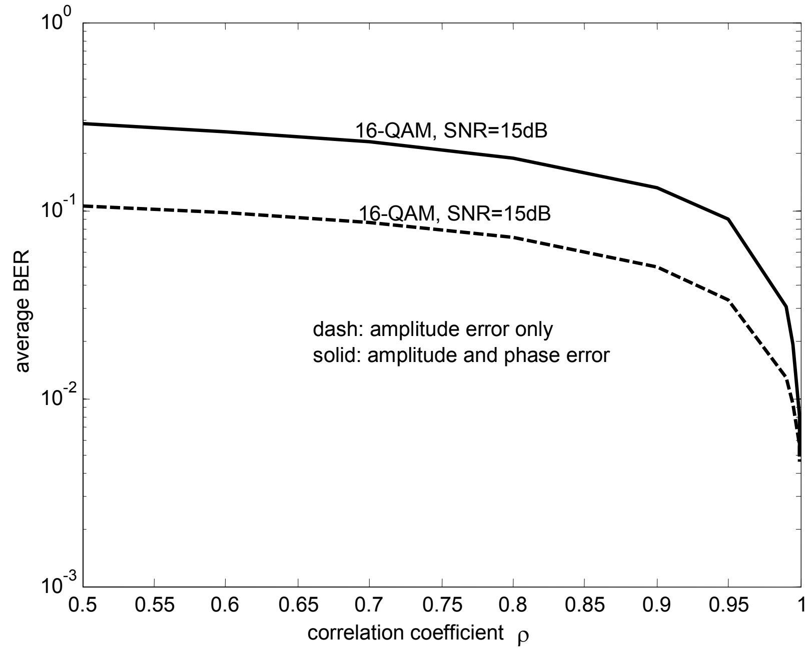

Fig.3.15 BER performance vs correlation coefficient ρ

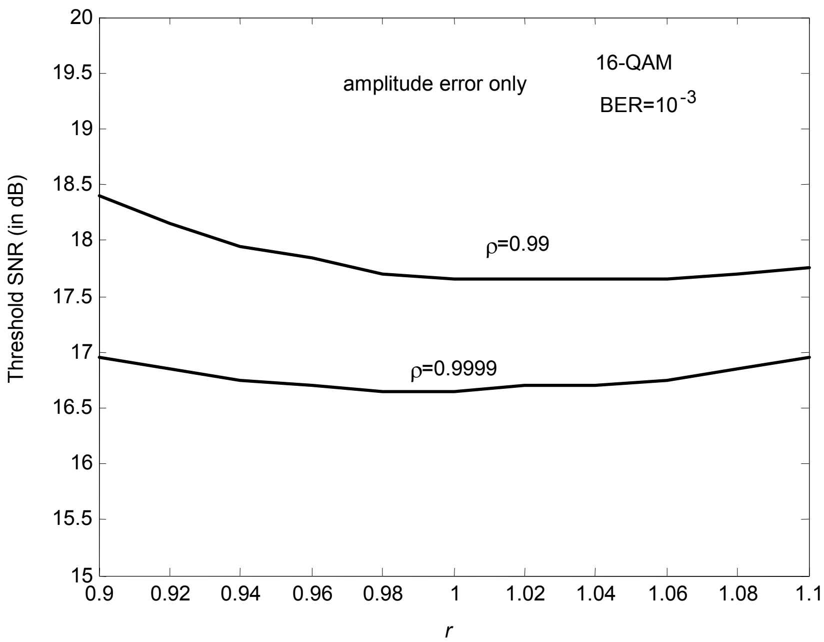

Fig.3.16 SNR threshold intervals vs r (for amplitude error only)

TABLE 3.1 Minimum SNR (in dB) for BER=10^{-3} with estimation error

$r=1$	Constellation size	$\rho=0.99$	$\rho=0.999$	$\rho=0.9999$
Amplitude error	BPSK	6.8	6.8	6.8
	QPSK	9.8	9.8	9.8
	16-QAM	X	17.65	16.65
	64-QAM	X	X	24
Amplitude and phase error	BPSK	X	7.1	6.85
	QPSK	X	10.7	9.9
	16-QAM	X	X	16.9
	64-QAM	X	X	25.8

Note: "X" means that this constellation size cannot satisfy the BER requirement due to the existence of error floor caused by estimation noise.

The SNR threshold intervals for the selection of M-QAM constellation to achieve BER=10^{-3} under imperfect channel estimation are listed in Table 3.2.

TABLE 3.2 SNR threshold intervals (in dB) for BER=10^{-3} with estimation error

Constellation bits/symbol i		Threshold interval	BPSK	QPSK	16-QAM	64-QAM
			1	2	4	6
Ideal estimation		$a_{th,i}^{new}$	6.8	9.8	16.6	22.6
		$b_{th,i}^{new}$	9.8	16.6	22.6	∞
Amplitude error	$\rho=0.9999$	$a_{th,i}^{new}$	6.8	9.8	16.65	24
		$b_{th,i}^{new}$	9.8	16.65	24	∞
	$\rho=0.999$	$a_{th,i}^{new}$	6.8	9.8	17.65	X
		$b_{th,i}^{new}$	9.8	17.65	∞	X
Amplitude & phase error	$\rho=0.9999$	$a_{th,i}^{new}$	6.9	9.9	16.9	25.8
		$b_{th,i}^{new}$	9.9	16.9	25.8	∞
	$\rho=0.999$	$a_{th,i}^{new}$	7.1	10.7	X	X
		$b_{th,i}^{new}$	10.7	∞	X	X

3.4.2 Channel capacity achieved under imperfect channel estimation

Once the new SNR threshold intervals under imperfect channel estimation are obtained for certain channel statistics, the channel capacity can be evaluated using (3-12), with the probability that one specific MQAM constellation is used being obtained as $P_i = \int_{a_{th,i}^{new}}^{b_{th,i}^{new}} f_\gamma(\gamma)d\gamma$, where $f_\gamma(\gamma)$ is the PDF of the received SNR and is defined in (3-9), with $\mu = \hat{\Omega}\bar{\gamma}_s$ and $\overline{\Omega}$ being the variance of the estimated fading gain. In this study, only four constellations BPSK, QPSK, 16QAM and 64QAM, are used.

Capacity obtained under imperfect channel estimation is shown in Fig.3.17. As average received SNR (μ) is small, for example below 18dB for amplitude error alone and 10dB for amplitude and phase error, the capacity loss caused by imperfect channel estimation is not significant. The reason is that, at low SNR, the shift of SNR threshold intervals caused by channel estimation error is marginal. And at low SNR, lower constellation, for example BPSK, dominates the transmission and less sensitive to estimation error. At higher SNR, the probability that higher order constellation is used increases, if perfect channel estimation is assumed. However, with estimation error, this probability decreases dramatically since higher order constellations are more sensitive to estimation error. In some cases the probability becomes zero. Significant capacity loss is then observed at high SNR.

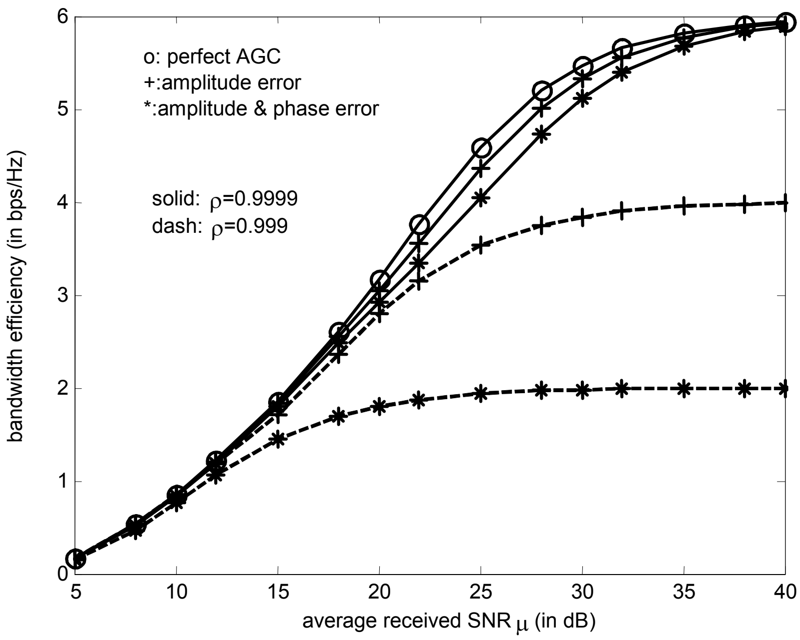

Fig.3.17 Capacity under certain degree of imperfect channel estimation (r=1, BER=10^{-3})

3.5 Effect of estimation error on capacity achieved by diversity reception and adaptive modulation

3.5.1 Diversity reception and combining techniques

Diversity reception is a promising technique designed to overcome channel fading by providing several replicas of the same information signal transmitted over different fading branches to receiver [61]. This concept exploits the fact that all diversity branches are simultaneously in deep fades is very low. A commonly used method to implement diversity reception is to use multiple antennas as shown in Fig.3.18. As these reception antennas are spaced sufficiently far apart, independently fading components of transmitted signal can be obtained. Combining techniques are then employed to form decision metric. The widely recognized diversity combining schemes are maximal ratio combining (MRC) [61], equal gain combining (EGC) [62] and selection combining (SC) [63]. The MRC combining maximizes the output SNR at the expense of implementation complexity. The SC scheme performs combining by selecting the strongest branch, however it achieves a lower diversity gain although it is considered as the least complicated means of combining. The symbol detection of diversity reception system is performed at the output of the combiner.

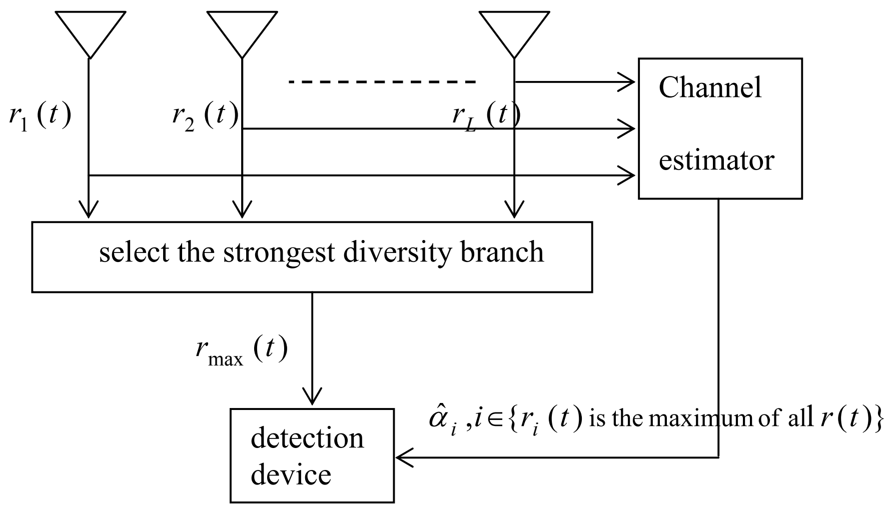

Fig. 3.18 A block diagram of SC diversity reception

As channel state information of all diversity branches are known at both receivers and transmitters, adaptive modulation can be combined with diversity reception technique to further improve system bandwidth efficiency, especially as there is a few receiver antennas [64]. When SC is used, the branch with the strongest received power is selected from all the diversity branches and this is assumed can be performed without decision error. The decision variable for coherent symbol detection is constructed based on the received signal of the selected branch. As adaptive modulation is used, the measured SNR of this branch is fed back to the transmitter, to control the parameters of the transmitted signal.

In this section, statistically independent and identical branches and SC combining are assumed. With SC combining, the combiner output is given by $r_c = r_i, i \in \{1,2,3,\cdots L\}$, with the ith branch selected based on the largest fading gain, i.e., $i = \arg[\max(\alpha_1, \alpha_2, \alpha_{i,} \cdots \alpha_L)]$. L is the number of diversity branch. The decision variable for symbol detection is then constructed as $r_d = r_c / \hat{\alpha}_i$.

3.5.2 Capacity achieved under perfect channel estimation

By employing SC technique, the output SNR under ideal channel estimation is expressed as [65]

$$f_\gamma(\gamma) = \sum_{k=1}^{L} \binom{L}{k} (-1)^{k-1} \frac{k}{\mu} \exp\left(-\frac{k\gamma}{\mu}\right), \tag{3-21}$$

where $\mu = \Omega \bar{\gamma}_s$ is the average received SNR per branch. With the SNR threshold intervals defined in Table 2.1, capacity can be easily calculated to be

$$C = \sum_i i \sum_{k=1}^{L} \binom{L}{k} (-1)^{k-1} \frac{k}{\mu} \left[\exp\left(-\frac{k a_{th,i}}{\mu}\right) - \exp\left(-\frac{k b_{th,i}}{\mu}\right) \right]. \tag{3-22}$$

Capacity obtained with SC technique is shown in Fig.3.19. It is seen that as more branches are employed in diversity reception, a higher channel capacity can be obtained.

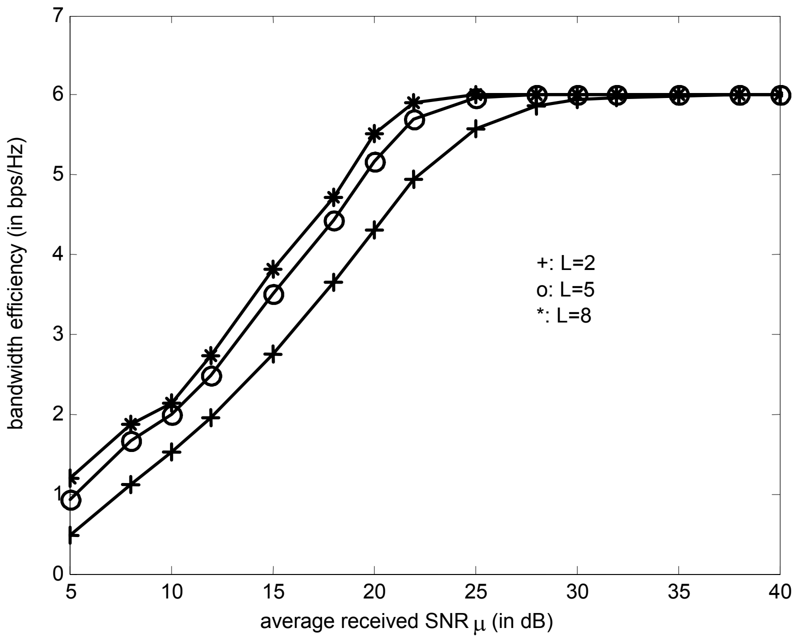

Fig.3.19 Capacity achieved for SC combining under perfect channel estimation

3.5.3 Capacity achieved under imperfect channel estimation

To investigate the effect of channel estimation error, the joint PDF of true channel fading gain $\alpha_{\max}$ and the estimated fading gain $\hat{\alpha}_{\max}$ will be derived first.

The joint cumulative distribution function (CDF) between $\alpha_{\max}$ and $\hat{\alpha}_{\max}$ can be expressed as

$$\begin{aligned} F_{\alpha_{\max},\hat{\alpha}_{\max}}(\alpha_{\max},\hat{\alpha}_{\max}) &= \sum_{i=1}^{L} P(\alpha_i \le \alpha_{\max}, \hat{\alpha}_i \le \hat{\alpha}_{\max} \mid \alpha_i \text{ is the maximum}) P(\alpha_i \text{ is the maximum}) \\ &= \sum_{i=1}^{L} P(\alpha_i \le \alpha_{\max}, \hat{\alpha}_i \le \hat{\alpha}_{\max}, \alpha_i \text{ is the maximum}) \\ &= \sum_{i=1}^{L} P(\alpha_i \le \alpha_{\max}, \hat{\alpha}_i \le \hat{\alpha}_{\max}, \alpha_1 \le \alpha_i, \alpha_2 \le \alpha_i, \cdots, \alpha_L \le \alpha_i) \end{aligned} \tag{3-23}$$

where L is the number of diversity branches and $P(X)$ is the probability of event X, and

$$P_{\alpha_{\max},\hat{\alpha}_{\max}}(\alpha_i \le \alpha_{\max}, \hat{\alpha}_i \le \hat{\alpha}_{\max}, \alpha_1 \le \alpha_i, \alpha_2 \le \alpha_i, \cdots, \alpha_L \le \alpha_i) = \int_0^{\alpha_{\max}} \int_0^{\hat{\alpha}_{\max}} \int_0^{\alpha_i} \int_0^{\alpha_i} \cdots \int_0^{\alpha_i}$$
$$f_{\alpha_i,\hat{\alpha}_i,\alpha_1,\alpha_2,\cdots,\alpha_L}(\alpha_i, \hat{\alpha}_i, \alpha_1, \alpha_2, \cdots, \alpha_L) d\alpha_i d\hat{\alpha}_i d\alpha_1 d\alpha_2 \cdots d\alpha_L \tag{3-24}$$

$$f_{\alpha_i,\hat{\alpha}_i,\alpha_1,\alpha_2,\cdots\alpha_L}(\alpha_i, \hat{\alpha}_i, \alpha_1, \alpha_2, \cdots, \alpha_L) = f_{\alpha_i,\hat{\alpha}_i}(\alpha_i, \hat{\alpha}_i) f_{\alpha_1,\alpha_2,\cdots\alpha_{j\ne i},\cdots\alpha_L}(\alpha_1, \alpha_2, \cdots \alpha_{j\ne i}, \cdots, \alpha_L)$$
$$= f_{\alpha_i,\hat{\alpha}_i}(\alpha_i, \hat{\alpha}_i) f_{\alpha_1}(\alpha_1) f_{\alpha_2}(\alpha_2) \cdots f_{\alpha_{j\ne i}}(\alpha_{j\ne i}) \cdots f_{\alpha_L}(\alpha_L) \tag{3-25}$$

In (3-25), $f_{\alpha_i,\hat{\alpha}_i}(\alpha_i, \hat{\alpha}_i)$ is the joint PDF of α_i and $\hat{\alpha}_i$, and $f_\alpha(\alpha)$ is the PDF of fading gain taking any distribution described in Chapter II.

$$P(\alpha_i \le \alpha_{\max}, \hat{\alpha}_i \le \hat{\alpha}_{\max}, \alpha_1 \le \alpha_i, \alpha_2 \le \alpha_i, \cdots, \alpha_L \le \alpha_i) = \int_0^{\alpha_{\max}} \int_0^{\hat{\alpha}_{\max}} \int_0^{\alpha_i} \int_0^{\alpha_i} \cdots \int_0^{\alpha_i}$$
$$f_{\alpha_i,\hat{\alpha}_i}(\alpha_i, \hat{\alpha}_i) f_{\alpha_1}(\alpha_1) f_{\alpha_2}(\alpha_2) \cdots f_{\alpha_{j\ne i}}(\alpha_{j\ne i}) \cdots f_{\alpha_L}(\alpha_L) d\alpha_i d\hat{\alpha}_i d\alpha_1 d\alpha_2 \cdots d\alpha_L$$

$$= \int_0^{\alpha_{\max}} \int_0^{\hat{\alpha}_{\max}} f_{\alpha_i,\hat{\alpha}_i}(\alpha_i, \hat{\alpha}_i) \prod_{j=1, j\ne i}^{L} F_{\alpha_i}(\alpha_i) d\alpha_i d\hat{\alpha}_i \tag{3-26}$$

where $F_{\alpha_i}(\alpha_i)$ is CDF of α_i. The joint PDF of α_i and $\hat{\alpha}_i$ is therefore given by

$$f_{\alpha_{\max},\hat{\alpha}_{\max}}(\alpha_{\max}, \hat{\alpha}_{\max}) = \frac{\partial^2 F_{\alpha_{\max},\hat{\alpha}_{\max}}(\alpha_{\max}, \hat{\alpha}_{\max})}{\partial \alpha_{\max} \partial \hat{\alpha}_{\max}}$$
$$= \sum_{i=1}^{L} \frac{\partial^2 P(\alpha_i \le \alpha_{\max}, \hat{\alpha}_i \le \hat{\alpha}_{\max}, \alpha_1 \le \alpha_i, \alpha_2 \le \alpha_i \cdots \alpha_L \le \alpha_i)}{\partial \alpha_{\max} \partial \hat{\alpha}_{\max}}$$
$$= \sum_{i=1}^{L} \left\{ f_{\alpha,\hat{\alpha}}(\alpha_{\max}, \hat{\alpha}_{\max}) \prod_{j=1, j\ne i}^{L} F_\alpha(\alpha_{\max}) \right\} \tag{3-27}$$

Assuming that all α and $\hat{\alpha}$ follow Rayleigh distribution, the joint PDF of $\alpha_{\max}$ and $\hat{\alpha}_{\max}$ can be obtained as

$$f_{\alpha_{\max},\hat{\alpha}_{\max}}(\alpha_{\max},\hat{\alpha}_{\max}) = \frac{L4\alpha_{\max}\hat{\alpha}_{\max}}{(1-\rho)\Omega\hat{\Omega}} \exp\left[-\frac{1}{1-\rho}\left(\frac{\alpha_{\max}^2}{\Omega}+\frac{\hat{\alpha}_{\max}^2}{\hat{\Omega}}\right)\right] I_0\left[\frac{\sqrt{\rho}\alpha_{\max}\hat{\alpha}_{\max}}{(1-\rho)\sqrt{\Omega\hat{\Omega}}}\right]\cdot$$

$$\left[1 - \exp\left(-\frac{\alpha_{\max}^2}{\Omega}\right)\right]^{L-1} \tag{3-28}$$

With this joint PDF, the SNR threshold intervals for the selection of MQAM constellation can be obtained following the method in Section 3.4. However, the PDF of $\lambda = \alpha_{\max} / \hat{\alpha}_{\max}$ is difficult to derive where L becomes larger.

Consider a two-antenna system, (3-28) is rewritten as

$$f_{\alpha_{\max},\hat{\alpha}_{\max}}(\alpha_{\max},\hat{\alpha}_{\max}) = \frac{L4\alpha_{\max}\hat{\alpha}_{\max}}{(1-\rho)\Omega\hat{\Omega}} \exp\left[-\frac{1}{1-\rho}\left(\frac{\alpha_{\max}^2}{\Omega}+\frac{\hat{\alpha}_{\max}^2}{\hat{\Omega}}\right)\right] I_0\left[\frac{\sqrt{\rho}\alpha_{\max}\hat{\alpha}_{\max}}{(1-\rho)\sqrt{\Omega\hat{\Omega}}}\right]\left[1 - \exp\left(-\frac{\alpha_{\max}^2}{\Omega}\right)\right]$$

$$= Lf_{\alpha_{\max},\hat{\alpha}_{\max}}(\alpha_{\max},\hat{\alpha}_{\max}) - Lf^1_{\alpha_{\max},\hat{\alpha}_{\max}}(\alpha_{\max},\hat{\alpha}_{\max})\,. \tag{3-29a}$$

Similar to (3-16), the PDF of λ is derived to be

$$f_{L=2}(\lambda) = f(\lambda) - f^1(\lambda)\,, \tag{3-29b}$$

where $f(\lambda)$ and $f^1(\lambda)$ are the PDF of λ obtained for the first term and second term of (3-29a), respectively. $f(\lambda)$ is defined in (3-16) and

$$f^1(\lambda) = \frac{4\lambda(1-\rho)W_2\left\{\left[W_2^2\tan^{-1}\sqrt{\dfrac{W_2+W_1}{W_2-W_1}} - \tan^{-1}\sqrt{\dfrac{W_2-W_1}{W_2+W_1}}\right] - W_1^2\left[\tan^{-1}\sqrt{\dfrac{W_2+W_1}{W_2-W_1}} + \tan^{-1}\sqrt{\dfrac{W_2-W_1}{W_2+W_1}}\right]\right\}}{\pi(W_2^2-W_1^2)^{3/2}\Omega\hat{\Omega}} \tag{3-30}$$

where $W_2 = \frac{1}{\hat{\Omega}} + \frac{\lambda^2}{\Omega}(2-\rho)$, $W_1 = \frac{2\sqrt{\rho}}{\sqrt{\Omega\hat{\Omega}}}\lambda$.

Now we proceed to derive the joint PDF of $\theta_{\max}$ and $\hat{\theta}_{\max}$. The CDF. of $\theta_{\max}$ and $\hat{\theta}_{\max}$ can be expressed as

$$F_{\theta_{\max},\hat{\theta}_{\max}}(\theta_{\max},\hat{\theta}_{\max}) = \sum_{i=1}^{L} P(\theta_i \le \theta_{\max}, \hat{\theta}_i \le \hat{\theta}_{\max} \mid \alpha_i \text{ is the maximum}) P(\alpha_i \text{ is the maximum}) \,. \tag{3-31}$$

Since α_i and θ_i are independent, (31) can be rewritten as

$$F_{\theta_{\max},\hat{\theta}_{\max}}(\theta_{\max},\hat{\theta}_{\max}) = \sum_{i=1}^{L} P(\theta_i \le \theta_{\max}, \hat{\theta}_i \le \hat{\theta}_{\max}) P(\alpha_i \text{ is the maximum}) \,. \tag{3-32}$$

Since all branches experience identical and independent channel fading,

$$P(\alpha_i \text{ is the maximum}) = \frac{1}{L}, \tag{3-33}$$

$$P(\theta_i \le \theta_{\max}, \hat{\theta}_i \le \hat{\theta}_{\max}) = F_{\theta_i,\hat{\theta}_i}(\theta_{\max},\hat{\theta}_{\max}), \tag{3-34}$$

where $F_{\theta_i,\hat{\theta}_i}(\theta_{\max},\hat{\theta}_{\max})$ is the CDF of θ_i and $\hat{\theta}_i$. Substitute (3-33) and (3-34) into (3-32), and take derivative with respect to $\theta_{\max}$ and $\hat{\theta}_{\max}$, the joint PDF of $\theta_{\max}$ and $\hat{\theta}_{\max}$ is obtained as

$$f_{\theta_{\max},\hat{\theta}_{\max}}(\theta_{\max},\hat{\theta}_{\max}) = f_{\theta,\hat{\theta}}(\theta_{\max},\hat{\theta}_{\max}), \tag{3-35}$$

where $f_{\theta,\hat{\theta}}(\theta_{\max},\hat{\theta}_{\max})$ is defined in (2-13). Hence the PDF of $\psi_{\max} = \theta_{\max} - \hat{\theta}_{\max}$ is also described by (2-14).

The SNR threshold intervals for SC technique with imperfect channel estimation can be obtained using (3-19) and (3-20), with $f(\lambda)$ derived from (3-29b) and $f_\psi(\psi)$ defined by in (2-14). With the knowledge of the SNR threshold intervals under the consideration of channel estimation error, system capacity can then be calculated as

$$C = \sum_i i \int_{a_{th,i}^{SC}}^{b_{th,i}^{SC}} f_\gamma(\gamma) d\gamma , \tag{3-36}$$

where $a_{th,i}^{SC}, b_{th,i}^{SC}$ are the SNR threshold intervals obtained for SC combining technique and $f_\gamma(\gamma)$ is defined in (3-21) with $\mu = \hat{\Omega}\bar{\gamma}_s$.

The BER performance curves obtained for SC technique under imperfect channel estimation are shown in Fig.3.20 to Fig.3.23. BER performance is more sensitive to imperfect channel estimation with both amplitude and phase errors. Compared to BER performance curves shown in Fig.3.10 to Fig.3.13, the combining technique can be seen to reduce the effect of channel estimation error on the SNR threshold intervals, as shown in Fig.3.22. This is achieved at the cost of implementation complexity caused by diversity reception. The SNR threshold intervals for SC combining are listed in Table 3.3.

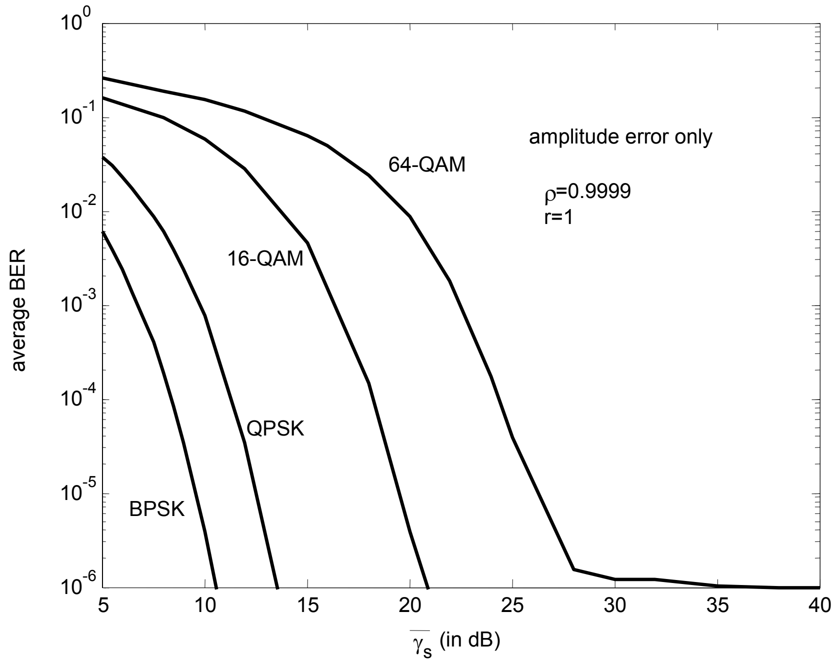

Fig.3.20 BER performance with amplitude error with diversity reception($\rho = 0.9999$*)*

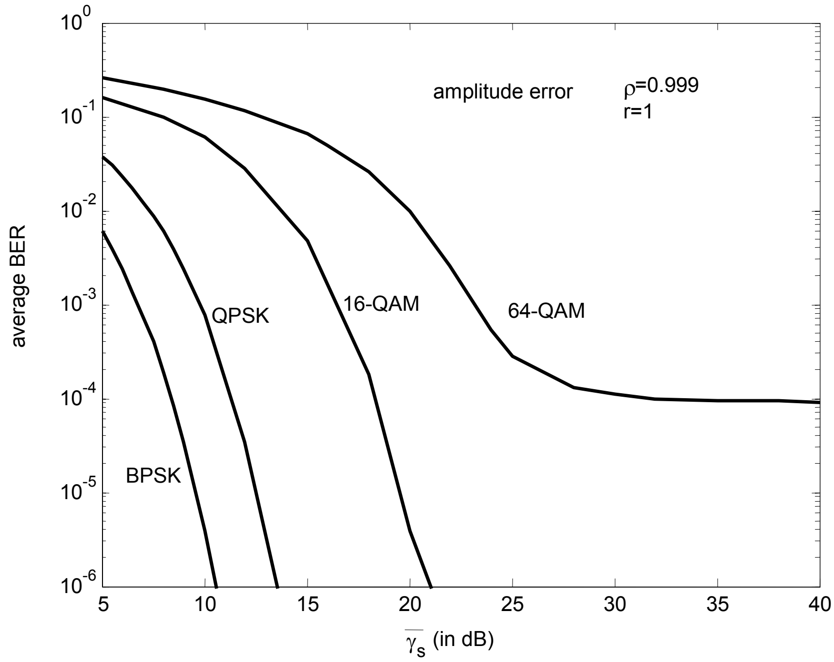

Fig.3.21 BER performance with amplitude error with diversity reception ($\rho = 0.999$*)*

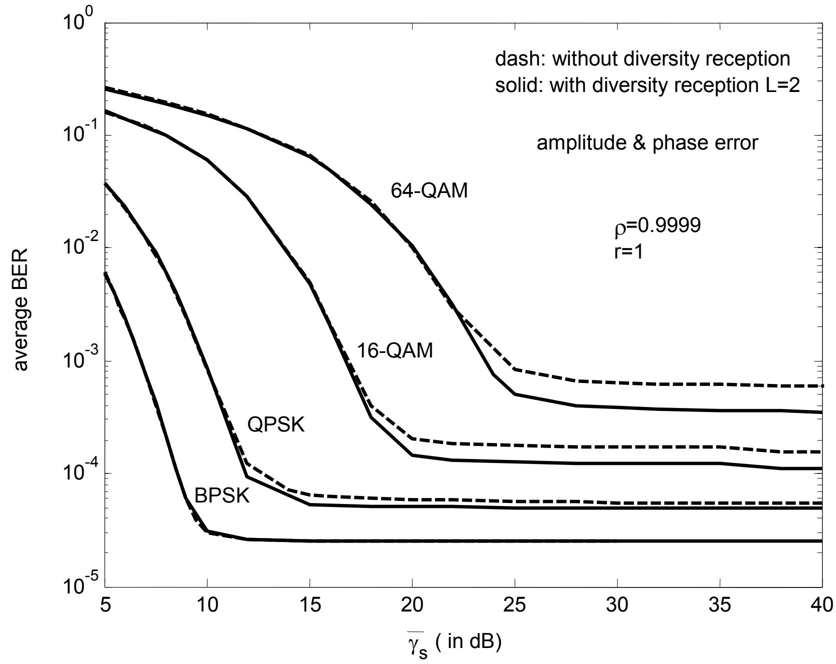

Fig.3.22 BER with amplitude and phase error (diversity reception, $\rho = 0.9999$)

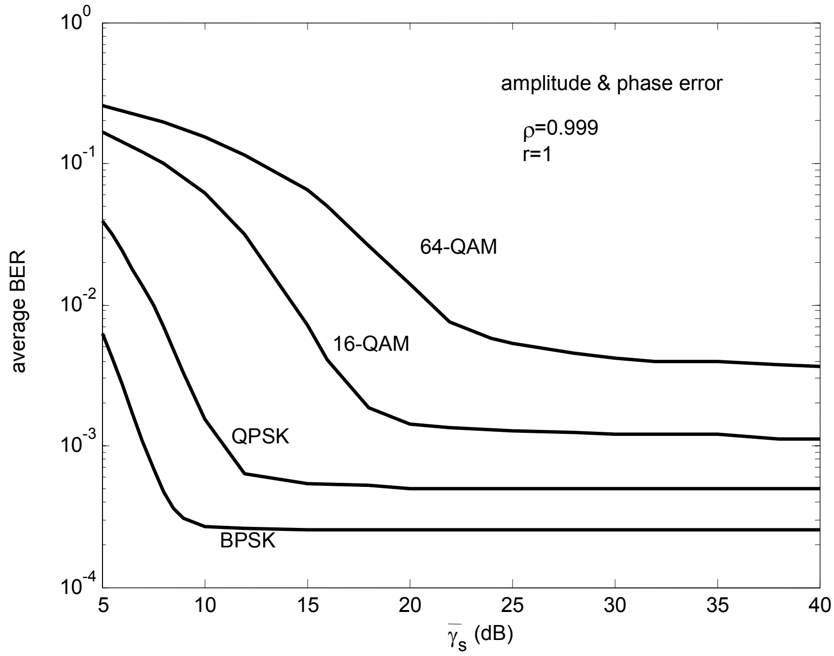

Fig.3.23 BER performance with amplitude and phase error (diversity reception $\rho = 0.999$)

TABLE 3.3 SNR threshold intervals for BER=10^{-3} for SC

Constellation Bits/symbol I		Threshold interval	BPSK 1	QPSK 2	16-QAM 4	64-QAM 6
Ideal estimation		$a_{th,i}^{SC}$	6.8	9.8	16.6	22.6
		$b_{th,i}^{SC}$	9.8	16.6	22.6	∞
Amplitude error	$\rho=0.9999$	$a_{th,i}^{SC}$	6.8	9.8	16.65	23
		$b_{th,i}^{SC}$	9.8	16.65	23	∞
	$\rho=0.999$	$a_{th,i}^{SC}$	6.8	9.8	17	24.5
		$b_{th,i}^{SC}$	9.8	17	24.5	∞
Amplitude &phase error	$\rho=0.9999$	$a_{th,i}^{SC}$	6.9	9.9	16.9	24.8
		$b_{th,i}^{SC}$	9.9	16.9	24.8	∞
	$\rho=0.999$	$a_{th,i}^{SC}$	7.1	9.9	x	x
		$b_{th,i}^{SC}$	9.9	∞	x	x

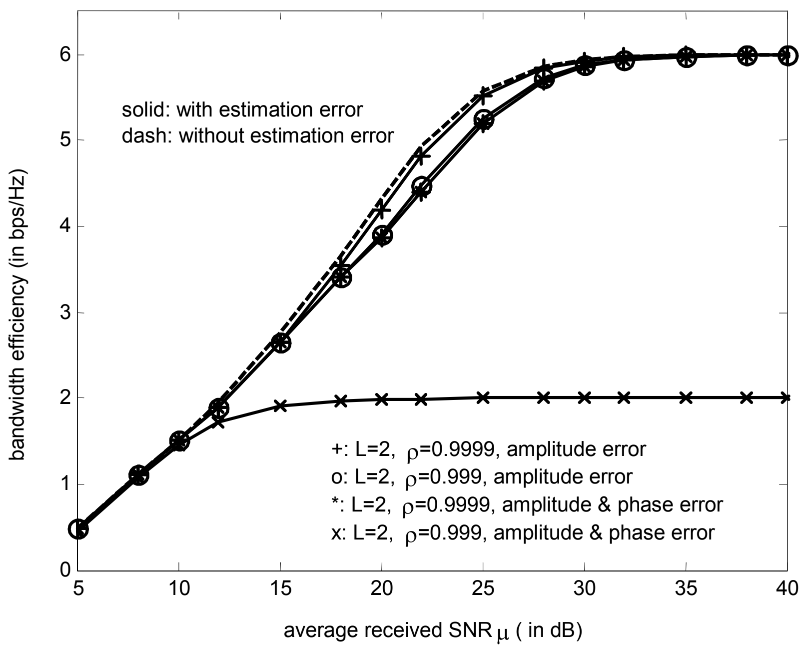

Fig.3.24 Capacity achieved with diversity reception under channel estimation error

Capacity achieved under imperfect channel estimation is shown in Fig.3.24. Compared with Fig.3.17, it can be seen that diversity reception slightly improves the capacity of adaptive modulation system under imperfect channel estimation for $L = 2$.

3.6 Summary

The Shannon capacity and the capacity achieved by adaptive MQAM technique have been investigated under single user environment. In the context of Shannon limit, it is observed that an adaptive rate adaptive power system achieves insignificant capacity gain over an adaptive rate system. The framework to study the effect of imperfect channel estimation on the capacity of a rate adaptive modulation system is proposed. The proposed framework enables designers to obtain the extra SNR margins needed in defining the SNR threshold intervals through analysis based on different channel and estimation statistics rather than assuming a few dB obtained by experiences. An equivalent receiver circuit is constructed where the effect of imperfect channel estimation is converted to an imperfect IQ receiver structure.

The proposed framework is then applied to the capacity analysis of rate adaptive MQAM systems with and without diversity reception. The SNR threshold intervals with channel estimation error are obtained. Under imperfect channel estimation, capacity loss is caused by the need to increase the link margin to overcome the effect of estimation error. Moreover, with imperfect channel estimation, some higher order modulation cannot be employed due to the error floor hence significant drop in achievable capacity is observed.

CHAPTER IV

CAPACITY OF RATE ADAPTIVE MODULATION SYSETM OVER MULTIPLE ACCESS FADING CHANNEL

As multiple users are allowed to share the radio link, the optimum channel allocation is that only the user observing the best channel conditions is allowed to transmit at any given transmission interval over the entire bandwidth [32]. The bandwidth efficiency, performance metrics such as the time duration for the fading process to stay in a particular MQAM constellation and the channel inter-access time of the optimal scheme are studied. A SNR-priority-based suboptimal channel allocation scheme which allows a number of users to share the bandwidth is then proposed to effectively reduce the channel inter-access time. A dual-class channel allocation scheme is further proposed to accommodate two classes of service. The capacity and the system throughput obtained by employing both the proposed channel allocation schemes and rate adaptive MQAM technique are studied. Although the schemes studied here are simple, no thorough analysis was performed before and hence is the main contribution of this chapter.

4.1 Channel capacity achieved by the optimal power allocation under multiple access environment

Under a multiple access environment, users are randomly located within a cell. The transmission environment varies vastly from user to user. Hence each user in the system experiences a different degree of fading at an observation time, making some users sensing better channel conditions than others. This observation leads to the possibility of employing a channel allocation scheme by allowing the user with the best instantaneous channel conditions to transmit at any transmission interval to improve bandwidth efficiency. The realization of such channel allocation scheme requires the base station to have the knowledge of channel state information for all mobile links in order to decide which mobile user is to transmit. In other words, to facilitate the operation of such a system, the BS should keep track of channel conditions for all users, and coordinate the transmission to make use of user diversity. Moreover, the channel state information is used not only for the selection of modulation mode at the transmitter but also for the channel allocation as shown in Fig. 4.1.

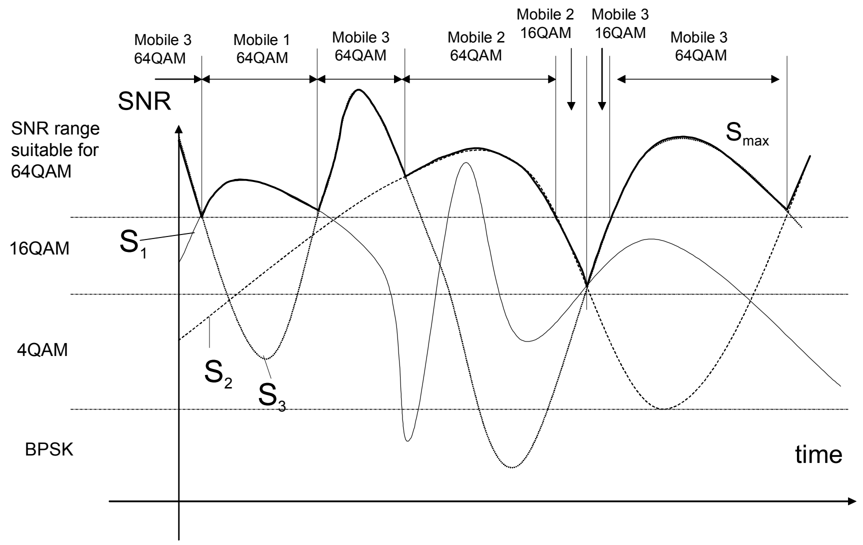

Fig.4.1 An illustration of channel allocation and modulation mode selection

Considering an isolated cell, where performance of the receiver is determined only by the received SNR. To make analysis free from the spatial distribution of mobile users over the cell, we assume that the BS performs regular ranging hence the distance between mobile users and the BS is known. Thus path loss can be accurately compensated for and the average received SNR for each mobile can be assumed to be independent and identically distributed (i.i.d.).

Let γ_m be the random variable denoting the instantaneous received SNR for the *m*th mobile (which is proportional to the square of the signal envelope, X_m). The PDF and CDF of γ_m are denoted by $f_{\gamma_m}(\gamma)$ and $F_{\gamma_m}(\gamma)$ respectively. Mathematically, the maximum SNR received at BS among N users, $\gamma_{\max}$, is given by

$$\gamma_{\max} = \max(\gamma_1, \gamma_2, \cdots \gamma_N). \tag{4-1}$$

The CDF of $\gamma_{\max}$ could be derived as

$$F_{\gamma_{\max}}(\gamma_{\max} < \gamma) = P(\gamma_1 < \gamma, \gamma_2 < \gamma, \cdots, \lambda_N < \gamma) = \prod_{m=1}^{N}[F_{\gamma_m}(\gamma_m < \gamma)]. \tag{4-2}$$

As γ_ms $(m = 1 \cdots N)$ are i.i.d., PDF of $\gamma_{\max}$ is obtained by taking the derivative of (4-2),

$$f_{\gamma_{\max}}(\gamma) = N[F_{\gamma_m}(\gamma_m < \gamma)]^{N-1} f_{\gamma_m}(\gamma). \tag{4-3}$$

As the adaptive power adaptive rate technique is employed, the Shannon capacity achieved by this optimal power control scheme is

$$C_{Shannon} = B\int_0^{\infty} f_{\gamma\max}(\gamma) \cdot \log_2 \frac{\gamma}{\gamma_0} d\gamma, \tag{4-4a}$$

where γ_0 is defined by $\int_{\gamma_0}^{\infty}\left(\frac{\bar{p}}{\gamma_0} - \frac{\bar{p}}{\gamma}\right) f_{\gamma_{\max}}(\gamma) d\gamma = \bar{p}$.

By assuming a constant transmission power rate adaptation system, the Shannon capacity achieved by this optimal channel allocation scheme is

$$C_{Shannon} = B\int_0^{\infty} f_{\gamma_{\max}}(\gamma)\cdot\left[\log_2(1+\gamma)\right]d\gamma \,. \tag{4-4b}$$

The BER performance of MQAM under AWGN is bounded by [49]

$$BER \le 0.2\exp\left[-1.5\gamma/(M-1)\right], \tag{4-5}$$

where M is the constellation size. If we assume that M in (4-5) can take any real value depending on the received SNR γ, or mathematically

$$M(\gamma) = 1 - 1.5\gamma/\ln(5\cdot BER)\,. \tag{4-6}$$

The channel capacity using MQAM technique without constellation constraint to satisfy a predefined BER performance is thus obtained by averaging over the fading statistics, or mathematically,

$$C_T = B\cdot E\left[\log_2 M(\gamma)\right] = B\cdot\int_0^{\infty} f_{\gamma_{\max}}(\gamma)\cdot\left[\log_2 M(\gamma)\right]\cdot d\gamma \,. \tag{4-7}$$

C_T gives the upper bound on the channel capacity when MQAM transmitter is used. In practical, $M = 2^i$ and it takes only some finite integers. In this study, i=1, 2, 4, 6, 8 are used. We partition $\gamma_{\max}$ into a finite number of SNR intervals $[a_{th,i}, b_{th,i})$ as shown in Fig.4.1. Each interval is associated with one constellation and only the constellation that can meet the minimum BER performance is assigned. The probability that a MQAM constellation is used is given by

$$P_i = \int_{a_{th,i}}^{b_{th,i}} f_{\gamma_{\max}}(\gamma)d\gamma \,, \tag{4-8}$$

where $a_{th,i}, b_{th,i}$ take on the values given in Table 2.1. The channel capacity with constellation constraint is given to be

$$C_{QAM} = \sum_{i=1}^{k} iB \cdot P_i \ . \qquad (4\text{-}9)$$

It is expected that $C_{QAM} < C_T < C_{Shannon}$.

4.1.1 Capacity achieved over Rayleigh fading channel

For Rayleigh fading channel, the PDF of SNR for the *m*th user is given by (3-9), while the CDF is given as $F(\gamma) = 1 - \exp(1 - \gamma / \mu)$. The PDF of $\gamma_{\max}$ is then obtained as

$$f_{\gamma_{\max}}(\gamma) = N\left[1 - \exp(-\frac{\gamma}{\mu})\right]^{N-1} \frac{1}{\mu}\exp(-\frac{\gamma}{\mu}). \qquad (4\text{-}10)$$

Fig.4.2 illustrates the PDF of $\gamma_{\max}$ under different channel conditions.

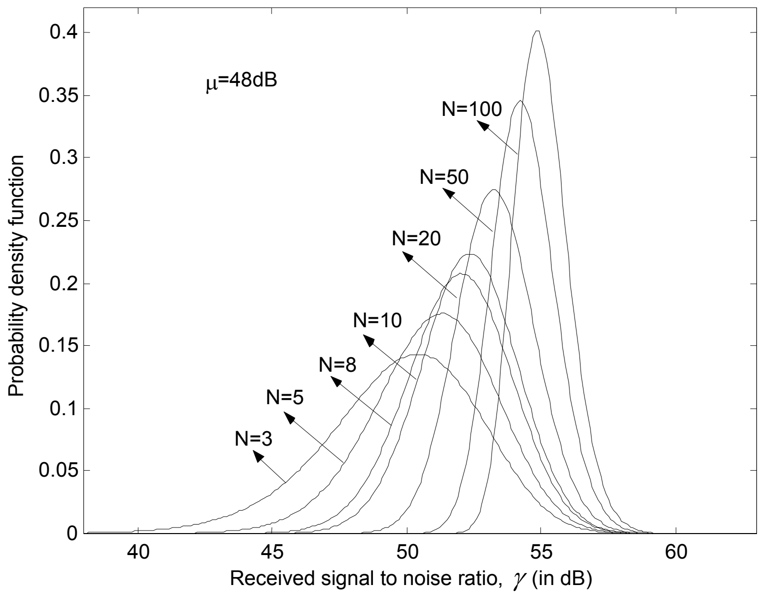

Fig.4.2 Illustration of PDF of $\gamma_{\max}$ over Rayleigh fading channel

The probability that one QAM constellation being used is given by

$$P_i = \int_{a_{th,i}}^{b_{th,i}} f_{\gamma_{\max}}(\gamma)d\gamma = \left[1-\exp(-\frac{b_{th,i}}{\mu})\right]^N - \left[1-\exp(-\frac{a_{th,i}}{\mu})\right]^N . \tag{4-11}$$

Channel capacities can therefore be calculated using (4-4b), (4-7) and (4-9). The results are shown in Fig.4.3 and Fig.4.4. It can be seen from Fig.4.3 and Fig.4.4 that as more users are allowed to contend for the access of channel, higher capacity can be obtained. It shows that C_{QAM} approaches $8B$ with only a few users at high received SNR. This is because at high received SNR, the channel condition is so good that higher level constellation (i>8) can be used but we are confined to $i \le 8$ in our example. On the other hand, C_T continues to increase since we do not restrict the maximum value of i used. The difference in capacities given by (4-7) and (4-9) shown in Fig.4.3 is due to the limited number of signal constellation used.

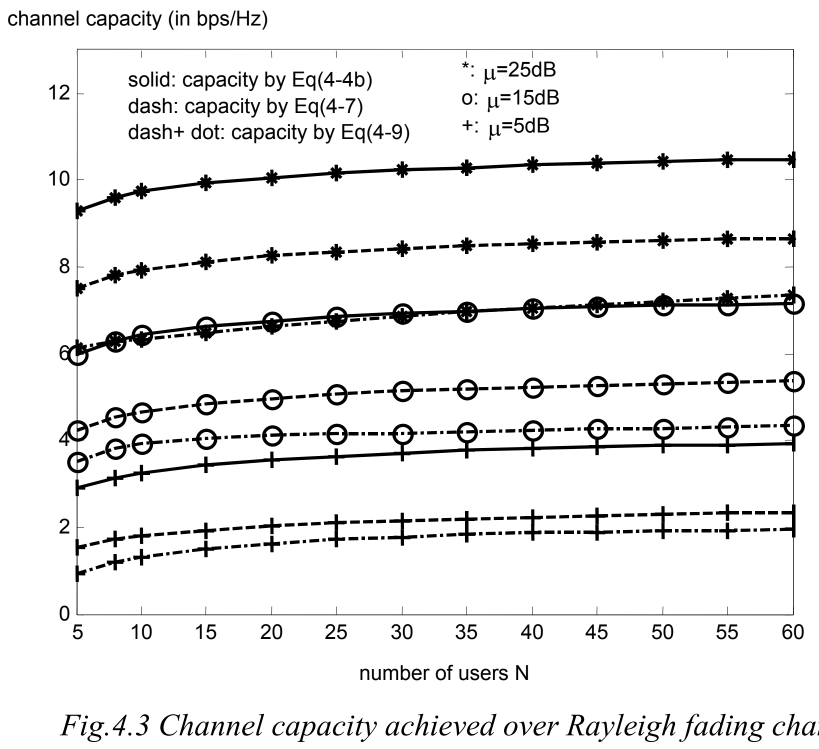

Fig.4.3 Channel capacity achieved over Rayleigh fading channel

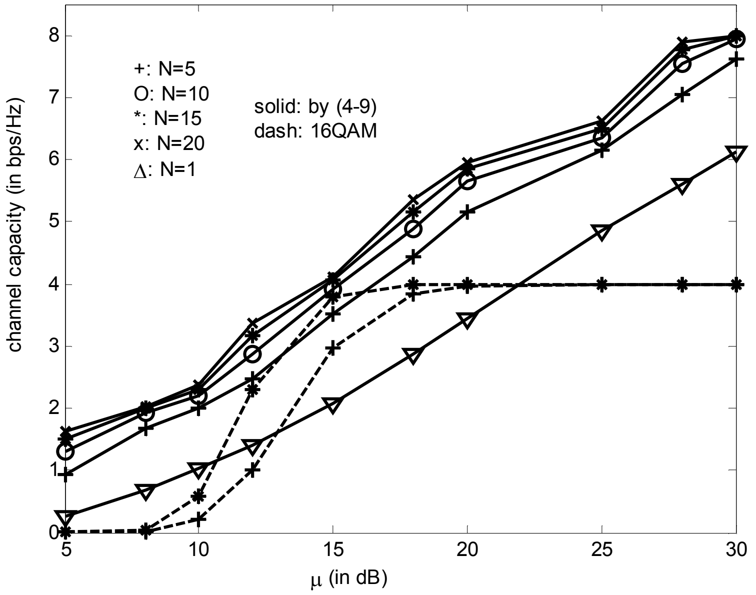

Fig.4.4 Channel capacity employing adaptive MQAM technique

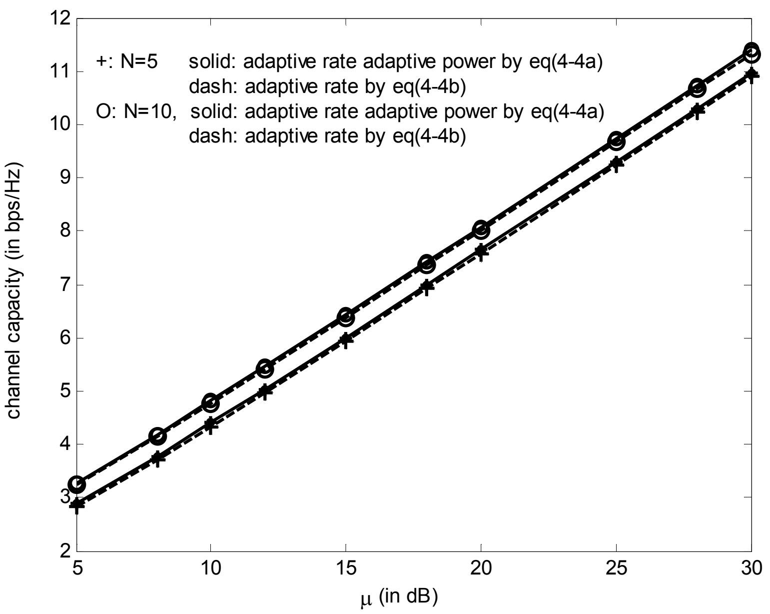

Fig.4.5 Channel capacity over Rayleigh fading channel with optimal power allocation

Fig.4.5 shows that the Shannon capacity achieved by the rate adaptive modulation with and without adaptive power allocation. It confirms the conclusion in Chapter II that rate adaptive modulation and adaptive rate adaptive power modulation achieve roughly the same information capacity, even under multiple access environments.

4.1.2 Capacity achieved over General Gamma fading channel

In earlier studies, only small-scale multipath fading is considered. As large-scale shadowing effect is taken into account, General Gamma distribution can be employed to characterize the statistical nature of channel with both multipath fading and shadowing effect. The effectiveness of this model has been studied in Section 2.1. In General Gamma fading channel, the PDF and CDF of instantaneous SNR γ can be derived to be

$$f_{\gamma_{\max}}(\gamma_{\max}=s)=\frac{1}{2\sqrt{\gamma}}\sqrt{\frac{1}{\bar{\gamma}_s}}\frac{c_g\left(\gamma/\bar{\gamma}_s\right)^{(c_g d_g-1)/2}}{\beta_g{}^{c_g d_g}\Gamma(d_g)}\exp\left[-\left(\frac{\gamma}{\beta_g^2\bar{\gamma}_s}\right)^{c_g/2}\right] \quad (4\text{-}12a)$$

and

$$F_{\gamma_m}(\gamma_m\le\gamma)=\frac{x^{d_g/2}e^{-t/2}M_{d_g/2,(d_g+1)/2}(x)}{d_g(d_g+1)\Gamma(d_g)}+\frac{x^{(d_g/2-1)}e^{-x/2}M_{d_g/2+1,(d_g+1)/2}(x)}{d_g\Gamma(d_g)},$$

(4-12b)

where $x=(\gamma/\beta_g^2\bar{\gamma}_s)^{c_g/2}$ and $M_{\lambda,\eta}(z)$ is the Whittaker function [60]. Whittaker function is related to Confluent Hypergeometric function $\Phi(x,y,z)$ through the relationship $M_{\lambda,\eta}(z)=z^{\eta+1/2}e^{z/2}\Phi(\eta-\lambda+\frac{1}{2},2\eta+1;z)$.

The PDF of $\gamma_{\max}$ over General Gamma fading channel can be obtained by (4-3). Fig.4.6 illustrates the distribution of $\gamma_{\max}$ under different number of users. Channel capacity achieved over General Gamma fading channel is shown in Fig.4.7.

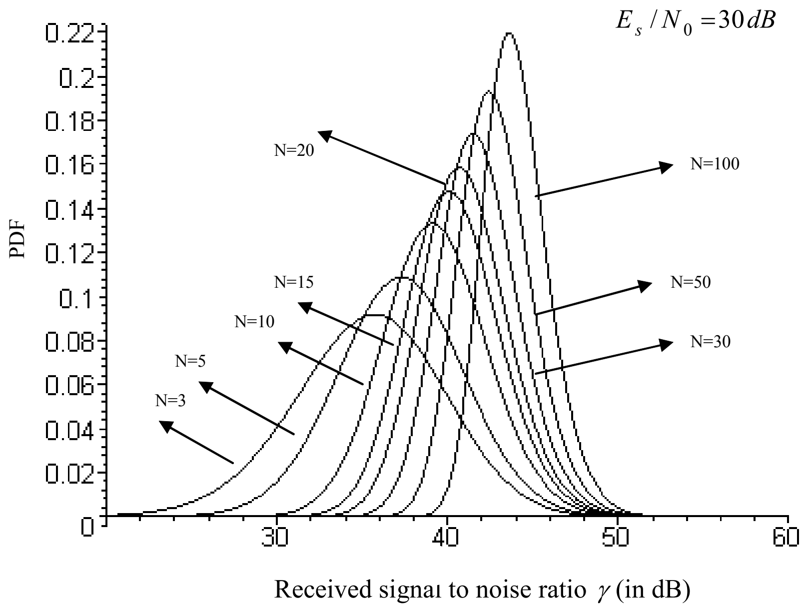

Fig.4.6 Illustration of PDF of $\gamma_{\max}$ over General Gamma fading channel

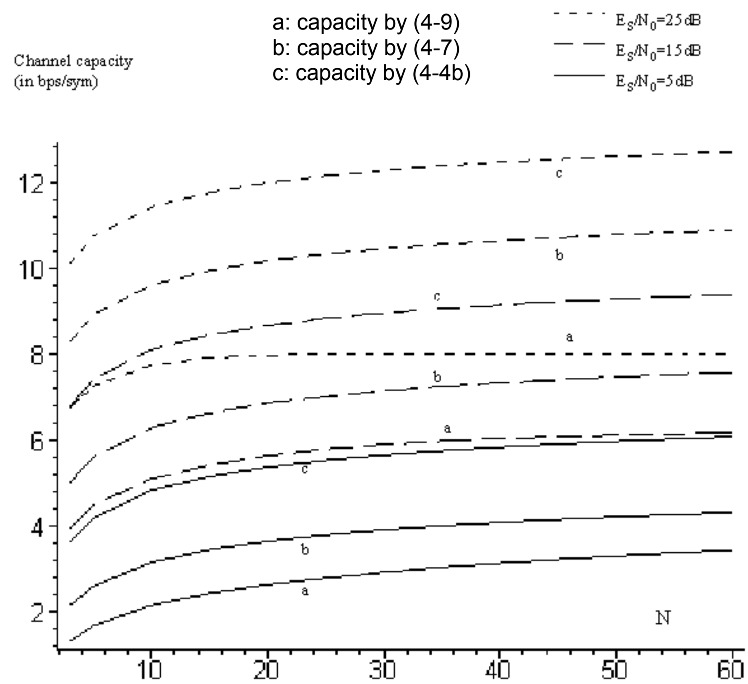

Fig.4.7 Capacity as a function of number of users over General Gamma fading channel

4.1.3 Average time duration for the optimal channel allocation scheme to remain in one MQAM constellation

The average time duration can be obtained from average level crossing rate (LCR) which is defined as the rate at which the amplitude of channel fading crosses the level α in a downward (upward) direction.

A. Derivation of LCR

Generally, the LCR is given by [66]

$$L_{CR}(\alpha)=\int_0^{\infty} \dot{\alpha} f_{\alpha,\dot{\alpha}}(\alpha,\dot{\alpha})d\dot{\alpha}\,, \tag{4-13}$$

where $\alpha,\dot{\alpha}$ are the fading amplitude and its derivative respectively, $f_{\alpha,\dot{\alpha}}(\alpha,\dot{\alpha})$ is the joint PDF of α and $\dot{\alpha}$. For Rayleigh fading channel, the PDF of $\dot{\alpha}$ is

$$f_{\dot{\alpha}}(\dot{\alpha})=\frac{1}{\sqrt{\pi\dot{\Omega}}}\exp(-\frac{\dot{\alpha}^2}{\dot{\Omega}})\,, \tag{4-14}$$

where Ω and $\dot{\Omega}=E\left[\dot{\alpha}^2\right]=2\pi^2 f_D^2\Omega$ are the variance of the random variable α and $\dot{\alpha}$, respectively. f_D is Doppler shift. The random variables α and $\dot{\alpha}$ are shown to be independent and the joint PDF is derived to be [66]

$$f_{\alpha,\dot{\alpha}}(\alpha,\dot{\alpha})=\frac{2\alpha}{\Omega\sqrt{\pi\dot{\Omega}}}\exp(-\frac{\alpha^2}{\Omega})\exp(-\frac{\dot{\alpha}^2}{\dot{\Omega}})\,, \tag{4-15}$$

If only the user observing the best SNR is allowed to transmit, the joint CDF of $\alpha_{\max}$ and $\dot{\alpha}_{\max}$ is given by

$$F_{\alpha_{\max},\dot{\alpha}_{\max}}(\alpha,\dot{\alpha}) = \sum_{m=1}^{N} P(\alpha_{\max} \le \alpha, \dot{\alpha}_{\max} \le \dot{\alpha} \mid \alpha_m \text{ is the largest}) P(\alpha_{\mathrm{m}} \text{ is the largest})$$

$$= \sum_{m=1}^{N} P(\alpha_{\max} \le \alpha, \dot{\alpha}_{\max} \le \dot{\alpha}, \alpha_m \text{ is the largest})$$

$$= \sum_{m=1}^{N} \int_0^{\alpha} \int_0^{\alpha_m} \cdots \int_0^{\alpha_m} f_{\alpha_1}(\alpha_1) \cdots f_{\alpha_N}(\alpha_N) da_1 \cdots d\alpha_N d\alpha_m F_{\dot{\alpha}_m}(\dot{\alpha})$$

$$= \sum_{m=1}^{N} \int_0^{\alpha} f_{\alpha_m}(\alpha_m) \prod_{k=1,k\neq m}^{N} F_{\alpha_k}(\alpha_m) F_{\dot{\alpha}_m}(\dot{\alpha}) \tag{4-16}$$

where $F_{\dot{\alpha}_m}(\dot{\alpha})$ is the CDF of $\dot{\alpha}$. The joint PDF of α and $\dot{\alpha}$ is obtained by differentiating (4-16) with respect to α and $\dot{\alpha}$,

$$f_{\alpha_{\max},\dot{\alpha}_{\max}}(\alpha,\dot{\alpha}) = \sum_{m=1}^{N} f_{\dot{\alpha}_m}(\dot{\alpha}) \prod_{k=1,k\neq m}^{N} F_{\alpha_k}(\alpha), \tag{4-17}$$

where $F_{\alpha}(\alpha) = 1 - \exp(-\frac{\alpha^2}{\Omega})$ is the CDF of α.

The LCR can be obtained as [67,68]:

$$L_{CR}(\alpha) = \sum_{m=1}^{N} \sqrt{\frac{\dot{\Omega}_m}{4\pi}} f_{\alpha_m}(\alpha) \prod_{k=1,k\neq m}^{N} F_{\alpha_k}(\alpha), \tag{4-18}$$

where $\dot{\Omega}_m$ is the variance of $\dot{\alpha}$ for the mth user and is identical to all users. Hence (4-18) can be rewritten as

$$L_{CR}(\alpha) = N f_D \sqrt{\frac{\Omega\pi}{2}} f_{\alpha}(\alpha) \left[F_{\alpha}(\alpha)\right]^{N-1}. \tag{4-19}$$

Since $\gamma = \alpha^2 \bar{\gamma}_s$, (4-19) can be expressed in terms of γ

$$L_{CR}(\gamma) = N f_D \sqrt{\frac{\Omega\pi}{2}} f_{\alpha}(\sqrt{\frac{\gamma}{\bar{\gamma}_s}}) \left[F_{\alpha}(\sqrt{\frac{\gamma}{\bar{\gamma}_s}})\right]^{N-1}. \tag{4-20}$$

Eq.(4-20) can be further written as

$$L_{CR}(\gamma)=Nf_D\sqrt{2\pi}\sqrt{\frac{\gamma}{\mu}}e^{-\frac{\gamma}{\mu}}\left(1-e^{-\frac{\gamma}{\mu}}\right)^{N-1}, \tag{4-21}$$

where $\mu=\Omega\bar{\gamma}_s$ is the average received SNR for one user.

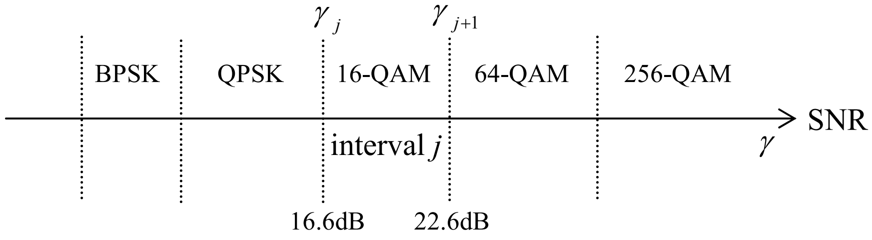

Fig.4.8 An illustration of SNR intervals

B. Derivation of average time duration to stay in one MQAM constellation

To obtain the average time duration for $\alpha_{\max}$ to stay in one MQAM constellation, we employ the first-order Markov model to characterize the fading process $\alpha_{\max}$.

For individual user (taking the *m*th user as an example), as the fading process varies very slowly over time, it has been shown that the higher order conditional probability can be adequately approximated by the first order conditional probability [69,70], or

$$P(\alpha_m(t)|\alpha_m(t-1),\alpha_m(t-2),\cdots\alpha_m(1))\approx P(\alpha_m(t)|\alpha_m(t-1)), \tag{4-22}$$

where $\alpha_m(t)$ is the channel fading gain at the frame time *t*. Hence the first order Markov model can be employed to characterize the slow fading process of individual user. The underlined assumption for Markov model is that the channel fading remains in one SNR interval over one frame period, and from a given SNR interval, the process can only remain in the same SNR interval or transit to the adjacent SNR intervals shown in Fig.4.8.

Now we verify that the first-order Markov model is also adequate to characterize $\alpha_{\max}$. Contradictorily, if we assume $\alpha_{\max}$ cannot be modeled as a Markovian process, the fading gain at frame time *t* will depend on the fading gains at both frame time (*t*-1) and frame time (*t*-2), or mathematically,

$$P(\alpha_{\max}(t) \mid \alpha_{\max}(t-1), \alpha_{\max}(t-2)) \neq P(\alpha_{\max}(t) \mid \alpha_{\max}(t-1)). \tag{4-23}$$

In the following, we consider two cases (a) where user *m* observes the best SNR at frame time *t*, (*t*-1) and (*t*-2), and (b) where user *m* observes the best SNR at frame time *t* while user *k* observes the best SNR at frame time (*t*-1).

Case (a): First we consider the situation where the *m*th user observes the best channel conditions at frame times *t,* (*t*-1) and (*t*-2), or

$$P\left(\alpha_{\max}(t) | \alpha_{\max}(t-1), \alpha_{\max}(t-2)\right) = P\left(\alpha_m(t) | \alpha_m(t-1), \alpha_m(t-2)\right). \tag{4-24}$$

From (4-23) and (4-24), it can be obtained

$$P\left(\alpha_m(t) | \alpha_m(t-1), \alpha_m(t-2)\right) \neq P\left(\alpha_m(t) | \alpha_m(t-1)\right). \tag{4-25a}$$

Eq.(4-25a) obviously contradicts with the conclusion drawn in (4-22) that the fading process for an individual user can be modeled as a Markovian process. Hence

$$P\left(\alpha_{\max}(t) | \alpha_{\max}(t-1), \alpha_{\max}(t-2)\right) \approx P\left(\alpha_{\max}(t) | \alpha_{\max}(t-1)\right). \tag{4-25b}$$

Next we consider the case where the *m*th user observes the best channel conditions at frame times *t* and (*t*-1) while the *k*th user observes the best SNR at frame time (*t*-2). Since

$\alpha_m(t)$ is uncorrelated with $\alpha_m(t-2)$, it should also be uncorrelated with $\alpha_k(t-2)$, hence mathematically,

$$\begin{aligned} P(\alpha_{\max}(t) \mid \alpha_{\max}(t-1), \alpha_{\max}(t-2)) &= P(\alpha_m(t) \mid \alpha_m(t-1), \alpha_k(t-2)) \\ &\approx P(\alpha_m(t) \mid \alpha_m(t-1)) \\ &= P(\alpha_{\max}(t) \mid \alpha_{\max}(t-1)) \end{aligned} \quad . \tag{4-26}$$

Case (b): Now we argue that (4-25b) is true for the case where another user k rather than user m observes the best SNR at frame time (t-1), i.e., $\alpha_{\max}(t-1) = \alpha_k(t-1)$, $\alpha_{\max}(t) = \alpha_m(t)$ and the channel at frame time (t-2) can be occupied by any user $j, j \in \{1, 2, \cdots N\}$. In this case,

$$\begin{aligned} P\big(\alpha_{\max}(t) \mid \alpha_{\max}(t-1), \alpha_{\max}(t-2)\big) &= P\big(\alpha_m(t) \mid \alpha_k(t-1), \alpha_j(t-2\big) \\ &\approx P\big(\alpha_m(t) \mid \alpha_k(t-1)\big) \\ &= P\big(\alpha_{\max}(t) \mid \alpha_{\max}(t-1)\big) \end{aligned} \quad . \tag{4-27}$$

From above discussions, we conclude that the higher order conditional probability of $\alpha_{\max}$ can be approximated by the first order conditional probability as well if the fading process for individual user is modeled as Markovian process, or mathematically

$$P\big(\alpha_{\max}(t) \mid \alpha_{\max}(t-1), \alpha_{\max}(t-2), \cdots \alpha_{\max}(1)\big) \approx P\big(\alpha_{\max}(t) \mid \alpha_{\max}(t-1)\big). \tag{4-28}$$

Using the first order finite-state Markov model, the transition probability from state j to state j+1 can be approximated by the average level crossing rate at γ_{j+1} divided by the average symbols per second as channel stays in the SNR interval j. Assuming a transmission rate R_j (symbols per second), the average symbols per second transmitted as channel stays in the SNR interval j is given as $R_t^j = R_t P_j = P_j / T_s$, where $T_s = 1/B$ is the symbol time, and P_j is the steady state probability which can be calculated as

$$P_j = \int_{\gamma_j}^{\gamma_{j+1}} f_{\gamma_{\max}}(\gamma) d\gamma . \tag{4-29}$$

Hence the transition probabilities between the SNR intervals $j \to (j+1), j \to (j-1)$ and $j \to j$ are given as

$$P_{j,j+1} = \frac{L_{CR}^{j+1}}{R_t^j} = \frac{L_{CR}^{j+1} T_s}{P_j}, \quad P_{j,j-1} = \frac{L_{CR}^{j}}{R_t^j} = \frac{L_{CR}^{j} T_s}{P_j}, \quad P_{j,j} = 1 - P_{j,j+1} - P_{j,j-1}, \tag{4-30}$$

where L_{CR}^j is the level crossing rate at γ_j which can be given as

$$L_{CR}^j = N f_D \sqrt{2\pi} \sqrt{\frac{\gamma_j}{\mu}} e^{-\frac{\gamma_j}{\mu}} \left(1 - e^{-\frac{\gamma_j}{\mu}} \right)^{N-1} . \tag{4-31}$$

The average time duration for the process to stay in the jth SNR interval can be obtained as

$$\tau_j = \frac{T_s}{1 - P_{j,j}} = \frac{T_s}{P_{j,j+1} + P_{j,j-1}} = \frac{P_j}{L_{CR}^{j+1} + L_{CR}^{j}} . \tag{4-32}$$

With the SNR threshold intervals defined in Table 2.1, the average time duration for each constellation can be obtained. Results are listed in Table 4.1 to Table 4.3.

TABLE 4.1 Average time duration (in second) for N=5, f_D=50Hz

μ	BPSK	QPSK	16QAM	64QAM	256QAM
5dB	4.612	5.087	2.099	1.052	0.4
15dB	0.914	4.204	11.077	3.347	1.264
25dB	0.26	0.652	1.621	2.843	4.154

TABLE 4.2 Average time duration (in second) for $\mu = 15dB$, f_D=50Hz

N	BPSK	QPSK	16QAM	64QAM	256QAM
5	0.914	4.204	11.077	3.347	1.264
8	0.628	2.688	16.913	3.363	1.264
10	0.509	2.152	22.032	3.374	1.264
15	0.341	1.435	35.928	3.401	1.264

TABLE 4.3 Average time duration (in second) for $\mu = 15dB$, N=5

f_D	BPSK	QPSK	16QAM	64QAM	256QAM
20	2.284	10.51	27.692	8.368	3.161
30	1.523	7.007	18.461	5.579	2.108
50	0.914	4.204	11.077	3.347	1.264
80	0.571	2.628	6.923	2.092	0.79
100	0.457	2.102	5.538	1.674	0.632

From these tables, it can be seen that, as transmitted SNR and the number of users contending for channel access increases, the time duration that the process stays in higher order modulation increases. For slow fading channel, or small Doppler shift, the process tends to stay in one modulation for longer duration than for the larger Doppler shift situation. This also means that the channel inter-access time increases with Doppler shift f_D. The analysis here is helpful to decide the frame period so that the fading process remains nearly constant over one frame period for reliable transmission.

4.1.4 Analysis of channel inter-access time

In a communication system, if data waiting for transmission queues at the buffer for a time interval exceeding the tolerable duration, outage will be declared to guarantee the transmission quality. Channel inter-access time is an important parameter directly relating to system performance. As channel fading varies slowly over time, a two-state Markov model can be employed to compute the average channel inter-access time as shown in Fig.4.9. The event that one particular user gains the channel access is denoted as state 1, while the event that one user loses the channel access is denoted as state 2. The transition probability from state 1 to state 2, state 1 to state 1, state 2 to state 1 and state 2 to state 2 are denoted as $P_{1,2}$,$P_{1,1}$,$P_{2,1}$,$P_{2,2}$ respectively.

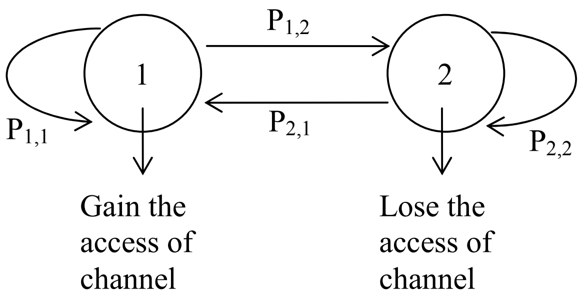

Fig.4.9 An illustration of two-state Markov model

The probability that one user loses the channel access in k consecutive transmission intervals is given as [71]

$$P_l^k = (P_{2,2})^{k-1}(1-P_{2,2}) . \tag{4-33}$$

The average channel inter-access time can be calculated as

$$T_{\text{inter-access}} = \sum_{k=1}^{\infty} kT_f P_l^k$$

$$= \frac{1}{1-P_{2,2}} T_f \ , \tag{4-34}$$

where T_f is the duration of each transmission interval or the frame size. In the following, we will illustrate how to derive the transition probability $P_{2,2}$. For time correlated Rayleigh fading channel, the joint PDF of two instantaneous SNRs separating by time interval τ for the mth user can be expressed as [53]

$$f_{\gamma(t),\gamma(t-\tau)}(\gamma,\gamma_\tau)=\frac{1}{\mu^2(1-\rho^2)}\exp\left(-\frac{(\gamma+\gamma_\tau)}{\mu(1-\rho^2)}\right)\cdot I_0\left(\frac{2|\rho|\sqrt{\gamma\gamma_\tau}}{\mu(1-\rho^2)}\right), \tag{4-35}$$

where $\rho=J_0(2\pi f_D\tau)$ is the correlation coefficient, and J_0 is zero-order first kind Bessel function.

For a system with a number of *N* users contending for the channel access, if each user experiences independent channel fading, the joint PDF for instantaneous SNRs for all users separating by τ is written as

$$f_{\gamma_1,\gamma_\tau^1,\gamma_2,\gamma_\tau^2\cdots\gamma_N,\gamma_\tau^N}(\gamma_1,\gamma_\tau^1,\gamma_2,\gamma_\tau^2\cdots\gamma_N,\gamma_\tau^N)=f_{\gamma_1,\gamma_\tau^1}(\gamma_1,\gamma_\tau^1)f_{\gamma_2,\gamma_\tau^2}(\gamma_2,\gamma_\tau^2)\cdots f_{\gamma_N,\gamma_N^{'}}(\gamma_N,\gamma_\tau^N) \tag{4-36}$$

In our analysis, we use $\tau=T_f$.

Now we track the process of the *i*th user. The probability that the *i*th user loses the channel access in the current transmission interval conditioned on its loss of the channel access in the previous transmission interval can be obtained using Bayes' rule and is given as

$$P_{2,2}=\frac{P(ith\text{ user stays in state 2 for }2T_f)}{P(\text{the steady state probability in state 2})}=\frac{\sum\limits_{m=1,m\neq i}^{N}\sum\limits_{k=1,k\neq i}^{N}P_{m,k}}{P_2}. \tag{4-37}$$

where $P(X)$ denotes the probability of event *X* occurring. $P_{m,k}$ is the probability that the *m*th user gains the channel access in the previous transmission interval and the *k*th user occupies the channel for the current transmission interval. $P_{m,k}$ is given as

$$P_{m,k}=\int\limits_{\gamma_m=0}^{\infty}\int\limits_{\gamma_1=0}^{\gamma_m}\cdots\int\limits_{\gamma_N=0}^{\gamma_m}\int\limits_{\gamma_\tau^k=0}^{\infty}\int\limits_{\gamma_\tau^1=0\cdots}^{\gamma_k}\int\limits_{\gamma_\tau^N=0\cdots}^{\gamma_k}f_{\gamma_1,\gamma_\tau^1,\gamma_2,\gamma_\tau^2\cdots\gamma_N,\gamma_\tau^N}(\gamma_1,\gamma_\tau^1,\gamma_2,\gamma_\tau^2\cdots\gamma_N,\gamma_\tau^N)d\gamma_\tau^N\cdots d\gamma_\tau^k d\gamma^1\cdots d\gamma^m \tag{4-38}$$

P_2 is the probability that user i loses the channel access in one transmission interval and is calculated to be

$$P_2 = \sum_{m=1,m\neq i}^{N} \int_0^{\infty} \int_{\gamma_1=0}^{\gamma_m} \cdots \int_{\gamma_N=0}^{\gamma_m} f_{\gamma_1}(\gamma_1) f_{\gamma_2}(\gamma_2) \cdots f_{\gamma_i}(\gamma_i) \cdots f_{\gamma_N}(\gamma_N) f_{\gamma_m}(\gamma_m) d\gamma_1 d\gamma_2 \cdots d\gamma_i \cdots d\gamma_N d\gamma_m$$

$$= \sum_{m=1,m\neq i}^{N} \int_0^{\infty} \left[1-\exp(-\frac{\gamma_m}{\mu})\right]^{N-1} \frac{1}{\mu}\exp(-\frac{\gamma_m}{\mu}) d\gamma_m$$

$$= \frac{N-1}{N}$$

(4-39)

The result obtained for P_2 is as expected. If all users have identical fading statistics, for a long run, each user has the equal probability to access the channel. Hence the probability that one user loses the channel access should be $1-1/N$.

There are two cases in computing $P_{m,k}$: 1) $P_{m,m} = P_{trans}$, denoting the case where the same user occupies the channel for two consecutive transmission intervals. 2) $P_{m,k} = P_{trans1}$, denoting the case where different users occupy the two consecutive transmission intervals. Hence

$$\sum_{m=1,m\neq i}^{N} \sum_{k=1,k\neq i}^{N} P_{m,k} = (N-1)P_{trans} + (N-1)(N-2)P_{trans1}. \quad (4\text{-}40a)$$

Substitute (4-40a) into (4-37), $P_{2,2}$ is given as

$$P_{2,2} = NP_{trans} + N(N-2)P_{trans1}. \quad (4\text{-}40)$$

Substitute (4-40) into (4-34), channel inter-access time can be obtained as

$$T_{\text{inter-access}} = \frac{1}{1 - NP_{trans} - N(N-2)P_{trans1}} T_f. \quad (4\text{-}41)$$

As fading channel is uncorrelated in the time domain, i.e., $f_D \to \infty$, under such circumstance, rate adaptive modulation technique is not advisable to employ, since channel changes very fast even within one frame period. However, the results obtained will give the limit of the channel inter-access time.

$$P_{trans} = P_{trans1} = \int_0^{\infty} \int_{\gamma_1=0}^{\gamma_m} \cdots \int_{\gamma_N}^{\gamma_m} \int_0^{\infty} \int_{\gamma_\tau^1=0}^{\gamma_\tau^m} \cdots \int_{\gamma_\tau^N=0}^{\gamma_\tau^m} f_{\gamma_1}(\gamma_1) f_{\gamma_2}(\gamma_2) \cdots f_{\gamma_N}(\gamma_N) f_{\gamma_m}(\gamma_m) \cdot$$

$$f_{\gamma_\tau^1}(\gamma_\tau^1) f_{\gamma_\tau^2}(\gamma_\tau^2) \cdots f_{\gamma_\tau^N}(\gamma_\tau^N) f_{\gamma_\tau^1}(\gamma_\tau^1) d\gamma_1 d\gamma_2 \cdots d\gamma_N d\gamma_m d\gamma_\tau^1 d\gamma_\tau^2 \cdots d\gamma_\tau^N d\gamma_\tau^k$$

$$= \frac{1}{N^2} \tag{4-42}$$

Therefore (4-40) is simplified as

$$P_{2,2} = N(N-1)\frac{1}{N^2} = \frac{N-1}{N}. \tag{4-43}$$

Hence as channel fading for individual user is uncorrelated over time, the channel inter-access time is obtained as

$$T_{\text{inter-access}} = NT_f. \tag{4-44}$$

In order to verify the theoretical analysis, a simulation is conducted. The probability mass function (p.m.f) of channel inter-access time is obtained from simulation. The average channel inter-access time is just the mean based on this p.m.f.

The channel inter-access time under different correlation conditions is shown in Fig.4.10. From this figure, we can see that the channel inter-access time strongly depends on channel correlation as expected. As channel fading of individual user becomes more time-correlated, the channel inter-access time increases. The reason is that as channel is more correlated, the user tends to stay in its current fading state for a longer period of time and takes longer time for its channel conditions to turn to be the best. In the extreme case where channel fading is too fast, the channel access by each user is totally random. The dependence of channel inter-access time on μ is not significant. This is due to the fact that all users in the system are assumed to have identical fading statistics. μ does not affect the probability that one user is selected to transmit or not. It can also be seen that, for this two-user system, as $f_D \to \infty$ or channel is uncorrelated, the channel inter-access time approaches $2T_f$ which can be predicted from (4-44). The p.m.f. of channel inter-access time and average channel inter-access time obtained from simulation are shown in Fig.4.10 (a) and Fig. 4.10 (b). It can be seen that the numerical results and simulation results match very well.

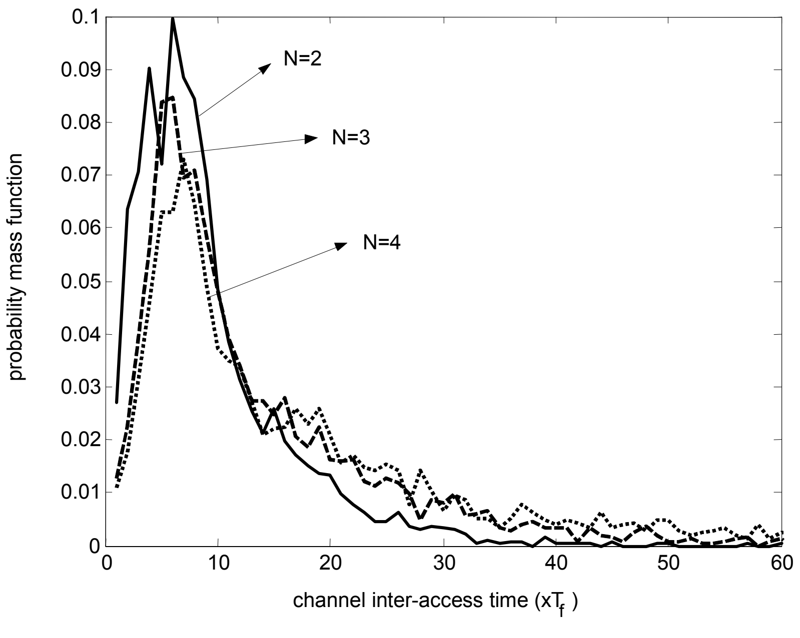

(a)

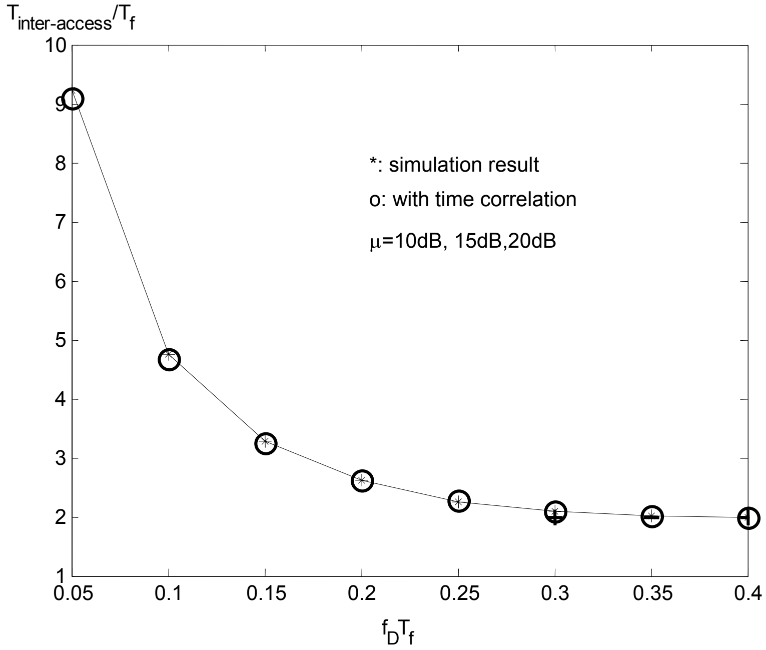

(b)

Fig.4.10 (a) Probability mass function of channel inter-access time (b) Average channel inter-access time for two-user system

4.2 Channel capacity achieved by suboptimal channel allocation scheme

A major drawback of the optimal channel allocation scheme studied in Section 4.1 is the possible long channel inter-access time before a mobile user can access the channel, since users who suffer severe channel fading would have to wait for a long period of time to be allowed to transmit. The channel inter-access time increases dramatically with the number of users admitted in the system. An alternative approach is to use a SNR-priority-based channel allocation scheme, by allowing a number of users observing the first few best channel conditions to share the channel during one transmission interval (frame) rather than allocating the entire bandwidth to only one user for the whole transmission interval (frame). This is a suboptimal multiple access scheme similar to TDMA systems as shown in Fig.4.11, except that the users transmitting simultaneously are selected from all users contending for the channel access. The users being selected observe the few best SNRs among all the users. For each user selected to transmit, adaptive MQAM modulation is employed so that the constellation used by each user is defined by its own channel conditions. Obviously, the tradeoff of this SNR-priority-based scheme is the reduction of bandwidth efficiency and the improvement of channel inter-access time performance.

In the following study, no power control is performed thus the transmission power is kept as a constant. Channel is assumed to vary slowly so that it remains constant for a few transmission frames. Channel estimation is performed at one transmission interval. In this system, the selection of mobile users to transmit is performed at the BS. Therefore the BS should have the knowledge of channel state information of all users and uses the information to decide which *K* mobiles should transmit. Other mobile users who do not have the permission to transmit must wait till their channel conditions are among the *K* best SNRs.

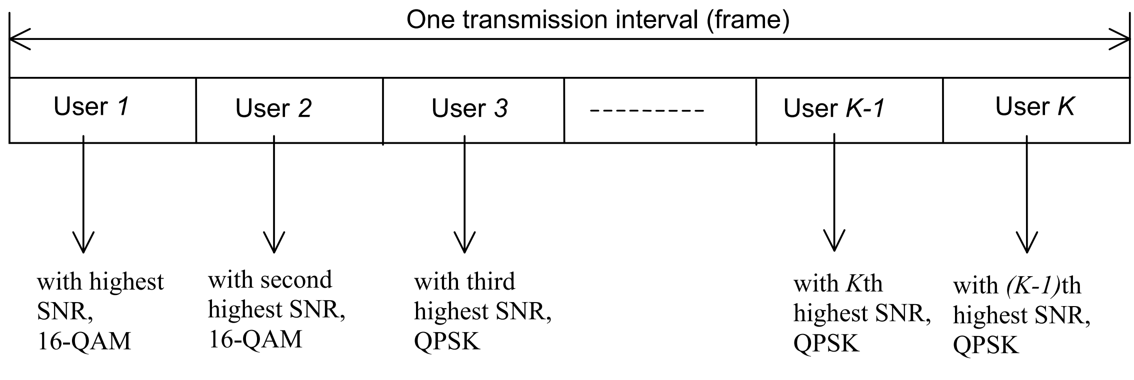

Fig.4.11 A frame structure for a SNR-priority-based system

4.2.1 Introduction of order statistic

Suppose that $T=\{\gamma_1,\gamma_2,\cdots\gamma_{N-1},\gamma_N\}$ is a set of N independent random variables, each with PDF $f_\gamma\ (\gamma)$ and CDF $F_\gamma\ (\gamma)$. If $\gamma_1,\gamma_2,\cdots\gamma_{N-1},\gamma_N$ are arranged in a descending order of magnitude and are denoted as $U_1,U_2,\cdots U_K\cdots U_N$, or mathematically,

$$\begin{aligned}
&U_1=\max(T)\\
&U_2=\max(T-\{U_1\})\\
&\vdots\\
&U_K=\max(T-\{U_1,\cdots U_{K-1}\})\\
&\vdots\\
&U_N=\max(T-\{U_1,\cdots U_{N-1}\})
\end{aligned}\quad, \tag{4-45}$$

where the operation "-" means excluding those elements listed in the given set. Obviously $U_1>U_2>U_3\cdots>U_K\cdots>U_N$. The PDF of U_k is given as [72]

$$\begin{aligned}
&f_{U_1}(u_1)=N[F_\gamma(U_1<u_1)]^{N-1}f_\gamma(u_1)\\
&f_{U_2}(u_2)=\frac{N!}{(N-2)!}\left[F_\gamma(U_2<u_2)\right]^{N-2}\left[1-F_\gamma(U_2<u_2)\right]f_\gamma(u_2)\\
&\vdots\\
&f_{U_k}(u_k)=\frac{N!}{(N-k)!(k-1)!}\left[F_\gamma(U_k<u_k)\right]^{N-k}\left[1-F_\gamma(U_k<u_k)\right]^{k-1}f_\gamma(u_k)
\end{aligned}\quad, \tag{4-46}$$

where $\infty>u_1>u_2>u_3>\cdots u_K\cdots>u_N>0$. The PDF of U_1 corresponds to the PDF of $\gamma_{\max}$ which is shown in (4-3).

The joint PDF for the first K order statistics ($U_k, k=1,\cdots K$) is given by [72]

$$f_{U_1,U_2\cdots U_K}(u_1,u_2\cdots u_K)=\frac{N!}{(N-K)!}\left[F(u_K)\right]^{N-K}f_\gamma(u_1)f_\gamma(u_2)\cdots f_\gamma(u_K). \tag{4-47}$$

In the proposed SNR-priority-based scheme, the first time slot will be occupied by the user observing the best channel conditions, the user observing the next best channel conditions uses the second time slot, and so on. Hence this scheme allows a number of K users observing the first K best SNRs among N users to transmit. It corresponds to a single order statistics with N independent random variables, while only the first K order statistics in a descending order of magnitude are considered.

4.2.2 Shannon capacity

Assuming that K time slots are available for allocation, for an individual user with the kth highest SNR, the achievable transmission rate is given as

$$R_{k,bestK} \leq \frac{B}{K}\log_2(1+u_k) \ . \tag{4-48}$$

The channel capacity for a given combination (U_k, $k=1\cdots K$) is given by

$$C_{bestK} = \sum_{k=1}^{K} R_{k,bestK} \ . \tag{4-49}$$

The average channel capacity is obtained by averaging (4-49) over all the fading states and is given as

$$\overline{C}_{bestK} = \frac{B}{K}\int_0^{\infty}\int_0^{u_1}\cdots\int_0^{u_{K-1}}\sum_{k=1}^{K}\log_2(1+u_k)\cdot f_{U_1,U_2\cdots U_K}(u_1,u_2\cdots u_K)\cdot du_K\cdots du_2 du_1 \ . \tag{4-50}$$

Largest $\overline{C}_{bestK}$ given in (4-50) is obtained when K=1 and the result is given in section 2.1. However, the channel inter-access time for only one user to gain the access of the channel is the largest. The SNR-Priority-based transmission scheme is expected to improve this situation at the expense of capacity.

Shannon capacity achieved is presented in Fig.4.12. It shows that as more users are allowed to share the channel, the channel capacity will be reduced.

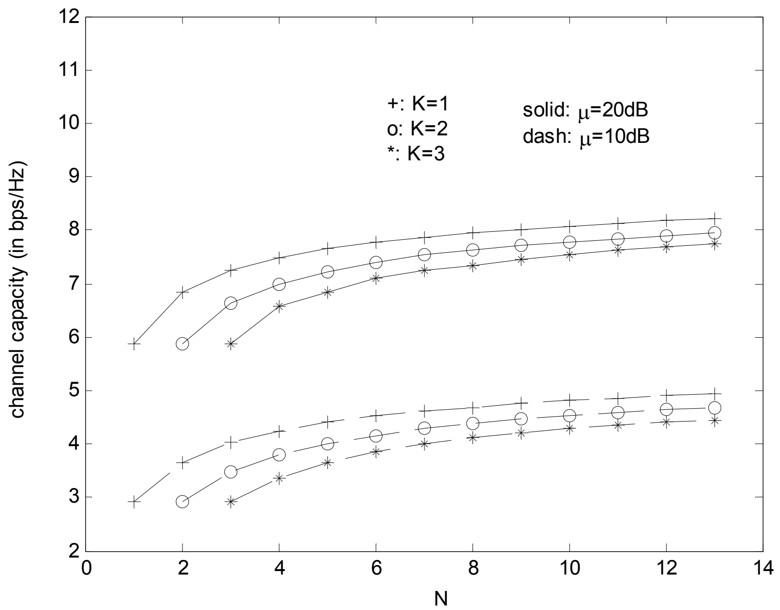

Fig.4.12 Shannon capacity of SNR-priority-based systems

4.2.3 Channel capacity achieved with adaptive MQAM technique

The probability that a given MQAM modulation constellation is used is given by

$$P_i = \int_{a_{th,i}}^{b_{th,i}} f_{U_k}(u_k)du_k\ , \quad \forall i \in \{0,1,2,4,6,8\}. \tag{4-51}$$

The channel throughput obtained by employing adaptive MQAM technique is given by

$$C_{BestK} = \frac{B}{K} \sum_{(i_1,i_2,\cdots i_K)} (i_1 + i_2 + \cdots + i_k + \cdots i_K) \cdot q_{i_1,i_2,\cdots i_K}\ , \tag{4-52}$$

where i_k indicates that the user with *k*th highest SNR transmits using constellation $M = 2^{i_k}$, and

$$q_{i_1,i_2,\cdots i_K} = \int_{a_{th,i_1}}^{b_{th,i_1}} \int_{a_{th,i_2}}^{b_{th,i_2}} \cdots \int_{a_{th,i_K}}^{b_{th,i_K}} f_{U_1,U_2\cdots U_K}(u_1,u_2\cdots u_K)\cdot du_K \cdots du_2 du_1. \tag{4-53}$$

A comment on evaluating $q_{i_1,i_2,\cdots i_K}$ is needed. Since $i_1 \geq i_2 \geq \cdots \geq i_{K-1} \geq i_K$, the limits of integration need to be chosen carefully. If $i_{k-1} > i_k > i_{k+1} > i_{k+2}$ for a given *k*, then $a_{th,i_k} \neq a_{th,i_{k+1}}$ and $b_{th,i_k} \neq b_{th,i_{k+1}}$, i.e. one of the ranges in Table 2.1 gives the limits of each of the integrals. If $i_{k-1} > i_k = i_{k+1} > i_{k+2}$, then $a_{th,i_{k+1}} = a_{th,i_k}$ and $b_{th,i_k} = b_{th,i_{k+1}}$. The same method should be extended to the case where there are more time slots using the same constellation.

The capacity obtained is shown in Fig.4.13. It confirms the results shown in Fig.4.12.

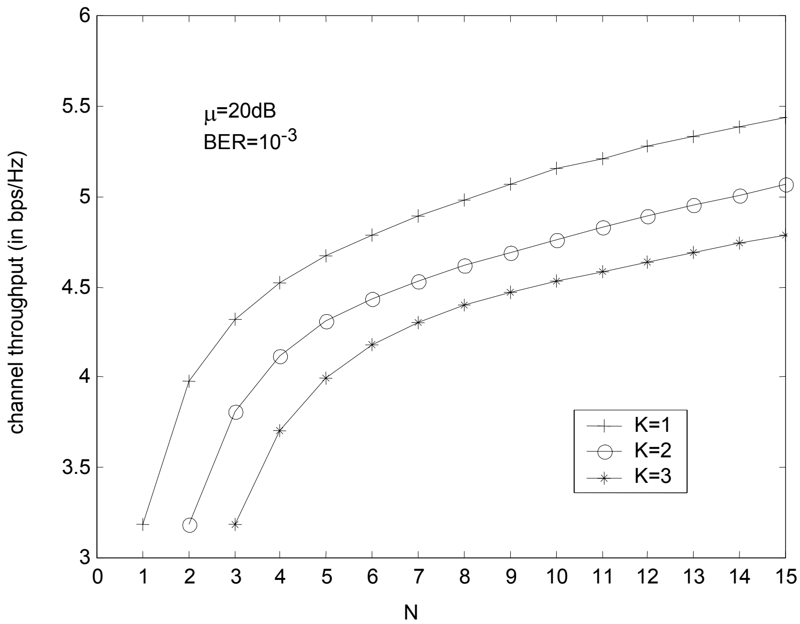

Fig.4.13 Channel throughput employing adaptive MQAM technique

In order to have a clearer picture of the proposed SNR-priority-based channel allocation system, comparison of channel capacity (Shannon capacity) achieved by the conventional TDMA system where all N users in the system are assigned one time slot during one transmission interval is performed and the results are listed in Table 4.4. It shows that the SNR-priority-based system achieves higher channel capacity than the conventional TDMA system.

TABLE 4.4 Capacity achieved with SNR-priority-based system

	R_1 (bps/Hz)	R_2(bps/Hz)	R_3(bps/Hz)	R_4(bps/Hz)	R_1+ R_2+ R_3 (bps/Hz)
Priority-based TDMA (K=2, N=2)	3.4152	2.4688	X	x	5.8840
Conventional TDMA (K=2, N=2)	2.9420	2.9420	X	x	5.8840
Priority-based TDMA (K=2, N=3)	3.6192	3.0073	X	x	6.6265
Conventional TDMA (K=3, N=3)	1.9614	1.9614	1.9614	x	5.8840
Priority-based TDMA (K=2, N=4)	3.7405	3.2555	X	x	6.9960
Conventional TDMA (K=4, N=4)	1.4710	1.4710	1.4710	1.4710	5.8840

4.2.4 Simulation to investigate capacity under a real transmission environment

In order to verify the numerical results obtained in Section 4.2.3, a simulation is conducted. The simulation assumes a more realistic situation. Each user is assumed to experience time-correlated Rayleigh fading with maximum Doppler shift f_d Hz. Clark and Gan's [73,74] model is used to simulate the Rayleigh channel fading observed by each mobile user as shown in Fig.4.12. The channel fading experienced by different user is independent and identically distributed with $\Omega=1$.

For simulation purpose we assume the channel estimation is perfect and the feedback delay is negligible. In practical, for the downlink transmission, the estimation of channel conditions are activated by the BS at a frame interval by sending a common preamble sequence to all the mobiles admitted in the system. Each mobile will estimate the channel conditions from their respectively received signal simultaneously. A dedicated uplink channel is used for the mobiles to send the channel information (an example is the SNR) back to the BS, at certain predefined order so that no contention will happen and the probability that the uplink channel encounters loss in data due to fading is assumed to be negligible. After receiving the channel state information for all mobile links, based on the above-mentioned SNR-priority-based channel allocation criterion, the BS then sets up connection with mobile users observing the first few best SNRs with a suitable MQAM constellation.

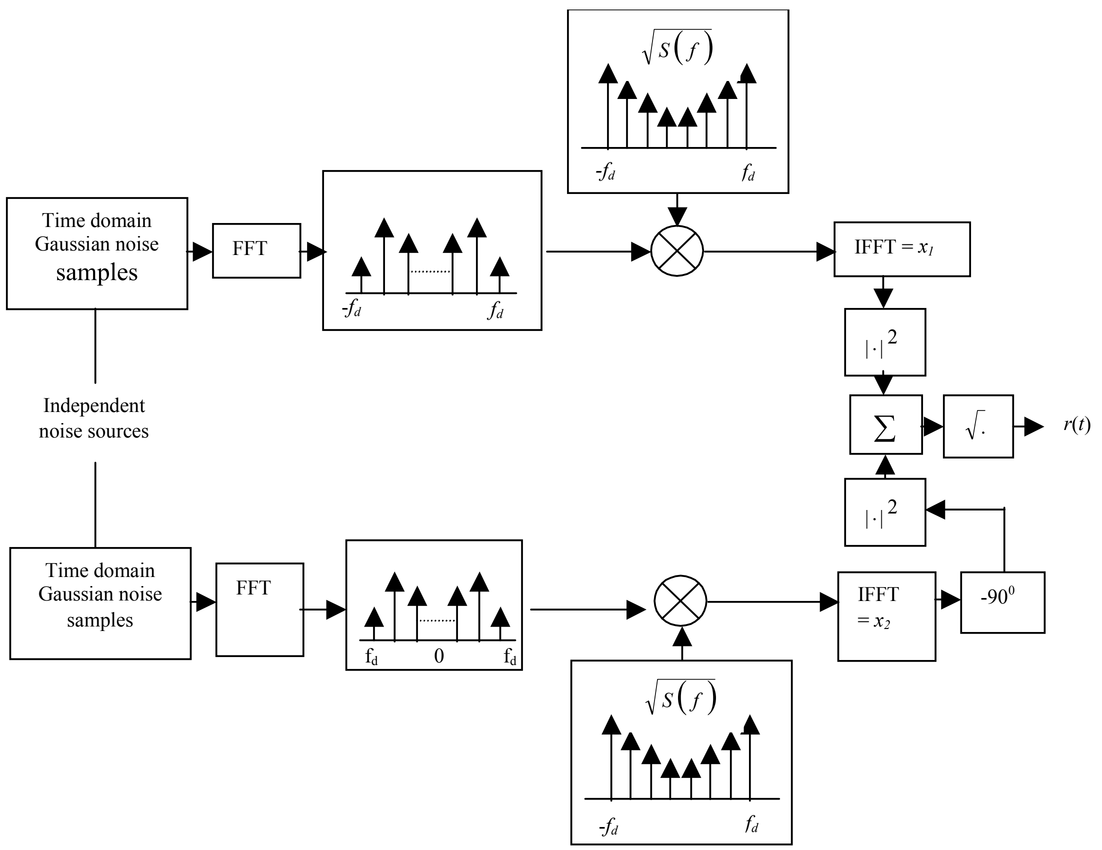

Fig.4.14 Clark and Gan's correlated Rayleigh generation model

The simulation program generates the fading amplitudes of each mobile at frame period. The fading amplitudes of all mobiles are used to decide which K mobiles should transmit. The criterion for the selection of MQAM constellation is shown in Table 2.1 (the fading amplitude α is related to the SNR γ through $\gamma = \alpha^2 \bar{\gamma}_s$). One frame consists of K time slots and the frame duration is fixed to be 0.005 second. Immediately after the channel estimation is done, K mobiles observing the best K channel conditions among all N mobile users are selected.

The results obtained from simulation are shown in Fig.4.15 and match well with the results obtained from numerical analysis.

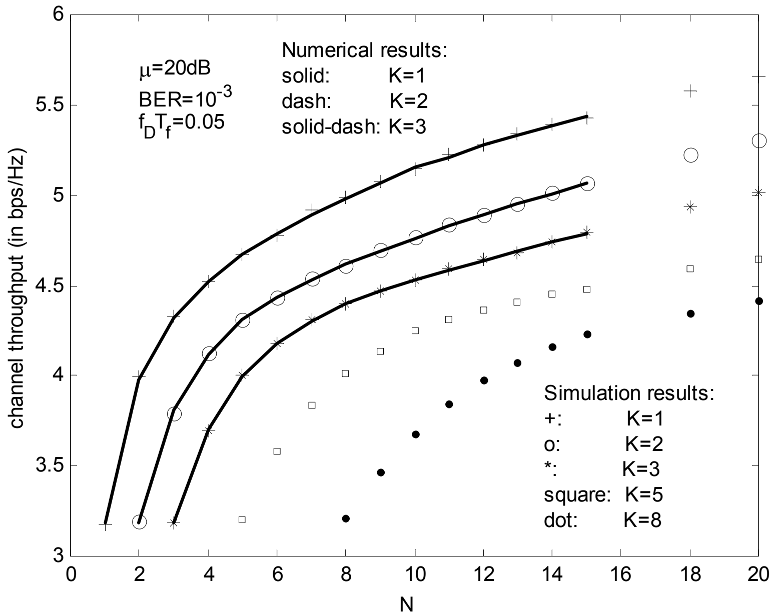

Fig.4.15 Channel throughput employing MQAM obtained from simulation (lines - theoretical result, markers- simulated result with $f_D T_f = 0.05$)

4.3 Throughput analysis of adaptive modulation system supporting dual-class services

In the proposed rate adaptive TDMA systems studied in Section 4.2.4, the duration of each time slot is fixed and hence the number of bits transmitted over one time slot is not a constant if adaptive modulation is employed in each time slot. Therefore, such systems can only be used to support delay non-sensitive services, where variation in transmission delay is not critical.

For delay sensitive services whose data from one user have to be transmitted at a constant rate, fixed time slot duration will not achieve higher bandwidth efficiency even if an adaptive modulation technique is used. This is due to the possibility that the remaining bandwidth when channel is in good conditions will be left unused. To improve system bandwidth efficiency when a rate adaptive technique is employed to support constant bit rate (CBR) services, we propose another channel allocation scheme where the time slot duration assigned to each service depends on its instantaneous channel conditions or modulation constellation used. We classify services supported in the system into two classes. One class is CBR services that demands constant bit rate, constant delay with no delay jitter tolerance. The other class is the best effort (BE) services with no QoS requirement. For each class of services, the transmission rate is adapted according to the instantaneous channel conditions. From hereafter, we will use the term QoS services to replace CBR services, since it is sufficient to classify the two classes of service. Priority is given to QoS services and the remaining bandwidth will then be used to transmit BE services. In conventional systems, for BE services, media access control (MAC) employs first-come-first-service scheme to allocate channel regardless of instantaneous physical link conditions. In this manner physical layer conditions are transparent to higher layer services. However in rate-adaptive wireless systems, MAC protocol should have the capability to schedule the transmission of BE services based on physical channel conditions of all services. This scheme is possible because of the fact that in multiple access environment, each mobile in the system experiences different degree of fading at any observation time. This scenario brings up the possibility to further improve the bandwidth efficiency of conventional adaptive TDMA systems.

The channel fading gain of each user is assumed to remain almost constant over a few TDMA frame periods and is independent of each other. Accurate estimation of channel conditions can be performed at receivers (BS for uplink and MS for downlink). Channel state information will then be fed back to transmitters and used to schedule transmission for the next frame. A simple way to realize such a system is to use a TDD system, where both the uplink and the downlink are time-sharing one frequency band but transmitting in different time slots. Since channels follow the same statistical model for both directions, channel fading gains for both uplink and downlink transmission can be simply obtained directly from downlink signals received at respective mobile through interpreting the common messages sent out from the BS. Mobiles then take turn to inform the BS the respective channel state information.

4.3.1 Channel allocation scheme

For convenience, only the downlink is considered in this study but the analysis holds true for the uplink. The users' data for transmission are grouped into frame formats as shown in Fig.4.16. We consider a frame format with fixed frame duration but variable slot durations, while the number of time slots is fixed. QoS services have higher priority to transmit while only one BE service is allowed to transmit when there is bandwidth available after satisfying the QoS services. For QoS services, channel estimation results are only used to decide the constellation size. Each QoS service will be guaranteed to have a time interval enough to transmit a given number of bits, thus guarantee transmission quality. If adaptive MQAM is used, the slot duration depends on constellation sizes. But it is still some integer multipliers of "mini-slot". Here a mini-slot is a unit of time used for the convenience of calculation. For example, as 256QAM is used, given that the information rate is common to all QoS services, time needed to transmit a packet is 3 mini-slots, while if BPSK is used, it should take 24 mini-slots. With the introduction of mini-slot and numbering these mini-slots in order over one TDMA frame period, transmitters should know exactly when to transmit based on scheduling instruction from the BS. Table 4.5 shows the dependency of the number of mini-slots on MQAM modulation constellations.

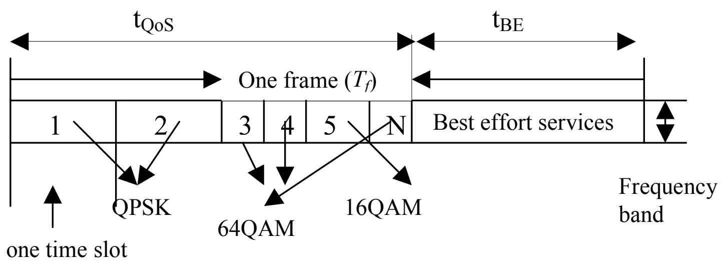

Fig.4.16. TDMA frame structure for dual classes system

TABLE 4.5 Mini-slot illustration for MQAM modulation

$i = \log_2 M$	8	6	4	2	1
Modulation	256QAM	64QAM	16QAM	QPSK	BPSK
Minimum SNR (in dB)	31	22.6	16.6	9.8	6.8

Number of mini-slot	3	4	6	12	24

The transmission of BE services depends on the availability of bandwidth after satisfying the bandwidth requirement of QoS services. The number of allowed BE services waiting for transmission is a design parameter which is related to the allowable queuing delay and the traffic model.

4.3.2 Probability mass function of transmission time

Based on the proposed adaptive modulation technique and the MAC scheme, the total transmission time occupied by QoS services and thus the transmission time for BE services are random variables depending on instantaneous channel conditions of all users. Therefore the system throughput is also a random variable. To evaluate the average system throughput, the p.m.f. of the total transmission time occupied by QoS services over a TDMA frame period employing the proposed transmission scheme should be studied.

A. QoS service

Assuming that the number of QoS services served in one TDMA frame is *N*. By assuming that in any TDMA frame, the number of QoS services that employs *i*th order MQAM constellation is N_i, then $N = N_0 + N_1 + N_2 + \cdots N_i + \cdots N_H$, where *H* denotes the number of constellation size available and zero denotes the situation where no transmission is allowed.

The probability for a given combination of QoS services $(N_0, N_1, N_2 \cdots N_H)$ over a TDMA frame can be derived as

$$P(N_0, N_1, N_2 \cdots N_H) = \binom{N}{N_0}\binom{N-N_0}{N_1}\cdots\binom{N_H}{N_H} P_0^{N_0} P_1^{N_1} P_2^{N_2} \cdots P_H^{N_H}, \qquad (4\text{-}54)$$

where $P_i = \int_{a_{th,i}}^{b_{th,i}} f_\gamma(\gamma)d\gamma$ is the probability that 2^i QAM constellation is used and $f_\gamma(\gamma)$ is the PDF of the received SNR. The values of $a_{th,i}, b_{th,i}$ are defined in Table 2.1. At every TDMA frame, each QoS service will use one QAM modulation constellation depending on channel conditions to transmit data. The transmission time allocated is then determined as $t_i = L_p/(iB)$ for $i > 0$ and $t_0 = 0$ for $i = 0$, where L_p and B are packet length and the symbol rate (channel bandwidth) respectively. The total transmission time occupied by N QoS services can be calculated as

$$t_{QoS} = N_1 t_1 + N_2 t_2 + N_3 t_3 + \cdots N_i t_i + \cdots N_H t_H. \qquad (4\text{-}55)$$

The p.m.f. of t_{QoS} can be obtained by calculating $P(N_0, N_1, N_2 \cdots N_H)$ for all possible combinations of N_i, where $N_i \in \{0,1,2,\cdots N\}$ and $\sum N_i = N$. For example, the probability of all QoS services employing BPSK modulation constellation is given by $P(N_0 = 0, N_1 = N, 0, 0\cdots 0) = \binom{N}{N_1 = N} p_1^N$, the total transmission time of N QoS services is Nt_1. The probability of $(N-1)$ QoS services employing BPSK and one service employing QPSK will be $P(0, N-1, 1, 0, \cdots 0) = \binom{N}{N-1}\binom{1}{1} P_1^{N-1} P_2$, the total transmission time for N QOS users is $(N-1)t_1 + t_2$.

If any QoS service predicts that a packet loss is going to happen due to the poor channel conditions, the bandwidth released by this user will be re-assigned to BE services.

B. BE services

For BE services, we assume the number of users waiting to access the channel is N_{BE}. The selection of N_{BE} is based on the ultimate queuing delay that a system can tolerate. For simplicity, we assume only one of the N_{BE} BE services and only the service with the best channel conditions (highest SNR among all the N_{BE} users) is allowed to transmit during each TDMA frame. The PDF $f_{\gamma_{\max}}(\gamma)$ of the best signal-to-noise-ratio ($\gamma_{\max}$) for N_{BE} is given in (4-3). The probability that a given QAM modulation constellation is used by the selected BE service observing the best SNR is given in (4-8).

Given the frame duration T_f, the transmission time available for BE services is given by

$$t_{BE} = \max(T_f - t_{QoS}, 0) \cdot \qquad \textit{(4-56)}$$

Therefore the p.m.f of t_{BE} can be obtained easily from the p.m.f of t_{QoS} if $T_f - t_{QoS} > 0$.

The probability mass functions for different system configurations are shown in Fig.4.17. As more QoS services are allowed in the system, the p.m.f of t_{QoS} shifts toward the high end.

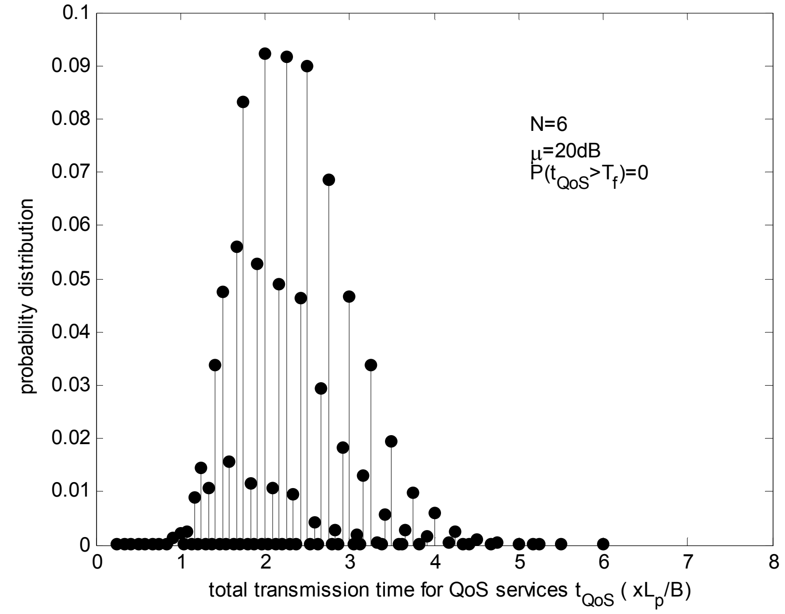

(a)

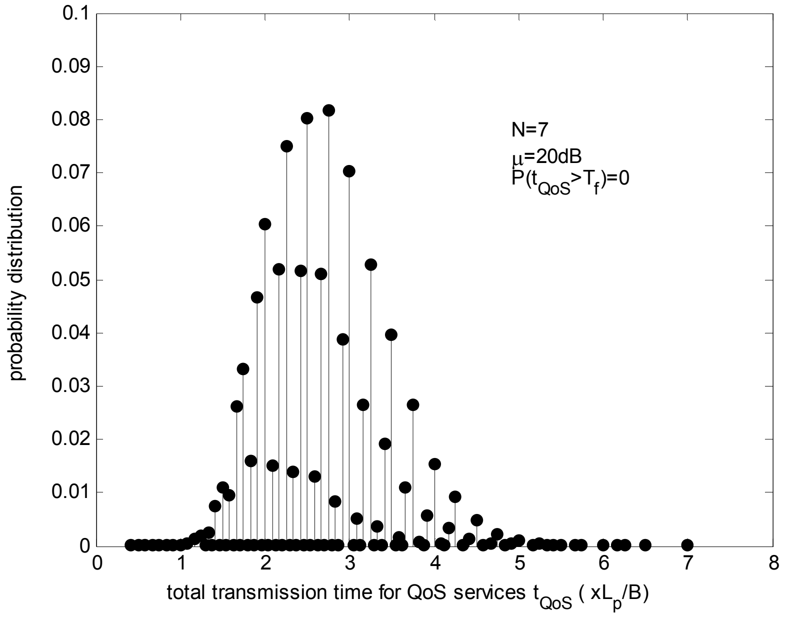

(b)

Fig.4.17 Probability mass function of t_{QoS} *normalized to* B/L_pT_f *(a) N=7,* μ *=20dB (b) N=6,* μ *=20dB*

4.3.3 System performance evaluation in terms of packet loss and average throughput

A. Probability of packet loss

We may expect that if more transmission time is allocated to BE services the system will achieve higher system throughput. On the other hand, QoS services can generate more revenues to service providers, therefore we may want to accommodate as many QoS services as possible. However as the number of QoS services supported in the system increases, it is possible that the bandwidth cannot fulfill the need of all QoS services if a few of the mobile's transmission links turn out to be poor simultaneously. Some QoS services may have to drop transmission due to insufficient frame time for all QoS services to transmit. Therefore the number of QoS users supported in the system has to be designed delicately. In practical, some QoS services can tolerate a small probability of packet loss, or mathematically the total transmission time occupied by QoS services in one TDMA frame can exceed the frame duration with a pre-defined small probability P_{ex}, i.e. $P(t_{QoS} > T_f) < P_{ex}$. The parameter P_{ex} is a design metric that should be satisfied when trying to accommodate more QoS services.

Two situations will cause packet loss in our proposed system. The first situation is when the channel conditions observed by a service is poor and instantaneously received SNR is smaller than the minimum required SNR to transmit using BPSK (lowest order of MQAM constellation). The transmission for this service has to be suspended and a packet loss occurs. The second situation is when $t_{QoS} > T_f$ happens, the services sensing the worst channel conditions will be forced to drop transmission since the available time in one TDMA frame cannot accommodate all the QoS services to transmit and hence results in packet loss. The former type of packet loss is determined by the transmission power and channel conditions, while the latter one is introduced by system design to generate more revenue. The total packet loss can be further reduced by increasing the transmission power, although in this study we have assumed a rate adaptive transmission scheme with constant power. In the following, we explain how these two terms are computed.

The average packet loss due to the channel fading can be derived as

$$\beta_{fading} = \sum_{i=1}^{N} i \binom{N}{i} P_0^i (1-P_0)^{N-i} = NP_0, \tag{4-57}$$

where N is the number of QoS users and P_0 is the probability that SNR is below minimum SNR requirement of BPSK. The packet loss due to the poor channel conditions will dominate the overall packet loss when N is small. As the number of QoS services N increases, the total transmission time of QoS services t_{QoS} may exceed the frame duration T_f. The maximum number of QoS services N that can be supported in the system with $P(t_{QoS} > T_f) = 0$ is given by $N_q = \lfloor T_f / t_1 \rfloor$, where $\lfloor x \rfloor$ is a function that returns the maximum integer less than X, $t_1 = L_p B$ is the transmission time needed for QoS services employing BPSK. If $N \le N_q$, the average packet loss is defined by (4-57). If $N > N_q$, $t_{QoS} > T_f$ happens, then the QoS service with the worst channel conditions may be forced to drop the packet transmitted. The average packet loss is the summation of these two types of packet loss, i.e.,

$$\beta_{loss} = \beta_{fading} + \beta_{QoS} \tag{4-58}$$

where β_{fading} is calculated by (4-57) and β_{QoS} is the packet loss caused by $t_{QoS} > T_f$. The calculation of β_{QoS} is not straightforward, we have to turn to computer program. We give two examples below to illustrate this.

Assuming $N_q = T_f / t_1$ is an integer, the computation can be done in a much simpler way. Supposing $N = N_q + 1$, $P(t_{QoS} > T_f)$ will happen if: (1) All QoS services are transmitting using BPSK, hence one of the QoS services will have to drop its packets. (2) The data from N_q QoS services are transmitting using BPSK while the data from the remaining services is transmitting at a constellation size above BPSK, therefore one of the QoS services that is transmitting using BPSK will have to drop its packets. Mathematically,

$$P(t_{QoS} > T_f) = (P_1)^{N_q+1} + \binom{N_q+1}{N_q}(P_1)^{N_q}\sum_{i=2}^{H} P_i \quad . \tag{4-59}$$

The average packet loss when $N = N_q + 1$ is given by

$$\beta_{loss} = (N_q + 1)P_0 + P(t_{QoS} > T_f) \,. \tag{4-60}$$

Similarly if $N = N_q + 2$, packet loss happens when (1) all QoS services are transmitting using BPSK so that each of the two services has to drop its packets, (2) $(N_q + 1)$ QoS services are transmitting using BPSK while the remaining QoS services are transmitting using higher modulation constellation so that two services transmitting using BPSK have to drop their packets, (3) N_q QoS services are transmitting using BPSK while the remaining two services are transmitting using higher modulation level so that one service transmitting using BPSK have to drop its packets. (4) One QoS service is forced to stop transmission due to poor channel conditions, while the remaining (N_q+1) QoS services are transmitting at BPSK and one of them has to drop its packets. (5) One QoS service is forced to stop transmission due to poor channel conditions and one QoS service are transmitting at a constellation above BPSK, while the remaining N_q QoS services are transmitting at BPSK. Hence one of QoS services using BPSK has to drop its packets. Mathematically, then the probability of $t_{QoS} > T_f$ can be derived as

$$p(t_{QoS} > T_f) = p_1^{N_q+2} + \binom{N_q+2}{N_q+1}(p_1)^{N_q+1}\sum_{i=2}^{K} p_i +$$

$$\binom{N_q+2}{N_q}\binom{2}{1}(p_1)^{N_q}\sum_{i=2}^{K}\sum_{j=2,j\neq i}^{K} p_i p_j + \binom{N_q+2}{N_q}(p_1)^{N_q}\sum_{i=2}^{K}(p_i)^2 + \tag{4-61}$$

$$\binom{N_q+2}{1}p_0(p_1)^{N_q+1} + \binom{N_q+2}{1}\binom{N_q+1}{N_q}p_0(p_1)^{N_q}\sum_{i=2}^{K} p_i$$

Accordingly, the average packet loss due to $t_{QoS} > T_f$ is given as

$$\beta_{QoS} = 2p_1^{N_q+2} + 2\binom{N_q+2}{N_q+1}(p_1)^{N_q+1}\sum_{i=2}^{K} p_i +$$

$$\binom{N_q+2}{N_q}\binom{2}{1}(p_1)^{N_q}\sum_{i=2}^{K}\sum_{j=2,j\neq i}^{K} p_i p_j + \binom{N_q+2}{N_q}(p_1)^{N_q}\sum_{i=2}^{K}(p_i)^2 + \tag{4-62}$$

$$\binom{N_q+2}{1}p_0(p_1)^{N_q+1} + \binom{N_q+2}{1}\binom{N_q+1}{N_q}p_0(p_1)^{N_q}\sum_{i=2}^{K} p_i$$

The average total packet loss will be given by

$$\beta_{loss} = (N_q+2)P_0 + \beta_{QoS}\,. \tag{4-63}$$

From the viewpoint of system design, we would like to know what the maximum number of QoS services will be given the constraint on the probability of $t_{QoS} > T_f$. We have illustrated the computation of packet loss using two examples, however, the computation of the probability of $t_{QoS} > T_f$ and the number of average packet loss will be of a very complicated form as N increases. To solve this problem, a computer program has to be used.

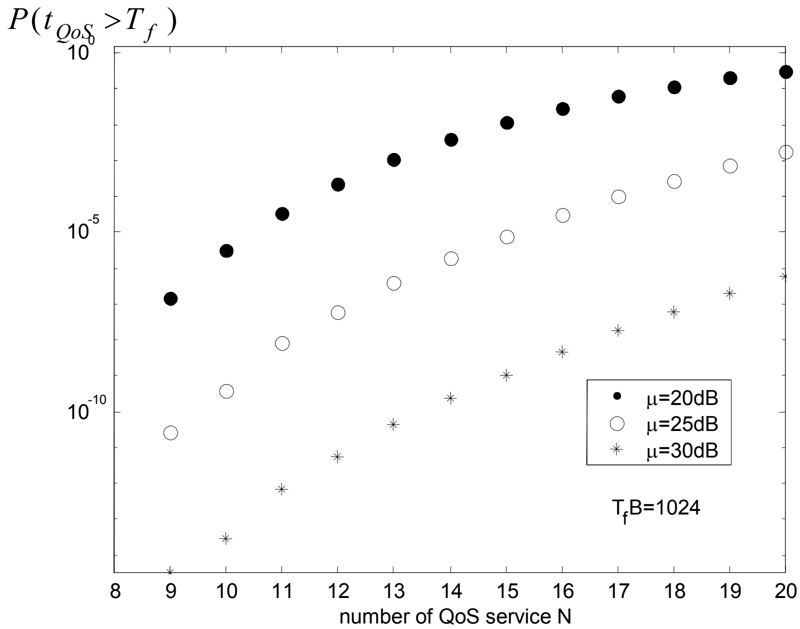

Fig.4.18. Investigation on $P(t_{QoS} > T_f)$

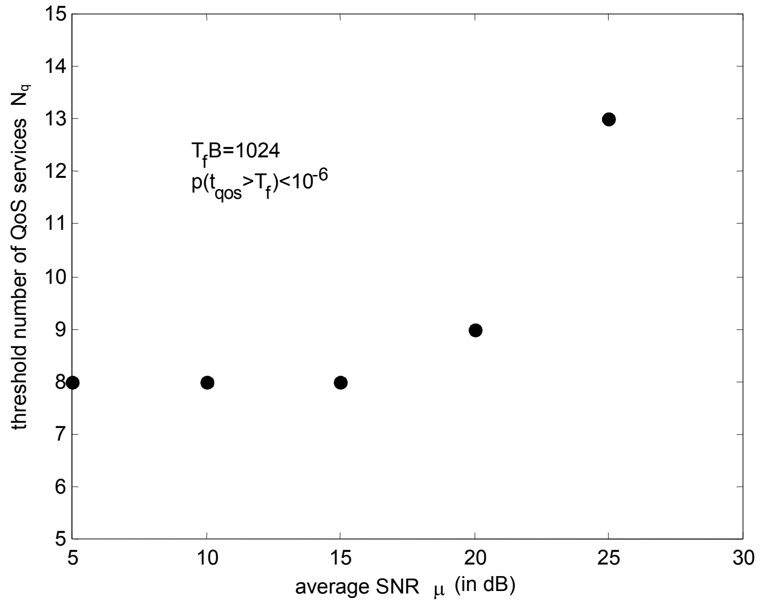

Fig.4.19 Investigation on N_q with respect to SNR

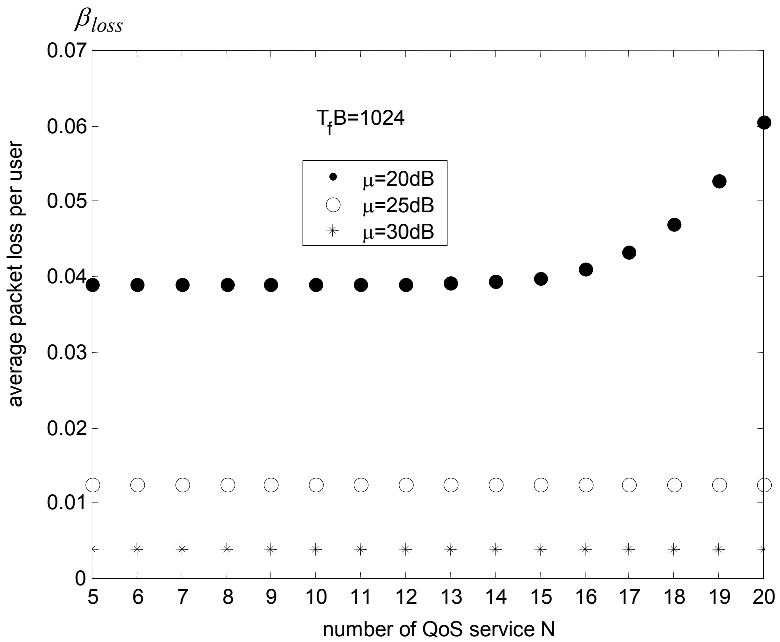

Fig.4.20 Average packet loss as a function of number of admitted QoS services

B. Average system throughput

The average system throughput is defined as the total number of data bits transmitted for both QoS services and BE services over one TDMA frame. We assume no constraint on data volume, i.e. user data is always available for transmission whenever there is bandwidth. This assumption is valid when evaluating the maximum system throughput. For simplicity, the signaling overheads are assumed to be part of the system throughput. Given the combination of number of QoS services ($N_0, N_1, N_2 \cdots N_H$), and assuming the BE service chosen from N_{BE} services employs $2^{i^{BE}}$ QAM modulation constellation during the transmission frame, the instantaneous system throughput in bits can be expressed as

$$C(N_0, N_1, N_2, \cdots N_H, N_i^{BE}=1) = (N_1 + N_2 + \cdots + N_H) \cdot L_p + t_{BE} i^{BE} B \quad . \quad (4\text{-}64)$$

where N_i^{BE} is the number of BE user employing $M = 2^{i^{BE}}$ constellation size to transmit and is always equal to 1 in our case. Assuming that both types of services are independent of each other, the probability of $C(N_0, N_1, N_2, \cdots N_H, N_i^{BE}=1)$ can be derived to be

$$P_C(N_0, N_1, N_2 \cdots N_H, 1) = P(N_0, N_1, N_2, \ldots N_H) P_i^{BE}, \quad (4\text{-}65)$$

where $P(N_0, N_1, N_2, \ldots N_H)$ and P_i^{BE} have been defined in (4-54) and (4-8) respectively.

Taking packet loss into account, the average system throughput will be given as

$$C_{av} = \frac{1}{T_f}\left[\sum C(N_0, N_1, N_2, \cdots N_H, 1) P_C(N_0, N_1, N_2, \cdots N_H, 1) - \beta_{QoS} L_p\right]. \quad (4\text{-}66)$$

The probability distribution of system throughput is shown in Fig.4.21. The average system throughput is shown in Fig.4.22. It can be seen that the system throughput increases with the decrease of the number of QoS services. The system throughput obtained for fixed TDMA systems where all time slots are assigned for QoS services with a fixed slot duration and BPSK modulation being used, the adaptive TDMA system with fixed time slot duration but adaptive modulation being used and the proposed system are compared in Table 4.6. It shows that the proposed system achieves a higher average system throughput than the other two systems. However as the same number of users are allowed to share the radio channel, the system throughput achieved by employing an adaptive MQAM with the proposed scheme performs worse than that achieved with the channel allocation scheme studied in Section 4.2. This is due to the fact that in the SNR-priority-based scheme, only users with the best few SNRs can be accommodated, whereas in the dual-class system, the QoS services have to be served regardless of their channel conditions thus insufficient usage of channel bandwidth is observed.

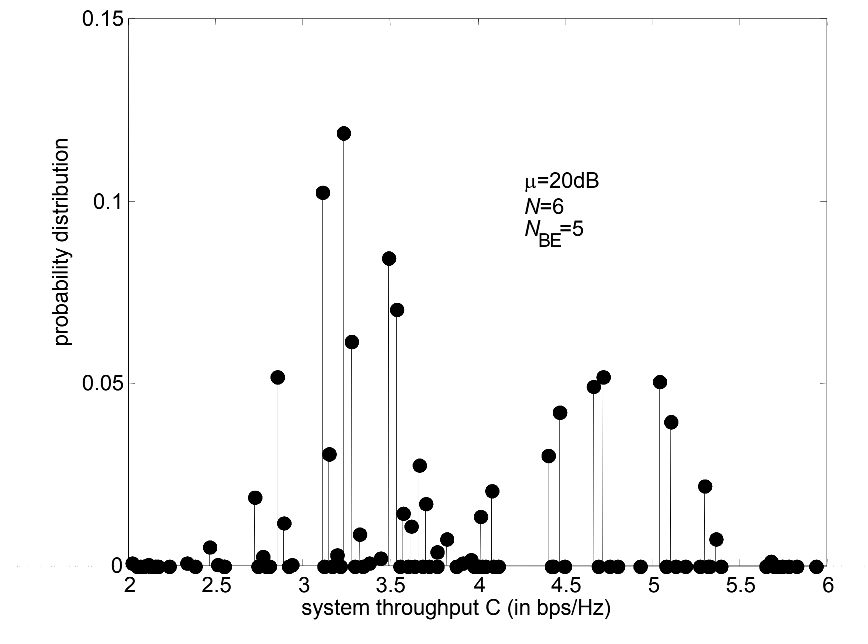

(a)

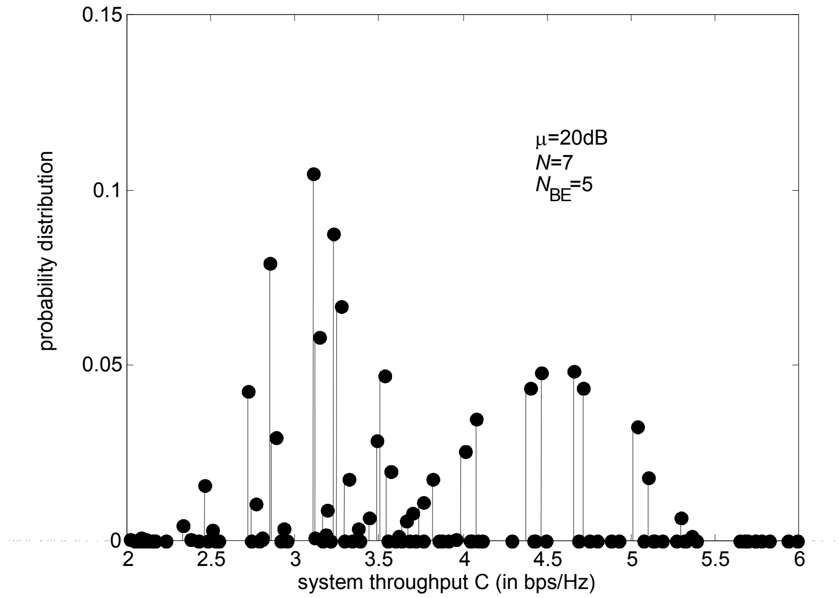

(b)

Fig.4-21 Probability distribution of system throughput (a) N=6 P(t_{QoS}>T_f)=0 and N=7, P(t_{QoS}>T_f)=0

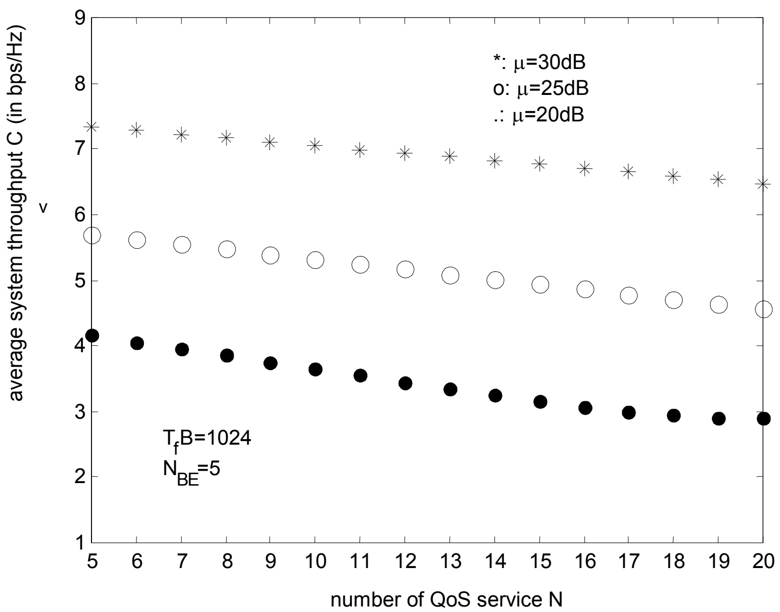

Fig.4-22 Average system throughput as a function of number of admitted QoS services

Table 4.6 Average system throughput comparison (SNR=15dB)

	No. of QoS service	No. of BE service	modulation	Packet size(bits)	Throughput (bps/Hz)
Fixed TDMA	8	0	BPSK	128	1
Adaptive TDMA	8	0	adaptive	Adaptive	2.08
Proposed system	8	1 out of 5	adaptive	128	2.91

4.4 Summary

The channel capacities achieved by the optimal channel and power allocation under multiple access environment are studied theoretically. It is observed that the capacity gain achieved by the combined rate and power adaptation over the rate adaptation only is insignificant employing this optimal system. Some performance metrics of the optimal channel allocation scheme are obtained. To overcome the difficulty of long channel inter-access time of the optimal channel allocation scheme, a suboptimal SNR-priority-based allocation scheme is proposed. The capacity achieved by this suboptimal scheme is studied by employing order statistics. The numerical results show that this proposed scheme can achieve a higher channel capacity than the conventional TDMA system and effectively alleviate the problem of the long channel inter-access time. A channel allocation scheme to accommodate QoS and BE services is also studied in this chapter. The average system throughput and the probability of packet loss have been investigated. This dual-class allocation scheme performs better in terms of average system throughput than the conventional fixed TDMA and the adaptive TDMA system with fixed time slot duration.

CHAPTER V

CAPACITY OF RATE ADAPTIVE CDMA SYSTEM OVER FREQUENCY SELECTIVE FADING CHANNEL

Rate adaptive modulation techniques can be applied to CDMA systems. In CDMA systems, users share the entire bandwidth simultaneously by employing spreading codes, unlike the systems studied in Chapter IV. Capacity of a CDMA system is then limited by both the channel characteristics and the multiple access interference. Most of currently deployed CDMA systems employ power control with fixed rate transmission. In this chapter, a variety of adaptive rate adaptive power control schemes is first proposed to improve the capacity of a CDMA system. These power control schemes make use of the information of channel conditions and location of mobile user. Capacity analysis is carried out on the uplink transmission under the constraint of a minimum required PG, the average transmission power and the BER performance of individual user.

5.1 System model description

5.1.1 RAKE receiver structure and combining techniques

As a wideband signal transmits over radio channels where the signal bandwidth is much greater than the coherent bandwidth of the radio channel, it experiences frequency selective fading. It will resolve the multipath components thus provide the receiver with several independently fading paths. Mathematically, frequency selective fading channel can be represented by (2-6). The commonly used receiver for processing such wideband signal is a RAKE receiver. It is designed to exploit the path diversity to overcome severe channel fading [75]. In fact, RAKE receiver attempts to collect the energy from all paths that fall within the span of the delay spread and carry the same information. RAKE receiver consists of a bank of L fingers defined by $L = \lfloor T_d / T_c \rfloor + 1$, where T_d ,T_c are the delay spread and the coherent time of channels or signal duration. $\lfloor X \rfloor$ is an operation taking the largest integer less than or equal to X. The finger output is then combined to form a decision variable.

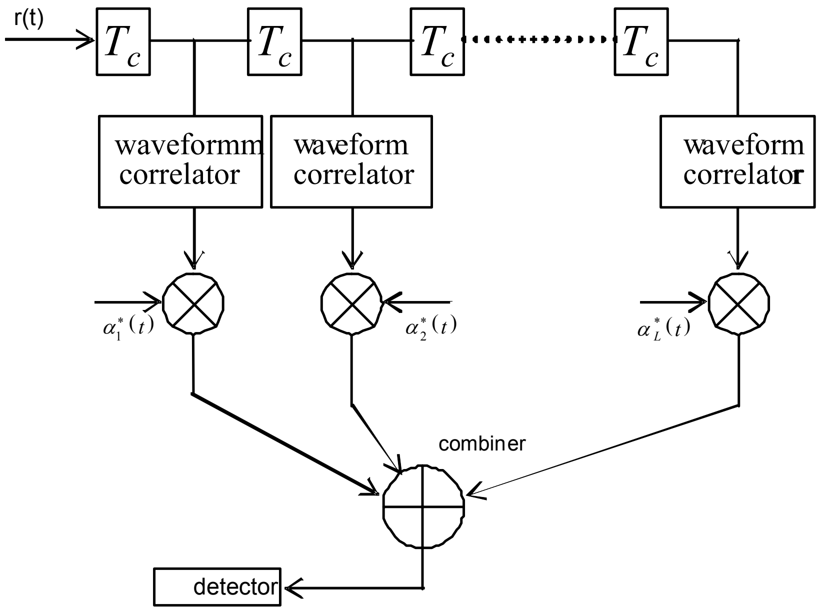

Fig.5.1 A block diagram of RAKE receivers

The structure of a RAKE receiver is shown in Fig.5.1. The RAKE receiver employs a single delay line model through which the received signal is passed. The time-varying tap weights $\{\alpha_l(t)\}$ corresponding to the L different delays are uncorrelated and complex-valued stationary random processes. At the output of the RAKE receiver, combining schemes can be employed to make use of the resolvable paths. The available diversity combining schemes are MRC [61], EGC [62] and SC [63]. In the subsequent study, MRC is assumed and the achieved system capacity is investigated. With MRC, the power received at the BS can be expressed as

$$p_r = \sum_{l=1}^{L} |h_l|^2 cz^{-n} p_t, \tag{5-1}$$

where $p_r, p_t, h_l = \alpha_l e^{j\theta_l}$ are the received power, the transmission power and the channel fading gain for the *l*th path respectively. c, n, z are path loss constant, path loss index and the distance between mobile users and the BS, respectively. In this study, we assume n=2. To avoid the singular point when performing analysis, a minimum distance z_0 between mobile users and the base station, which denotes the situation where mobile users are much closer to the base station so that the transmission is forced to stop, is defined in this study. The amplitude of the channel fading gain α_l takes any form of distribution introduced in Section 2.1 of Chapter II. The channel fading for each tap can be estimated precisely if the fading changes sufficiently slowly.

5.1.2 Detection techniques for CDMA systems

Assuming K mobile users are admitted in a CDMA system, the optimal maximum likelihood (ML) detector for a CDMA system must compute a large number of correlation metrics and select the K sequences that correspond to the largest correlation metric. Obviously this optimal detector has a computational complexity which grows exponentially with the number of users K. Some suboptimal detectors with computational complexity which grows linearly with K are employed, for example, conventional single-user detector, decorrelating detector and minimum mean-square-error (MMSE) detector [76-78]. Among them, multiuser detection techniques including decorrelating detectors and MMSE detectors are promising solution to combat MAI. However the major obstacle to the deployment of multiple user detector (MUD) is the high complexity of the algorithms. Therefore, the conventional single user matched filter based detector remains popular due to its simplicity. In this study, we employ the single user detector and analyze the capacity and the performance of some adaptive rate adaptive power control schemes.

In conventional single user detectors, the received signal is first correlated (or matched-filtered) with the signature sequence of the desired user. The output from the correlator is then passed to the detector, which makes decision based on the single correlator output. Thus the conventional detector treats signals from other co-channel users as interference. For the transmission over uplink, MAI is unavoidable since the long spreading codes or random codes are not perfectly orthogonal. In the extreme case, the interference is excessive if the power levels of some users are larger than the power level of the desired user. This leads to near-far end problem. The adoption of some kind of power control strategies is thus necessary in a CDMA system.

Two categories of power control schemes are widely employed in a CDMA system, one is strength-based power control scheme which maintains the received power for each user at the BS at a desired level, while the other is signal-to-interference ratio (SIR, defined as the ratio of signal power to interference power) based [79,80] power control scheme which maintains the received SIR at a desired level. In strength-based schemes, the strength of a signal arriving at the base station from one mobile is measured to control the transmission power, whereas in the SIR-based design, the quantity metric is the SIR with the interference consisting of both the channel noise and the MAI. In reality, the strength-based power control seems to be impractical due to the difficulty in the measurement of signal power, while the SIR-based power control is more realistic and desirable since it is the SIR which is directly related to the received bit error probability. It suffices to maintain the SIR at an acceptable level in order to guarantee the BER requirement. Generally adaptive transmission systems adopt the SIR based power control strategy and adjust transmission parameters such as transmission power and transmission rate accordingly.

In this chapter, three SIR-based power control schemes are proposed and studied. In each case, the transmission rate is adaptive to the received SIR while the transmission power of mobile users can be designed to adapt to the mobile location and the channel fading. In power control scheme I, we assume that path loss is compensated for at any time. The transmission power after path loss has been compensated for is kept as a constant, while the transmission rate is adapted to the received SIR. In scheme II, the transmission power is distributed according to the instantaneous channel conditions of individual mobile user. In scheme III, the location of each mobile user is taken into consideration. The transmission power is a function of the distance from the base station – the transmission power is adapted to path loss rather than just to compensate for it.

5.1.3 Rate adaptive modulation technique in CDMA system

Rate adaptive modulation can be employed in CDMA systems. The adaptation can be achieved by not only adaptive constellation size and coding, but also adaptive PG, adaptive chip rate and adaptive number of sub-channels for multi-carrier systems. The capacity and the BER performance of MQAM in CDMA systems was studied in [35,36]. The capacity of multi-rate CDMA systems realized through multi-code techniques was studied intensively in [81,82]. The adaptive PG is another solution to achieve adaptive modulation where the chip rate is kept as a constant while the processing gain is adjusted accordingly [33]. The capacity of CDMA systems achieved with rate adaptive modulation techniques over multipath fading channel has been investigated in [42] in terms of lower bound.

However, when the rate adaptive modulation is realized through adapting the PG to the channel conditions, these reported works generally do not set a minimum value on the PG and thus the conclusions are not accurate. In CDMA systems, user data is spread using a PN code with the chip rate much higher than the data rate to enable multiple access capability and to overcome the multipath channel fading and the MAI, therefore, there should have a minimum PG ($G_{\min}$). It is obvious that with this PG constraint, the transmission rate achieved by rate adaptive CDMA systems cannot go beyond the maximum rate defined by $R_{\max} = B / G_{\min}$ even if the channel conditions are extremely good. In this chapter, we propose a combined adaptive PG and adaptive MQAM technique which does not need to expand the spreading bandwidth while overcome the minimum PG constraint. Some power control schemes can be developed to increase the system capacity achieved by this technique. Detailed description of this technique is given later in this chapter.

In this study, the transmission rate for users in the proposed adaptive CDMA systems fluctuates with the channel fading or the user location. This fluctuation causes varying transmission delay for services. However this issue is above the scope of this study. Like most of the works in the literatures, without looking into the details of implementation, capacities of adaptive CDMA systems achieved by different adaptive rate adaptive power control schemes based on some available information of users such as channel fading gain and location are studied. However, since the performance of the proposed power control schemes relies on the estimation of SIR, channel fading gains and user location, with channel estimation error or location tracking error, the power control schemes are not able to allocate the transmission power to make use of the instantaneous conditions and user locations, resulting in the loss of bandwidth efficiency. The effect of estimation errors on the achieved system capacity is not studied in this thesis and is left for future

5.2 Interference analysis of adaptive CDMA system

Generally, for asynchronous transmission, there are a few symbols from interference users sharing the radio channel interfering with the desired symbol to be detected, resulting in MAI. Conventionally the uplink transmission suffers much severe degradation of system performance than the downlink transmission. CDMA is said to be uplink interference limited.

Assuming a multiple access DS/CDMA system in a single cell and signal transmitted over radio channel experiences both large-scale path loss and small-scale multi-path fading (the effect due to shadowing is neglected in this study to simplify the analysis). The received baseband signal $r(t)$ can be expressed as

$$r(t)=\sum_{m=1}^{K}\sqrt{2p_{m,t}(t)cz_m^{-n}}\sum_{l=1}^{L}h_{m,l}(t)b_m(t-\tau_{m,l})a_m(t-\tau_{m,l})+n(t) \quad , \tag{5-2}$$

where $b_m(t)$ is the transmitted binary signal, $a_m(t)$ is the spreading signal and $n(t)$ is

AWGN with double sided power spectrum density $N_0/2$. $p_{m,t}(t)$ is transmission power for the mth user. $h_{m,l}(t)=\alpha_{m,l}(t)e^{j\theta_{m,l}(t)}$ is fading gain for the mth user over the lth path with $\alpha_{m,l}(t)$, $\theta_{m,l}(t)$ being the amplitude and the phase of the fading gain, respectively. K is the number of users allowed to transmit simultaneously, $\tau_{m,l}=lT_c$ is the delay for the mth user over the lth path. The power delay profile employed in this study can be uniformly distributed or has any other distributions. For uniformly distributed power delay profile, the variance for each path is $2\sigma^2=\Omega=1/L$. For exponential distribution, $2\sigma_l^2=\Omega_l=A\exp(-(l-1)T_d/T_c)$, where A is the normalized factor. c is the path loss constant and z_m is the distance between the base station and the m^{th} user. n is the path loss index.

The RAKE receiver is employed and MRC is performed at the output of the receiver. In the lth path of the RAKE receiver of the mth user, the interference power received at the base station can be derived to be

$$\begin{aligned} I_{m,l} &= p_{m,t}cz_m^{-n}\sum_{j\neq l}^{L}|h_{m,j}|^2 + \sum_{j=1,j\neq m}^{K}p_{j,t}cz_j^{-n}\sum_{l=1}^{L}|h_{j,l}|^2 \\ &= p_{m,t}cz_m^{-n}\sum_{j\neq l}^{L}(\alpha_{m,j})^2 + \sum_{j=1,j\neq m}^{K}p_{j,t}cz_j^{-n}\sum_{l=1}^{L}(\alpha_{j,l})^2 \quad . \end{aligned} \tag{5-3}$$

In the right hand side of (5-3), the first term gives the self interference power from other paths of the mth user whilst the second term gives the interference from other users sharing the frequency band. In practical, the second term is much larger than the first term, i.e. self-interference can be neglected, (5-3) can be written as

$$I_m \approx \sum_{i=1,i\neq m}^{K} p_{i,t}cz_i^{-n}\sum_{l=1}^{L}(\alpha_{i,l})^2 \ . \tag{5-4}$$

In CDMA systems, for coherent BPSK receivers, the BER performance can be approximated by $P_e \approx Q\left(\sqrt{2(E_b/N_0)}\right)$ [83,84]. The E_b/N_0 for the *m*th user can be expressed as [85]

$$\left(\frac{E_b}{N_0}\right)_m = \frac{p_{m,r}/R_m}{2T_c I_m/3 + N_0}, \tag{5-5}$$

where $p_{m,r}$,R_m are the received power and the instantaneous transmission rate for the *m*th user. The constant 2/3 arises in (5-5) since rectangular chip pulses are assumed. However for different pulse shapes, it has different value. If thermal noise is negligible and substitute (5-4) to (5-5), E_b/N_0 is obtained

$$\frac{E_b}{N_0} = \frac{3}{2T_c}\frac{\sum_{l=1}^{L}(\alpha_{m,l})^2 p_{m,t} c z_m^{-n} T_b}{\sum_{i=1,i\neq m}^{K} p_{i,t} c z_i^{-n}\sum_{l=1}^{L}(\alpha_{i,l})^2} = \frac{\sum_{l=1}^{L}(\alpha_{m,l})^2 p_{m,t} c z_m^{-n}}{\sum_{i=1,i\neq m}^{K} p_{i,t} c z_i^{-n}\sum_{l=1}^{L}(\alpha_{i,l})^2}\frac{3B}{2R_m}. \tag{5-6}$$

In (5-6), $T_b/T_c = B/R_m = G$ is defined as the PG. Generally in CDMA systems, to maintain the capability of combating multipath fading, one symbol cannot be spread by less than one chip, i.e., the PG must be kept larger than a pre-defined $G_{\min}$ with $G_{\min} > 1$. This PG constraint limits the system to make use of the advantage offered by the adaptive transmission efficiently. For example, although one user observes channel conditions where higher transmission rate can be employed, it has to transmit at a rate equal to $B/G_{\min}$. Hence the better channel conditions cannot be fully exploited. This fact has not been considered in most of the reported works [41,42] and results in inaccurate conclusion. In the following, various adaptive transmission schemes are proposed and the performance in terms of system capacity under the PG constraint is studied.

5.3 Capacity of rate adaptive CDMA system with path loss being compensated for

Conventionally, the capacity of a CDMA system is evaluated in terms of the maximum number of users supported in the system. This is fair in a single rate CDMA system. As adaptive rate or multi-rate is used, this definition turns out to be inappropriate. Here we adopt alternative definition where the system capacity is defined as the sum of the average transmission rate from all users in the system, or mathematically,

$$C = \sum_{m=1}^{K} \overline{R}_m \ , \tag{5-7}$$

where $\overline{R}_m$ is the average transmission rate for the mth user.

5.3.1 Power control scheme I—adaptive rate constant transmission power

In this rate adaptive power control scheme, we assume that path loss can be compensated for at any time instant. This scheme is similar to conventional CDMA systems except no intention for closed loop power control to combat fast fading but rather rate adaptive being employed. This compensation can be performed very easily once the position of the mobile is known and the path loss model is well defined. Alternatively we could average the received signal over a sufficient observation period to estimate path loss. The transmission power after path loss is totally compensated for remains constant for all mobile users. Therefore the received power at the base station for the mobiles is different only as a result of the fast channel fading and the instantaneous transmission rate is adapted to the respectively received SIR.

Considering BPSK modulation, from (5-6), the instantaneous transmission rate for the mth user can be obtained as

$$R_m = \frac{\sum_{l=1}^{L}(\alpha_{m,l})^2 p_{m,t} c z_m^{-n}}{\sum_{j=1,j\neq m}^{K} p_{j,t} c z_j^{-n} \sum_{l=1}^{L}(\alpha_{j,l})^2} \frac{3B}{2\gamma_{\min}} \tag{5-8}$$

where $\gamma_{\min}$ is the predefined E_b/N_0 requirement to guarantee the transmission quality and $B = 1/T_c$ is the spreading bandwidth.

Setting $\alpha_L = \sum_{l=1}^{L}(\alpha_{m,l})^2$ and $\alpha_K = \sum_{j=1,j\neq m}^{K}\sum_{l=1}^{L}(\alpha_{j,l})^2$ and assuming uniformly distributed power delay profile, the PDF of α_L and α_K can be derived as

$$f_{\alpha_L}(\alpha_L) = \frac{\left[1/(2\sigma^2)\right]^L}{(L-1)!}(\alpha_L)^{L-1}\exp\left[-\frac{\alpha_L}{2\sigma^2}\right] \tag{5-9}$$

and

$$f_{\alpha_K}(\alpha_K) = \frac{\left[1/(2\sigma^2)\right]^{(K-1)L}}{\left[(K-1)L-1\right]!}\alpha_K^{(K-1)L-1}\exp\left[-\frac{\alpha_K}{2\sigma^2}\right], \tag{5-10}$$

where $2\sigma^2 = \Omega$ is the variance of the channel fading for each path. For a non-uniform distribution, the following expressions can be derived [86],

$$f_{\alpha_L}(\alpha_L) = \sum_{l=1}^{L}\overline{\alpha}_{L,l}^{L-2}\exp\left(-\frac{\alpha_L}{\overline{\alpha}_{L,l}}\right)\prod_{j=1,j\neq l}^{L}\frac{1}{\overline{\alpha}_{L,l}-\overline{\alpha}_{L,j}}, \tag{5-11}$$

and

$$f_{\alpha_K}(\alpha_K) = \sum_{l=1}^{(K-1)L}\overline{\alpha}_{K,l}^{(K-1)L-2}\exp\left(-\frac{\alpha_K}{\overline{\alpha}_{K,l}}\right)\prod_{j=1,j\neq l}^{(K-1)L}\frac{1}{\overline{\alpha}_{K,l}-\overline{\alpha}_{K,j}}, \tag{5-12}$$

where $\alpha_{L,l} = |h_{m,l}|^2$, $\alpha_{K,l} = |h_{j,l}|^2$ are the power gain of the lth path for the mth desired user and the jth interference user. $\overline{\alpha}_{L,l}, \overline{\alpha}_{K,l}$ are the mean values of $\alpha_{L,l}, \alpha_{K,l}$ respectively.

Since large scale path loss is needed to be totally compensated for at the BS, the transmission power for the *m*th mobile user before path loss being compensated for will have to overcome the power attenuation caused by path loss and has the form of

$$p_{m,t} = \overline{p} z_m^n / c , \tag{5-13}$$

where $\overline{p}$ is the transmission power after path loss is compensated for. Substitute (5-13) into (5-8), the received E_b / N_0 for the *m*th user can be rewritten as

$$\frac{E_b}{N_0} = \frac{\sum_{l=1}^{L} (\alpha_{m,l})^2 \overline{p} T_b}{\frac{2T_c}{3} \sum_{j=1, j\neq m}^{K} \overline{p} \sum_{l=1}^{L} (\alpha_{j,l})^2} = \frac{\alpha_L}{\alpha_K} \frac{3G}{2} . \tag{5-14}$$

The PDF of E_b / N_0 can be derived to be

$$f_\gamma(\gamma) = \frac{\left[1/(2\sigma^2)\right]^{KL} [KL-1]!}{\left[(K-1)L-1\right]! [L-1]!} \left(\frac{2\gamma}{3G_{\min}} \right)^{L-1} \frac{2}{3G_{\min}} \left(\frac{1}{2\sigma^2} + \frac{2\gamma}{6G_{\min}\sigma^2} \right)^{-KL} . \tag{5-15}$$

The PDF of E_b / N_0 is shown in Fig.5.2. It can be seen that, with higher PG constraint, the PDF of γ moves toward high E_b / N_0 end.

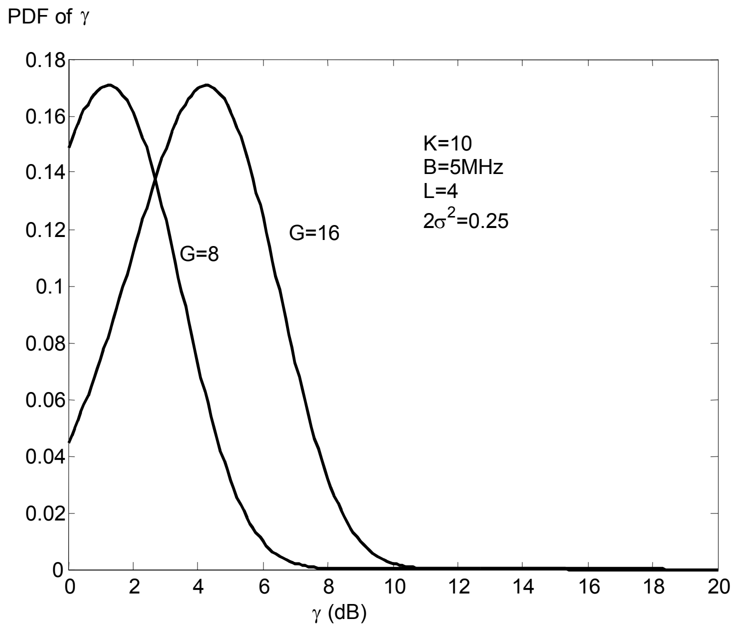

Fig.5.2 A PDF of instantaneous E_b/N_0

Likewise, the PDF of R (the subscript *m* is dropped since it is identical to all users) is derived to be

$$f_R(R)=\frac{\left[1/(2\sigma^2)\right]^{KL}[KL-1]!}{\left[(K-1)L-1\right]![L-1]!}\left(\frac{2\gamma_{\min}R}{3B}\right)^{L-1}\frac{2\gamma_{\min}}{3B}\left(\frac{1}{2\sigma^2}+\frac{2\gamma_{\min}R}{6B\sigma^2}\right)^{-KL}. \qquad (5\text{-}16)$$

As more users are allowed in the system, the interference experienced by each user increases, hence the probability that one user transmits at a high data rate decreases, as observed from Fig.5.3.

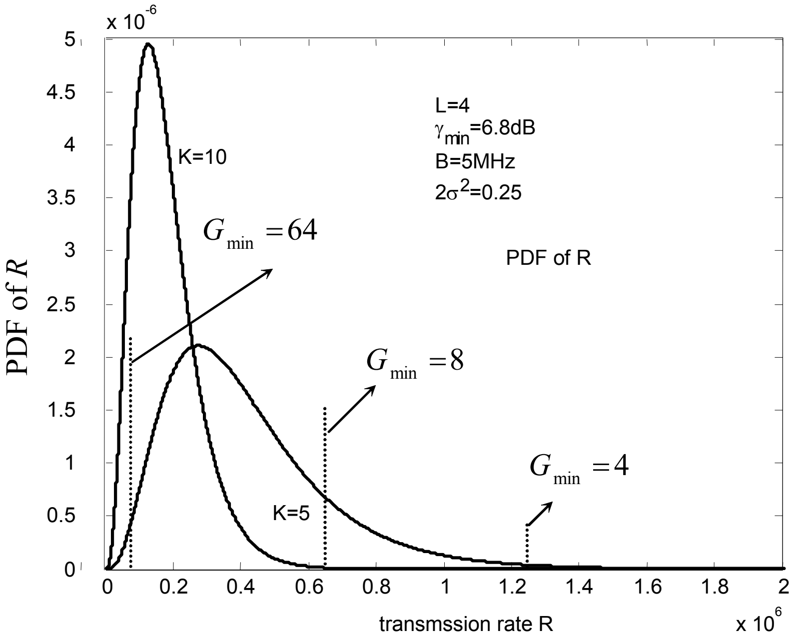

Fig.5.3 A PDF of instantaneous rate R

A. System capacity employing adaptive PG only

As PG can take any value larger than $G_{\min}$, the average system capacity is given as

$$C = K\left(\int_{0}^{R_{\max}} R f_R(R)\,dR + \int_{R_{\max}}^{\infty} R_{\max} f_R(R)\,dR \right), \tag{5-17}$$

where the first term is the average system capacity achieved as $G < G_{\min}$ and the second term is the system capacity achieved as $G > G_{\min}$.

In multi-rate systems where the PG can only take a value from a set of discrete PGs $G = \{G_1, G_2, \cdots G_j, G_{j+1}, \cdots G_D\}$, the system capacity is given as

$$C = K \sum_j \frac{B}{G_j} \int_{B/G_j}^{B/G_{j+1}} f_R(R)\,dR\,. \tag{5-18}$$

For the purpose of comparison, the system capacity achieved by the fixed rate perfect power control scheme where both path loss and fast fading are compensated for (or the power received at the BS remains constant) is computed. When thermal noise is not taken into account, the transmission rate can be expressed as: $R = \frac{3B}{2\gamma_{\min}(K-1)}$ and $G = \frac{2(K-1)\gamma_{\min}}{3}$. If $G \geq G_{\min}$, then $C = KR$. In case $G \leq G_{\min}$, $C = KR_{\max}$.

The system capacity achieved by adaptive continuous and discrete PG is shown in Fig.5.4 and Fig.5.5 respectively, with the transmission power defined by (5-13). As continuous PG is used, it can be seen that there exists a maximum system capacity. Before reaching this maximum capacity, the SIRs experienced by most of the users are high. However users have to transmit at $R_{\max}$ due to $G_{\min}$ even though they can transmit at a data rate higher than $R_{\max}$. Therefore the system is in an underloading state because of the $G_{\min}$ constraint. After reaching the maximum capacity, most users in the system are transmitting at a rate defined by (5-8). The system capacity decreases with the number of users. For discrete PG, as the number of users increases, the system capacities achieved by different sets of PG approach the same value. Another observation is, with the PG constraint, the capacity achieved by discrete PGs cannot be better than that achieved by continuous PG due to the limited number of PGs being used. As fewer users are supported in the system, the rate adaptive system employing adaptive PG performs not better than the fixed rate or the ideal power control system as shown in Fig.5.4, while with the increase of number of users in the system, it will achieve the same system capacity. The explanation is as follows. With a small number of users, due to the low

MAI, the system is in an underloading state. The received SIR for individual user is high, adaptive PG can be used to make use of the good conditions, thus to improve bandwidth efficiency. At a large number of users, since the MAI is large, the received SIR is low most of the time. Therefore the capacity gain achieved by employing adaptive PG is very limited.

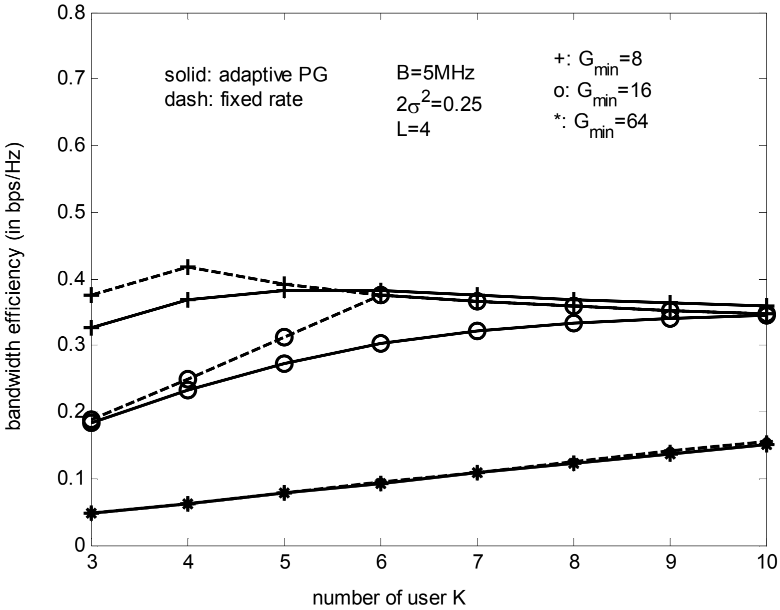

Fig.5.4 Capacity achieved by adaptive continuous PG

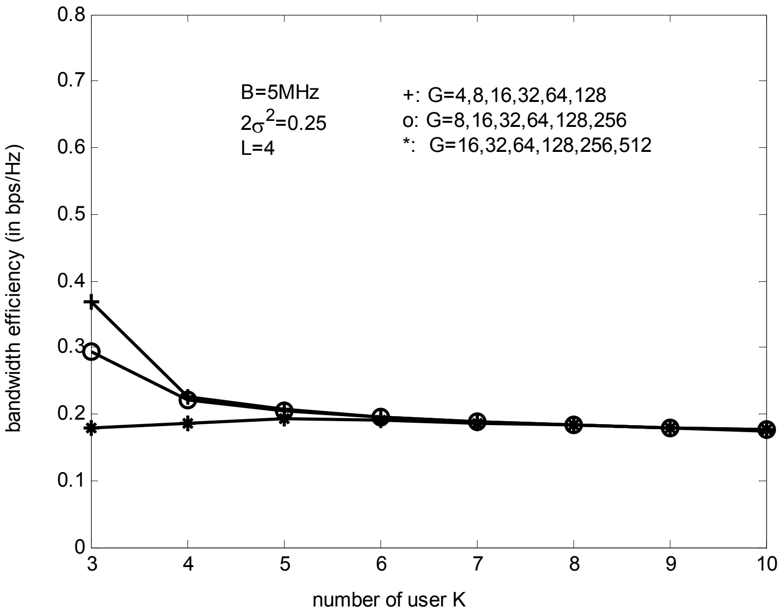

Fig.5.5 Capacity achieved by adaptive discrete PG

B. System capacity employing combined adaptive PG and adaptive MQAM

In previous study, as there exists a minimum processing gain constraint, $G_{\min}$, even if the SIR observed by one mobile user is good, the instantaneous transmission rate cannot exceed $R_{\max}$. One solution to overcome this problem is to employ the rate adaptive MQAM modulation once the PG required to achieve desired a E_b/N_0 threshold ($\gamma_{\min}$) is smaller than $G_{\min}$. The rationale behind this solution is: in case that higher R can be employed but a transmission rate of $R_{\max}$ has to be used, the instantaneous E_b/N_0 obtained for one mobile user might exceed the minimum E_b/N_0 requirement (or $\gamma_{\min}$), hence a higher order MQAM constellation can be used to exploit the extra E_b/N_0 resulted from good SIR conditions while the required BER performance can still be guaranteed. As MQAM is used, the transmission rate is calculated as $R = R_{\max}\log_2 M$, where $M = 2^i$ is the constellation size. For BPSK modulation, $i=1$ and the $\gamma_{\min}$ required to achieve the BER performance of 10^{-3} is 6.8dB. For QPSK, $i=2$ and $\gamma_{\min} = 9.8\text{dB}$. With the combination of adaptive PG and adaptive MQAM, the system capacity is expected to increase. Hence with this combination, the system capacity achieved can be expressed as

$$C = K(\overline{\Re}_1 + \overline{\Re}_2), \tag{5-19}$$

where $\overline{\Re}_1$ and $\overline{\Re}_2$ are the portion of capacity when only adaptive PG takes place and when PG takes the values $G_{\min}$, respectively.

$$\overline{\Re}_1 = \int_0^{R_{\max}} R f_R(R)\, dR \quad , \tag{5-20}$$

and

$$\overline{\Re}_2 = R_{\max} \int_{\gamma_{\min}}^{\infty} \log_2[M(\gamma)] f(\gamma)\, d\gamma, \tag{5-21}$$

where $M(\gamma) = 1 - \dfrac{1.5\gamma}{\ln(5 \cdot BER)}$. The adaptive MQAM will be employed once $\gamma > \gamma_{\min}$.

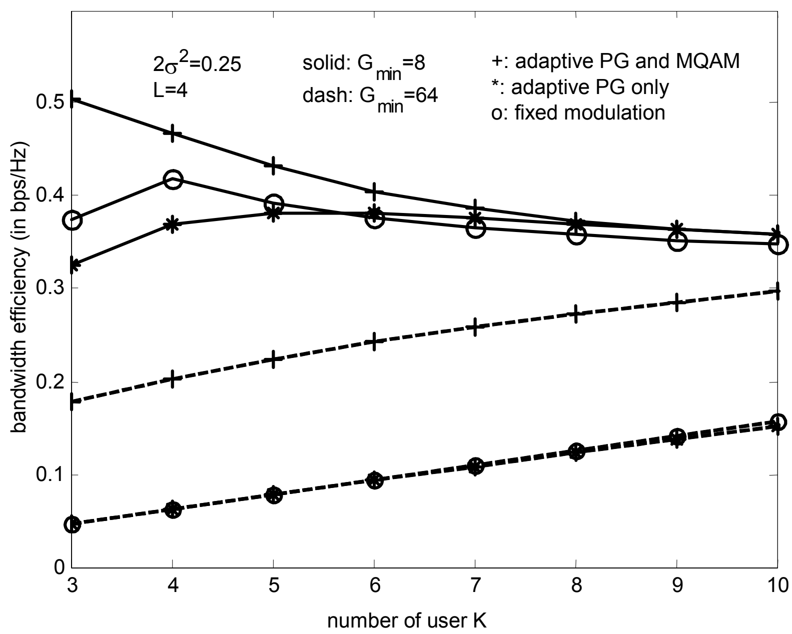

Fig.5.6 Capacity achieved by adaptive continuous PG and continuous MQAM

The system capacity achieved by the combined adaptive PG and MQAM technique is shown in Fig.5.6 with B=5MHz. From Fig.5.6, it can be seen that with the combined adaptive PG and MQAM, the system capacity can be improved noticeably. The improvement in terms of bandwidth efficiency is significant as $G_{\min}$ is higher. However with the increase of the number of users, the capacity gain achieved by the combined adaptive PG and MQAM technique becomes insignificant, for example, the bandwidth approaches 0.35 as $G_{\min} = 8$. This can be explained by the fact that with the increase of K, the probability of $R > R_{\max}$ becomes insignificant. With the combination of adaptive PG and adaptive MQAM, unlike systems with adaptive PG only, the achieved system capacity can be higher than the fixed rate perfect power control systems, especially under small a number of users in the system and a higher $G_{\min}$.

5.3.2 Power control scheme II--adaptive rate adaptive power

As the instantaneous channel information is available at both transmitters and receivers, not only the transmission rate but also the transmission power can be adapted. The implementation of the optimal power control is complicated for interference limited systems since the increase of the power level of each user will cause interference to other users in CDMA systems. Most of the previous works aim to look into the optimal power allocation to maximize information capacity over fading channel with the help of iterative algorithms [87]. The optimal rate and power adaptation for multi-rate CDMA systems over fading channel was studied in [88]. Here we proposed a simple power allocation scheme based on the knowledge of the fast channel fading, for which no complicated algorithm is needed and the attainable system capacity is still improved. In this power control scheme, the transmission power is distributed according to mobile user's individual channel conditions, like the single user water-filling strategy. User will be assigned more power and transmits more data when it observes better channel conditions. Part of the transmission power will, however, still be used to compensate for respective path loss, with the amount depending on the distance from mobile users to the BS. Therefore, in this case, both the transmission power and the transmission rate are adapted accordingly, unlike the power control scheme I studied in Section 5.3.1 where only the transmission rate is adapted. Comparing to the scheme with rate adaptation constant transmission power, the power control scheme studied in this section gives more privilege to the user observing better channel conditions. However, in the extreme case, no power will be allocated to the user with poor channel conditions, and transmissions for these users have to be delayed to a later time.

In this scheme, the transmission power of the mth mobile is of the form

$$p_{m,t} = \frac{Dz_m^n}{c}\left(\sum_{l=1}^{L}(\alpha_{m,l})^2\right)^q, \tag{5-22}$$

where both D and q are power control parameters. The received power for the mth user is

$$p_{m,r} = D\left(\sum_{l=1}^{L}(\alpha_{m,l})^2\right)^{q+1}. \tag{5-23}$$

As adaptive transmission schemes are used, the sum of instantaneous transmission power for all mobile users in the system will fluctuate according to the instantaneous locations of all mobile users. To fairly evaluate the performance of power control schemes, we are looking at maintaining the long-term average total transmission power at a constant. To keep the average transmission power as a constant, and assuming that users are likely occur in anywhere of the cell over the observation period, coefficient D can be derived as

$$D = \frac{(L-1)!\,\overline{p}}{(2\sigma^2)^q\,(L+q-1)!}. \tag{5-24}$$

By setting $w = \left[\sum_{l=1}^{L}(\alpha_{j,l})^2\right]^{q+1}$, based on (5-9), the PDF of w is given as

$$f_w(w) = \left(\frac{1}{2\sigma^2}\right)^L \frac{1}{(L-1)!(q+1)} w^{\frac{L-q-1}{q+1}} e^{-\frac{w^{\frac{1}{q+1}}}{2\sigma^2}}. \tag{5-25}$$

Substitute (5-22) into (5-6), the transmission rate for each user (the subscript m is dropped) is derived to be

$$R = \left(D\left[\sum_{l=1}^{L}(\alpha_{m,l})^2\right]^{q+1} \Big/ D\sum_{j=1,j\neq m}^{K}\left[\sum_{l=1}^{L}(\alpha_{j,l})^2\right]^{q+1} \right)\frac{3B}{2\gamma_{\min}} \\ == \frac{3B}{2\gamma_{\min}}\frac{w_m}{\sum_{j=1,j\neq m}^{K} w_j} \quad . \tag{5-26}$$

The capacity achieved by the adaptive PG and adaptive MQAM can be obtained as

$$\overline{\Re}_1 = \frac{3B}{2\gamma_{\min}}\int_{w_K=0}^{\infty}\int_{w_1=0}^{\infty}\cdots\int_{0}^{w=\frac{2\gamma_{\min}}{3G}\sum_{j=1,j\neq m}^{K-1}w_j}\frac{w_m}{\sum_{j=1,j\neq m}^{K-1}w_j}f_{w_m}(w_m)f_{w_1}(w_1)\cdots f_{w_K}(w_K)dw_m dw_1\cdots dw_K \tag{5-27}$$

$$\overline{\Re}_2 = R_{\max}\int_{w_K=0}^{\infty}\int_{w_1=0}^{\infty}\cdots\int_{w_m=\frac{2\gamma_{\min}}{3G}\sum_{j=1,j\neq m}^{K-1}w_j}^{\infty}\log_2 M(\gamma)f_{w_m}(w_m)f_{w_1}(w_1)\cdots f_{w_K}(w_K)dw_m dw_1\cdots dw_K \tag{5-28}$$

where

$$\gamma = \frac{3B}{2R_{\max}}\frac{w_m}{\sum_{j=1,j\neq m}^{K} w_j}. \tag{5-29}$$

Capacity achieved by the adaptive rate and adaptive power scheme is shown in Fig.5.7, where $q=0$ corresponds to the case presented in section 5.3.1. It is observed that the increase of q leads to the improvement of the system capacity. However as $G_{\min}$ is larger, the increase of the system capacity with q is very insignificant. Fig.5.8 shows the dependence of the system capacity on the number of users *K*. This dependence varies with the $G_{\min}$ as seen in this figure. The system capacities achieved from different schemes are listed in Table 5.1. It can be seen that with the combined adaptive PG and MQAM, the adaptive rate adaptive power scheme studied in this section achieves higher system capacity than scheme I studied in Section 5.3.1 and the conventional perfect power control scheme.

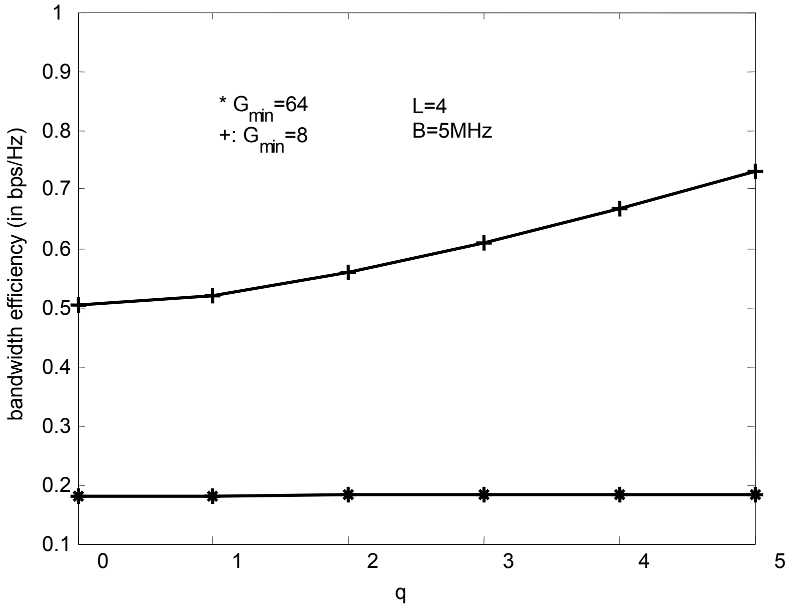

Fig.5.7 Capacity achieved with different power control coefficient q (K=3, $2\sigma^2 = 0.25$)

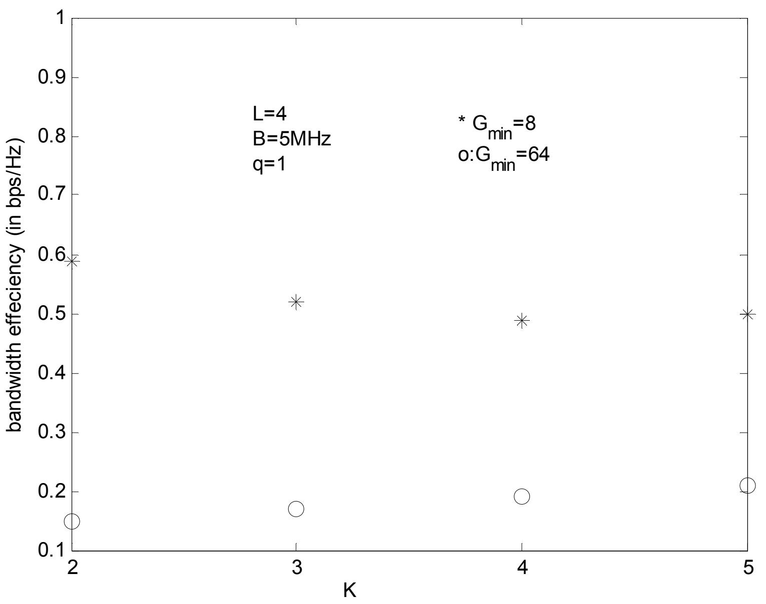

Fig.5.8 Capacity achieved with different number of users K ($2\sigma^2 = 0.25$)

TABLE 5.1 Bandwidth efficiency comparison (K=3)

Scheme	$G_{\min}$	With MQAM	Without MQAM
Adaptive rate	4	0.65	0.43
	8	0.5	0.33
Adaptive rate adaptive power	4, q=3	0.8	0.25
	8, q=3	0.61	0.15
Perfect	4,8	0.375	0.375

5.3.3 Dual-class services employing adaptive PG only

In wireless systems, more than one class of services will have to be accommodated. For different services with different transmission requirements, the power allocation strategy can be different. Here assuming a dual-class CDMA system supporting voice and data services, the power control strategies are specified as: 1) Voice service is transmitted at a fixed rate (using BPSK) in order to maintain constant delay performance, a constant received power for voice user is then required. 2) Power control scheme I is employed for data users which has no stringent requirement on delay performance: the received power fluctuates with the channel conditions of individual user and the transmission rate is adapted to the received SIR by changing PG. The transmission power for data users is defined by (5-13). The co-existence of these two power control schemes makes the total transmission power of dual-class systems not a constant. In the following, the system capacity and the power consumption will be studied.

Assuming that the number of voice users and data users supported in the system is K_v and K_d, respectively, and the transmission rate of voice user is R_v. For the voice and data users, their respective E_b / N_0 expression (5-5) can be written as

$$\gamma^{(v)} = \frac{p_{m,r}^{(v)}}{\sum_{j=1,j\neq m}^{K_v} p_{j,r}^{(v)} + \sum_{j=1}^{K_d}\sum_{l=1}^{L} (\alpha_{j,l})^2 \,\overline{p}_d} \frac{3B}{2R_v}, \tag{5-30a}$$

$$\gamma^{(d)} = \frac{\sum_{l=1}^{L} (\alpha_{m,l})^2 \,\overline{p}_d}{\sum_{j=1}^{K_v} p_{j,r}^{(v)} + \sum_{j=1,j\neq m}^{K_d}\sum_{l=1}^{L} (\alpha_{j,l})^2 \,\overline{p}_d} \frac{3B}{2R_d}, \tag{5-30b}$$

where $p_{j,r}^{(v)}, \overline{p}_d$ are the received power for the *j*th voice and the average transmission power for the data user respectively. The first term and the second term in the denominator of (5-30a) and (5-30b) represent the interference from voice users and data users, respectively. To ensure the fixed rate transmission for voice users, the received power has the relationship

$$p_{1,r}^{(v)} = p_{2,r}^{(v)} = \cdots = p_{K_v,r}^{(v)} = p_r^{(v)}. \tag{5-31}$$

To satisfy the BER requirement, $\gamma^{(v)} \geq \gamma_{\min}^{(v)}$. Substitute (5-31) into (5-30a), the received power for voice user is obtained as

$$p_r^{(v)} = \frac{\sum_{j=1}^{K_d}\sum_{l=1}^{L} (\alpha_{j,l})^2 \,\overline{p}_d}{3B/2\gamma_{\min}^{(v)} - (K_v - 1)R_v} R_v. \tag{5-32}$$

A. System capacity investigation

To ensure the transmission quality, $\gamma^{(d)} \geq \gamma_{\min}^{(d)}$. Therefore from (5-30b), the transmission rate for data users can be obtained as

$$R_d = \frac{\sum_{l=1}^{L} (\alpha_{m,l})^2 \,\overline{p}_d}{\sum_{j=1}^{K_v} p_{j,r}^{(v)} + \sum_{j=1,j\neq m}^{K_d}\sum_{l=1}^{L} (\alpha_{j,l})^2 \,\overline{p}_d} \frac{3B}{2\gamma_{\min}^{(d)}}. \tag{5-33}$$

Substitute (5-32) into (5-33), the transmission rate of data users can be rewritten as

$$R_d = \frac{1}{\left[3B/2\gamma_{\min}^{(v)} + R_v\right]\xi + K_v R_v}\left[\frac{3B}{2\gamma_{\min}^{(v)}} - (K_v - 1)R_v\right]\frac{3B}{2\gamma_{\min}^{(d)}}, \tag{5-34}$$

where

$$\xi = \sum_{j=1,j\neq m}^{K_d}\sum_{l=1}^{L} |\alpha_{j,l}|^2 \Big/ \sum_{l=1}^{L}|\alpha_{m,l}|^2 . \tag{5-35}$$

The PDF of ξ is derived to be

$$f_\xi(\xi) = \frac{(K_d L - 1)!}{\left[(K_d - 1)L - 1\right]!(L-1)!}\xi^{(K_d - 1)L - 1}\frac{1}{(\xi + 1)^{K_d L}} . \tag{5-36}$$

Due to the existence of voice users, as seen from (53), R_d is limited by $R_d^{\max}$ with

$$R_d^{\max} = \frac{1}{K_v R_v}\left[\frac{3B}{2\gamma_{\min}^{(v)}} - (K_v - 1)R_v\right]\frac{3B}{2\gamma_{\min}^{(d)}} . \tag{5-37a}$$

Here $R_d^{\max} \neq R_{\max}$. If $R_d^{\max} < R_{\max}$, only adaptive PG is used to realize the rate adaptation. As $R_d^{\max} > R_{\max}$, adaptive PG is employed for $R \le R_{\max}$, while adaptive MQAM is used for $R_{\max} < R \le R_d^{\max}$. $R_d^{\max}$ depends $K_v, K_d, \gamma_{\min}$ and R_v.

The average transmission rate for data users can be obtained

$$\overline{R}_d = \int_{\xi_0}^{\infty} \frac{3B}{2\gamma_{\min}^{(d)}}\left[\frac{3B}{2\gamma_{\min}^{(v)}} - (K_v - 1)R_v\right]\frac{f_\xi(\xi)}{\left(3B/2\gamma_{\min}^{(v)} + R_v\right)\xi + K_v R_v}d\xi + \int_0^{\xi_0}\frac{B}{G_{\min}}f_\xi(\xi)d\xi, \tag{5-37b}$$

where

$$\xi_0 = \frac{\left[3B/2\gamma_{\min}^{(v)} - (K_v - 1)R_v\right]3G_{\min}/2\gamma_{\min}^{(d)} - K_v R_v}{3B/2\gamma_{\min}^{(v)} + R_v}. \tag{5-38}$$

The first term in (5-37) corresponds to the case with $R_d \le B/G_{\min}$, while the second term corresponds to the case with $R_d > B/G_{\min}$. The average system capacity for the dual classes of services systems is given as

$$C = K_v R_v + K_d \overline{R}_d. \tag{5-39}$$

The bandwidth efficiency is then obtained as C/B.

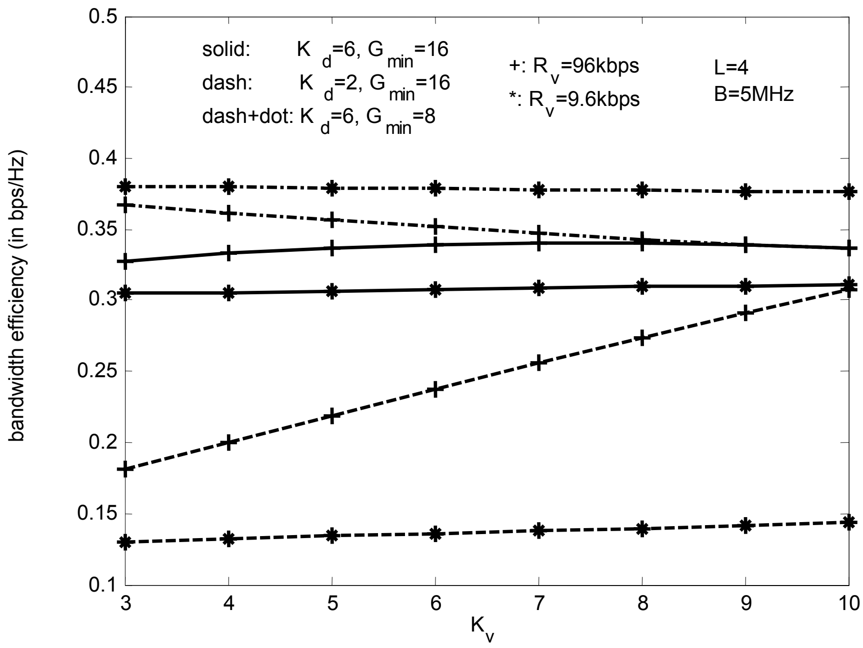

Fig.5.9 System capacity for dual-class CDMA system

The system capacity calculated from (5-39) is presented in Fig.5.9. It is observed that the system capacity first increases with K_v. It is expected that there exists a K_v leading to a maximum system capacity. After the maximum capacity is reached, the system capacity will decreases with the increase in K_v, as for the case with $G_{\min} = 16, R_v = 96$kbps shown in Fig.5.9. The reason is as follows. As the number of voice user is low, the MAI experienced by the data users is low hence data users can transmit at higher bit rate. However due to the PG constraint, the data users can only transmit at a rate $R_d \le R_{\max}$. Therefore the system is under-loaded and a large number of voice users are favorable to exploit the good conditions. As the maximum system capacity is reached, more voice user will result in the reduction of transmission rate of data user and thus the degradation of the system capacity. The explanation holds true for the dependence of the system capacity on $G_{\min}$. Another observation is that given the number of voice users, the system capacity increases with the number of data users. The reason is that data users are able to exploit the channel conditions. The above observations suggest that in a dual-class system, in order to use the bandwidth efficiently, K_v, K_d and R_v have to be chosen carefully, given a $G_{\min}$.

B. Power consumption investigation

Unlike the analysis in Section 5.3.1 and Section 5.3.2 where for comparison purpose the long term average transmission power is kept as a constant, for a practical system defined in this section, the total transmission power is not fixed. When comparing the capacity of this dual class system for different conditions, the total transmission power is not taken into account. Therefore it is necessary to investigate the power consumption for different number of voice and data users. From (5-32), under the consideration of both path loss and channel fading, the transmission power for the *m*th voice user located at a distance *z* can be rewritten as

$$p_{m,t}^{(v)} = \frac{z^n \overline{p}_d}{c} \frac{R_v}{3B/2\gamma_{\min}^{(v)} - (K_v - 1)R_v} \xi_p, \tag{5-40}$$

where c is path loss constant and

$$\xi_p = \sum_{j=1}^{K_d} \sum_{l=1}^{L} (\alpha_{j,l})^2 \Big/ \sum_{l=1}^{L} (\alpha_{m,l})^2 . \tag{5-41}$$

The PDF of ξ_p and z are given as

$$f_{\xi_p}(\xi_p) = \frac{[(K_d + 1)L - 1]!}{(K_d L - 1)!(L-1)!} \frac{\xi_p^{K_d L - 1}}{(\xi_p + 1)^{(K_d + 1)L}}, \tag{5-42}$$

$$f_z(z) = 2z/\varsigma^2 \tag{5-43}$$

with ς denoting the cell radius.

The average transmission power for voice users is obtained by integrating (5-40) over z and ξ_p and is given as

$$\overline{p}^{(v)} = \int_0^\infty \frac{R_v \overline{p}_d}{c} \frac{z^n \xi_p f_z(z) f_{\xi_p}(\xi_p) dz d\xi_p}{3B/2\gamma_{\min}^{(v)} - (K_v - 1)R_v} = \frac{c_p R_v \overline{\xi}_p}{3B/2\gamma_{\min}^{(v)} - (K_v - 1)R_v}, \tag{5-44}$$

where $c_p = \left[2(\varsigma^{n+2} - z_0^{n+2})\overline{p}_d\right] / \left[c\varsigma^2 (n+2)\right]$ and $\overline{\xi}_p = E[\xi_p]$. The total transmission power is the sum of the average transmission power from voice and data users and is given as

$$\overline{p}_{tot} = c_p \left[\frac{K_v R_v \overline{\xi}_p}{3B/2\gamma_{\min}^{(v)} - (K_v - 1)R_v} + K_d \right]. \tag{5-45}$$

The power consumption of dual-class CDMA systems is shown in Fig.5.10. As more voice users are allowed and transmit at a higher transmission rate, the total transmission power increases. It indicates that the received interference power of data users increases.

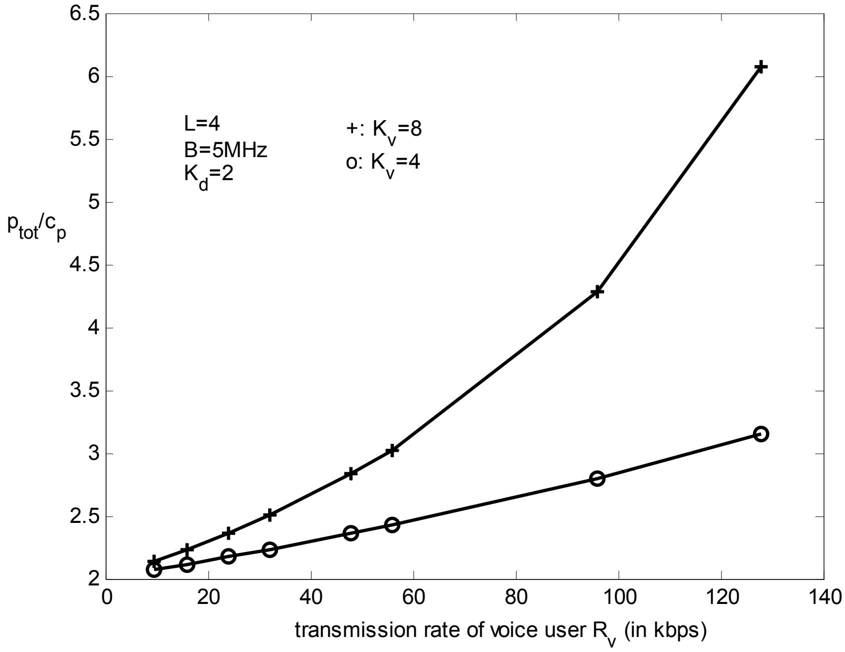

Fig.5.10 Power consumption for dual-class CDMA system

5.4 Power control scheme III—adaptive rate and location-based adaptive power

In previous analysis, we assume that path loss has been totally compensated for. With the development of location tracking and positioning technologies, it is possible to take advantage of location information rather than just to compensate for it. Location-based power control scheme was first studied in infostation systems for delay non-sensitive services [89] for TDMA systems. It was proven to be effective to increase the system capacity of TDMA systems. For single user systems, it has been shown that as more power is allocated to users near to the BS, higher system capacity is achieved. In this section, we consider a location-based power control scheme for CDMA systems employing adaptive continuous PG and MQAM modulation technique.

The proposed location-based power control scheme is in the form of

$$p_{m,t} = Az^{g}, \tag{5-46}$$

where A is a constant and g is the power control coefficient which can take any integer value and defines how the transmission power depends on its distance. z is the distance between a mobile user and the BS and its PDF is defined in (5-41). As g takes a positive value, it indicates that mobile users near to the border of home cell will be allocated more power, while mobile users near to the BS will transmit at lower power. The power allocation strategy with a positive g will try to compensate for the power attenuation caused by path loss, however it will result in large interference to mobile users in neighboring interference cells (or other cells). As g takes a negative value, the power allocation strategy will favor mobile users near to the BS. In this case, the interference inflicted by home cell users to other interference cell users is expected to decrease. The investigation of the effect of g on the system capacity with and without other cell interference will be investigated.

To make the comparison fair, the total transmission power for the whole system is kept as a constant, hence

$$K\int_{z_0}^{\varsigma} Az^{g} f_z(z)dz = p_{tot}, \tag{5-47a}$$

The constant A is given as

$$A = \frac{\varsigma^{n+2} - z_0^{n+2}}{\varsigma^{g+2} - z_0^{g+2}} \frac{g+2}{n+2} \frac{\overline{p}}{c}. \tag{5-47b}$$

With this power allocation strategy, the instantaneous received power for the *m*th user at distance z_m from the base station is given by

$$p_{m,r} = \sum_{l=1}^{L} (\alpha_{m,l})^2 \, Acz_m^{g-n} \; . \tag{5-48}$$

5.4.1 Capacity without other cell interference

Without the consideration of interference cells, the interference is from the users sharing the bandwidth in the home cell only. The instantaneous transmission rate is given as

$$R = \frac{3B}{2\gamma_{\min}} \left(\sum_{l=1}^{L} (\alpha_{m,l})^2 z_m^{g-n} \right) \Bigg/ \left(\sum_{j=1, j\neq m}^{K} \sum_{l=1}^{L} (\alpha_{j,l})^2 z_j^{g-n} \right) \quad . \tag{5-49}$$

Setting $u = \sum_{l=1}^{L} (\alpha_{m,l})^2 \, z_m^{g-n}$ and $v = g - n$, the PDF of *u* is derived to be

$$f_u(u) = \frac{1}{(L-1)!} \left(\frac{1}{2\sigma^2} \right)^{2/v} \frac{2u^{(2/v)-1}}{v\varsigma^2} \left[\Gamma(L - \frac{2}{v}, \frac{u}{2\sigma^2 \varsigma^v}) - \Gamma(L - \frac{2}{v}, \frac{u}{2\sigma^2 z_0^v}) \right] \text{ for } v > 0 \tag{5-50}$$

and

$$f_u(u) = \frac{1}{(L-1)!} \left(\frac{1}{2\sigma^2} \right)^{2/v} \frac{2u^{(2/v)-1}}{|v| \varsigma^2} \left[\Gamma(L - \frac{2}{v}, \frac{uz_0^{|v|}}{2\sigma^2}) - \Gamma(L - \frac{2}{v}, \frac{u\varsigma^{|v|}}{2\sigma^2}) \right] \text{ for } v < 0 . \tag{5-51}$$

As $R \le R_{\max}$, this portion of capacity can be evaluated by

$$\begin{aligned} \overline{\Re}_1 = \int_{u_K=0}^{\infty} \int_{u_1=0}^{\infty} \cdots \int_{u_m=0}^{\frac{2\gamma_{\min}}{3G_{\min}} \sum_{j=1,j\neq m}^{K-1} u_j} \frac{3B}{2\gamma_{\min}} u_m \Bigg/ \left(\sum_{j=1,j\neq m}^{K} u_j \right) \\ f_{u_m}(u_m) f_{u_1}(u_1) \cdots f_{u_K}(u_K) \, du_m du_1 \cdots du_K \end{aligned} \; . \tag{5-52}$$

After PG reaches $G_{\min}$, the E_b / N_0 can be expressed as

$$\gamma = \frac{3G_{\min}}{2} u_m \Big/ \sum_{j=1, j\neq m}^{K} u_j \ . \tag{5-53}$$

Thus the capacity with adaptive continuous MQAM is given by

$$\overline{\Re}_2 = R_{\max} \int_{u_K=0}^{\infty} \int_{u_1=0}^{\infty} \cdots \int_{u_m=\frac{2\gamma_{\min}}{3G_{\min}} \sum_{j=1, j\neq m}^{K-1} u_j}^{\infty} \log_2 M(\gamma) f_{u_m}(u_m) f_{u_1}(u_1) \cdots f_{u_K}(u_K)\, du_m du_1 \cdots du_K \tag{5-54}$$

The system capacity achieved by the location-based power control scheme is presented in Fig.5.11. *g-n=v=0* corresponds to the case employing power control scheme I. It can be seen that without the consideration of the other cell interference, the system capacity achieves either A maximum or A minimum value around v=0, depending on $G_{\min}$. As $G_{\min}$ takes small value, the location-based power control scheme performs better than the power control scheme I. However, as $G_{\min}$ takes large valueS, the proposed power control scheme exhibits no significant capacity gain. Therefore, the proposed location-based power control scheme is not promising if the other cell interference is ignored.

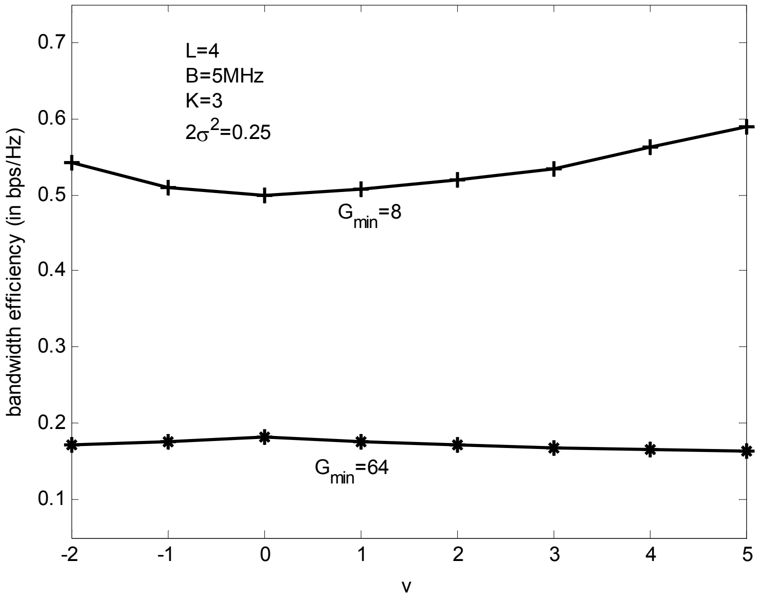

Fig.5.11 System capacity achieved by location-based power control scheme

5.4.2 Capacity with other cell interference

Under the consideration of the other cell interference, it is expected that as power allocation schemes favor the users nearer to the BS of the home cell, system will achieve higher system capacity since the other cell interference is reduced. In this study, we consider the first tier interference cells. Power control is performed by the home cell BS. The model to characterize the other cell interference is shown in Fig.5.12. The other cell interference is modeled as Gaussian random variable [90]. In the following we first derive the mean and the variance of other cell interference when the proposed location-based power control scheme is employed. The interference power received at the home cell BS contributed by the *m*th user in the *k*th interference cell is given by

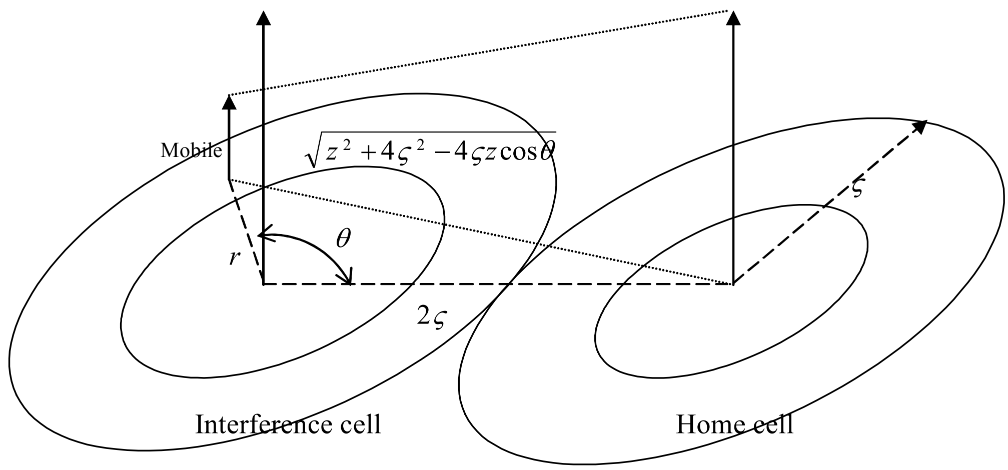

Fig.5.12 Other cell interference model

$$p_{m,r}^{k}=\sum_{l=1}^{L}(\alpha_{m,l}^{k})^{2}\,bc\frac{z_m^{g}}{\left(z_m^2+4\varsigma^2-4\varsigma z_m\cos\theta\right)^{n/2}}=Ac\alpha_L\frac{z_m^{g}}{\left(z_m^2+4\varsigma^2-4\varsigma z_m\cos\theta\right)^{n/2}},$$

(5-55)

where θ is a random variable uniformly distributed over 0 to 2π. The distribution of α_L and z are defined in (5-9) and (5-41) respectively.

The other cell interference is then given to be

$$I_{oth}=\sum_{k}\sum_{m}p_{m,r}^{k}. \quad (5\text{-}57)$$

Assuming that all users experience independent path loss and multipath fading, the mean and the variance of I_{oth} can be obtained as

$$\bar{I}_{oth}=E\left[I_{oth}\right]=\sum_{k}\sum_{m}E\left[p_{m,r}^{k}\right], \quad (5\text{-}58)$$

and

$$\sigma_{oth}^2 = \mathrm{var}[I_{oth}] = E\left[(I_{oth} - \bar{I}_{oth})^2\right] \\ = E\left[(I_{oth})^2\right] - \left(\bar{I}_{oth}\right)^2 , \tag{5-59}$$

where

$$E\left[(I_{oth})^2\right] = \sum_k \sum_m E\left[(p_{m,r}^k)^2\right] + \sum_k \sum_{k'} \sum_m \sum_{m'} E\left[p_{m,r}^{(k)}\right] E\left[p_{m',r}^{k'}\right], \tag{5-60}$$

$$E\left[(p_{m,r}^k)^2\right] = \int_0^\infty \int_{z_0}^{\varsigma} \int_0^{2\pi} (p_{m,r}^k)^2 f_\alpha(\alpha) f_Z(z) f_\theta(\theta)\, d\alpha dz d\theta , \tag{5-61}$$

$$E\left[p_{m,r}^k\right] = \int_0^\infty \int_{z_0}^{\varsigma} \int_0^{2\pi} p_{m,r}^k f_\alpha(\alpha) f_Z(z) f_\theta(\theta)\, d\alpha dz d\theta . \tag{5-62}$$

With the knowledge of the mean and the variance, the PDF of I_{oth} is obtained as

$$f_{I_{oth}}(I_{oth}) = \frac{1}{\sqrt{2\pi\sigma_{oth}^2}} e^{-\frac{(I_{oth} - \bar{I}_{oth})^2}{2\sigma_{oth}^2}} . \tag{5-63}$$

Under the consideration of the other cell interference, the instantaneous transmission rate for mobile users in the home cell is expressed as

$$R = \frac{3B}{2\gamma_{\min}} \left(\sum_{l=1}^{L} (\alpha_{m,l})^2 z_m^{g-n} \right) \Big/ \left(\sum_{j=1, j\neq m}^{K} \sum_{l=1}^{L} (\alpha_{j,l})^2 z_j^{g-n} + \frac{I_{oth}}{Ac} \right). \tag{5-64}$$

The average transmission rate for one mobile user is

$$\overline{\Re}_1 = \int_0^\infty \int_{u_K=0}^\infty \int_{u_1=0}^\infty \cdots \int_{u_m=0}^{\frac{2\gamma_{\min}}{3G_{\min}} \sum_{j=1, j\neq m}^{K-1} u_j + \frac{1}{Ac} I_{oth}} \frac{3B}{2\gamma_{\min}} u_m \Big/ \left(\sum_{j=1, j\neq m}^{K} u_j + \frac{I_{oth}}{Ac} \right) \bullet \\ f_{u_m}(u_m) f_{u_1}(u_1) \cdots f_{u_K}(u_K) f_{I_{oth}}(I_{oth}) du_m du_1 \cdots du_K dI_{oth} , \tag{5-65}$$

and

$$\overline{\Re}_2 = R_{\max} \int_0^{\infty} \int_{u_K=0}^{\infty} \int_{u_1=0}^{\infty} \cdots \int_{u_m = \frac{2\gamma_{\min}}{3G_{\min}}\left(\sum_{j=1,j\neq m}^{K-1} u_j + \frac{1}{Ac} I_{oth}\right)}^{\infty} \log_2 M(\gamma) f_{u_m}(u_m)$$

$$f_{u_1}(u_1)\cdots f_{u_K}(u_K) f_{I_{oth}}(I_{oth}) du_m du_1 \cdots du_K dI_{oth} \quad , \qquad (5\text{-}66)$$

where

$$\gamma = \frac{3G_{\min}}{2} u_m \Big/ \left(\sum_{j=1,j\neq m}^{K} u_j + \frac{1}{Ac} I_{oth} \right). \qquad (5\text{-}67)$$

The total capacity achieved is computed using (5-19).

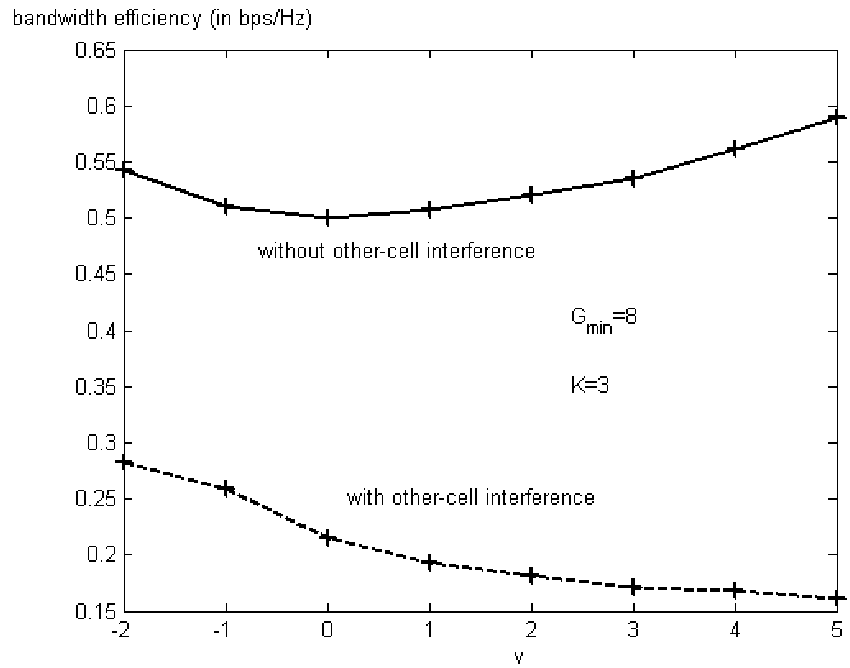

Fig.5.13 System capacity achieved by location-based power control scheme with consideration of other cell interference

The system capacity achieved under the consideration of the other cell interference is numerically computed and shown in Fig.5.13. *g-n=v=0* corresponds to the case WITH power control scheme I. Unlike the case without the other cell interference, the system capacity decreases with *g* ($g = v + n$) regardless of $G_{\min}$, given the path loss index *n*. It indicates that as more power is allocated to the users near to the BS of the home cell, systems can achieve a higher capacity. The reason is that the other cell interference can be effectively suppressed through reducing the transmission power of interference mobile users near to the border of other cells. From Fig.5.13, we can see that with the consideration of the other cell interference, scheme III achieves higher system capacity than scheme I as $v<0$. However the capacity gain is achieved at the expense of the transmission rate for users near to the cell border.

5.5 Summary

A combined adaptive PG and MQAM modulation technique for CDMA systems is proposed in this chapter. A flaw present in the capacity study of adaptive CDMA systems in most of the literatures is corrected by considering a minimum PG constraint ($G_{\min}$). A dual-class CDMA system supporting both voice and data services is also proposed and studied. Three power control schemes are proposed under the constraint of the total average transmission power. The capacities achieved by these power control schemes with the combined adaptive PG and MQAM technique are studied. The descriptions of these power control schemes are summarized as follows:

1) Scheme I: The transmission power is defined by $p_{m,t} = \bar{p} z_m^n / c$. The transmission power is a constant after path loss is compensated for and the transmission rate is adapted to the received SIR. Generally, the conventional power control scheme has better bandwidth efficiency (system capacity) than scheme I with adaptive PG only, but inferior to scheme I with combined adaptive PG and MQAM.

2) Scheme II: The transmission power is defined by $p_{m,t} = D\left(\sum_{l=1}^{L}(\alpha_{m,l})^2\right)^q$. The transmission power after path loss is compensated for is allocated based on the fast fading of individual user while the transmission rate is adapted to the received SIR. Generally, scheme II with combined adaptive PG and MQAM achieves higher bandwidth efficiency than scheme I. Bandwidth efficiency increases with the increase of positive q.

3) Scheme III: The transmission power is defined by $p_{m,t} = Az^g$. The transmission power is allocated based on the location of the mobile user while the transmission rate is adapted to the received SIR. It is more efficient to overcome the other cell interference. Scheme III with combined adaptive PG and MQAM outperforms scheme I as $v < 0$, under the consideration of other cell interference.

CHAPTER VI

ANALYSIS ON MULTIPLE ACCESS INTERFERENCE AND CAPACITY OF MULTIPLE CHIP RATE CDMA SYSTEM

The capacity of rate adaptive CDMA systems employing adaptive PG is investigated in Chapter V. Another solution to realize rate adaptive capability in a CDMA system is to vary THE spreading chip rate while keep the processing gain unchanged. In the study conducted in Chapter V, an interference model where mobile users can have different data rates but the chip rate remains the same for all users is assumed. In this chapter, we consider a multiple chip rate (MCR) system. The variance of MAI of a MCR system with constant processing gain is derived under a model, where the asynchronous transmission of signals with different chip rate at different carrier frequencies and the effect of power spectral density (PSD) of signals are taken into account. With the knowledge of the variance of MAI, different configurations of MCR systems are evaluated in terms of system capacity. Comparison of capacity between MCR systems and multiple processing gain (MPG) constant chip rate systems is then performed for the first time.

6.1 Introduction of MCR systems

Wideband CDMA is selected as a candidate for the future generation wireless systems to accommodate a wide variety of services with information bit rates ranging from a few kb/s to 2Mb/s [91]. The multi-rate capability of wideband CDMA systems can be achieved by employing MCR systems where the spreading chip rate varies with the transmission rate while the processing gain remains unchanged. In a MCR system, users requesting different bit rate services will share the entire frequency band in a manner where data transmitted at different rates will be spread with different bandwidth. The system bandwidth is selected according to the maximum transmission rate supported in the system [92,93]. The users requesting highest bit rate service will occupy the entire bandwidth, while other users requesting lower transmission rate will be allocated part of the bandwidth in the same frequency band. The architecture of MCR systems can be represented by a spectral layer structure shown in Fig.6.1. We define each subsystem as a spectral layer supporting the same bit rate services but with different carrier frequencies. In a MCR system shown in Fig.6.1, there is only one wideband subsystem with bandwidth B_w, while the number of narrowband subsystem with bandwidth B_n is 4, 1 and 1 for configuration (a), configuration (b) and configuration (c), respectively. The number of subsystems can be designed flexibly and tailored to meet the requirements of traffic load and service quality. The MCR system was proposed by the Code Division Testbed (CODIT) [94]. In the experimental CODIT testbed, three different chip rates were proposed, with the bandwidth of 1MHz, 5MHz and 20MHz respectively, where 1MHz is allocated to low-rate voice services, 5MHz can be used as an option for providing a higher QoS services.

The justification of spectrally overlaid arrangement of a MCR system is that it is not necessary that users requesting lower bit rate service occupy the whole frequency band. With the control of MCR system configurations shown in Fig.6.1, the MAI from users with different spreading bandwidth can be different. This chapter will look into the capacity of a MCR system with different configurations.

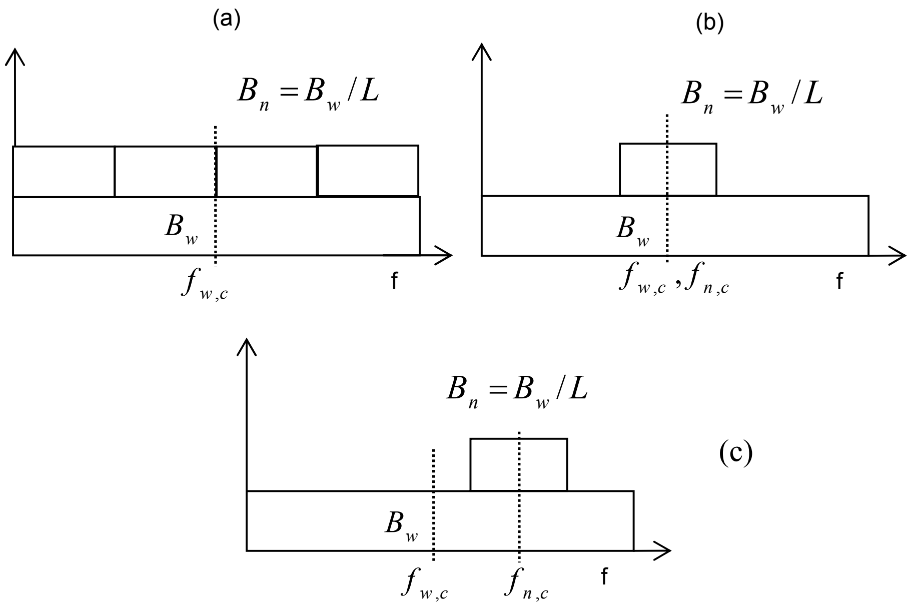

Fig.6.1 Examples of MCR system configurations

6.2 Interference analysis

6.2.1. System model

Due to the spectral overlay of subsystems with different spreading bandwidth, the MAI of MCR systems exhibits different statistical characteristics from that of single chip rate systems. The co-existence of different chip rates affects system performance through three effects: (1) The non-orthogonality of spreading codes with the same and different spreading bandwidth, for example, spreading codes with bandwidth B_n and B_w as shown in Fig.6.1. (2) The difference of carrier frequencies for different subsystems, for example, the difference between $f_{t,c}$ and $f_{r,c}$ as shown in Fig.6.2, where $f_{t,c}, f_{r,c}$ are carrier frequencies for the interference signal and the desired signal, respectively. (3) The effect due to the receiver filter for the desired user and the PSD of the interference signals with different spreading bandwidth, for example, the effect of $H_r(f)$ on $S_g(f)$ as shown in Fig.6.2, where $S_g(f)$ and $H_r(f)$ are the PSD of the interference signal and the ideal transfer function of the receiver filter for the desired user, respectively. [95]. An interference coefficient χ is introduced to characterize the effect (2) and (3). Obviously, χ depends on the shape of PSD, the ratio of spreading bandwidth of the desired and the interference user, and the difference between $f_{t,c}$ and $f_{r,c}$. The computation of χ is shown in Appendix B.

The statistical characteristics of MAI of MCR systems were studied through computation in [96]. The interference analysis taking both the effect (1) and (2) into account was conducted and a closed form solution was obtained in [97]. However, in all the previous works on the capacity analysis of a MCR system [98-100], the MAI model was oversimplified by assuming that the MAI of a MCR system has the same statistical nature as that of a single chip rate system, by treating the interference caused by interference users with spreading bandwidth B_I to desired users with bandwidth B_S as $p_I \cdot B_S / B_I$, where p_I is the received power of the interference user. This simplification will definitely lead to inaccuracy on the evaluation of the system capacity. Therefore the study on the capacity of a MCR system under a more practical environment, which considers all these effects, is imperative and valuable for the design of such system.

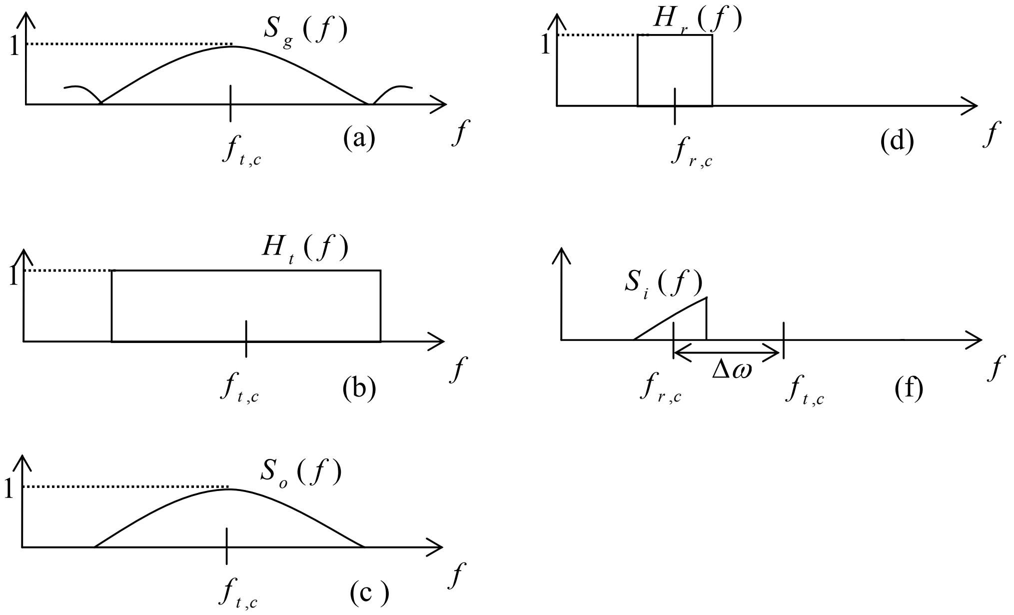

Fig.6.2 A illustration of effect of PSD and center frequency

For a multi-rate CDMA system, assuming that the system can support Q classes of service (or Q different data rates or subsystems), the transmitted signal of user k of class i can be expressed as

$$s_{ik}(t)=\sqrt{2p_i}\,b_{ik}(t)a_{ik}(t)\cos(\omega_{ik,c}t+\theta_{ik}), \tag{6-1}$$

where p_i is the transmission power for the ith class of service. $a_{ik}(t)$ and $b_{ik}(t)$ are of the form

$$a_{ik}(t)=\sum_{n=-\infty}^{\infty}\sum_{m=0}^{\Lambda-1}a_{ik}^{m}\Phi\left[\frac{t-(m+n\Lambda)T_{ci}}{T_{ci}}\right], \tag{6-2}$$

and

$$b_{ik}(t)=\sum_{n=-\infty}^{\infty}b_{ik}^{n}\Phi\left[\frac{t-nT_{bi}}{T_{bi}}\right]. \tag{6-3}$$

In (6-2) and (6-3), Λ is the PG and $\Phi(t)$ represents the unit impulse function and is given by

$$\Phi(t) = \begin{cases} 1 & 0 \le t \le 1 \\ 0 & \text{otherwise} \end{cases}, \tag{6-4}$$

where b_{ik}^{n} is the nth data bit of user k of the ith class and a_{ik}^{m} is the mth chip of spreading code for user k of class i under the assumption that data and spreading chip are of rectangular pulse shapes. Both a_{ik}^{m} and b_{ik}^{n} take values of (-1,1). $\omega_{ik,c}$ is the carrier frequency for the kth user in the ith class, θ_{ik} is the initial phase offset.

Assuming a power control scheme which totally compensates for the channel fading and path loss, signals are then transmitted over a channel equivalent to AWGN channel, the signal received at the base station is given as

$$r(t) = \sum_{i=1}^{Q} \sum_{k=1}^{K_i} s_{ik}(t - \tau_{ik}) + n(t), \tag{6-5}$$

where τ_{ik} is the relative delay for user k of class i, $n(t)$ is AWGN with two-sided power spectral density $N_0/2$. K_i is the number of services for the ith class.

The received signal contains both the desired signal and the interference signals from other services, either in the same class or in different classes. The signal is down-converted to baseband, correlated by the spreading code of the desired user and integrated over one bit period. By adopting a single user detector, the decision variable for the nth bit of the desired user (lth user of jth class of service) is constructed by correlating the received signal with the desired user's spreading sequence and is given as

$$Z_{jl} = \int_{nT_{bj}}^{(n+1)T_{bj}} r(t)a_{jl}(t)\cos(\omega_{jl,c}t)dt \,. \tag{6-6}$$

Substitute (6-5) into (6-6), the matched filter output can be written as

$$Z_{jl} = \int_{nT_{bj}}^{(n+1)T_{bj}} \sum_{i=1}^{I} \sum_{k=1}^{K_i} \sqrt{2p_i}\, b_{ik}(t-\tau_{ik})a_{ik}(t-\tau_{ik})\cos\left[\omega_{ik,c}(t-\tau_{ik})+\theta_{ik}\right]a_{jl}(t)\cos(\omega_{jl,c}t)dt$$

$$= S_{jl} + I + \zeta \tag{6-7}$$

where the first term is the contribution from the desired user, the second term is the MAI from other interference users sharing the same bandwidth, the third term is from AWGN and

$$S_{jl} = \int_{nT_{bj}}^{(n+1)T_{bj}} \sqrt{2p_j}\, b_{jl}(t)a_{jl}(t)\cos\left[\omega_{jl,c}(t-\tau_{jl})+\theta_{jl}\right]a_{jl}(t)\cos(\omega_{jl,c}t)dt \,. \tag{6-8}$$

Assuming ideal coherent detection and perfect phase and timing synchronization between the desired user and the receiver, (6-8) can be rewritten as

$$S_{jl} = \sqrt{\frac{p_j}{2}}\, b_{jl}^{n} T_{bj} \,. \tag{6-9}$$

The noise term is given by

$$\zeta = \int_{nT_{bj}}^{(n+1)T_{bj}} n(t)a_{jl}(t)\cos(\omega_{jl,c}t)dt \,. \tag{6-10}$$

The mean and the variance of ζ is derived to be [101]

$$E[\zeta] = 0 \tag{6-11a}$$

and

$$\mathrm{var}[\zeta] = \frac{N_0 T_{bj}}{4} \,. \tag{6-11b}$$

The MAI term is given by

$$I = \sum_{i=1}^{Q} \sum_{k=1, ik \neq jl}^{K_i} I_{ik} , \tag{6-12}$$

where

$$\begin{aligned} I_{ik} &= \int_{nT_{bj}}^{(n+1)T_{bj}} \sqrt{2p_i} b_{ik}(t-\tau_{ik}) a_{ik}(t-\tau_{ik}) \cos\left[\omega_{ik,c}(t-\tau_{ik}) + \theta_{ik}\right] a_{jl}(t) \cos(\omega_{jl,c} t) dt \\ &= \sqrt{\frac{p_i}{2}} \int_{nT_{bi}}^{(n+1)T_{bi}} b_{ik}(t-\tau_{ik}) a_{ik}(t-\tau_{ik}) a_{jl}(t) \cos(\Delta\omega t + \varphi_{ik}) dt \end{aligned} \tag{6-13}$$

$\varphi_{ik} = \theta_{ik} - \omega_{ik,c}\tau_{ik}$, and $\Delta\omega = \omega_{ik} - \omega_{jl}$. Eq.(6-13) is obtained by ignoring the high frequency term $\omega_{ik,c} + \omega_{ik,c}$. It can be seen from (6-13) that the MAI is obtained from the integration over one data bit duration (or T_{bj}) of the desired user.

Conventionally, the MAI can be modeled as a zero mean Gaussian random variable. Hence it is sufficient to investigate the variance of the MAI in order to evaluate the BER performance of CDMA systems. In the following analysis, the variance of the MAI is first derived by assuming that the pulse shape of $a_{ik}(t)$ and $a_{jl}(t)$ is rectangular. The resulting interference due to the receiver filter for the desired *l*th user and the PSD of the spreading signal $a_{ik}(t)$ of the interference user is included and described by the interference coefficient χ [95].

6.2.2 Derivation of variance of MAI

It can be shown that each of the multiple access interferers are uncorrelated [102]. The variance of the MAI is then obtained as

$$\mathrm{var}[I]=E\left[\left(\sum_{i}^{Q}\sum_{k}^{K_i} I_{ik}\right)^2\right]=\sum_{i}^{I}\sum_{k}^{K_i} E[I_{ik}^2]. \tag{6-14}$$

In the following, $\mathrm{var}[I]$ is studied in three cases where $T_{cj}=T_{ci}$, $T_{cj}>T_{ci}$, $T_{cj}<T_{ci}$, with T_{ci}, T_{cj} being chip the duration for the *i*th and the *j*th subsystem or class of service respectively. These three cases correspond to the situations: 1) $T_{cj}=T_{ci}$ or the desired user *j* and the interference user *i* have the same spreading bandwidth, 2) $T_{cj}>T_{ci}$ or the desired user *j* has a smaller spreading bandwidth than the interference user *i*, 3) $T_{cj}<T_{ci}$ or the desired user *j* has a larger spreading bandwidth than the interference user *i*.

A. Variance of MAI for the case where $T_{cj}=T_{ci}$

In this case, $\Delta\omega=0$ and $\mathrm{var}[I]$ is similar to that of single spreading chip rate systems. The variance of the MAI of a single rate system is [83,84]

$$\mathrm{var}[I]=\frac{GT_c^2}{6}\sum_k p_k , \tag{6-15}$$

where G is the PG, T_c is the chip duration and p_k is the received power for the *k*th user at the base station.

B. Variance of MAI for the case where $T_{cj}>T_{ci}$

In this case, we denote a narrowband subsystem as a subsystem with a smaller spreading bandwidth (or larger chip duration T_{cj}), whereas a wideband subsystem as the one having a larger spreading bandwidth (or smaller chip duration T_{ci}), respectively. For the narrowband users with chip duration T_{cj}, the interference caused by the wideband user with chip duration T_{ci} is illustrated in Fig.6.3 where $\vartheta = 3, G = 12$, with $\vartheta = T_{cj} / T_{ci}$ denoting the chip rate ratio of the two subsystems. Generally, the MAI imposed on the data bit b_{jl}^{1} of the desired user is caused by $(\vartheta + 1)$ data bits of the interference user for asynchronous systems. The data bits in both subsystems are spread by the same PG, denoted by G. Each chip of narrowband subsystems with duration T_{cj} will span over a number of chips of the wideband subsystem with duration T_{ci}. The delay of the data bit of the interference user k relative to the data bit of the desired user l is denoted as $\tau_{ik} = \varepsilon_{ik} T_{ci} + \Delta_{ik}$, where ε_{ik} can be expressed as $\varepsilon_{ik} = w\vartheta + v$ with w and v being integers.

The integration of (6-13) over one data bit duration of T_{bj} can be partitioned into three cases: 1) I_1: the correlation between chips a_{ik}, a_{jl} with duration of Δ_{ik}, as shown in Fig.6.3 (b). 2) I_2: the correlation between chips a_{ik}, a_{jl} with duration of $T_{ci} - \Delta_{ik}$, as shown in Fig.6.3 (c). 3) I_3, I_4: the correlation between chips a_{ik}, a_{jl} with duration of T_{ci}, as shown in Fig.6.3 (d). I_3, I_4 are used to distinguish the correlation for v wideband chips a_{ik} on the right hand side of I_1 and $(\vartheta - v - 1)$ wideband chips a_{ik} on the left hand side of I_2, as represented by the two different shadowed regions shown in Fig.6.3.(d). This differentiation is necessary given that v wideband chips a_{ik} correlate with b_{ik}^{1} while $(\vartheta - v - 1)$ wideband chips a_{ik} correlate with b_{ik}^{2}.

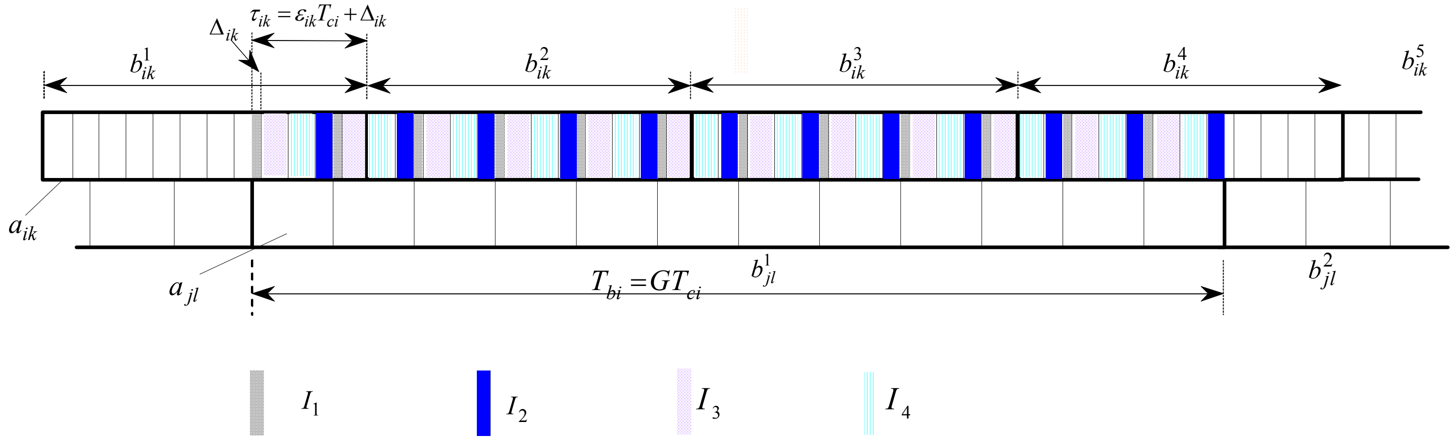

(a) Diagram to evaluation various components of the MAI for a wideband user imposed on the narrowband user. In this illustration, we use $T_{cj}/T_{ci} = \vartheta = 3$, PG for both users are given by G=12, hence $G/\vartheta = 4$, $\varepsilon_{ik} = 4$ or $w = 1\,(\varepsilon_{ik} = 1\cdot\vartheta + 1)$

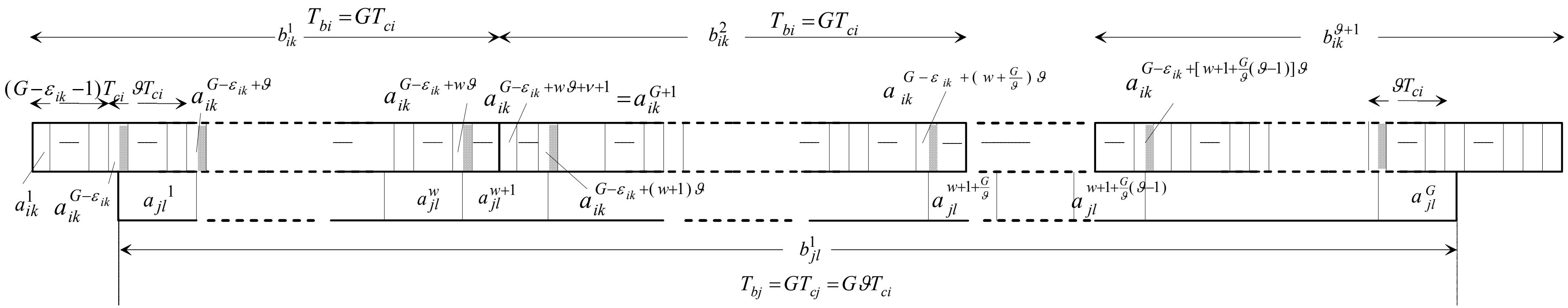

(b) Diagram for computation of I_1

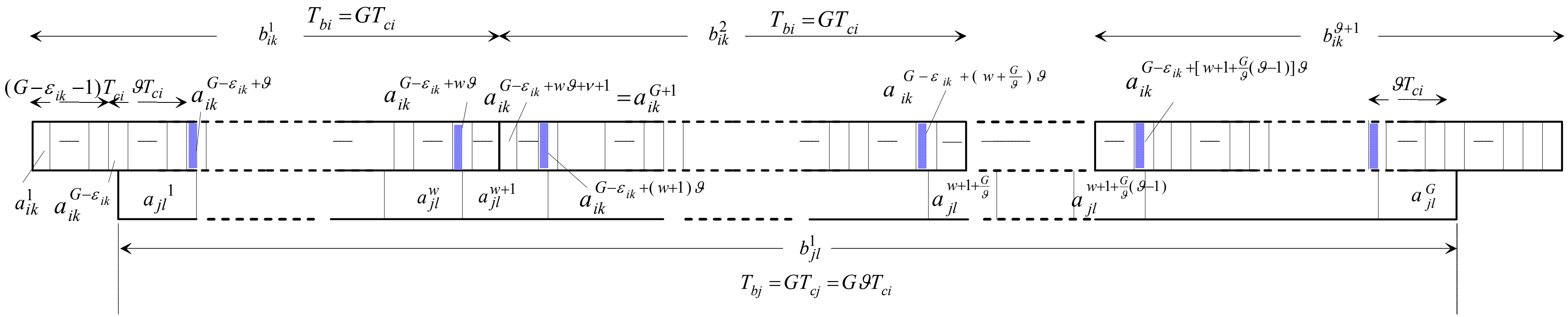

(c) Diagram for the computation of I_2

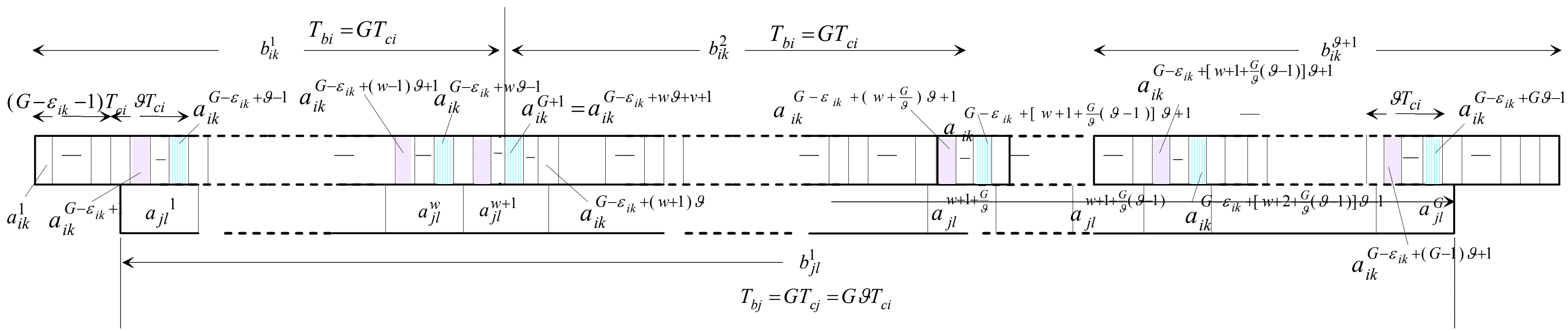

(d) Diagram for the computation of I_3 *and* I_4

Fig.6.3 Schematic diagram of correlation for $T_{cj} > T_{ci}$

With this partition, (6-13) can be rewritten as

$$I_{ik} = \sqrt{\frac{p_{ik}}{2}} \left[(I_1 + I_2 + I_3 + I_4) \right], \tag{6-16}$$

Denote

$$T_1(x) = \int_{x-\Delta_{ik}}^{x} \cos(\omega t + \varphi_{ik}) dt ,$$

$$T_2(x) = \int_{x-T_{ci}}^{x-\Delta_{ik}} \cos(\Delta\omega t + \varphi_{ik}) dt ,$$

$$T_3(x) = \int_{x-T_{ci}}^{x} \cos(\Delta\omega t + \varphi_{ik}) dt .$$

I_1, I_2, I_3, I_4 are calculated as follows respectively.

$$\begin{aligned} I_1 = \Bigg[\; & b_{ik}^1 \sum_{n=1}^{w+1} a_{jl}^n a_{ik}^{G-\varepsilon_{ik}+\vartheta(n-1)} T_1\left(\left[G - \varepsilon_{ik} + \vartheta(n-1)\right] T_{ci}\right) + \\ & b_{ik}^2 \sum_{n=w+2}^{w+1+\frac{G}{\vartheta}} a_{jl}^n a_{ik}^{G-\varepsilon_{ik}+\vartheta(n-1)} T_1\left(\left[G - \varepsilon_{ik} + \vartheta(n-1)\right] T_{ci}\right) + \\ & \cdots + b_{ik}^{\vartheta+1} \sum_{n=w+2+\frac{G}{\vartheta}(\vartheta-1)}^{G} a_{jl}^n a_{ik}^{G-\varepsilon_{ik}+\vartheta(n-1)} T_1\left(\left[G - \varepsilon_{ik} + \vartheta(n-1)\right] T_{ci}\right) \Bigg] , \end{aligned} \tag{6-17a}$$

where the subscript n denotes the nth chip of narrowband subsystems. Fig.6.3 can help to identify these chip and bit positions. The terms in (6-17a) correspond to the correlation from interference data bits $b_{ik}^1, b_{ik}^2, b_{ik}^3 \cdots b_{ik}^{\vartheta}, b_{ik}^{\vartheta+1}$. After some arrangements, (6-17a) can be rewritten as

$$I_1 = b_{ik}^1 a_{jl}^1 a_{ik}^{G-\varepsilon_{ik}} T_1\left(\left[G - \varepsilon_{ik}\right] T_{ci}\right) + \sum_{n=2}^{G} b_{ik} a_{jl}^n a_{ik}^{G-\varepsilon_{ik}+\vartheta(n-1)} T_1\left(\left[G - \varepsilon_{ik} + \vartheta(n-1)\right] T_{ci}\right) \tag{6-17b}$$

where $b_{ik} \in \left\{ b_{ik}^1, b_{ik}^2, b_{ik}^3 \cdots b_{ik}^{\vartheta-1}, b_{ik}^{\vartheta} \right\}$. The reason to use this notation for $b_{ik}^1, b_{ik}^2, b_{ik}^3 \cdots b_{ik}^{\vartheta-1}, b_{ik}^{\vartheta}$ is that the actual values will not affect the computation of interference in the following.

$$I_2 = \Bigg[\; b_{ik}^1 \sum_{n=1}^{w} a_{jl}^n a_{ik}^{G-\varepsilon_{ik}+\vartheta n} T_2\left(\left[G-\varepsilon_{ik}+\vartheta n\right]T_{ci}\right) + b_{ik}^2 \sum_{n=w+1}^{w+\frac{G}{\vartheta}} a_{jl}^n a_{ik}^{G-\varepsilon_{ik}+\vartheta n} T_2\left(\left[G-\varepsilon_{ik}+\vartheta n\right]T_{ci}\right) +$$

$$\cdots + b_{ik}^{\vartheta+1} \sum_{n=w+1+\frac{G}{\vartheta}(\vartheta+1)}^{G} a_{jl}^n a_{ik}^{G-\varepsilon_{ik}+\vartheta n} T_2\left(\left[G-\varepsilon_{ik}+\vartheta n\right]T_{ci}\right) \Bigg]$$

$$= \sum_{n=2}^{G} b_{ik} a_{jl}^{n-1} a_{ik}^{G-\varepsilon_{ik}+\vartheta(n-1)} T_2\left(\left[G-\varepsilon_{ik}+\vartheta(n-1)\right]T_{ci}\right) + b_{ik}^G a_{jl}^G a_{ik}^{G-\varepsilon_{ik}+G\vartheta} T_2\left(\left[G-\varepsilon_{ik}+G\vartheta\right]T_{ci}\right) \tag{6-18}$$

$$I_3 = \sum_{q=1}^{v} \Bigg\{ \; b_{ik}^1 \sum_{n=1}^{w+1} a_{jl}^n a_{ik}^{G-\varepsilon_{ik}+\vartheta(n-1)+q} T_3\left(\left[G-\varepsilon_{ik}+\vartheta(n-1)+q\right]T_{ci}\right) +$$

$$b_{ik}^2 \sum_{n=w+2}^{w+\frac{G}{\vartheta}+1} a_{jl}^n a_{ik}^{G-\varepsilon_{ik}+\vartheta(n-1)+q} T_3\left(\left[G-\varepsilon_{ik}+\vartheta(n-1)+q\right]T_{ci}\right) + \cdots +$$

$$b_{ik}^{\Lambda} \sum_{n=w+2+\frac{G}{\vartheta}(\vartheta-1)}^{G} a_{jl}^n a_{ik}^{G-\varepsilon_{ik}+\vartheta(n-1)+q} T_3\left(\left[G-\varepsilon_{ik}+\vartheta(n-1)+q\right]T_{ci}\right) \Bigg\}$$

$$= \sum_{q=1}^{v} \Bigg\{ \; b_{ik}^1 a_{jl}^1 a_{ik}^{G-\varepsilon_{ik}+1} T_3\left(\left[G-\varepsilon_{ik}+1\right]T_{ci}\right) + \sum_{n=2}^{G} b_{ik} a_{jl}^n a_{ik}^{G-\varepsilon_{ik}+\vartheta(n-1)+1} T_3\left(\left[G-\varepsilon_{ik}+\vartheta(n-1)+1\right]T_{ci}\right) \Bigg\} \tag{6-19}$$

$$I_4 = \sum_{q=1}^{\vartheta-v-1} \Bigg\{ \; b_{ik}^1 \sum_{n=1}^{w} a_{jl}^n a_{ik}^{G-\varepsilon_{ik}+\vartheta(n-1)+v+q} T_3\left(\left[G-\varepsilon_{ik}+\vartheta(n-1)+v+q\right]T_{ci}\right) +$$

$$b_{ik}^2 \sum_{n=w+1}^{w+\frac{G}{\vartheta}} a_{jl}^n a_{ik}^{G-\varepsilon_{ik}+\vartheta(n-1)+v+q} T_3\left(\left[G-\varepsilon_{ik}+\vartheta(n-1)+v+q\right]T_{ci}\right) + \cdots$$

$$b_{ik}^{\vartheta} \sum_{n=w+2+\frac{G}{\vartheta}(\vartheta-1)}^{G-1} a_{jl}^n a_{ik}^{G-\varepsilon_{ik}+\vartheta(n-1)+v+q} T_3\left(\left[G-\varepsilon_{ik}+\vartheta(n-1)+v+q\right]T_{ci}\right) +$$

$$b_{ik}^{\vartheta+1} a_{jl}^G a_{ik}^{G(\vartheta+1)-\varepsilon_{ik}-\vartheta+v+q} T_3\left(\left[G(\vartheta+1)-\varepsilon_{ik}-\vartheta+v+q\right]T_{ci}\right) \Bigg\}$$

$$= \sum_{q=1}^{\vartheta-v-1} \Bigg\{ \; \sum_{n=2}^{G} b_{ik} a_{jl}^n a_{ik}^{G-\varepsilon_{ik}+\vartheta n+v+q} T_3\left(\left[G-\varepsilon_{ik}+\vartheta(n-1)+v+q\right]T_{ci}\right) +$$

$$b_{ik}^{\vartheta+1} a_{jl}^G a_{ik}^{G(\vartheta+1)-\varepsilon_{ik}-\vartheta+v+q} T_3\left(\left[G(\vartheta+1)-\varepsilon_{ik}-\vartheta+v+q\right]T_{ci}\right) \Bigg\} \tag{6-20}$$

Substitute (6-17b), (6-18), (6-19), and (6-20) into (6-16), and using $\int_a^b \cos(x)dx = \sin b - \sin a$, the MAI caused by the kth interference user is obtained as

$$I_{ik} = \sqrt{\frac{p_{ik}}{2}}(A+B), \tag{6-21}$$

where

$$A = \sum_{n=2}^{G} \frac{1}{\Delta\omega}\Bigg[b_{ik} a_{jl}^{n} a_{ik}^{\Lambda-\varepsilon_{ik}+\vartheta(n-1)} Q_1\left(\left[G-\varepsilon_{ik}+\vartheta(n-1)\right]T_{ci}\right)+$$

$$b_{ik} a_{jl}^{n-1} a_{ik}^{G-\varepsilon_{ik}+\vartheta(n-1)} Q_2\left(\left[G-\varepsilon_{ik}+\vartheta(n-1)\right]T_{ci}\right)+$$

$$\sum_{\mathrm{q=1}}^{\mathrm{v}} b_{ik} a_{jl}^{n} a_{ik}^{G-\varepsilon_{ik}+\vartheta(n-1)+q} Q_3\left(\left[G-\varepsilon_{ik}+\vartheta(n-1)+q\right]T_{ci}\right)+$$

$$\sum_{\mathrm{q=1}}^{\vartheta\text{-v+1}} b_{ik} a_{jl}^{n} a_{ik}^{G-\varepsilon_{ik}+\vartheta n+v+q} Q_3\left(\left[G-\varepsilon_{ik}+\vartheta n+v+q\right]T_{ci}\right) \Bigg] \quad , \tag{6-22}$$

and

$$B = \frac{1}{\Delta\omega}\Big[b_{ik}^{1} a_{jl}^{1} a_{ik}^{G-\tau_{ik}} Q_1\left(\left[G-\varepsilon_{ik}\right]T_{ci}\right) + b_{ik}^{G} a_{jl}^{G} a_{ik}^{G-\tau_{ik}+G\vartheta} Q_2\left(\left[G-\varepsilon_{ik}+G\vartheta\right]T_{ci}\right)+$$
$$\sum_{\mathrm{q=1}}^{\mathrm{v}} b_{ik}^{1} a_{jl}^{1} a_{ik}^{G-\tau_{ik}+q} Q_3\left(\left[G-\varepsilon_{ik}+q\right]T_{ci}\right)+$$
$$\sum_{\mathrm{q=1}}^{\vartheta\text{-v+1}} b_{ik}^{L+1} a_{jl}^{G} a_{ik}^{G(L+1)-\tau_{ik}-L+q+v} Q_3\left(\left[G(\vartheta+1)-\varepsilon_{ik}-\vartheta+v+q\right]T_{ci}\right) \tag{6-23}$$

In (6-22) and (6-23),

$$Q_1(a) = \sin(\Delta\omega a + \varphi_{ik}) - \sin(\Delta\omega a - \Delta\omega\Delta_{ik} + \varphi_{ik}),$$

$$Q_2(a) = \sin(\Delta\omega a - \Delta\omega\Delta_{ik} + \varphi_{ik}) - \sin(\Delta\omega a - \Delta\omega T_{ci} + \varphi_{ik})),$$

and

$$Q_3(a) = \sin(\Delta\omega a + \varphi_{ik}) - \sin(\Delta\omega a - \Delta\omega T_{ci} + \varphi_{ik})).$$

Here we consider random data and random spreading sequences. Since all terms in (6-22) and (6-23) represent independent random variables and both the data and the spreading sequence have zero mean, $E[AB]=0$. The variance of I_{ik} can then be calculated as

$$E[I_{ik}^2]=\frac{p_{ik}}{2}\left(E[A^2]+E[B^2]\right), \tag{6-24}$$

where $E[A^2]$ and $E[B^2]$ can be obtained as

$$E[A^2]=\sum_{n=2}^{G}\frac{1}{(\Delta\omega)^2}\Bigg[\left(Q_1([G-\varepsilon_{ik}+\vartheta(n-1)]T_{ci})\right)^2+\left(Q_2([G-\varepsilon_{ik}+\vartheta(n-1)]T_{ci})\right)^2+$$
$$\sum_{\text{q}=1}^{\text{v}}\left(Q_3([G-\varepsilon_{ik}+v(n-1)+q]T_{ci})\right)^2+\sum_{\text{q}=1}^{\vartheta\text{-v}+1}\left(Q_3([G-\varepsilon_{ik}+\vartheta n+v+q]T_{ci})\right)^2\Bigg]$$

(6-25)

and

$$E[B^2]=\frac{1}{(\Delta\omega)^2}\Bigg[\left(Q_1([G-\varepsilon_{ik}]T_{ci})\right)^2+\left(Q_2([G-\varepsilon_{ik}+G\vartheta]T_{ci})\right)^2+\left(Q_3([G-\varepsilon_{ik}+1]T_{ci})\right)^2+$$
$$\sum_{\text{q}=1}^{\text{v}}\left(Q_3([G-\varepsilon_{ik}+q]T_{ci})\right)^2+\sum_{\text{q}=1}^{\vartheta\text{-v}+1}\left(Q_3([G(\vartheta+1)-\varepsilon_{ik}-\vartheta+v+q]T_{ci})\right)\Bigg]$$

(6-26)

Averaging over φ_{ik} which is uniformly distributed over 0 to 2π, (6-25) and (6-26) become

$$E[A^2]=\frac{1}{(\Delta\omega)^2}\sum_{n=2}^{G}\Bigg[\left[1-\cos(\Delta\omega\Delta_{ik})\right]+\left[1-\cos(\Delta\omega(T_{ci}-\Delta_{ik})\right]+\left[1-\cos(\Delta\omega(T_{ci})\right]+$$
$$\cdots+\left[1-\cos(\Delta\omega(T_{ci})\right]+\left[1-\cos(\Delta\omega(T_{ci}))\right]+\cdots+\left[1-\cos(\Delta\omega T_{ci})\right]\Bigg]$$
$$=\frac{1}{(\Delta\omega)^2}\sum_{n=2}^{G}\Bigg[\left[1-\cos(\Delta\omega\Delta_{ik})\right]+\left[1-\cos(\Delta\omega(T_{ci}-\Delta_{ik}))\right]+(\vartheta-1)\left[1-\cos(\Delta\omega T_{ci})\right]\Bigg]$$

(6-27)

$$E\left[B^2\right]=\frac{1}{(\Delta\omega)^2}\Big[\ [1-\cos(\Delta\omega\Delta_{ik})]+[1-\cos(\Delta\omega(T_{ci}-\Delta_{ik})]+[1-\cos(\Delta\omega(T_{ci})]+\cdots+$$

$$[1-\cos(\Delta\omega(T_{ci})]+[1-\cos(\Delta\omega(T_{ci})]+\cdots+[1-\cos(\Delta\omega(T_{ci})]\ \Big]$$

$$=\frac{1}{(\Delta\omega)^2}E\Big[\ [1-\cos(\Delta\omega\Delta_{ik})]+[1-\cos(\Delta\omega(T_{ci}-\Delta_{ik}))]+(\vartheta-1)[1-\cos(\Delta\omega T_{ci})]\ \Big]$$

(6-28)

Substitute (6-27) and (6-28) into (6-24), we obtain

$$E\left[I_{ik}^2\right]=\frac{p_{ik}G}{2(\Delta\omega)^2}\left[\ 2\sin^2\frac{\Delta\omega\Delta_{ik}}{2}+2\sin^2\frac{\Delta\omega(T_{ci}-\Delta_{ik})}{2}+2(\vartheta-1)\sin^2\frac{\Delta\omega T_{ci}}{2}\ \right]. \tag{6-29}$$

Considering the two cases where $\Delta\omega=0$,and $\Delta\omega\neq 0$.

I) $\Delta\omega=0$

Taking limit on the right hand side, (6-29) becomes

$$E\left[I_{ik}^2\right]=\frac{p_{ik}G}{4}\left[\Delta_{ik}^2+(T_{ci}-\Delta_{ik})^2+(\vartheta-1)T_{ci}^2\right]. \tag{6-30}$$

Averaging over Δ_{ik} which is uniformly distributed over T_{ci}, (6-30) can be simplified as

$$E\left[I_{ik}^2\right]=\frac{(3\vartheta-1)GT_{ci}^2}{12}p_{ik}. \tag{6-31}$$

II) $\Delta\omega\neq 0$

$$E\left[I_{ik}^2\right]=\frac{p_{ik}G}{2(\Delta\omega)^2}\left[\ 2-\frac{2\sin(\Delta\omega T_{ci})}{\Delta\omega T_{ci}}+(\vartheta-1)(1-\cos(\Delta\omega T_{ci}))\ \right] \tag{6-32}$$

C. Variance of MAI for the case where $T_{cj} < T_{ci}$

In this case, as shown in Fig.6.4, two data bits b_{ik}^1, b_{ik}^2 of the narrowband user k in class i will correlate with the data bit b_{jl}^1 of the wideband user. We consider the case where $G = \lambda\vartheta$, $\varepsilon_{ik} = Gw + v$. Similar to the case with $T_{cj} > T_{ci}$, the integration in (6-13) can be partitioned into I_1, I_2, I_5, I_6 as shown in Fig.6.4 (a). The definition of I_1, I_2 is defined in Section 6.2.2.B. I_5, I_6 are defined as the integration with duration T_{cj}. I_6 denotes the integration for the first and the last interference chips a_{ik} correlating with b_{jl}^1, while I_5 denotes the integration for other interference chips a_{ik}. Hence the MAI from user k in class i is obtained as

$$I_{ik} = \sqrt{\frac{p_{ik}}{2}}\left[I_1 + I_2 + I_5 + I_6\right], \tag{6-33}$$

where I_1, I_2, I_5, I_6 are defined in the following.

$$\begin{aligned} I_1 &= b_{ik}^1 \sum_{n=1}^{w+1} a_{jl}^{\vartheta(n-1)+1+v} a_{ik}^n T_1\left(\left[\vartheta(n-1)+1+v\right]T_{cj}\right) + b_{ik}^2 \sum_{n=w+2}^{\lambda} a_{jl}^{\vartheta(n-1)+1+v} a_{ik}^n T_1\left(\left[\vartheta(n-1)+1+v\right]T_{cj}\right) \\ &= \sum_{n=2}^{\lambda} b_{ik} a_{jl}^{\vartheta(n-1)+1+v} a_{ik}^n T_1\left(\left[\vartheta(n-1)+1+v\right]T_{cj}\right) + b_{ik}^1 a_{jl}^{v+1} a_{ik}^1 T_1\left(\left[v+1\right]T_{cj}\right) \end{aligned} \tag{6-34}$$

where $b_{ik} \in \{b_{ik}^1, b_{ik}^2\}$.

$$\begin{aligned} I_2 &= b_{ik}^1 \sum_{n=2}^{w+1} a_{jl}^{\vartheta(n-2)+1+v} a_{ik}^n T_2\left(\left[\vartheta(n-2)+1+v\right]T_{cj}\right) + b_{ik}^2 \sum_{n=w+2}^{\lambda+1} a_{jl}^{\vartheta(n-2)+1+v} a_{ik}^n T_2\left(\left[\vartheta(n-2)+1+v\right]T_{cj}\right) \\ &= \sum_{n=2}^{\lambda} b_{ik} a_{jl}^{\vartheta(n-2)+1+v} a_{ik}^n T_2\left(\left[\vartheta(n-2)+1+v\right]T_{cj}\right) + b_{ik}^2 a_{jl}^{\vartheta(\lambda-1)+1+v} a_{ik}^{h+1} T_2\left(\left[\vartheta(\lambda-1)+1+v\right]T_{cj}\right) \end{aligned} \tag{6-35}$$

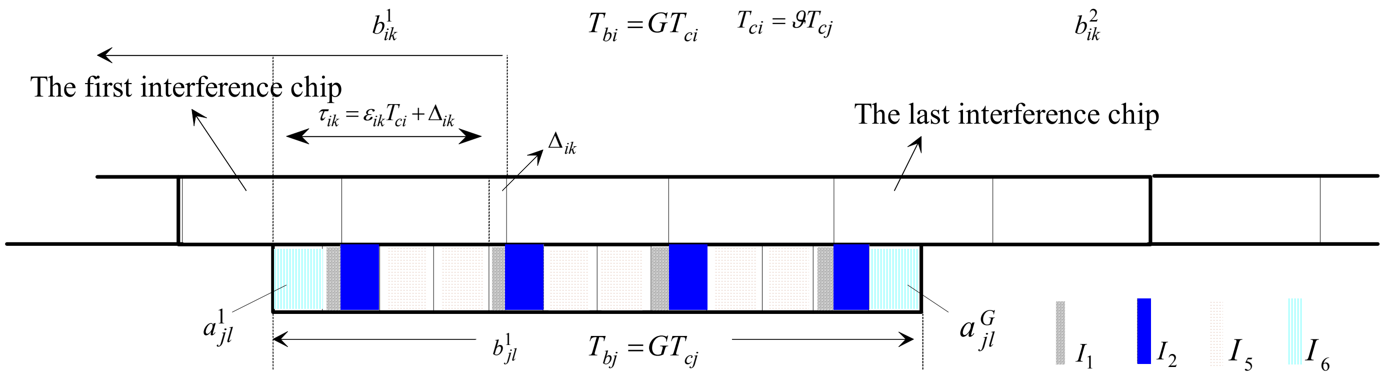

(a) Diagram to evaluation various components of the MAI for a narrowband user imposed on the wideband user. In this illustration, we use $T_{ci}/T_{cj} = \vartheta = 3$, PG for both users are given by G=12, hence $\lambda = G/\vartheta = 4$, $\varepsilon_{ik} = 4$ or $w = 1$ ($\varepsilon_{ik} = 1 \cdot \vartheta + 1$).

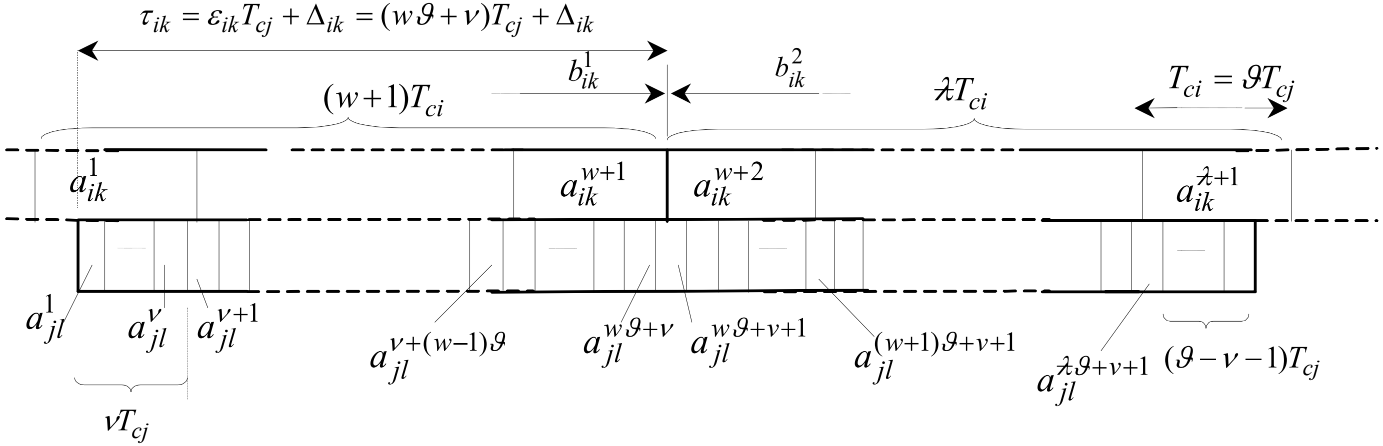

(b) Index number for the sequence

Fig.6.4 Schematic diagram of correlation for $T_{cj} < T_{ci}$

$$I_5 = \sum_{q=1}^{\vartheta-1} \left\{ b_{ik}^1 \sum_{n=2}^{w+1} a_{ik}^n a_{jl}^{\vartheta(n-2)+v+1+q} T_3\left(\left[\vartheta(n-2)+v+1+q\right]T_{cj}\right) + b_{ik}^2 \sum_{n=w+2}^{\lambda} a_{ik}^n a_{jl}^{\vartheta(n-2)+v+1+q} T_3\left(\left[\vartheta(n-2)+v+1+q\right]T_{cj}\right) \right\}$$
$$= \sum_{q=1}^{\vartheta-1} \sum_{n=2}^{\lambda} b_{ik} a_{ik}^n a_{jl}^{\vartheta(n-2)+v+1+q} T_3\left(\left[\vartheta(n-2)+v+1+q\right]T_{cj}\right) \qquad (6\text{-}36)$$

$$I_6 = \sum_{q=1}^{v} b_{ik}^1 a_{ik}^1 a_{jl}^q T_3\left(qT_{cj}\right) + \sum_{q=1}^{\vartheta-v-1} b_{ik}^2 a_{ik}^{\lambda+1} a_{jl}^{\vartheta\lambda-\vartheta+v+1+q} T_3\left(\left[\vartheta\lambda-\vartheta+v+1+q\right]T_{cj}\right) \qquad (6\text{-}37)$$

Based on (6-34), (6-35), (6-36) and (6-37), (6-33) can be simplified as

$$I_{ik} = \sqrt{\frac{p_{ik}}{2}}(A_1 + B_1), \qquad (6\text{-}38)$$

where

$$A_1 = \sum_{n=2}^{\lambda} \Bigg[b_{ik} a_{jl}^{\vartheta(n-1)+1+v} a_{ik}^n T_1\left(\left[\vartheta(n-1)+1+v\right]T_{cj}\right) + b_{ik} a_{jl}^{\vartheta(n-2)+1+v} a_{ik}^n T_2\left(\left[\vartheta(n-2)+1+v\right]T_{cj}\right) + \sum_{q=1}^{\vartheta-1} b_{ik} a_{ik}^n a_{jl}^{\vartheta(n-2)+v+1+q} T_3\left(\left[\vartheta(n-2)+v+1+q\right]T_{cj}\right) \Bigg]$$

(6-39)

and

$$B_1 = b_{ik}^1 a_{jl}^{v+1} a_{ik}^1 T_1\left(\left[1+v\right]T_{cj}\right) + b_{ik}^2 a_{jl}^{\vartheta(\lambda-1)+1+v} a_{ik}^{\lambda+1} T_2\left(\left[\vartheta(\lambda-1)+1+v\right]T_{cj}\right) + \sum_{q=1}^{v} b_{ik}^1 a_{ik}^1 a_{jl}^q T_3\left(qT_{cj}\right) + \sum_{q=1}^{\vartheta-v-1} b_{ik}^2 a_{ik}^{\lambda+1} a_{jl}^{\vartheta\lambda-\vartheta+v+1+q} T_3\left(\left[\vartheta\lambda-\vartheta+v+1+q\right]T_{cj}\right) \qquad (6\text{-}40)$$

Therefore the variance of I_{ik} caused by the narrowband user to the wideband user is

$$E\left[I_{ik}^2\right] = \frac{p_{ik}}{2}\left(E\left[A_1^2\right] + E\left[B_1^2\right]\right). \qquad (6\text{-}41)$$

Similar to the case where $T_{cj} > T_{ci}$,

$$E\left[A_1^2\right]=\frac{1}{(\Delta\omega)^2}\sum_{n=2}^{\lambda}\left[\ \left[1-\cos(\Delta\omega\Delta_{ik})\right]+\left[1-\cos(\Delta\omega(T_{cj}-\Delta_{ik}))\right]+(\vartheta-1)\left[1-\cos(\Delta\omega T_{cj})\right]\ \right] \tag{6-42}$$

$$E\left[B_1^2\right]=\frac{1}{(\Delta\omega)^2}\left[\ \left[1-\cos(\Delta\omega\Delta_{ik})\right]+\left[1-\cos(\Delta\omega(T_{cj}-\Delta_{ik}))\right]+(\vartheta-1)\left[1-\cos(\Delta\omega T_{cj})\right]\ \right] \tag{6-43}$$

Substitute (6-42) and (6-43) into (6-41), we got

$$E\left[I_{ik}^2\right]=\frac{p_{ik}\lambda}{2(\Delta\omega)^2}\left[\ 2\sin^2\frac{\Delta\omega\Delta_{ik}}{2}+2\sin^2\frac{\Delta\omega(T_{cj}-\Delta_{ik})}{2}+2(\vartheta-1)\sin^2\frac{\Delta\omega T_{cj}}{2}\ \right] \tag{6-44}$$

Averaging (6-44) over Δ_{ik}, we obtain

$$E\left[I_{ik}^2\right]=\begin{cases}\dfrac{(3\vartheta-1)GT_{cj}^2}{12\vartheta}p_{ik} & \Delta\omega=0\\[2ex] \dfrac{p_{ik}G}{2(\Delta\omega)^2\vartheta}\left[\ 2-\dfrac{2\sin(\Delta\omega T_{cj})}{\Delta\omega T_{cj}}+(\vartheta-1)(1-\cos(\Delta\omega T_{cj}))\ \right] & \Delta\omega\neq 0\ .\end{cases} \tag{6-45}$$

The results obtained in this section confirmed the results published in [97] although we use a different approach. In the following, we compute the capacity obtained from MCR and multiple processing gain (MPG) systems. The MAI is approximated as a Guassian random variable. This approximation is proven to be accurate for large signal to noise ratio and many users, or alternatively for a few users with large processing gain.

6.3 Capacity obtained for MCR systems

In this study, a dual-service system accommodating wideband and narrowband users will be considered. There is only one wideband subsystem, however the number of narrowband subsystems on top of the wideband subsystem is flexible as shown in Fig.6.1. By modeling MAI as a Gaussian random variable, the BER performance of CDMA systems employing BPSK can be determined from the decision variable defined in (6-7). The BER can be obtained as $P_e = Q\left[\sqrt{\dfrac{(S_{jl})^2}{\chi \cdot \mathrm{var}[I] + \mathrm{var}[\zeta]}}\right]$ [101].

The introduction of χ is due to the effect caused by the receiver filter for the desired user and the PSD of the spreading signals of the interference user. The significance of χ is: for the wideband desired users $\chi = 1$, since all the interference power from the narrowband users can pass through the receiver filter for the desired wideband users, while for the narrowband desired user, $\chi < 1$ since only a portion of the interference power from the wideband users can pass through the receiver filter for the narrowband desired users and the actual value of χ depends on the difference in their carrier frequencies and the PSD of the spreading interference signals. The computation of χ caused by wideband user to narrowband is shown in Appendix B.

Substitute (6-9) and (6-11b) to this BER expression, BER can be rewritten as

$$P_e = Q\left[\sqrt{\frac{2pT_b^2}{4\chi \mathrm{var}[I] + N_0 T_b}}\right]. \tag{6-46a}$$

Compared with $P_e = \sqrt{2E_b / N_0}$ for BPSK, E_b / N_0 for CDMA systems is defined as

$$\gamma = \frac{pT_b^2}{4\chi \mathrm{var}[I] + N_0 T_b} \tag{6-46b}$$

where $\mathrm{var}[I]$ takes different expressions shown in (6-15), (6-31), (6-32) and (6-45).

We employ the perfect power control scheme is employed for each subsystem. Therefore, the received power for users in one specific subsystem is kept as a constant. For computation simplicity, the QoS requirement which is only defined by E_b / N_0 for users in the same spectral layer (narrowband or wideband subsystems) are identical, however in a practical implementation, it can be different for users in different subsystems of the same spectral layer. The system capacity is defined as the sum of the average transmission rate from all users in both wideband and narrowband subsystems. The bandwidth for high data rate (or the wideband subsystem) and low data rate (narrowband subsystems) users are assumed to be $B_n = 1/T_{cn}, B_w = 1/T_{cw}$ respectively. The E_b / N_0 requirements for both wideband and narrowband subsystems are γ_w, γ_n, hence, in (6-46b), $T_b \in \{T_{bn}, T_{bw}\}, \gamma \in \{\gamma_n, \gamma_w\}$ for the narrowband and the wideband subsystems, respectively. In our analysis, the transmission rates R_w, R_n are fixed for the wideband and narrowband users. The number of narrowband users K_n is also fixed. The number of wideband users K_w accommodated in the system is determined by K_n, γ_w, γ_n and B_w, B_n. The system capacity will be investigated in detail for the MCR configuration (a), (b) and (c) shown in Fig.6.1.

6.3.1 Capacity achieved by configuration (a)

In this configuration, there will be ϑ narrowband subsystems on top of the wideband subsystem. Narrowband users are evenly distributed among ϑ narrowband subsystems. It is expected that with such arrangement, the interference experienced by narrowband users is minimized so that the system capacity can be improved.

In this case, $\Delta\omega \neq 0$. Setting $\eta(\Delta\omega,\vartheta) = 2 - \dfrac{2\sin(\Delta\omega T_{cw})}{\Delta\omega T_{cw}} + (\vartheta - 1)(1 - \cos(\Delta\omega T_{cw})$, and substitute (4-32) and (4-45) into (4-46b), the E_b / N_0 expressions for narrowband users in the qth narrowband subsystem and wideband users become

$$\gamma_n = \frac{p_{n,q,l} T_{bn}}{\dfrac{2\chi_q \eta(\Delta\omega_q, \vartheta)}{(\Delta\omega_q)^2\, \vartheta T_{cw}} \sum_{k=1}^{K_w} p_{w,k} + \dfrac{2\vartheta T_{cw}}{3} \sum_{k=1,k\neq l}^{K_{n,q}} p_{n,q,k}}, \qquad q = 1 \cdots \vartheta \quad , \tag{6-47}$$

and

$$\gamma_w = \frac{p_{w,l} T_{bw}}{\dfrac{2}{\vartheta T_{cw}} \sum_{q=1}^{\vartheta} \dfrac{\eta(\Delta\omega_q, \vartheta)}{(\Delta\omega_q)^2} \sum_{k=1}^{K_{n,q}} p_{n,q,k} + \dfrac{2T_{cw}}{3} \sum_{k=1,k\neq l}^{K_w} p_{w,k}} \quad , \tag{6-48}$$

where $T_{bn} = 1/R_n$, $T_{bw} = 1/R_w$ and $K_{n,q} = K_n / \vartheta$ is the number of narrowband users in the qth narrowband subsystem if narrowband users are distributed uniformly over all the narrowband subsystems. $p_{n,q,l}$, $p_{w,l}$ denote the received power for the lth user in the qth narrowband subsystem and the lth user in wideband subsystem respectively. They are the same for all users in the same subsystem. χ_q is the interference coefficient caused by the wideband user to the user in the qth narrowband subsystem. χ_qs obtained for different narrowband subsystems are listed in Table 6.1 with

B=5MHz. As the carrier frequency of the narrowband subsystem is located far away from the carrier frequency of the wideband subsystem, χ_q decreases.

TABLE 6.1 χ_q for different narrowband subsystems

	$\vartheta=8$				$\vartheta=4$		$\vartheta=2$
$\Delta\omega$ (MHz)	2.1875	1.5625	0.9375	0.3125	1.875	0.625	1.25
χ_q	0.0078	0.0638	0.1697	0.2588	0.0715	0.4285	0.5

From (6-47), it can be obtained

$$\frac{p_{n,q,l}}{p_{w,k}}=\frac{2\chi_q\eta(\Delta\omega_q,\vartheta)K_w}{(\Delta\omega_q)^2\,\vartheta T_{cw}\left[1/(\gamma_n R_n)-\left(2\vartheta T_{cw}(K_{n,q}-1)/3\right)\right]},\tag{6-49}$$

where $K_{n,q}<\dfrac{3B}{2\gamma_n R_n\vartheta}+1$ to ensure $\dfrac{p_{n,q,l}}{p_{w,k}}>0$.

Substitute (6-49) into (6-48), for a given number of users in all the narrowband subsystems, the number of users supported in the wideband subsystem can be obtained as

$$K_w=\frac{2/3+B/(\gamma_w R_w)}{\dfrac{4B^3}{\vartheta^2}\sum_{q=1}^{\vartheta}\dfrac{\chi_q\eta(\Delta\omega_q,\vartheta)^2K_{n,q}}{(\Delta\omega_q)^4}\dfrac{3B\gamma_n R_n}{\left(3B-2\vartheta\gamma_n R_n(K_{n,q}-1)\right)}+2/3}.\tag{6-50}$$

Therefore the system capacity is obtained as

$$C=K_nR_n+K_w\vartheta R_n=(K_n+\vartheta K_w)R_n.\tag{6-51}$$

The system capacity obtained with different narrowband and wideband transmission rate is shown in Fig.6.5. For configuration (a), the increase in the transmission rate of narrowband and wideband users R_n, R_w, the spreading bandwidth ratio ϑ and the number of narrowband users supported in the system result in higher system capacity.

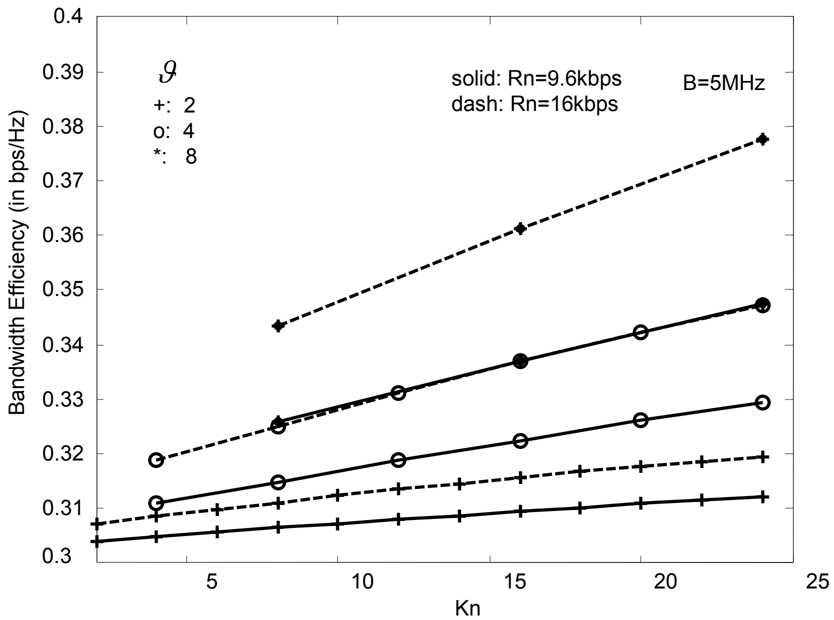

Fig.6.5 System capacity achieved by configuration (a)

6.3.2 Capacity achieved by configuration (b)

Under this configuration, all narrowband users are in one narrowband subsystem. The carrier frequency of the narrowband subsystem is the same as that of the wideband subsystem, or $\Delta\omega = 0$. In this case, $\chi_q, p_{n,q,l}$ of (6-47) and (6-48) can be replaced by $\chi, p_{n,l}$.

As $\Delta\omega = 0$, by substituting (6-31,45) into (6-46b), we obtain

$$\gamma_n = \frac{p_{n,l} T_{bn}}{\frac{\chi(3\vartheta - 1)T_{cw}}{3\vartheta} \sum_{k=1}^{K_w} p_{w,k} + \frac{2\vartheta T_{cw}}{3} \sum_{k=1,k\neq l}^{K_n} p_{n,k}} \quad , \tag{6-52}$$

and

$$\gamma_w = \frac{p_{w,l} T_{bw}}{\frac{(3\vartheta - 1)T_{cw}}{3\vartheta} \sum_{k=1}^{K_n} p_{n,k} + \frac{2T_{cw}}{3} \sum_{k=1,k\neq l}^{K_w} p_{w,k}} \quad . \tag{6-53}$$

The interference coefficient χ for different ϑ is listed in Table 6.2.

TABLE 6.2 Interference coefficients χ for $\Delta\omega = 0$

ϑ	2	4	8
χ	0.8570	0.5178	0.2722

The number of users supported in the system is obtained as

$$K_w = \frac{3B/(\gamma_w R_w) + 2}{\chi K_n (3 - 1/\vartheta)^2 \Big/ \big(3B/(\gamma_n R_n) - 2\vartheta(K_n - 1)\big) + 2} \tag{6-54}$$

The system capacity can be obtained using (6-51) and results are shown in Fig.6.6. Unlike configuration (a), the system capacity decreases with increase of the number of narrowband users K_n. As K_n is small, the system capacity is higher with the increase of R_n, however as K_n reaches a certain value, the observation reverses.

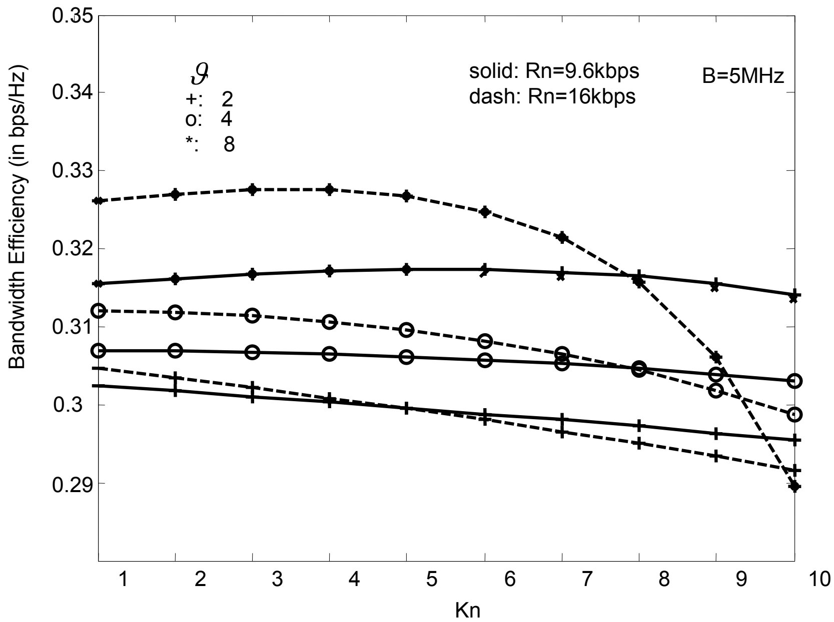

Fig.6.6 System capacity achieved by configuration (b) ($\Delta\omega = 0$)

6.3.3 Capacity achieved by configuration (c)

In this case, $\Delta\omega \neq 0$, by substituting (6-32) and (6-45) into (6-46b), the E_b / N_0 requirement for narrowband and wideband users can be obtained as

$$\gamma_n = \frac{p_{n,l} T_{bn}}{\frac{2\chi\eta}{(\Delta\omega)^2 \, \vartheta T_{cw}} \sum_{k=1}^{K_w} p_{w,k} + \frac{2\vartheta T_{cw}}{3} \sum_{k=1,k\neq l}^{K_n} p_{n,k}} \quad , \tag{6-55}$$

and

$$\gamma_w = \frac{p_{w,l} T_{bw}}{\frac{2\eta}{(\Delta\omega)^2 \, \vartheta T_{cw}} \sum_{k=1}^{K_n} p_{n,k} + \frac{2T_{cw}}{3} \sum_{k=1,k\neq l}^{K_w} p_{w,k}} \quad . \tag{6-56}$$

The number of wideband users K_w supported in the system is obtained as

$$K_w = \frac{\left[B/(\gamma_w R_w) + 2/3\right]}{4\chi\eta^2 B^3 K_n \Big/ \left[(\Delta\omega)^4 \, \vartheta^2 \left(1/(\gamma_n R_n) - 2\vartheta(K_n - 1)/(3B)\right)\right] + 2/3} . \tag{6-57}$$

The interference coefficient and the system capacity obtained using (6-51) are shown in Table 6.3 and Fig. 6.7 respectively.

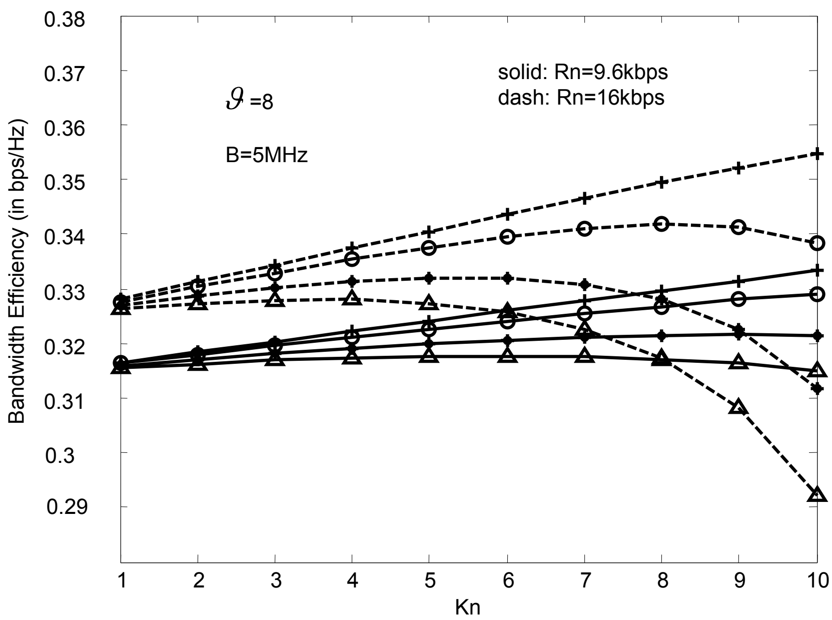

+: $\Delta\omega 1$ o: $\Delta\omega 2$ *: $\Delta\omega 3$ Δ: $\Delta\omega 4$

Fig.6.7 System capacity achieved by configuration (c) ($\Delta\omega \neq 0$)

TABLE 6.3 Interference coefficients χ for $\Delta\omega \neq 0$

	1	2	3	4
$\Delta\omega$ (MHz)	2.1875	1.5625	0.9375	0.3125
χ	0.0078	0.0638	0.1696	0.2588

The system capacity obtained for $\Delta\omega \neq 0$ is shown in Fig.6.7. From Fig.6.5 to Fig.6.7, it can be concluded that configuration (a) outperforms configuration (b) in terms of system capacity. This observation confirms the conclusion in [89,91] although the interference model considered in their works is oversimplified. However as there is only one narrowband subsystem, system capacity achieved by configuration (c) ($\Delta\omega \neq 0$) is higher than that of configuration (b) ($\Delta\omega = 0$) while in [89,91] all narrowband subsystems achieve the same system capacity. In terms of bandwidth efficiency, configuration (a) outperforms configuration (c) if there are more narrowband users supported. Therefore in case the system has to support a large number of users while not to degrade the system capacity, configuration (a) can be a choice. In configuration (a), distributing the narrowband users unevenly over the all narrowband subsystems will further improve the system capacity, although it is not investigated here. The results obtained here indicate that in MCR systems, with a delicate design of spectrally overlaid structure, more users can be accommodated and the system capacity can be enhanced also.

6.4 Capacity obtained for multiple processing gain (MPG) system

For comparison purpose, the system capacity obtained for multi-rate systems realized by MPG with single chip rate is investigated in this section. In MPG systems, users requesting different bit rate services have different PG, while spreading bandwidth are identical for all users. The variance of MAI received by the jth desired user is shown to be [38,103]

$$\mathrm{var}[I] = \begin{cases} \sum_{i}^{Q} \frac{G_i T_c^2}{6} \vartheta \sum_{k=1}^{K_i} p_{ik} & \Lambda_j > \Lambda_i \\ \sum_{i}^{Q} \frac{G_j T_c^2}{6} \sum_{k=1}^{K_i} p_{ik} & \Lambda_j < \Lambda_i \end{cases}, \tag{6-58}$$

where G_j, G_i are PGs and $\vartheta = G_j / G_i$ is the ratio between PG for high data rate and low data rate users. $T_c = 1/B$ is the chip duration. The first expression denotes the MAI caused by low rate users to high rate users. The second expression of (6-58) represents the MAI caused by high rate users to low rate users, Consider a dual-rate system and $Q=2$. The PG for low data rate and high data rate users are G_1 and G_2 respectively and $\vartheta = G_1 / G_2$. Substitute (6-58) into (6-46b), the E_b / N_0 for low rate data users and high data rate users are given by

$$\gamma_1 = \frac{p_{1,l} T_{b1}}{\frac{2}{3} T_c \sum_{k=1}^{K_2} p_{2,k} + \frac{2}{3} T_c \sum_{k=1, k \neq l}^{K_1} p_{1,k}}, \tag{6-59}$$

and

$$\gamma_2 = \frac{p_{2,l} T_{b2}}{\frac{2}{3} T_c \sum_{k=1}^{K_1} p_{1,k} + \frac{2}{3} T_c \sum_{k=1, k \neq l}^{K_2} p_{2,k}}, \tag{6-60}$$

where K_1, K_2 are the number of users requesting low data rate and high data rate services respectively. $T_{b1} = 1/R_1, T_{b2} = 1/R_2$ are the bit durations of low data rate and high data rate users. $p_{1,l}, p_{2,l}$ are the transmission power for low data rate and high data rate users.

Assuming that for low data rate and high data rate users, the E_b / N_0 requirement is the same for all users requesting service with the same data rate. γ_1, γ_2 are the

E_b / N_0 requirements for low data rate and high data rate users respectively. For the ideal constant received power control, (6-59) and (6-60) can then be rewritten as

$$\gamma_1 = \frac{1}{K_2 \frac{p_2}{p_1} + (K_1 - 1)} \frac{3B}{2R_1}, \tag{6-61}$$

and

$$\gamma_2 = \frac{1}{K_1 \frac{p_1}{p_2} + (K_2 - 1)} \frac{3B}{2R_2}. \tag{6-62}$$

The number of high rate users K_2 supported in the system is obtained as

$$K_2 = \frac{3B}{2\gamma_2 R_2} - K_1 \mathrm{X} + 1,$$

(6-63)

where $X = \frac{(3B + 2\gamma_2 R_2)\gamma_1 R_1}{(3B + 2\gamma_1 R_1)\gamma_2 R_2}$, and $K_1 < \frac{3B}{2\gamma_1 R_1} + 1$.

The system capacity obtained for MPG systems is shown in Fig.6.8. At lower ϑ, the effect of the number of low data rate users on the system capacity is not significant, while with the increase of ϑ, the system capacity drops with the increase of K_1.

The capacity comparison for MCR and MPG systems is shown in Table 6.4. From the investigation on the capacity of MCR and MPG systems, given the same conditions (the number of narrowband users K_1 or K_n, high data rate R_2 (or R_n) and low data rate R_1 (or R_w), the ratio of high data rate to low data rate ϑ, the system bandwidth B or B_w), MCR systems with $\Delta\omega = 0$ achieve nearly the same performance with MPG systems. However the full assignment configuration (a) and configuration (c) of MCR systems achieve higher system capacity than MPG systems. The reason is that with the control of spectrally overlaid structure, the MAI of MCR systems can be reduced significantly.

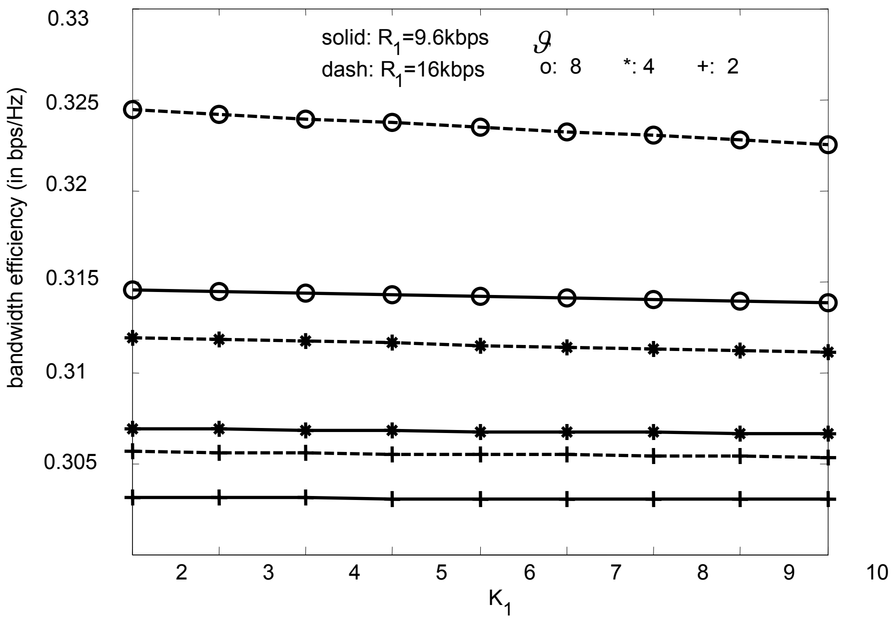

Fig.6.8 System capacity obtained for MPG system

TABLE 6.4 Capacity comparison for MCR and MPG systems

System	MCR (a)	MCR (b)	MCR (c)	MPG
$R_n = R_1 = 16kbps$	0.344	0.314	0.35	0.326
$R_n = R_1 = 9.6kbps$	0.325	0.314	0.33	0.314

6.5 Summary

In this chapter, the expression for the variance of MAI for MCR systems with asynchronous chip alignment and different carrier frequencies is derived. With the knowledge of the variance of MAI, capacity of MCR systems with wideband and narrowband subsystems is investigated for different spectral configurations. For the first time in the literatures, a capacity comparison is conducted for MCR and MPG systems. The results obtained show that with proper control of the spectrally overlaid structure, MCR systems can achieve higher capacity than that of MPG systems.

CHAPTER VII

CONCLUSIONS

Adaptive modulation is a promising technique to overcome the detrimental effect of channel fading. Adaptive modulation can be implemented by changing the transmission rate and the transmission power. However this study shows that adaptive modulation with both rate and power adaptation achieves negligible capacity gain over adaptive modulation with rate adaptation only under a given average power constraint.

The performance of adaptive modulation techniques relies on the precise tracking of channel conditions and the reliable feedback of channel state information from receivers to transmitters. In coherent detection systems, the study on the effect of imperfect channel estimation shows that the BER performance under imperfect channel estimation strongly depends on the correlation coefficient ρ (correlation between the estimated and the true fading gain), whilst the dependence of BER performance on r ($\Omega/\hat{\Omega}$, the ratio of variance of the true fading gain and the estimated fading gain) is not significant. Higher ρ leads to less degradation of BER performance under imperfect channel estimation. Under imperfect channel estimation, the BER error floor which does not exist under perfect channel estimation is present. Under imperfect channel estimation, the complexity in BER computation employing an exact method introduced in [29] grows with the increase of constellation size. An approximate method is proposed to overcome this difficulty under the assumption of higher ρ. Using this approximate method, a closed form solution for the BER performance with amplitude estimation error only is obtained.

The complexity in BER computation is reduced dramatically while sufficiently good approximation is provided. The analysis shows that at higher ρ and within a practical SNR range, the approximate method can predict the BER performance with good accuracy.

In adaptive modulation systems, the estimated channel fading gain is used not only for the coherent symbol detection, but also for the selection of suitable modulation mode at the transmitter. Under imperfect channel estimation, it is expected that extra margins should be given in the SNR threshold intervals for the selection of MQAM constellation in order to maintain the targeted BER performance. A framework to investigate the effect of imperfect channel estimation on channel capacity is introduced for adaptive modulation systems with and without diversity reception. An equivalent circuit which converts the effect of channel estimation error into an imperfect IQ receiver structure is conceived to quantify the extra margins required in the SNR threshold intervals. Prior to this work, these extra margins under the consideration of channel estimation error are just assumed to be a few dB through experience, without any quantitative analysis. This framework enables these extra margins to be obtained from quantitative analysis based on channel and estimation techniques. The studies show that smaller ρ causes larger extra SNR margins, while r does not affect these margins significantly. Employing the proposed framework, the BER performance curves which define the SNR threshold intervals are obtained. It is shown that some higher order constellations cannot be used due to the existence of error floors. In adaptive systems with diversity reception employing SC technique, it can be seen that the error floor in BER performance curves can be improved.

As multiple users are allowed to share radio channel, the optimal channel allocation strategy is to allow only the user with the best channel conditions to transmit at any transmission interval. Analysis on capacity obtained from this optimal scheme shows that the channel capacity gain achieved by adaptive rate adaptive power over rate adaptive only is insignificant as in single user systems. Some performance metrics such as the time duration for the process to stay in one MQAM constellation and the channel inter-access time are studied by employing the first order Markovian process. The channel inter-access time is a parameter directly related to the system performance in terms of service delay. A methodology is introduced to obtain the channel inter-access time through analysis based on channel statistics and the number of users in the system. Analytical results show that the channel inter-access time increases with the decrease of Doppler shift.

A suboptimal SNR-priority-based channel allocation scheme which allows a number of users observing the first few best channel conditions rather than only one user to transmit is proposed to overcome the long channel inter-access time of the optimal channel allocation scheme. Order statistics is employed to study the channel capacity achieved by the SNR-priority-based channel allocation scheme combined with adaptive modulation. Numerical analysis shows that this suboptimal channel allocation scheme can achieve higher capacity than the the fixed modulation system while it performs inferior to the optimal system. Another channel allocation scheme to accommodate dual classes of service (QoS and BE service) is proposed where all QoS services are allowed to transmit at any transmission interval while for BE services, the optimal channel allocation scheme is employed. As fewer QoS services are allowed, higher throughput is achieved. Although the schemes studied here are simple, the analysis conducted is concrete and new and is valuable for designers to perform system design.

Adaptive modulation techniques can be extended to CDMA systems. A combined adaptive MQAM and adaptive PG is proposed to study the system capacity achieved by a variety of adaptive rate adaptive power control schemes without considering the implementation details. A flaw present in the study of capacity of adaptive CDMA systems in most of the literatures is corrected by considering PG constraint ($G_{\min}$). Three power control schemes with rate adaptive capability are proposed. Scheme I aims to compensate for path loss and the transmission rate is adjusted based on the received SIR. Scheme II aims to compensate for path loss and allocate the transmission power based on the fast fading of individual user. The transmission rate is adapted to the received SIR as well. Scheme III aims to allocate the transmission power based on the mobile user location and the transmission rate is adapted to the received SIR. All these schemes are promising to improve system capacity. The studies show that the system capacity achieved by scheme II is higher than that obtained by scheme I. Scheme III is a power control strategy having the potential to reduce the other cell interference. The studies show that under the consideration of other cell interference, scheme III achieves higher system capacity than scheme I where path loss is totally compensated for, regardless of $G_{\min}$ constraint.

One way to realize rate adaptive modulation in CDMA systems is through varying spreading chip rate. As adaptive chip rate is employed, with the co-existence of multiple spreading bandwidth, the MAI exhibits unique characteristics. The study on the variance of MAI under a practical model, which takes into account the non-orthogonality of spreading codes, the offsets of carrier frequencies, the effect due to the PSD of the transmitted interference signals and the receiver filters for the desired user, is conducted. The system capacities achieved by several configurations of MCR systems is investigated based on this practical interference model. It can be concluded that the configuration where the narrowband users are distributed over different narrowband subsystems can achieve higher system capacity. As there is only one narrowband subsystem on top of the wideband subsystem, higher system capacity can be achieved by separating the carrier frequency of the narrowband subsystem apart from that of the wideband subsystem as far as possible. For the first time, the comparison study on the capacity achieved by MCR and MPG systems is conducted. It shows that the capacity achieved by MCR systems is not lower than that of MPG systems regardless of the configurations of MCR systems. The proper control of spectrally overlaid structure of MCR systems can achieve efficient usage of bandwidth.

REFERENCES

[1] J. F. Hayes, “Adaptive feedback communications”, *IEEE Trans. Commun. Technol.*, vol. COM-16, pp. 29-34, Feb. 1968.

[2] J. K. Cavers, “Variable-rate transmission for Rayleigh fading channels”, *IEEE Trans. Commun.*, vol. COM-20, pp.15-22, Feb. 1972.

[3] V. O. Jemtinen, “Error performance for adaptive transmission on fading channels”, *IEEE Trans. Commun.*, vol. COM-22, pp. 1331-1337, Sept. 1974.

[4] CCITT Draft recommendation V.34: A modem operating at data signaling rates up to 28.8Mbps for use on the general switched telephone network and on leased point to point 2-wire telephone-type circuits”, 1993.

[5] Cable television laboratories, Inc. (1998). DOCSIS: *Radio frequency interface specification: interim specification SP-RF1-104-980724*.

[6] S. Nanda, K. Balachandran, S. Kumar, “Adaptation techniques in wireless packet data services”, *IEEE Commu. Mag.*, pp. 54-64, Jan. 2000.

[7] Motorola and Nokia, “IXTREME”, 3GPP2, S00-20000321-019, March 2000.

[8] B. Classon, K. Blankenship, V. Desai, “Channel coding for 4G systems with adaptive modulation and coding”, *IEEE Wireless Communications*, vol. 9, pp. 8-13, Apr. 2002.

[9] S. Otsuki, S. Sampei, N. Morinaga, “Square-QAM adaptive modulation/TDMA/ TDD systems using modulation level estimation with Walsh function”, *Electron. Lett.*, vol. 31, pp. 169-171, Feb. 1995.

[10] W. T. Webb, R. Steele, “Variable rate QAM for mobile radio”, *IEEE. Trans. Commun*., vol. 43, pp. 223-2230, July 1995.

[11] Y. Kamio, S. Sampei, H. Sasaoka, N. Morinaga, “Performance of modulation-level-controlled adaptive-modulation under limited transmission delay time for land mobile communications”, in *Proc. IEEE VTC’95*, pp. 221-225,Chicago, IL, July 1995.

[12] B. Vucetic, “An adaptive coding scheme for time-varying channels”, *IEEE Trans. Commun*., vol. 39, pp. 653-666, May 1991.

[13] J. Torrance, H. Hanzo, “Optimization mode-switching levels for adaptive modulation in a slow Rayleigh fading channel”, *Electron. Lett.*, vol. 32, pp. 1167-1169, June 1996.

[14] C. Wong, R. S. Cheng, K. Letaief, R. D. Murch, “Multiuser OFDM with adaptive subcarrier, bit and power allocation”, *IEEE J. Selected Areas in Commun*., vol. 17, no. 10, pp. 1747-1758, Oct. 1999.

[15] A. J. Goldsmith, S. G. Chua, “Adaptive coded modulation for fading channels”, in *Proc. IEEE ICC’96*, vol. 3, pp. 1488-1492, June. 1997.

[16] F. F. Digham, M.-S. Alouini, “Adaptive M-FSK modulation for power limited systems”, *IEEE VTC-Fall*, 2002, vol. 2, pp. 1202 -1206, 2002.

[17] B. J. Choi, L. Hanzo, “Optimum mode-switching levels for adaptive modulation systems*”, IEEE GLOBALCOM’01*, 2001.

[18] A. J. Goldsmith, S. G. Chua, “Variable rate variable power MQAM for fading channels”, *IEEE Trans. Commun*., vol. 45, no. 10, pp. 1218-1229, Oct. 1997.

[19] M-S. Alounini, A. J. Goldsmith, “Capacity of Rayleigh fading channels under different adaptive transmission and diversity-combining technique”, *IEEE Trans. Veh. Technol*., vol. 48, pp. 1165-1181, July 1999.

[20] A. J. Goldsmith, P. P. Varaiya, “Capacity of fading channels with channel side information”, *IEEE Trans. Inform. Theory*, vol. 43, no. 6, pp. 1986-1992, Nov. 1997.

[21] M-S. Alounini, A. J. Goldsmith, "Comparison of fading channel capacity under different CSI assumptions", *IEEE VTS-Fall VTC'00*, vol. 4, pp. 1844-1849, 2000.

[22] S. T. Chung, A. J. Goldsmith, "Degrees of freedom in adaptive modulation: a unified view", *IEEE Trans. Commu*., vol. 49, no. 9, pp. 1561-1571, Sept. 2001.

[23] C. Kose, D. I. Goeckel, "On power adaptation in adaptive signaling system", *IEEE Trans. Commun*., vol. 48, pp. 1769 -1773, Nov. 2000.

[24] S. Sampei, S. Komaki, N. Morinaga, "Adaptive modulation/TDMA scheme for personal multi-media communication systems", in *Proc. IEEE GLOBALCOM'94*, pp. 989-993.

[25] T. Ue, S. Sampei, N. Morinaga, K. Hamaguchi, "Symbol rate and modulation level-controlled adaptive modulation/TDMA/TDD system for high-bit-rate wireless data transmission*", IEEE Trans. Veh. Technol*., vol. 47, pp. 1134-1147, Nov. 1998.

[26] T. Ikeda, S. Sampei, N. Morinaga, "TDMA-based adaptive modulation with dynamic channel assignment for high-capacity communication systems", *IEEE Trans. Veh. Technol.*, vol. 49, no. 2, pp. 404-412, Mar. 2000.

[27] J. Matsuoka, S. Sampei, N. Morrinaga, Y. Kamio, "Adaptive modulation system with variable coding rate concatenated code for high-quality multi-media communication systems", in *Proc. IEEE VTC'96*, pp. 487-491, 1996.

[28] X. Qiu, K. Chawla, "On the performance of adaptive modulation in cellular systems", *IEEE Trans. Commun*., vol. 47, no. 6, pp. 884-895, June. 1999.

[29] E. Erkip, B. Aazhang, "A Comparative study of multiple accessing schemes", Conference Record of the *Thirty-First Asilomar Conference on Signals, Systems & Computers*, vol. 1, pp. 614 –619, 1998.

[30] A. J. Goldsmith, "The capacity of downlink fading channels with variable rate and power", *IEEE Trans. Veh. Technol*., vol. 46, no. 3, pp. 569-580, Aug. 1997.

[31] P. Viswanath, David N. C. Tse, V. Anantharam, " Asymptotically optimal water-filling in vector multiple-access channels", *IEEE Trans. Inform. Theory*, vol. 47, pp. 241-267, Jan. 2001.

[32] R. Knopp, P. A. Humblet, "Information capacity and power control in single-cell multiuser communications", *IEEE ICC'95*, vol. 1, pp. 331-335, June 1995.

[33] F. Adachi, M. Sawahashi, H. Suda, "Wideband DS-CDMA for next-generation mobile communications systems", *IEEE Commun. Mag.*, vol. 36, pp. 56-69, Sept. 1998.

[34] T. Minn, K. Y. Siu, "Variable chip rate CDMA", in *Proc. of IEEE VTC'00*, vol. 3, pp. 2267-2271, Tokyo, 2000.

[35] R. R. Gejji, "MQAM/CDMA for increased cellular capacity", *in Proc. of VTC'93*, pp. 46-48, May 1993.

[36] L. B. Milstein, M. S. Lim, "On the performance of a higher order alphabet size in CDMA", *IEEE Commun. Letts*, vol. 1, pp. 9-11, Jan. 1997.

[37] S. J. Lee, H. W. Lee, D. K. Sung, "Capacities of single-code and multicode DS-CDMA systems accommodating multiclass services", *IEEE Trans. Veh. Technol*., vol. 48, pp. 376-384, Mar. 1999.

[38] T. Ottoson, A. Svensson, "Multi-rate schemes in DS/CDMA systems", *Proc.IEEE VTC'95*, pp. 1006-1010, July 1995.

[39] X. Tang, A. J. Goldsmith, "Admission control and adaptive CDMA for integrated voice and data systems", in *Proc. of IEEE VTC'01*, vol. 1, pp. 506 -510, 2001.

[40] V. K. N. Lau, S. V. Maric, "Variable rate adaptive modulation for DS-CDMA", *IEEE Trans. Commun*., vol. 47, pp. 577-589, April 1999.

[41] S. W. Kim, "Adaptive rate and power DS/CDMA communications in Fading channel", *IEEE Commun. Lett.*, vol. 3, pp. 85-87, 1999.

[42] S. W. Kim, Y. H. Lee, "Combined rate and power adaptation in DS/CDMA communications over Nakagami fading channels", *IEEE Trans. Commun.* vol. 48, pp. 162-168, 2000.

[43] M. D. Yacoub, *Foundations of Mobile Radio Engineering*, CRC Press, 1993.

[44] J. P. Linnarta, *Narrowband Land-mobile Radio Networks*, Artech House, 1993.

[45] G. C. Hess, *Land-mobile Radio Systems Engineering*, Artech House, 1993.

[46] R. C. French, "The effect of fading and shadowing on channel reuse in mobile radio", *IEEE Trans. Veh. Technol*., vol. 28, no. 3, pp. 171-181, Aug. 1979.

[47] H. Suzuki, "A Statistical Model for Urband Radio Propagation", *IEEE Trans. Commun*., COM-25, (7), pp. 673-680, 1997.

[48] A. J. Coulson, A. G. Williamson, R. G. Vaughan, "Improved Fading Distribution for Mobile Radio", *IEE Proceedings*, vol. 145, no. 3, pp. 197-202, June 1998.

[49] J. Griffiths, J. P. Mcgeehan, "Interrelationship between some Statistical Distributions used in Radio-wave Propagation", *IEE Proc. F, Commun*, Radar Signal Process, 129 (6), pp. 411-417, 1982.

[50] F. Davarian, "Mobile digital communications vis tone-calibration", *IEEE Trans. Veh. Technol.*, May 1987.

[51] J. K. Cavers, "An analysis of pilot symbol assisted modulation for Rayleigh fading channels", *IEEE Trans. Veh. Technol*., vol. 40, pp. 686-693, Apr. 1991.

[52] D. G. Godard, "Self-recovering equalization and carrier tracking in two-dimensional data communication systems", *IEEE Trans. Commun*., vol. COM-28, pp. 1867-1875, Nov. 1980.

[53] M. Nakagami, "The m-distribution: A general formula of intensity distribution of rapid fading", *Statistical Methods in Radio Wave propagation*, Oxofrd: Pergamon Press, 1960.

[54] W. B. Davenport, W.L.Root, *Random Signals and Noise*, New York: McGraw-Hill, 1958.

[55] X. Tang, M-S. Alounini, A. J. Goldsmith, “Effect of channel estimation error on M-QAM BER performance in Rayleigh fading”, *IEEE Trans. Commun*., vol. 47, pp. 1856-1864.

[56] G. J. Foschini, J. Salz, “Digital communications over fading radio channels”, *Bell Syst. Tech. J*., pp. 429-456, Feb. 1983.

[57] J. Lu, K. B. Letaief, J. C-I. Chunag, M. L. Liou, “M-PSK and M-QAM BER computation using signal-space concepts”, *IEEE Trans. Commun*., vol. 47, no. 2, pp. 181-184, Feb.,1999.

[58] J. Craig, “A new, simple and exact result for calculating the probability of error for two-dimension signal constellation*”, IEEE MILCOM’91*, pp. 571-575, 1991.

[59] S. Sampei, T. Sunaga, “Rayleigh fading compensation for QAM in land mobile radio communications”, *IEEE Trans. Veh. Technol*., vol. 42, pp. 137-147, May 1993.

[60] I. S. Gradshteyn, I. M. Ryzhik, *Table of Inegrals, Series, and Products*. New York: Academic, 1980.

[61] J. Kim, I. Kim, S. Ro, D. Hong, C. Kang, “Performance analysis of adaptive modulation system combined with transmitter/receiver diversity”, in *Proc. IEEE VTC’96*, vol. 2, pp. 837-841, 1996.

[62] N. C. Beaulieu, A. S. Abu-Dayya, “Analysis of equal gain diversity on Nakagami fading channels”, *IEEE Trans. Commun*, vol. 39, pp. 225-234, Feb. 1991.

[63] F. J. Altman, W. Sichak, “Simplified diversity communication system for beyond-the-horizon links”, *Electrical Commun*., vol. 33, pp. 151-160, June. 1956.

[64] D. G. Brennan, “ Linear diversity combining techniques”, *Proc. IRE*, vol. 47, pp. 1075-1101, June 1959.

[65] S. Chennakeshu, J. B. Anderson, “Error rates for Rayleigh fading multichannel reception of MPSK signals”, *IEEE Trans. Commun*., vol. 43, pp. 338-346, 1993.

[66] S. O. Rice, “Statistical properties of a sine wave plus noise”, *Bell Syst. Tech. J*., vol. 27, pp. 109-157, Jan. 1948.

[67] C. D. Iskander, P. Takis, “Analytical level crossing rates and average fade durations for diversity techniques in Nakagami fading channels”, *IEEE Trans. Commun*., vol. 50, no. 8, pp. 1301-1309, Aug. 2002.

[68] X. Dong, N. C. Beaulieu, “Average level crossing rate and average fade duration of selection diversity”, *IEEE Communications Letters*, vol. 5, no. 10, pp. 396-398, Oct. 2001.

[69] H. S. Wang, N. Moayeri, “Finite-state markov channel-A useful model for radio communication channels”, *IEEE Trans. Veh. Technol*., vol. 44, pp. 163-171, Feb. 1995.

[70] H. S. Wang, P. -C. Chang, “On verifying the first-order Markovian assumption for a Rayleigh fading channel model”, *IEEE Trans. Veh. Technol*., vol. 45, pp. 353-357, May 1996.

[71] A. Papoulis, *Probability, Random Variables, and Stochastic Processes*, New York: McGraw-Hill, 1991.

[72] H. A. David, *Order Statistics*, 2th edition, John Wiley and Sons, 1980.

[73] M. J. Gans, “A power spectral theory of propagation in the mobile radio environment”, *IEEE Trans. Veh. Technol*., vol. VT-21, pp. 27-38, Feb. 1972.

[74] R. H. Clarke, “A statistical theory of mobile-radio reception”, *Bell Syst. Tech. J*., vol. 47, pp. 957-1000, 1968.

[75] G. L. Turin, "Introduction to spread-spectrum anti-multipath techniques and their application to urban digital radio", *Proc. of IEEE*, vol. 68, pp. 328-353, Mar. 1980.

[76] S. Verdu, *Multiuser Detection*, Cambridge University press, 1998.

[77] R. Lupas, S. Verdu, "Linear multiuser detection for synchronous code-division multiple-access channel", *IEEE Trans. Inform. Theory*, vol. 35, pp. 123-136, Jan. 1989.

[78] M. Varanasi, B. Aazhang, "Near optimum detection in synchronous code-division multiple-access systems", *IEEE Trans. Commun*., vol. 39, pp. 725-736, May 1991.

[79] S. Ariyavisotakul, L. F. Chang, "Signal and Interference Statistics of a CDMA System with Feedback Power Control", *IEEE Trans. Commun*., vol. 41, pp. 1626-1634, Nov. 1993.

[80] S. Ariyavisotakul, "SIR based Power Control in CDMA System", in *Proc. IEEE GLOBECOM'92*, Orlando FL, pp. 868-873, Dec. 1992.

[81] C.-L. I, R. D. Gitlin, "Multi-code CDMA wireless personal communication networks", in *Proc. ICC'95*, Seatle, pp. 1060-1064, Jun. 1995.

[82] S. J. Lee, H. W.Lee, D. K. Sung, "Capacities of single-code and multicode DS-CDMA systems accommodating multiclass services", *IEEE Trans. Veh. Technol*., vol. 48, pp. 376-384, Mar.1999.

[83] M. B. Pursley, "Performance evaluation for phase-coded spread-spectrum multiple-access communication-part I: system analysis", *IEEE Trans. Commun*., vol. 25, no. 8, pp. 795-799, 1977.

[84] M. B. Pursley, D. V. Sarwate, W.E. Stark, "Performance evaluation for phase-coded spread-spectrum multiple-access communication-part II: code sequence analysis", *IEEE Trans. Commun*., vol. COM-25, no. 8, pp. 800-803, 1987.

[85] E. Geraniotis, B. Ghaffari, "Performance of binary and quaternary direct-sequence spread-spectrum multiple-access systems with random signature sequences", *IEEE Trans. Commun.*, vol. 39, pp. 713-724, 1991.

[86] Y. D. Yao, A. U. H. Sheikh, "Outage probability analysis for microcell mobile radio systems with co-channel interferers in Rician/Rayleigh fading environment", *Elec. Lett.*, vol. 26, no. 13, pp. 864-866, June 1990.

[87] W. Yu, W. Rhee, S. Boyd, J. M. Cioff, "Iterative water-filling for vector multiple access channels", *IEEE Int. Symp. Info. Th.*, 2001.

[88] S. A. Jafar, A. Goldsmith, "Optimal rate and power adaptation for multirate CDMA", in *Proc. IEEE VTC-FALL* 2000, vol. 3, pp. 994-1000, 2000.

[89] R. H. Frenkiel, T. Imielinski, "Infostations: The joy of 'many-time, many-where' communications", *Tech. Rep. TR-119*, Wireless Information Networks Laboratory (WINLAB), Rutgers, the State University of New Jersey, Apr. 1996.

[90] K. S. Gilhousen, I. M. Jacobs, R. Padovani, A. J. Viterbi, L. A. Weaver, Jr., C.E. Wheatley III, "On the capacity of a cellular CDMA system", *IEEE Trans. Veh. Technol.*, vol. 40, no. 2, pp. 303-312, May 1991.

[91] P. G. Andermo, L. M. Ewerbring, "A CDMA-based radio access design for UMTS", *IEEE Personal Commun.*, vol. 2, no. 1, pp. 48-53, 1995.

[92] A. Baier, U. C. Fiebig, W. Granzow, W. Koch, P. Teder, J. Thielecke, "Design study for a CDMA-based third-generation mobile radio system", *IEEE. J. Select. Areas Commun.*, vol. 12, no. 4, pp. 733-743, 1994.

[93] R. E. Fisher, A. Fukasawa, T. Sato, Y. Takizawa, T. kato, M. Kawade, "Wideband CDMA system for personal communications services", in *Proc. IEEE VTC'96*, pp. 1652-1655, April 1996.

[94] A. Baier, U. -C. Fiebig, W. Granzow, W. Kocj, P. Teder, "Design study for a CDMA-based third-generation mobile radio system", *IEEE J. Select. Areas Commun*., vol. 12 ,no. 4, pp. 733-743, 1994.

[95] Y. W. Kim, S. J. Lee, J. H. Kim, Y. H. Kwon, D. K. Sung, "Capacity estimation in multiple-chip-rate DS/CDMA systems supporting multimedia services", *Wireless Personal Commun.*, vol. 4, pp. 29-47, 2000.

[96] X. H. Chen, T. Lang, " Multiple chip rate division DS/CDMA system and its statiscal BER using a novel co-channel interference model", in *Proc. IEEE ICSP'96*, pp. 1659-1661, 1996.

[97] D. Lyu, I. Song, Y. Han, H. M. Kim, "Analysis of the performance of an asynchronous multiple-chip rate DS/CDMA system", *Int. J. Electron. Commun*., vol. 51, Issue 4, pp. 213-218, 1997.

[98] D. G. Jeong; II. G. Kim; D. Kim. "CAPACITY analysis of spectrally overlaid multiband CDMA mobile networks", *Trans. on Veh. Techn.*, vol. 47, No. 3, pp. 798-807, 1998.

[99] Il. G Kim; D. Kim; D. G. Jeong. "FORWARD link capacity of spectrally overlaid narrow band and wide band CDMA systems", in *Proc. VTC'97*, May, pp. 1445-1449, 1997.

[100] R. H. Mo, Y. H. Chew, C. C. Ko, "Uplink capacity analysis of a spectrally overlaid multi-band CDMA system with inter- and intra-cell interferences", in *Proc. of IEEE ICC'2001*, pp. 3005-3011, Jun. 2001.

[101] T. S. Rapport, *Wireless Communications: Principles and Practice,* Prentice Hall PTR: NJ, 1999.

[102] J. S. Lehnert, M. B. Pursley, "Error probabilities for binary direct-sequence spread-spectrum communications with random signature sequences", *IEEE Trans. Commun*., vol. 35, no. 1, Jan. 1987.

[103] E. Hamelin, L. A. Rusch, P. Fortier, “New cross-correlation results for multi-reate CDMA”, Conference Record, in *Proc. ICC’98*, vol. 2, pp. 693-698, Jun. 1998.

[104] S. Haykin, *Digital communications*, John Willey and Sons, 1988.

LIST OF PUBLICATIONS / SUBMISSIONS

1 R. Mo, Y.H. Chew, "Throughput analysis of rate adaptive TDMA system supporting two class services", accepted by *Wireless Network.*

2 Y.H. Chew, R. Mo, C.C. Ko, “Channel capacity in time sharing multiple-access flat fading channels employing variable rate MQAM transmitter”, *Electron. Lett.*, vol.37, no.17, pp.1084-1086, 2001.

3 R. Mo, Y.H. Chew, C.C. Ko, “Uplink capacity analysis of a spectrally overlaid multi-band CDMA system with Inter- and Intra-cell Interferences”, in *Proc. of ICC’2001*, Helsinki, Finland, Section G72 CDMA, cr1735.pdf (1-7), 2001

4 R. Mo, Y.H. Chew, C.C. Chai, “Capacity of DS-CDMA system under multipath fading with different adaptive rate adaptive power schemes”, in *Proc. of IEEE WCNC’2003,* New Oleans, Louisiana, USA, 2003.

5 R. Mo, Y.H. Chew, "Capacity and throughput analysis over Flat Fading channels using an Optimal TDMA scheme", in *Proc. of IEEE GLOABLCOM2003,* San Francisco, USA, 2003.

6 R. Mo, X. Hu, Y.H. Chew. “On the capacity analysis of overlaid CDMA system supporting dual classes of services employing rate adaptive transmission techniqu”, in *Proc. IEEE PIMRC2003*, Bejing, China, 2003.

7 R. Mo, Y.H. Chew, “Capacity of rate adaptive MQAM system in the presence of channel estimation error”, submitted to *IEEE Trans. Commun*.

8 R. Mo, Y.H. Chew, “Capacity of rate adaptive MQAM systems in the presence of channel estimation error”, submitted to *IEEE Trans. Commun*.

9 Ronghong Mo, Yong Huat Chew, “On the analysis of capacity and channel inter-access time for SNR-priority-based channel allocation scheme”, submitted to *IEEE Trans. Commun*.

10 Ronghong Mo, Yong Huat Chew, Chin Choy Chai, “Capacity of adaptive rate

adaptive power CDMA systems over frequency selective fading channels", submitted to *IEEE Trans. Veh. Technol*.

11 Ronghong Mo, Yong Huat Chew, "On the analysis of time correlated SNR with diversity reception over Rayleigh fading channel", submitted to *IEEE Commun*. Letters.

APPENDIX A

COEFFICIENTS FOR THE COMPUTATION OF BER

TABLE A.1 BPSK(amplitude error)

w_j	a_j	b_j
1	$\sqrt{2}$	0

TABLE A.2 QPSK(amplitude error)

w_j	a_j	b_j
1	1	0

TABLE A.3 16-QAM(amplitude error)

j	$w_j\ (\times 1/4)$	$a_j\ (\times 1/\sqrt{5})$	$b_j\ (\times 1/\sqrt{5})$
1	1	3	0
2	1	1	0
3	1	3	-2
4	-1	3	2
5	1	-1	2
6	1	1	2

TABLE A.4 64-QAM (amplitude error)

j	$w_j\ (\times 1/12)$	$a_j\ (\times 1/\sqrt{21})$	$b_j\ (\times 1/\sqrt{21})$	j	$w_j\ (\times 1/12)$	$a_j\ (\times 1/\sqrt{21})$	$b_j\ (\times 1/\sqrt{21})$
1	1	1	0	15	1	7	2
2	1	3	0	16	-1	7	6
3	1	5	0	17	1	-5	6
4	1	7	0	18	1	5	-2
5	1	7	-4	19	-1	5	2
6	-1	7	4	20	1	5	6
7	1	5	-4	21	1	-3	6
8	-1	5	4	22	1	3	-2
9	1	-3	4	23	-1	3	2
10	1	3	4	24	1	3	6
11	1	-1	4	25	1	-1	2
12	1	1	4	26	-1	-1	6
13	1	7	-6	27	1	1	2
14	-1	7	-2	28	-1	1	6

TABLE A.5 BPSK(amplitude and phase error)

w_j	a_{1j}	a_{2j}	b_j
1	$\sqrt{2}$	0	0

TABLE A.6 QPSK(amplitude and phase error)

w_j (x 1/2	a_{1j}	a_{2j}	b_j
1	1	1	0
1	1	-1	0

TABLE A.7 16-QAM (amplitude and phase error)

j	w_j (× $1/8$)	a_{1j} (× $1/\sqrt{5}$)	a_{2j} (× $1/\sqrt{5}$)	b_j (× $1/\sqrt{5}$)	j	w_j (× $1/8$)	a_{1j} (× $1/\sqrt{5}$)	a_{2j} (× $1/\sqrt{5}$)	b_j (× $1/\sqrt{5}$)
1	1	3	1	0	7	-1	3	1	2
2	1	3	3	0	8	-1	3	3	2
3	1	1	1	0	9	1	-1	1	2
4	1	1	3	0	10	1	-1	3	2
5	1	3	1	-2	11	1	1	1	2
6	1	3	3	-2	12	1	1	3	2

TABLE A.8 64-QAM (amplitude and phase error)

j	w_j (× $1/48$)	a_{1j} (× $1/\sqrt{21}$)	a_{2j} (× $1/\sqrt{21}$)	b_j (× $1/\sqrt{21}$)	j	w_j (× $1/48$)	a_{1j} (× $1/\sqrt{21}$)	a_{2j} (× $1/\sqrt{21}$)	b_j (× $1/\sqrt{21}$)
1	1	7	7	0	57	1	7	3	0
2	1	5	7	0	58	1	5	3	0
3	1	3	7	0	59	1	3	3	0
4	1	1	7	0	60	1	1	3	0
5	1	7	7	-4	61	1	7	3	-4
6	-1	7	7	4	62	-1	7	3	4
7	1	5	7	-4	63	1	5	3	-4
8	-1	5	7	4	64	-1	5	3	4
9	1	-3	-7	4	65	1	-3	-3	4
10	1	3	7	4	66	1	3	3	4
11	1	-1	-7	4	67	1	-1	-3	4
12	1	1	7	4	68	1	1	3	4
13	1	7	7	-6	69	1	7	3	-6
14	-1	7	7	-2	70	-1	7	3	-2
15	1	7	7	2	71	1	7	3	2
16	-1	7	7	6	72	-1	7	3	6
17	1	-5	-7	6	73	1	-5	-3	6

18	1	5	7	-2	74	1	5	3	-2
19	-1	5	7	2	75	-1	5	3	2
20	1	5	7	6	76	1	5	3	6
21	1	-3	-7	6	77	1	-3	-3	6
22	1	3	7	-2	78	1	3	3	-2
23	-1	3	7	2	79	-1	3	3	2
24	1	3	7	6	80	1	3	3	6
25	1	-1	7	2	81	1	-1	3	2
26	-1	-1	7	6	82	-1	-1	3	6
27	1	1	7	2	83	1	1	3	2
28	-1	1	7	6	84	-1	1	3	6
29	1	7	5	0	85	1	7	1	0
30	1	5	5	0	86	1	5	1	0
31	1	3	5	0	87	1	3	1	0
32	1	1	5	0	88	1	1	1	0
33	1	7	5	-4	89	1	7	1	-4
34	-1	7	5	4	90	-1	7	1	4
35	1	5	5	-4	91	1	5	1	-4
36	-1	5	5	4	92	-1	5	1	4
37	1	-3	-5	4	93	1	-3	-1	4
38	1	3	5	4	94	1	3	1	4
39	1	-1	-5	4	95	1	-1	-1	4
40	1	1	5	4	96	1	1	1	4
41	1	7	5	-6	97	1	7	1	-6
42	-1	7	5	-2	98	-1	7	1	-2
43	1	7	5	2	99	1	7	1	2
44	-1	7	5	6	100	-1	7	1	6
45	1	-5	-5	6	101	1	-5	-1	6
46	1	5	5	-2	102	1	5	1	-2
47	-1	5	5	2	103	-1	5	1	2
48	1	5	5	6	104	1	5	1	6
49	1	-3	-5	6	105	1	-3	-1	6
50	1	3	5	-2	106	1	3	1	-2
51	-1	3	5	2	107	-1	3	1	2
52	1	3	5	6	108	1	3	1	6
53	1	-1	5	2	109	1	-1	1	2
54	-1	-1	5	6	110	-1	-1	1	6
55	1	1	5	2	111	1	1	1	2
56	-1	1	5	6	112	-1	1	1	6

APPENDIX B

COMPUTATION OF INTERFERENCE COEFFICIENTS OF MCR/CDMA SYSTEM

In this appendix, the interference coefficients will be calculated from the viewpoint of PSD of spreading signals and filters.

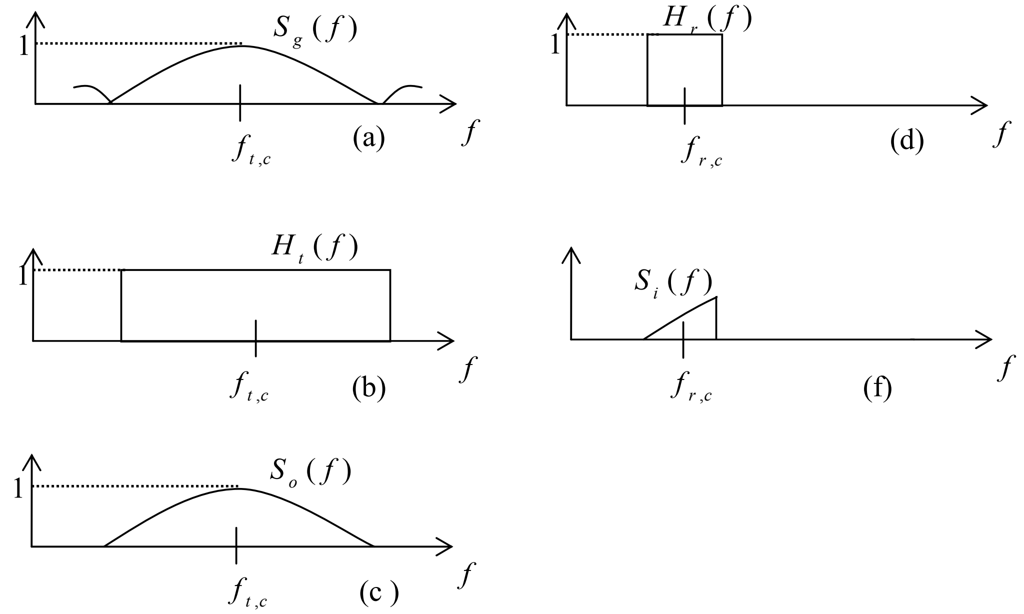

Fig.B.1 Illustration of PSD

Assuming that the PSD of spreading signal is $S_g(f)$. For QPSK signal, the normalized PSD is expressed as [104],

$$S_g(f) = \operatorname{sinc}^2\left\lfloor 2(f - f_{t,c})T_t \right\rfloor, \tag{B-1}$$

where $f_{t,c}$ is the central frequency of transmitter bandpass filter and $1/T_t$ is bandwidth of transmitter bandpass filter. For BPSK signal,

$$S_g(f) = \operatorname{sinc}^2\left[(f - f_{t,c})T_t\right]. \tag{B-2}$$

The bandpass filters in the transmitter and receiver are assumed to have ideal transfer function $H_t(f), H_r(f)$, where the frequency response equals to one during the passband while the frequency response is zero elsewhere as shown in Fig.B.1(b) and Fig.B.1(d), and the linear phase response is assumed within passband. The transfer functions of the filters can be expressed as

$$H_t(f) = \left\{\prod\left[\left(f - f_{t,c}\right)T_t\right]\right\}e^{-j2\pi f t_0} \tag{B-3}$$

and

$$H_r(f) = \left\{\prod\left[\left(f - f_{r,c}\right)T_r\right]\right\}e^{-j2\pi f t_0}, \tag{B-4}$$

where $f_{r,c}$ and $1/T_r$ are the central frequency and the bandwidth of transmitter and receiver bandpass filter respectively. The function $\prod\left[(f - f_c)T\right]$ is defined as

$$\prod[(f - f_c)T] = \begin{cases} 1 & f_c - \dfrac{1}{2T} \le f \le f_c + \dfrac{1}{2T} \\ 0 & \text{elsewhere} \end{cases}.$$

The PSD of spreading signal at the output of transmitter bandpass filter is

$$S_o(f) = |H_t(f)|^2\, S_g(f). \tag{B-5}$$

Assuming an ideal radio channel and no distortion is imposed on signals transmitted over air interface, the PSD of received signal at the output of receiver bandpass filter is

$$S_i(f) = |H_r(f)|^2\, S_o(f). \tag{B-6}$$

Substituting (B-5) into (B-6), the PSD of received signal can be rewritten as

$$
\begin{aligned}
S_i(f) &= |H_r(f)|^2 \, |H_t(f)|^2 \, S_g(f) \\
&= \left| \prod\left[(f - f_{t,c}) T_t \right] \right|^2 \left| \prod\left[(f - f_{r,c}) T_r \right] \right|^2 S_g(f)
\end{aligned}
\quad . \tag{B-7}
$$

The autocorrelation function $R(\tau)$ of the received signal separated by a time interval τ can be obtained by taking Fourier transform of (B-7) and is expressed as

$$
\begin{aligned}
R(\tau) &= F^{-1}\left[S_i(f) \right] \\
&= \int_{-\infty}^{\infty} \left| \prod\left[(f - f_{t,c}) T_t \right] \right|^2 \left| \prod\left[(f - f_{r,c}) T_r \right] \right|^2 S_g(f) e^{j2\pi f\tau} df \, . \\
&\approx \int_{f_{r,c}-1/(2T_r)}^{f_{r,c}-1/(2T_r)} S_g(f) e^{j2\pi f\tau} df
\end{aligned}
\tag{B-8}
$$

The average power of signals passing through the receiver bandpass filter is then given by

$$
R_i(0) = \int_{f_{r,c}-1/(2T_r)}^{f_{r,c}-1/(2T_r)} S_g(f) df \, . \tag{B-9}
$$

Similarly, the average power of transmitted signal can be obtained as

$$
R_t(0) = \int_{f_{t,c}-1/(2T_t)}^{f_{t,c}-1/(2T_t)} S_g(f) df \, . \tag{B-10}
$$

It can be noted that the integration regions of (B-9) and (B-10) are different. The interference coefficient is defined as the ratio of the average power of signal passing through the bandpass filter to the average power of transmitted signal, or

$$
\chi = \frac{R_i(0)}{R_t(0)} \, . \tag{B-11}
$$